DELIVERABLE REPORT

Thermal treatment for radioactive waste minimisation and hazard reduction

Initiative:	EU Horizon 2020 - Euratom Research and training programme
Grant Agreement No:	755480
Start date:	01.06.2017 Duration: 36 Months
Project Coordinator:	VTT Technical Research Centre of Finland Ltd

WP No:	4
Deliverable No:	D4.2
Title:	**Characterization of thermally treated waste products**
Lead beneficiary:	AND
Contributors:	AND, NNL, SCK•CEN, CEA, FZJ, USFD, VTT, VUJE
Dissemination level:	Public/~~Confidential~~

Due date of deliverable:	**July 2019**
Actual submission date:	**31/07/2019**

History Chart			
Type of revision	Document name	Partner	Date
Outline Table of Contents	THERAMIN D4.2 Report v1.1	Andra	01.05.19
Full draft for review and comment by project partners	THERAMIN D4.2 Report v1.2	Andra	03.07.19
First issue	THERAMIN D4.2 Report v1.3	All	31.07.19

REVIEW/OTHER COMMENTS:

The report has been reviewed by THERAMIN Consortium members and approved by THERAMIN WP4 leader. The THERAMIN coordinator has reviewed and approved the report for submission.

APPROVED FOR SUBMISSION:

This report has been approved by:

Table of Content

Acknowledgement

This project has received funding from the European Union’s Horizon 2020 Euratom research and innovation programme under Grant Agreement No 755480.

THERAMIN Project Partners

Andra	Agence nationale pour la gestion des déchets radioactifs – France
ORA	Orano – France
CEA	Commissariat à l'énergie atomique et aux énergies alternatives – France
GSL	Galson Sciences Limited – UK
FZJ	Forschungszentrum Juelich GmbH – Germany
LEI	Lithuanian Energy Institute – Lithuania
NNL	National Nuclear Laboratory – UK
ONDRAF/NIRAS	Organisme National des Déchets RAdioactifs et des matières Fissiles enrichies – Belgium
SCK•CEN	The Belgian Nuclear Research Centre – Belgium
USFD	University of Sheffield – UK
VTT	Teknologian Tutkimuskeskus VTT Oy (VTT Technical Research Centre of Finland Ltd)
VUJE	VUJE a.s. – Slovakia

THERAMIN End User Group

Andra	Agence nationale pour la gestion des déchets radioactifs – France
CEA	Commissariat à l'énergie atomique et aux énergies alternatives – France
EDF	Electricité de France – France
Fortum	Fortum Oyj – Finland
IGD-TP	Implementing Geological Disposal of Radioactive Waste Technology Platform
Nagra	Nationale Genossenschaft für die Lagerung Radioaktiver Abfälle – Switzerland
ONDRAF/NIRAS	Organisme National des Déchets RAdioactifs et des matières Fissiles enrichies – Belgium
RWM	Radioactive Waste Management Ltd – UK
Sellafield	Sellafied Ltd – UK
TVO	Teollisuuden Voima Oyj – Finland

List of acronyms

AAS	Atomic absorption spectrometry
DIW	Deionized water
DL	Detection Limit
EC	European Commission
EMP	Electron microprobe
GDF	Geological Disposal Facility
ICP	Inductively coupled plasma
ILW	Intermediate-Level Waste
ISG	International Simple Glass
JÜV50/2	JÜV 50/2 Jülicher Verbrennungsanlage
JEN	Jülicher Entsorgungsgesellschaft für Nuklearanlagen mbH
LLW	Low-Level Waste
MS	Mass spectrometry
OES	Optical emission spectroscopy
PCT	Product Consistency Test
RN	Radionuclides
RT	Room Temperature
SEM	Scanning electron microscopy
TRL	Technology Readiness Level
WAC	Waste Acceptance Criteria
WMO	Waste Management Organisation
WP	Work Package
XRD	X-ray diffraction
XRF	X-ray fluorescence spectrometry

1 Introduction

1.1 Background

The **Th**ermal treatment for **ra**dioactive waste **min**imisation and hazard reduction (THERAMIN) project is a European Commission (EC) programme of work jointly funded by the Horizon 2020 Euratom research and innovation programme and European nuclear waste management organisations (WMOs). The THERAMIN project is running in the period June 2017 – May 2020. Twelve European WMOs and research and consultancy institutions from seven European countries are participating in THERAMIN.

The overall objective of THERAMIN is to provide improved safe long-term storage and disposal of intermediate-level wastes (ILW) and low-level wastes (LLW) suitable for thermal processing. The work programme provides a vehicle for coordinated EU-wide research and technology demonstration designed to provide improved understanding and optimisation of the application of thermal treatment in radioactive waste management programmes across Europe, and will move technologies higher up the Technology Readiness Level (TRL) scale. The THERAMIN project is being carried out in five work packages (WPs). WP1 includes project management and coordination and is being led by VTT. WP2 evaluates the potential for thermal treatment of particular waste streams across Europe; this WP is led by GSL. In WP3, the application of selected thermal treatment technologies to radioactive waste management is demonstrated and evaluated; this WP is led by NNL. In WP4, the disposability of the thermally treated radioactive waste products is assessed; this WP is led by Andra. WP5 concerns synthesis of the project outcomes and their dissemination to other interested organisations; this WP is also led by GSL.

WP4 aims to carry out an evaluation of the disposability of thermally treated waste products and of the manageability of the resulting secondary waste, depending on the waste stream/treatment process combinations and depending on the disposal concepts in each participating country. WP4 is divided into three tasks:

- Task 4.1: Identification and review of criteria and requirements for the disposability of thermally treated waste products

  Under this task, Waste Acceptance Criteria (WAC) of interest and requirements in terms of behaviour and performance of waste products will be identified. Moreover, required characterization tests will be determined.

- Task 4.2: Study of thermally treated waste products and secondary waste

  Under this task, characterization tests will be carried out on thermally treated waste products and secondary waste. Some relevant existing data will be shared.

- Task 4.3: Downstream / Safety Case implications

  This task is focused on the disposability of thermally treated waste based on the identified criteria and the experimental data from the two previous tasks.

This deliverable covers all the work which has been realized in the Task 4.2.

1.2 Objectives of this Report

The objectives of this report are to present the characterization methods selected and adapted to the requirement of the project and also to compile the results of characterization tests carried out on thermally treated waste products in subtask 4.2.

The experimental methods were first compared and contrasted to select a set of simple tests which can provide basic information on the samples studied in WP4. The characterization tests selected for the project THERAMIN and adapted to the requirement of the project have already been described in the report MS12. These choices did not prevent partners from carrying out other tests.

Tests were performed on samples produced in WP3 but also on samples from treatment tests outside the project in order to get some informations about the homogeneity, the chemical composition, the microstructure and the chemical durability (leaching tests). They started mid-2018 and end mid-2019.

All the obtained results will be useful for the last task developed in WP4, i.e. the downstream/safety case implication.

1.3 Scope of this Report

This report gathers the results of characterization tests.

1.4 Report Structure

The remainder of this report is set out as follows:

- Section 2 presents the characterization tests which were selected for the project and how they were adapted
- Section 3 provides information on the thermally treated waste products which have been studied in the subtask 4.2.
- Section 4 compiles the results of characterization tests performed on thermally treated waste products, by each participating THERAMIN partner.
- Section 5 sets out the conclusions of this report.
- Section 6 lists the references used in this report.

2 Definition and adaptation of characterization tests

The characterization panel was discussed and chosen during a consensus discussion held during the WP4 meeting at Marcoule, the 2nd of February 2018 (see Minutes of WP4 meeting, 2018).

2.1 Short reminder of characterization method of interest for thermally treated waste products

The first part of WP4 was dedicated to the identification of characterization requirements to evaluate the disposability of thermally treated waste products. This work was achieved through the following methodology (see report D4.1 for more details):

- Identification of relevant WAC for thermally treated waste products,
- Review of WAC to select the ones requiring characterization tests,
- Identification of physicochemical parameters which relate to the list of identified criteria,
- Identification of characterization tools which can provide data on the identified criteria,
- Selection of tests which will be carried out in the project.

As a result, the following table was produced. It contains the list of WAC requiring characterization and the potential tools which could be used. Because of the duration of the project and the financial limitation, it is not possible to carry out all these tests in WP4, and some of them have been selected. The result of this selection is detailed in part 2.2.

Waste Acceptance Criteria	**Characterization tools which can be used**
No free liquid or gas	TGA, XRF, electron microscopy ...
Permeability and/or diffusivity of the waste sufficient to evacuate gas or other products	XRF, electron microscopy ...
No or limited content of hazardous materials (combustible, pyrophoric, reactive, etc.)	XRF, XRD, ICP after dissolution ...
Immobilisation of radionuclides	α spectrometry, autoradiography, Raman spectroscopy ...
Limited voids / limited porosity	WAXS, BET (open porosity) ...
No hot spots	XRF, electron microscopy ...
Leaching behaviour of the waste product	leaching tests, ICP, IC, UV-Vis spectroscopy, α spectrometry ...
Mechanical resistance of the waste product (mechanical constraint in disposal, impacts, etc.)	hardness, Young's modulus, toughness ...
No metal with a redox lower than 0.84 V HSE	XRF, electron microscopy ...
Thermal conductivity of the waste product (especially for self-heating waste)	thermal conductivity measurement ...

Table 1: WAC and associated characterization tools

2.2 Selected characterization techniques

A common basis for solid characterizations is chosen to test:

- the degree of homogeneity of the sample and to verify the absence of free liquid or gas,
- the overall chemical composition of a homogeneous sample or the local compositions of a heterogeneous sample,

- the amorphous or crystalline nature of a sample and the structure of the crystals present in a crystallized sample.

The analytical techniques that constitute the common basis of characterizations are listed below and are accessible to all THERAMIN partner laboratories.

- Scanning electron microscopy (a technique that produces high resolution images of a sample surface using electron–matter interactions. It can be associated with X-ray energy dispersive microanalysis to study the chemical composition of the sample by using the X-radiation caused by the electron beam).
- X-ray fluorescence spectrometry (a technique for the chemical analysis of the composition of the sample).
- *And/or* electron microprobe (non-destructive technique used to determine the chemical composition of small volumes of solid materials).
- *And/or* inductively coupled plasma analysis after dissolution of the solid (a physical method of chemical analysis that allows for the quantification of almost all dissolved elements simultaneously).
- X-ray diffraction (provides access to a variety of information contained in the arrangement of elements within a sample).

Depending on the nature of the samples and the national radioactive waste management context, partners may also be required to use other techniques, e.g.:

- total organic and inorganic carbon analyzes,
- gas physisorption to determine the specific surface area of a powder sample,
- thermal conductivity,
- transmission electron microscopy.

Finally, the chemical durability of the samples against the hydrolysis process will be estimated by leaching tests based on the ASTM Standard Test Method C 1285 – 14 “Standard Test Methods for Determining Chemical Durability of Nuclear, Hazardous, and Mixed Waste Glasses and Multiphase Glass Ceramics: The Product Consistency Test (PCT)” (ASTM International 2014) and described in the following paragraph.

2.3 Leaching tests method

As a common basis for leaching tests, the PCT-B procedure described in the ASTM Standard Test Method C 1285 – 14 (ASTM International 2014) was chosen and adapted collaboratively (Table 2). This procedure is useful to obtain initial information about chemical durability and alteration mechanisms and will avoid the findings to be limited to a specific repository concept. This methodology will enable partners to take the obtained results into account in their national context. Nevertheless, this common basis represents the reference case and does not prevent partners from carrying out additional tests, in other conditions.

	ASTM PCT-B Test Method	**Selected conditions**
Type of wasteform	Radioactive, mixed, simulated, hazardous	Sample to be tested in the framework of WP4
Usage	Scoping tests, crystallization studies, comparative wasteform evaluation	Comparative wasteform evaluation
Test vessel	Unsensitised Type 304L stainless steel or PFA TFE-fluorocarbon vessel related to >0.5 MPa	Unsensitised Type 304L stainless steel or PFA TFE-fluorocarbon vessel related to >0.5 MPa
Test duration	7 days ± 2% or varying times	≥ 28 days
Leachant	ASTM Type 1 water or other solutions	High quality pure water High pH solutions or groundwater as additional tests
Condition	Static	Static
Minimum sample mass	≥ 1g	Refer to “Leachant volume”
Particle size	U.S. Standard ASTM – 100 to + 200 mesh (0.149 to 0.274 mm) or other sizes which are <40 mesh (0.420 mm)	0.125 to 0.250 mm (a particle size more adapted for heterogeneous samples)
Leachant volume	10 ± 0.5 $cm^3 \cdot g^{-1}$ of sample mass or other volume/sample mass	A sample-surface-area to solution-volume ratio (SA/V) of 10 m^{-1}
Temperature	90 ± 2°C or other temperature provided that any changes in reaction mechanism are noted	90 ± 2°C
Atmosphere	Air or CO_2-free air	Air
Type of system	Open to transport in PFA TFE-fluorocarbon, closed to transport in stainless steel	Closed to transport

Table 2: Experimental conditions of leaching tests compared to those recommended by the standard ASTM Standard PCT-B Test Method (ASTM International 2014).

If obtaining a powdered sample is not possible because of the quality or nature of the sample, leaching test on monoliths are possible, based on ASTM Standard Test Method C 1220 – 17

“Standard Test Method for Static Leaching of Monolithic Wasteforms for Disposal of Radioactive Waste” (ASTM International 2017). In this second test method suitable for radioactive wasteform material specimens, a specimen of known geometric surface area is immersed in a known volume of leachant in a test vessel (PTFE, steel, titanium, fused silica; Figure 1) that is sealed and placed in an oven (± 1°C) set at a defined temperature for a defined time period without agitation. Aliquots of the leachate solution are removed and analyzed for pH and various components that were released from the specimen during the test. The concentrations of dissolved soluble components are used to determine the extent of reaction. A separate test is conducted to provide data for each test condition (duration, temperature, *S*/*V* ratio, leachant composition, etc.). The saw-cut specimens are polished using successively finer grit paper with water (or absolute alcohol) lubrication. Saw-cut specimens will have a surface finish similar to 200-grit. For typical glasses, the test specimen surface finish is 600-grit. The selected test conditions – test duration, leachant, *S*/*V* ratio, temperature and atmosphere – are identical to those described in the third column of Table 2.

Figure 1: Examples of PFA TFE-fluorocarbon reactor and support (left) and Type 304-L steel test vessel, support and closure fitting (right) (ASTM International 2017).

3 Short reminder of studied samples

The different samples characterized are gathered in the *Table 3*.

THERAMIN partner	Sample identification	Initial waste
CEA	THERAMIN-SHIVA-VDM1 sample	Mixture of zeolites, diatoms and IER
CEA	THERAMIN-INCAN-BST sample	Ashes from technological waste incineration
FZJ	Sample from JÜV 50/2	Mixed radioactive waste from German research reactor
NNL	TH 01 Geomelt ICV sample	Simulated cemented package representing conditioned waste such as failing cemented packages and sea dump drums
NNL	TH 02 Geomelt ICV sample	Heterogenous sludge
NNL	HIP-1 sample	Surrogates for uranium
NNL	HIP-2 sample	
USFD	Glass 6 – Geomelt sample	PCM/Magnox sludge simulants
USFD	Glass 12 – Geomelt sample	Pile fuel cladding/SIXEP
USFD	Plasma vitrified PCM – cold crucible	PCM
USFD	HIP-Ce sample	Magnox sludge simulant
USFD	HIP-U sample	
VTT	Thermal gasification sample	Organic IER
VUJE	Chrompik vitrification	Chrompik liquors
SCK.CEN	Concentrate slag – Simuli-2	Cemented concentrates
SCK.CEN	Concentrate slag – Simuli-3A	Cemented concentrates
SCK.CEN	Resin slag – R2 IRN-78	Cemented anionic resins

Table 3. Samples characterized in the subtask 4.2 by THERAMIN partners

In addition to the tests carried out on the different samples in the framework of WP4, an intercomparison of the results obtained by the different partner laboratories has been conducted. It is based on a leaching test under the conditions defined in *Table 4* on an international reference glass of nuclear interest, called ISG [Gin *et al*., 2013] provided by CEA and constituted by the six main oxides of the typical French borosilicate glass SON68 used to vitrify high-level waste.

The International Simplified Glass (ISG), was produced in 2012 by MoSci Corporation (Rolla, MO, USA). Three individual batches yielding approximately 25 kg of glass cullet each were produced by blending powdered raw materials in a V-blender. Each batch was melted in high purity fused silica crucibles in an electric furnace at 1300 °C and water quenched to produce glass frit. After drying in an electric oven the three batches of frit were blended together to create a master lot. This frit was then re-melted in platinum–rhodium crucibles in an electric furnace at 1300 °C for approximately four hours, stirred once with a quartz rod, and cast into a graphite mold. The ingots were annealed at 569 °C for 6 h in an electric oven and cooled to room temperature at a rate of 50 °C per hour [Gin *et al*. 2015].

For the standardised tests (ultrapure water and 90 °C) ISG glass powder with a 125 – 250 µm size fraction was prepared at CEA Marcoule by crushing and sieving a glass rod. The powder was washed by an iterative decanting process in acetone and absolute ethanol to remove fine particles. The specific surface area of 0.0345 $m^2 \cdot g^{-1}$ was determined by BET using Kr as adsorbent gas (MICROMERITICS ASAP 2020) after degassing at 200 °C under vacuum of 0.13 Pa minimum for 24 hours. The experimental uncertainty on the BET measurement was not specified. This value gives a classical shape factor of ≈ 2.8 with respect to the geometric surface area of the grains assimilated to spheres.

Oxide	**SiO_2**	**B_2O_3**	**Na_2O**	**Al_2O_3**	**CaO**	**ZrO_2**	
wt%	56.2 ± 1.5	17.3 ± 0.9	12.2 ± 0.7	6.1 ± 0.8	5.0 ± 0.6	3.3 ± 0.5	
mol%	60.1	16.0	12.7	3.8	5.7	1.7	
Element	**Si**	**B**	**Na**	**Al**	**Ca**	**Zr**	**O**
wt%	26.3	5.4	9.0	3.2	3.6	2.4	50.1
mol%	18.0	9.6	7.6	2.3	1.7	0.5	60.3

Table 4. Nominal composition of ISG.

4 Characterization results of thermally treated waste products

The results of characterization tests for each sample are presented below by using a Template (See Appendix A)

4.1 THERAMIN-SHIVA-VDM1 (CEA)

Both CEA and VUJE characterized THERAMIN-SHIVA-VDM1 samples. These characterization results are presented distinctly.

General information	
Partner:	CEA VUJE
Sample id:	THERAMIN-SHIVA-VDM1
Contact person:	CEA: Maxime Fournier VUJE:
Origin and macroscopic description - CEA	
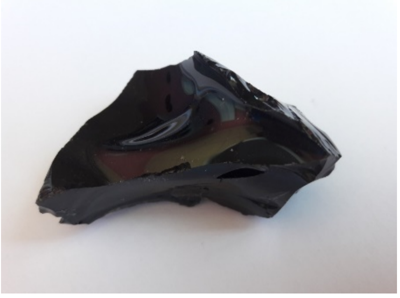 *Figure 2: Sample extracted from the wasteform produced by the SHIVA process.* ***For more information, refer to report THERAMIN D3.3*** *(revised version of June 2019)*	In the framework of the THERAMIN WP3, the **SHIVA process** was used for the thermal treatment of a waste containing a mixture of zeolites, diatoms, and ion exchange resins. The simulated glass wasteform was sampled at the center of the SHIVA cold crucible melter after cooling of the glass (Figure 2). **Thermal treatment technology** SHIVA is an incineration–vitrification process in a single reactor. It is well suited to the treatment of organic and mineral waste of low and medium activity. **Waste feeds** **Waste: 38 wt.%** (25 kg) composed of **zeolites** (45 wt.%, SOMEZ Siliz$^{®}$14), **diatoms** (44 wt.%, LAFFORT Diatomyl P0), strong acid and base **ion exchange resins** (5.5 wt.%, LENNTECH Amberlite^{TM} IRN77 and IRN78). **Glass frit: 62 wt.%** (40 kg) chosen for its good response to induction (5.2 wt.% Al_2O_3, 14.7 wt.% B_2O_3, 4.1 wt.% CaO, 0.7 wt.% CoO, 4.0 wt.% Fe_2O_3, 2.0 wt.% Li_2O, 10.0 wt.% Na_2O, 7.3 wt.% Nd_2O_3, 0.5 wt.% NiO, 46.6 wt.% SiO_2, 2.5 wt.% ZnO, 2.4 wt.% ZrO_2).
Origin and macroscopic description - VUJE	
	Sample of Shiva glass was produced by CEA using SHIVA process- incineration- vitrification process used for the thermal treatment of a

 Figure 3: Picture of SHIVA glass block prepared in VUJE´s laboratory	waste containing a mixture of zeolites, diatoms and ion exchange resins. The SHIVA sample (approx. 250 g) was sent to VUJE, Slovakia for chemical durability analysis using the modified ASTM C1220. Sample form SHIVA glass was prepared for siutable form for this analysis in VUJE´s laboratory: The sample of SHIVA glass was insert to an oven and melted using temperature regime of 10°C/ min 1220°C, holding time 1 hour at 1220°C. Monoliths were molted on the metal pad after remelting of approx. size 1.5 x 2 x 1.5-2 cm. After cooling to about 500- 600°C, the monoliths were transferred to a second furnace and tempered for 4 hours at 550°C.

Microstructure - CEA

Method(s):	☒ SEM ☒ XRD ☐ Other:
Operating conditions:	**XRD:** X-ray diffraction pattern is acquired with a Phillips X'PERT Pro equipped with a Bragg–Brentano θ–2θ diffractometer and operated with monochromatic $\text{Cu-K}\alpha_1$ radiation at 40 mA–40 kV. Acquisition is performed on the 2θ range extending from 10° to 90° with a speed of $0.27°\cdot\text{min}^{-1}$ and a step of 0.017° (2θ). Data are processed by DIFFRAC.EVA software (Bruker). **SEM:** Scanning electron microscopy images are acquired with a Zeiss Supra^{TM} 55 device operated with an acceleration voltage of 15 kV and equipped with secondary and backscattered electron detectors. The polished cross section is prepared by embedding the sample in an epoxy resin, polishing by diamond abrasive clothes and suspensions (up to 1 µm) before being coated with a carbon deposit.
Homogeneity:	The polished cross section observed by SEM is shown in Figure 4. As examples, Figure 5 and Figure 6 show regions of interest (ROI) number 1 and 4, respectively, at two different magnifications: ×50 and ×500. 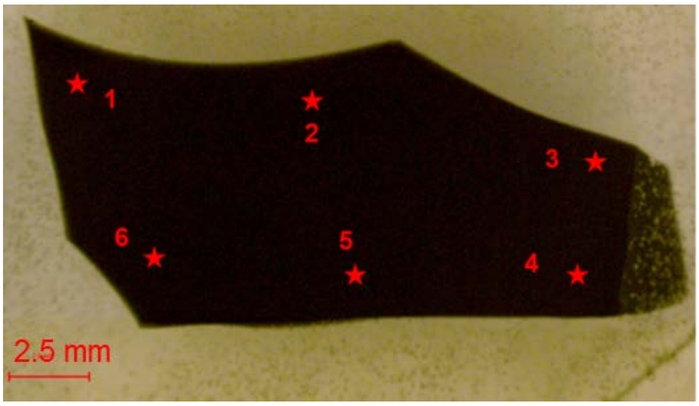 *Figure 4: View of a sample of the SHIVA-VDM1 waste glass sample prepared as a polished cross section.*

	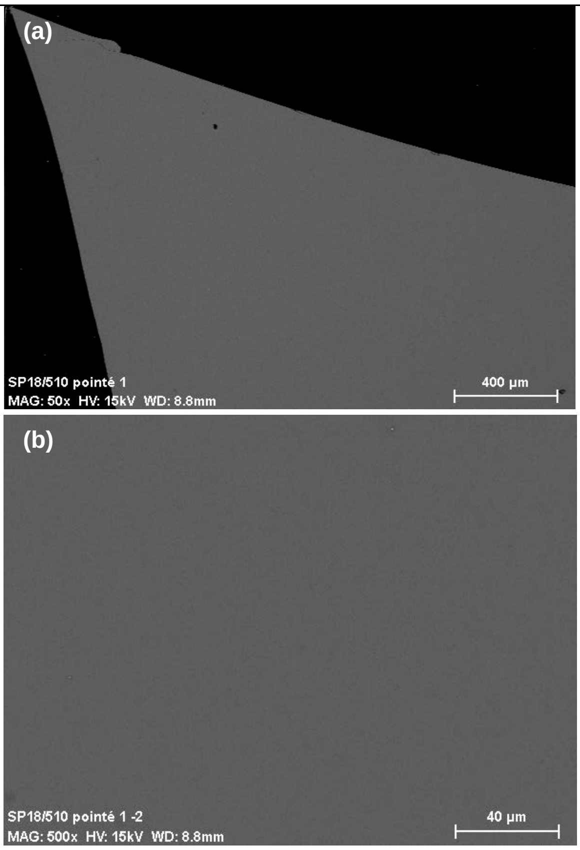 *Figure 5: SEM observation of ROI 1 with two magnifications (a) ×50 and (b) ×500.* 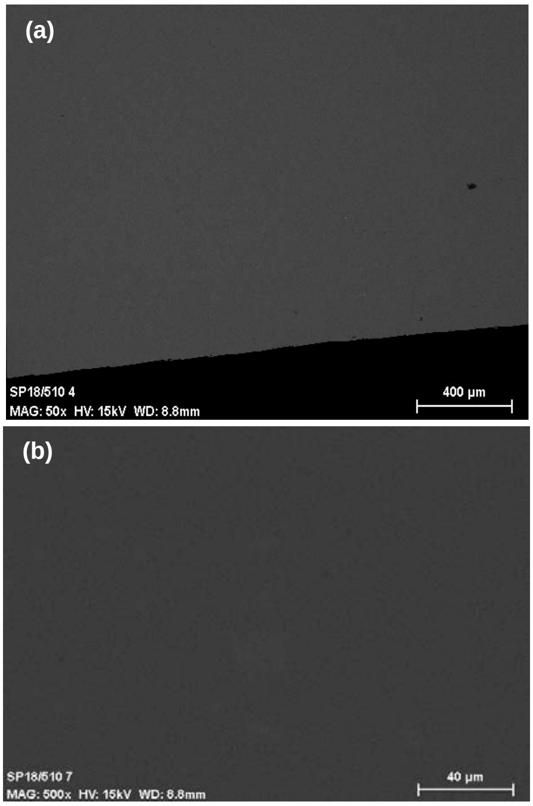

	Figure 6: SEM observation of ROI 4 with two magnifications (a) ×50 and (b) ×500.
Free liquid or gas:	Absence
Crystalline composition:	The XRD pattern acquired between 10 and 90° (2θ) shows no diffraction peak characteriztic of the presence of crystalline phases and has a diffusion halo characteriztic of vitreous materials (Figure 7). The sample is therefore **100% vitreous and amorphous**. 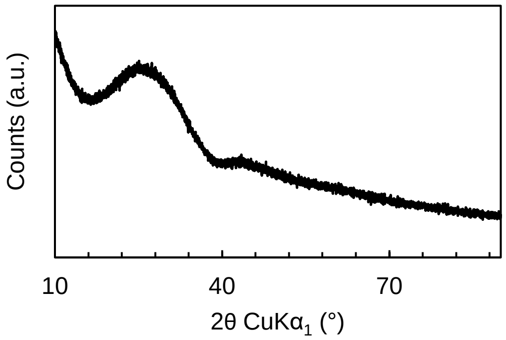 *Figure 7: XRD pattern of the SHIVA waste glass.*
Comments and discussion:	**The vitreous matrix produced by the SHIVA process in the framework of the THERAMIN project is homogeneous at the micrometric scale. The matrix is amorphous, exhibiting no crystallization visible in SEM or identifiable in XRD.**

Microstructure - VUJE

Method(s):	☒ SEM ☒ XRD ☐ Other:
Operating conditions:	**XRD:** Rigaku MiniFlex 600 Diffractometer: Cu X-ray tube + Ni Kβ filter, NaI scintillation counter: Tl detector; measurements in the range of 10° - 80° 2θ at room temperature a step of 0.02° 2θ, using an glass pad (powder). The measured data were compared with the ICDD PDF-2 database (version 2013). **SEM**: Scanning electron microscope with acceleration voltage of 15 kV in reflected electron (BEI) and secondary electron (SEI) modes using tungsten fiber. The microscope allows to change the acceleration voltage in the range of 0.3 - 30kV and, depending on the sample type, the magnification up to 300,000x. Microscope is a powerful multi-purpose scanning electron microscope with low vacuum capability. The microscope is equipped with an EDS silicon based X-Max 80 Premium detector (Figure 6-5) with an active area of 80 mm^2. the detector forms the basis of the analytical system AZTec Energy from Oxford Instruments.
Homogeneity:	Homogenous.

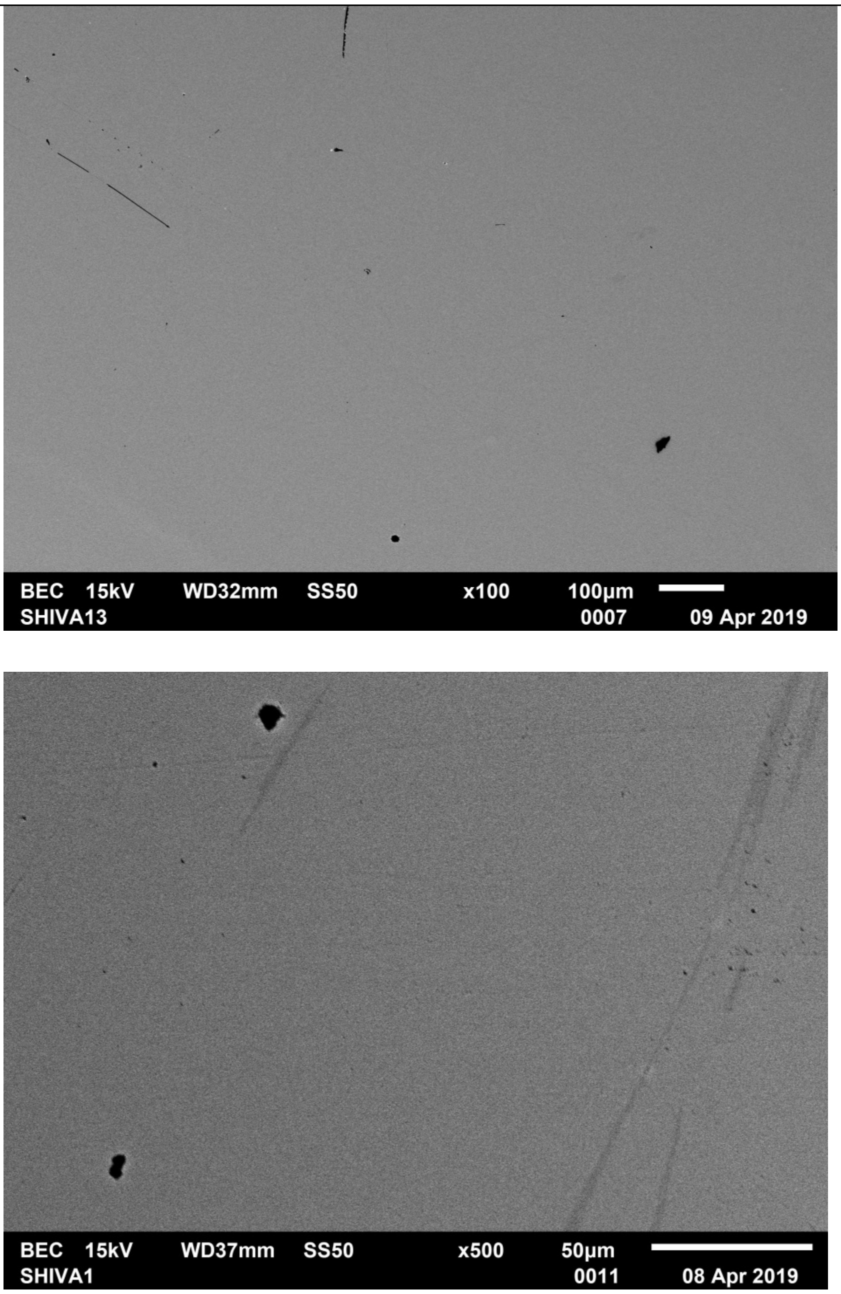

Figure 8: *SEM observation of SHIVA glass surface with two magnifications x 100 and x 500.*

	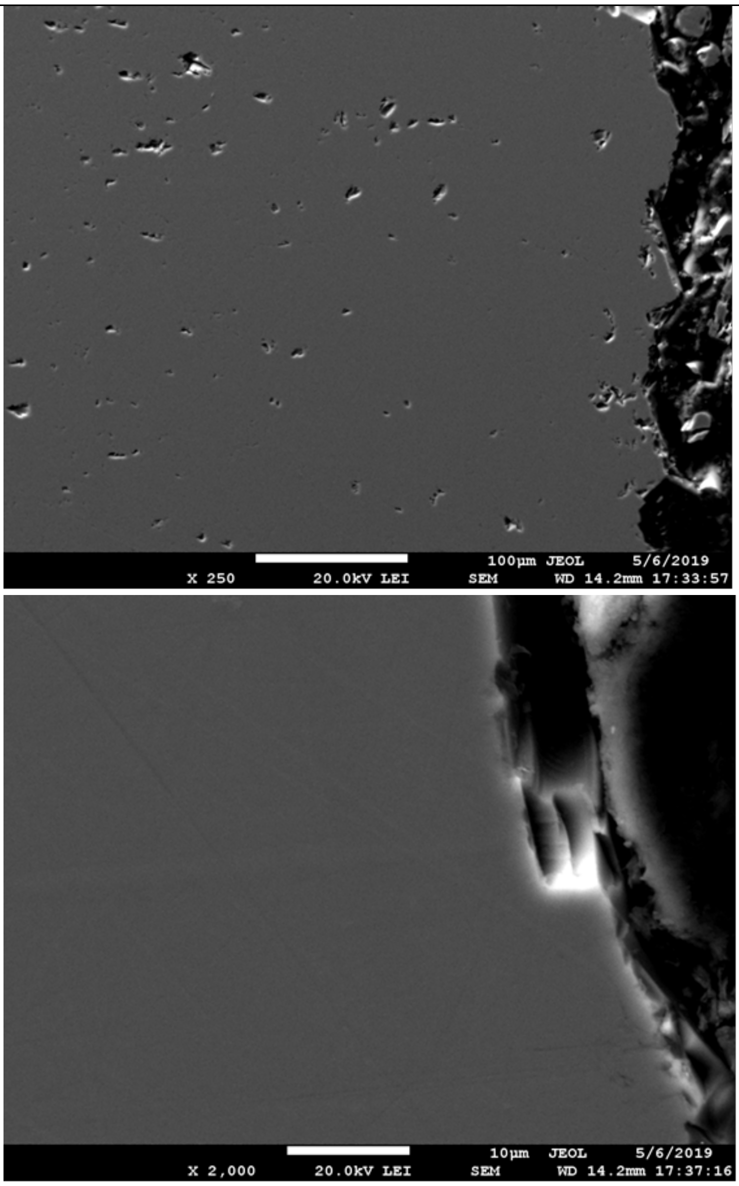 *Figure 9: SEM/EDX observation of SHIVA glass cross section*
Free liquid or gas:	Absence. No indication of free liquid or gas contained within the sample.
Crystalline composition:	Amorphous with a very small amount of crystalline silica present.

	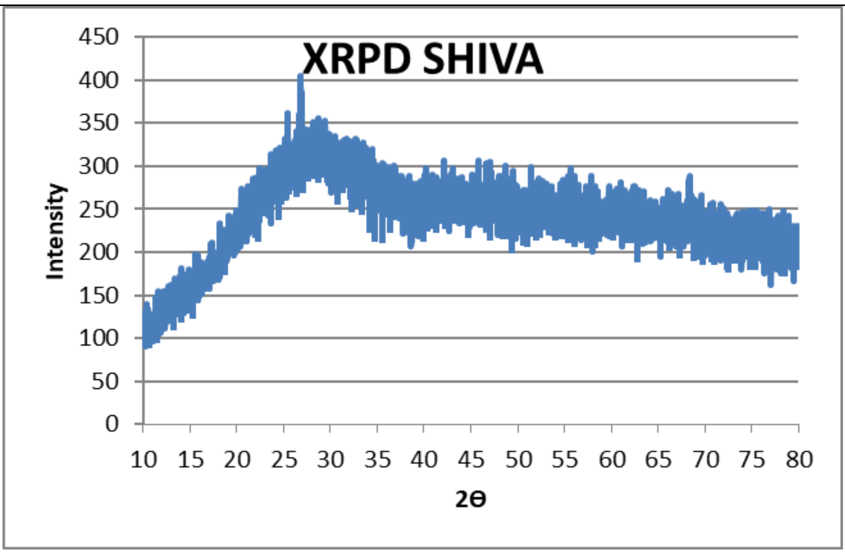 *Figure 10: Diffraction pattern of Shiva glass* Crystalline phases were detected in a Shiva glass sample where a very small amount of crystalline silica was present, a = 4.9133 Å, c= 5,4053 Å; Z = 3
Comments and discussion:	The SHIVA glass sample prepared within THERAMIN project shown no indication of free liquid or gas. The sample of SHIVA glass remelted in VUJE´s laboratory was homogenous, amorphous with a very small amount of crystalline silica present- the diffuse scattering region observed between 10° - 40° 2θ.

Chemical composition - CEA

Method(s):	☐ EMP ☒ ICP-OES/MS ☐ XRF ☒ Other: SEM/EDS
Operating conditions:	**ICP-OES:** A sample of the SHIVA-VDM1 wasteform is crushed and then dissolved in a mixture 10 HCl: 5 HNO_3: 2 HF (10 HCl: 5 HNO_3 for analysis of Nd_2O_3 content) before analysis of the solution by ICP-OES. **SEM/EDS:** The SEM described in the section “Microstructure” is coupled with a lithium-doped silicon detector for elemental analysis in energy-dispersive X-ray spectrometry.
Chemical composition:	The theoretical chemical composition (Table 5) is calculated based on the compositions of the glass frit and simulated waste, and the proportions of each in the mixture (refer to THERAMIN D3.3). This composition is verified by two methods: the dissolution of the material followed by the analysis of the solution by ICP-OES, and the analysis by EDS coupled with SEM observation. In SEM/EDS, six regions of interest (Figure 4) are analyzed giving close results (standard deviation ≤ 0.3) as shown by the superposition of EDS spectra in Figure 11. The values presented in Table 5 are the average of the six measurements. Since boron and lithium are too light to be analyzed by this method, the composition is normalized using the theoretical contents of these two elements.

	Theoretical	ICP-OES	SEM/EDS
Al_2O_3	7.2	5.6	5.7
B_2O_3	9.8	12.1	n.a
CaO	3.8	4.2	3.9
CoO	0.5	0.6	0.6
Fe_2O_3	3.4	4.2	4.0
K_2O	0.9	0.5	0.6
Li_2O	1.3	1.5	n.a
MgO	0.3	0.2	0.4
Na_2O	7.1	8.7	8.0
Nd_2O_3	4.9	6.2	6.1
NiO	0.3	0.4	0.3
SiO_2	57.2	50.7	52.2
TiO_2	0.1	0.6	0.5
ZnO	1.7	2.3	2.1
ZrO_2	1.6	2.2	2.1

Table 5: SHIVA-VDM1 waste glass composition (n.a.: not analyzed)

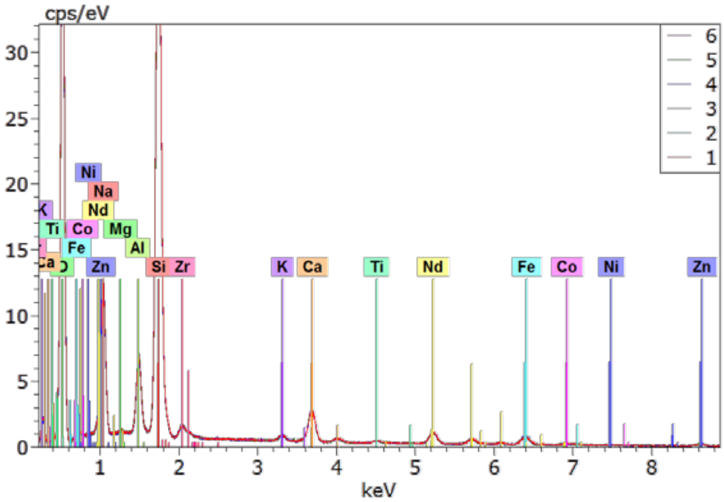

Figure 11: EDS analyzes on the 6 regions of interest shown on Figure 4. The six spectra of EDS analyzes are superimposed.

Comments and discussion:	**The analysis of the glass composition by two techniques gives consistent results. The glass contains mainly SiO_2, B_2O_3, Nd_2O_3 and Al_2O_3 that represent ≈ 85 wt.% of the glass composition. These contents are of the same order of magnitude as those of the inactive surrogate of the French reference glass R7T7.** **Significant differences are noted between the compositions of the analyzed samples taken from the center of the SHIVA crucible and the theoretical composition. They can be explained by an inhomogeneous incorporation of the waste into the matrix or a waste load lower than expected. This later hypothesis is unlikely because the masses of waste and glass frit were weighted before their introduction in the process. To validate the first hypothesis, a higher number of analyzes must be realized with a protocol of sampling in different localizations of the SHIVA crucible.**

Chemical composition - VUJE

Method(s):	☐EMP ☐ ICP-OES/MS ☒ XRF ☒ Other: SEM/EDX
Operating conditions:	**XRF:** Niton XL3t 900 GOLDD analyzer: 2W Ag X-ray tube, large-area Si drift detector. Three measurement modes: Main, Low, Light Internal calibration corresponds to a limited number of the most common elements with uncertain reliability, so it should be taken as a semiquantitative determination. Detected elements (vertical lines according to NIST X-ray Transition Energies, or just informative text) are listed in the measured spectra below. **SEM/EDX:** The measurement was performed on an electron microscope JEOL 7600F using an X-MAS 50 mm^2 EDX analyzer.

Chemical composition:

The theoretical chemical composition of SHIVA glass (Table 6) was provided by CEA. The chemical composition was verified by two methods XFR and SEM/EDX and results are presented in table 1 and compared with CEA results.

wt %	Theoretical	XRF	SEM/EDX
SiO_2	57.2	40.92	55.43
Al_2O_3	7.2	7.0	6.0
K_2O	0.9	ND	0.41
Na_2O	7.1	NA	6.05
Fe_2O_3	3.4	2.99	2.22
TiO_2	0.1	0.842	0.33
CaO	3.8	ND	3.31
MgO	0.3	ND	ND
B_2O_3	9.8	ND	ND
Li_2O	1.3	ND	ND
CoO	0.5	ND	0.36
ZnO	1.7	1.977	1.10
ZrO_2	1.6	1.458	ND
Nd_2O_3	4.9	NA	1.56
NiO	0.3	0.25	0.22

Table 6: SHIVA glass composition

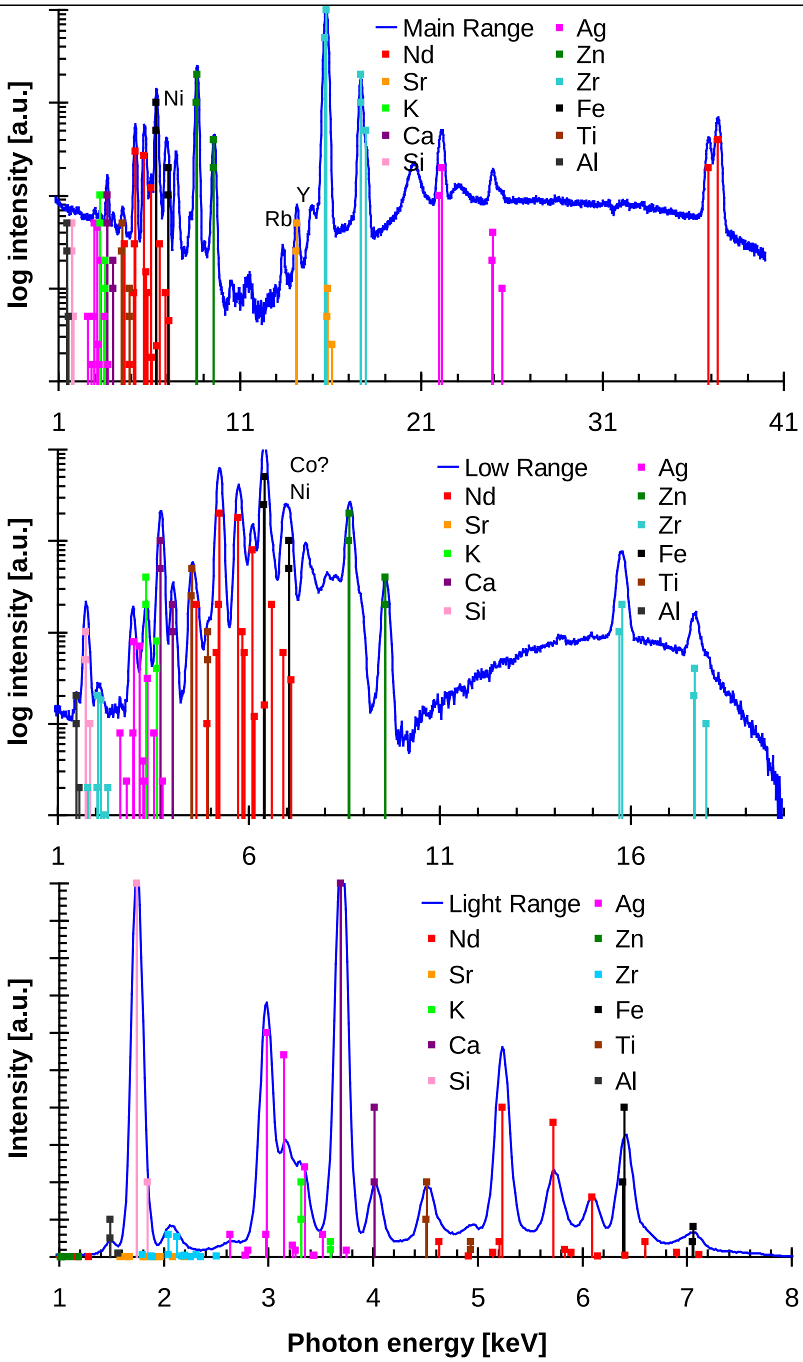

Figure 12: XRF pattern of the SHIVA glass

Comments and discussion:	The analysis of the prepared glass composition was measured by two techniques. Results from SEM/EDX analysis give consistent results between theoretical chemical composition and SHIVA glass composition. Results from XRF analysis varied from theoretical SHIVA glass composition, especially by SiO_2 wt % - this may be caused by different sample preparation.

Chemical durability - CEA

Method(s):	☒ As described in MS12 Report (p. 12-13), adapted from ASTM C1285

	☐ As described in MS12 Report (p. 14), adapted from ASTM C1220 ☐ Other:
Clarifications:	Solution samples, taken at regular intervals, are filtered with a cutoff of 0.45 µm, acidified with ultrapure grade HNO_3 and analyzed by ICP-OES (Thermo Scientific iCAP^{TM} 6000 Series). The concentrations are used to calculate normalized mass losses NL_i: $\mathrm{NL}_i = C_i/(x_i \times S/V)$ with C_i the concentration of the element i, x_i the mass percentage of i in the glass (using the analyzed sample composition: $x_{\mathrm{Al}} = 0.030$, $x_{\mathrm{B}} = 0.038$, $x_{\mathrm{Ca}} = 0.030$, $x_{\mathrm{Li}} = 0.007$, $x_{\mathrm{Na}} = 0.065$, $x_{\mathrm{Si}} = 0.237$), S/V the specific-surface-area-to-solution-volume ratio. The alteration rate, $r = \mathrm{d}NL_i/\mathrm{d}t$, is calculated by linear regression. Note that B is known to be an alteration tracer, that means that it is not retained in alteration products while released from the glass.
Results and discussion:	The stoichiometric dissolution of the glass during the first days (Figure 13.a) becomes gradually non-stoichiometric with a retention of Ca and Al of respectively 4 and 30% (relative to B) after one month. The rather unusual shape of the curve $NL_i = f(t)$ is explained by the conjunction of two phenomena: (i) the effect of the pH variation on the rate of hydrolysis and (ii) the effect of the formation of a surface layer on the alteration rate. The pH increases from 7 to 8.5 (Figure 13.b), value at which it stabilizes: this variation causes the increase in the rate of hydrolysis (v_0) of the vitreous matrix. This effect of pH is illustrated by the grey dashed curve on Figure 13.a calculated according to: $v_0 = k_+ \times [\mathrm{H}^+]^n \times e^{-E_a/(R\times T)}$, where k_+ is estimated from the NL_{B} value at 1 day (0.12 g·m^{-2}), n is the pH dependence coefficient, E_a the apparent activation energy, R the ideal gas constant and T the temperature. In this calculation, $n = 0.4$ and $E_a = 76$ kJ·mol^{-1} are assumed to be equal to those of the R7T7 glass. The progressive divergence between the calculated and the experimental data is explained by the decrease of the alteration rate with the formation of a surface layer.

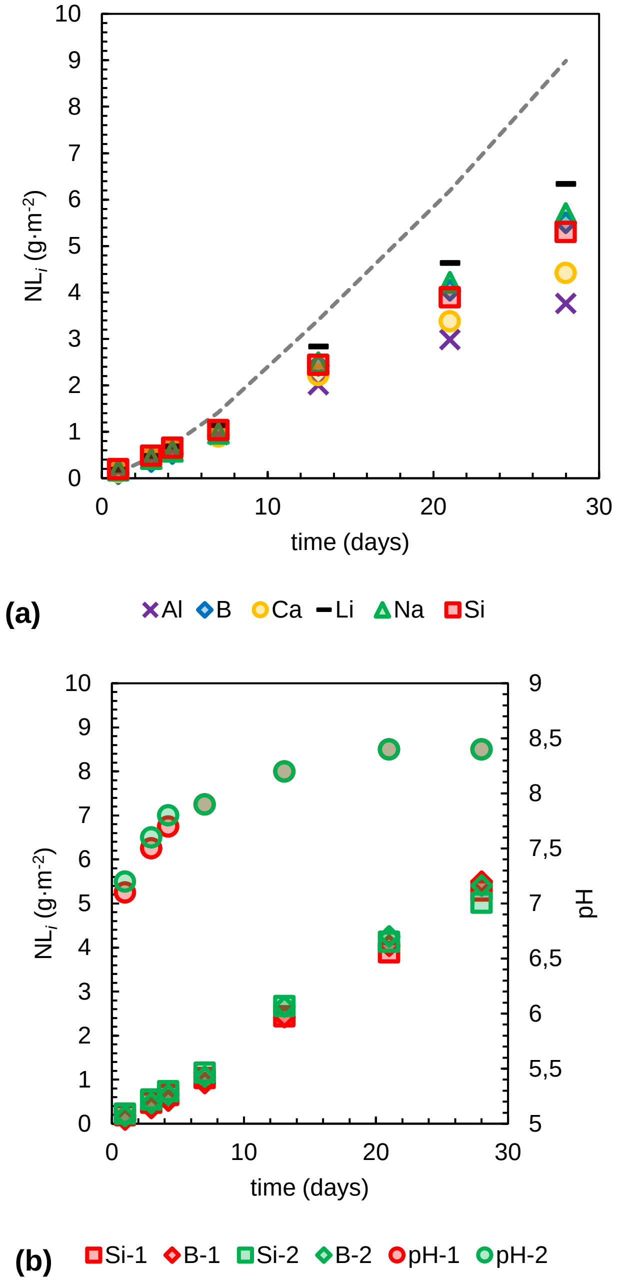

Figure 13: Evolution (a) of NL as a function of time at 90°C, S/V = 10 m^{-1} without stirring and (b) of pH and NL$_{B,\ Si}$ during duplicate leaching tests of SHIVA-VDM1 sample.

The comparison of the results obtained with the SHIVA-VDM1 and ISG samples (Figure 14) shows a similar (and classical) evolution of the pH of the solutions, being basified by the release of alkaline species from the samples. The pH stabilizes at values close to 8 at 90°C under these experimental conditions of low *S/V* ratio.

The hydrolysis rate of the ISG (based on B release) is higher by approximately one order of magnitude than the one of the SHIVA-VDM1 sample. The dissolution of the ISG is prematurely non-stoichiometric and so goes along with the formation of an alteration layer. Because of the diffusion of elements through this alteration layer, **the alteration rate of ISG drops earlier than for the SHIVA-VDM1 sample**. Concluding about the long-term behaviour of the SHIVA-VDM1 wasteform would require further investigation but these first results are encouraging when given the possibility of attributing to it a good behaviour for longer durations.

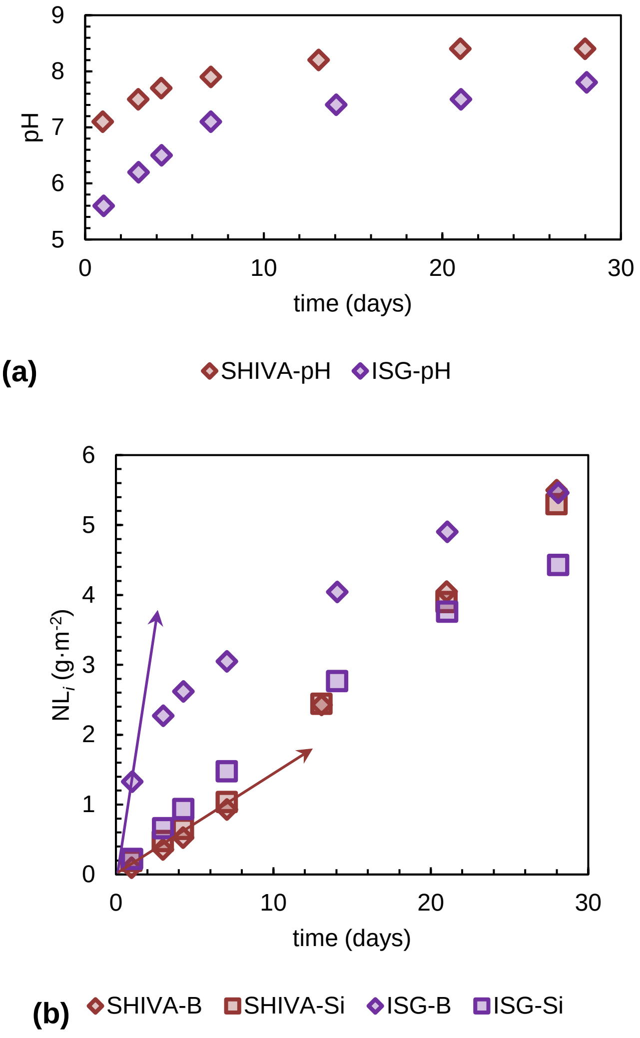

Figure 14: Compared evolutions of (a) pH and (b) NL of Si and B during the leaching of ISG and SHIVA-VDM1 samples. The arrows are a guide for the eyes to estimate the minimum hydrolysis rate of the matrices.

Chemical durability - VUJE

Method(s):	☐ As described in MS12 Report (p. 12-13), adapted from ASTM C1285 ☐ As described in MS12 Report (p. 14), adapted from ASTM C1220 ☒ Other: modified ASTM C1220

Clarifications:	Samples were prepared by pouring into cuboid monoliths of approx. 1.5 x 2x 1.5-2 cm. The formula was used to calculate the normalized mass: $NL = \frac{(m_0 - m_t)}{S_0}$, where m_0 is the weight of the monolith at the start of the experiment, m_t is the mass of the monolith at time t, S_0 is the surface of the sample. The amount of leaching solution was determined by the ratio *S/V* = 1/10, where *V* is the volume of the solution. Leaching was carried out in an oven at 90°C. Samples were gradually removed from the oven at 1, 3, 7, 14, and 28 days. Subsequently, the samples were washed with demi water, rinsed with acetone and freely dried in the air. After drying, the samples were weighed. The pH, conductivity and determined Na^+ content using AAS were measured in the leaching solution. The Na^+ content was measured in the leaching solution and calculated to the amount of Na^+ released from the sample (glass monolith) by the equation: $NL_i = \frac{c_i}{x_i \frac{S}{V}}$, where NL_i is the normalization loss of the sample element (i = Na^+), c_i is the concentration of the element in the solution, x_i is the mass fraction of the element i in the glass, is the surface of the sample, V is the volume of the leaching solution.
Results and discussion:	Leaching at 90°C in oven: 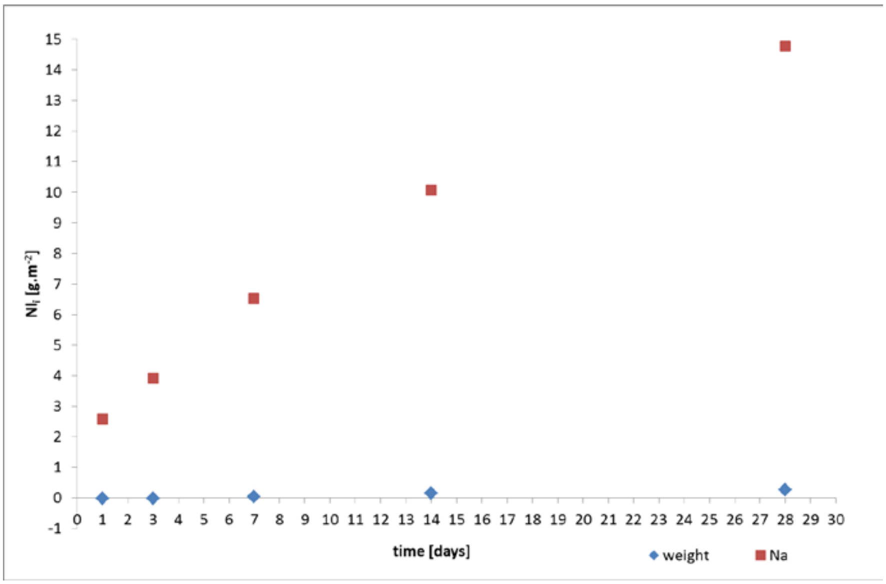 *Figure 15: Evolution of NLweight, Na as a function of time at 90°C, S/V=1/10 m-1 without stirring during repeated leaching tests of SHIVA sample (average value)*

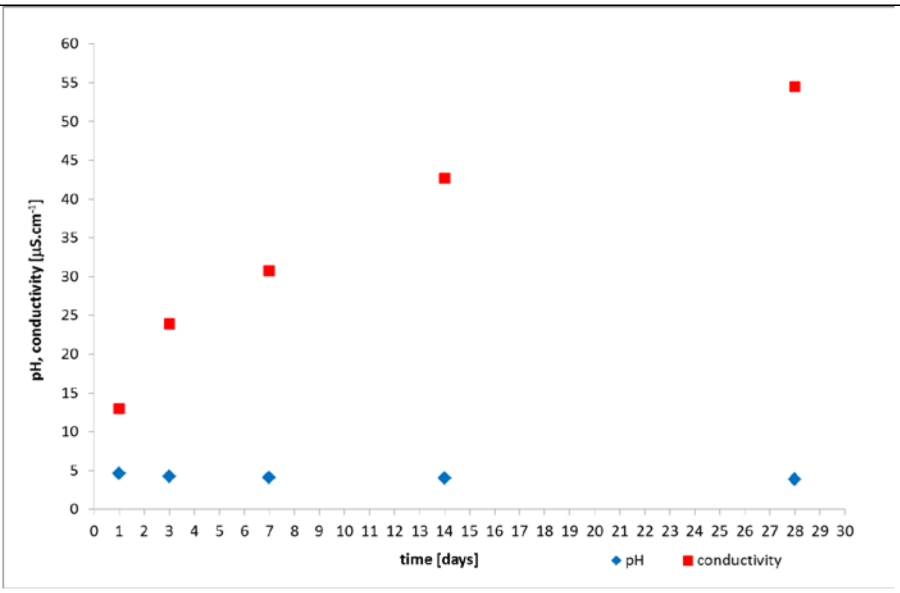

Figure 16: *Evolution of pH and conductivity as a function of time at 90°C, S/V=1/10 m-1 without stirring during repeated leaching tests of SHIVA sample (average value)*

The pH value decrease slightly. The pH stabilizes close to 4 at 90°C under these experimental conditions and SHIVA glass monolith preparation.

The conductivity increases in proportionally to the Na content in leaching solution. K content is in a very small amount in glass, so it was not possible to determine its leachability.

Other tests and characterizations - CEA

Specific surface area measurement

The specific surface area of the glass powder is measured by krypton adsorption on the surface of the sample (Micromeritics ASAP 2020). The samples were degassed at 200°C under vacuum of 0.13 Pa minimum for 24 hours. The quantity of gas required to form a monoatomic layer on the surface of the sample is estimated by the Brunauer–Emmett–Teller theory.

The specific surface of the SHIVA-VDM1 powder (125-250 µm) is **280 $cm^2 \cdot g^{-1}$**. This value gives a classical shape factor of ≈ 2.3 with respect to the geometric surface area of the grains assimilated to spheres.

Other tests and characterizations - VUJE

Specific surface area measurement:

Samples were prepared by pouring into cuboid monoliths of approx. 1.5 x 2x 1.5-2 cm.Surface of the original surface (without cutting and polishing the sample) using a 3D scanner Zeiss Comet L3D - Optical scanner.

Surface 1247.9217 mm^2 - 1557.3898 mm^2

Volume 3405.9709 mm^3 - 4815.0034 mm^3

deviation ± 0.004 mm

Conclusions and Outlooks - CEA

The SHIVA-VDM1 sample was produced by incineration-vitrification using the SHIVA process of a waste consisting of a mix of absorbing media. The final product consists of an amorphous glass mainly composed of SiO_2, B_2O_3, Nd_2O_3, and Al_2O_3. Differences are observed between the theoretical composition of the glass and the composition analyzed by two techniques, probably explained by a too low convection in the melter.

Leaching tests conducted at 90°C and a low glass-surface-area-to-solution-volume ratio show that the hydrolysis rate of SHIVA-VDM1 glass is significantly lower than that of the International Simple Glass. Concluding about the long-term behaviour of the SHIVA-VDM1 wasteform would require further investigation but these first results are encouraging considering the objective of demonstration of a good behaviour for longer durations. Finally, the vitreous nature of the matrix and the presence of boron — known to be a tracer of the alteration — make it possible to apply to this matrix the proven methodologies for the study of chemical durability and long-term behaviour.

Conclusions and Outlooks - VUJE

Shiva glass sample was produced by incineration-vitrification using the SHIVA process of a waste consisting of an absorbing media mixture.

In SHIVA glass monolith prepared in VUJE´s laboratory there was no free liquid or gas, sample was homogeneous and amorphous with a very small amount of crystalline silica, this may be caused by glass monolith preparation. Also the chemical composition of this wasteform is compatible with both results. Chemical composition of glass was analyzed by two techniques, there were small differences observed between theoretical composition XRF results and SEM/EDX results.

Leaching tests were performed according to the modified ASTM C1220. The pH value decrease slightly. The pH stabilizes close to 4 at 90°C under these experimental conditions and SHIVA glass monolith preparation.

Concluding about the long-term behaviour of SHIVA waste glass form would require further investigation.

4.2 THERAMIN-INCAN-BST sample (CEA)

General information

Partner:	CEA
Sample id:	THERAMIN-INCAN-BST
Contact person:	Maxime Fournier

Origin and macroscopic description

Figure 17: Wasteform produced by the bench scale test preceding the In-Can Melter full-scale trial. Operating conditions were identical between these two tests, except that the ash was not pelletized for the bench scale test.

For more information, refer to report THERAMIN D3.3
(revised version of June 2019)

In the framework of the THERAMIN WP3, studies were carried out on the treatment and conditioning of ash coming from the incineration of technological surrogate waste. Ash vitrification was based on the CEA **In-Can Melting** process consisting in a metallic crucible melter heated in a simple refractory furnace using electrical resistors. Prior to the full-scale trial (≈ 50 kg), laboratory-scale (≈ 10 g), and bench scale (≈ 1 kg) tests were conducted to select optimized operating conditions. This trial also made it possible to begin the technical reflection required for the introduction of very powdery solids into the can while avoiding the emission of dust: in this trial, a temporary densification by pelletizing was implemented.

Important note: To respect the deadlines imposed for the delivery of WP4 reports, **the material resulting from the bench scale test (BST) was characterized** (Figure 17). Operating conditions of BST were identical to the ones of the full-scale trial (FST), except that the ash was not pelletized. The thermal history of the test consists of heating at 300°C·h^{-1} and maintaining at 800°C for 8h**. First points of comparison between the materials from BST and FST are provided at the end.**

Thermal treatment technology

The In-Can Melter is a metallic crucible heated in a refractory furnace using electrical resistors allowing in-container vitrification.

Waste feeds

Waste: 50 wt.% (400 g) for BST and **49 wt.%** (26.1 kg) for FST of **ash** mainly composed of: Al, Zn, Ca, Si, Bi, K, Mg, and P; and containing also: Ba, Cl, Cr, Fe, Na, Ni, S, Sb, and Ti.

Glass frit: 50 wt.% (400 g) for BST and **49 wt.%** (26 kg) for FST composed of 32.4 wt.% B_2O_3, 32.1 wt.% Na_2O, 35.5 wt.% SiO_2).

Adjuvant: 0 wt.% for BST and **2 wt.%** for FST of **bentonite** used as a **pelletizing binder** in proportion equivalent to 10% of the mass of pelletized ash.

Microstructure

Method(s):	☒ SEM ☒ XRD ☒ Other: Optical microscopy
Operating conditions:	**Optical microscopy:** A preparatory work of observation is carried out with a Zeiss Axio Imager 2 optical microscope. The entire surface of the polished cross sections is imaged by a motorized stage and an Axiocam 305 Color camera allowing to realize a mosaic of images. **SEM:** Scanning electron microscopy images are acquired with a Zeiss Supra^{TM} 55 device operated with an acceleration voltage of 15 kV and equipped with secondary and backscattered electron detectors. The polished cross sections are prepared by embedding the samples in an epoxy resin, polishing by diamond abrasive clothes and suspensions (up to 1 µm) before being coated with a carbon deposit. **XRD:** X-ray diffraction pattern is acquired with a Phillips X'PERT Pro equipped with a Bragg–Brentano θ–2θ diffractometer and operated with monochromatic Cu-Kα_1 radiation at 40 mA–40 kV. Acquisition is performed on the 2θ range extending from 10° to 90° with a speed of 0.27°·min^{-1} and a step of 0.017° (2θ). Data are processed by DIFFRAC.EVA software (Bruker).
Homogeneity:	Two polished cross sections were prepared from the wasteform shown in Figure 17: one with a sample taken from the center (Figure 18.a and Figure 19) and the other with a sample taken from a contact zone between the wasteform and the Inconel crucible (Figure 18.b and Figure 20). No major differences are observed between the microstructures of the two samples analyzed by SEM: they both present a vitreous matrix in which crystals are included. The distribution of these crystals in the matrix is homogeneous with the exception of the contact zone with the crucible — of about one millimeter thick — in which the crystals appear substantially more numerous (Figure 18.b and Figure 20.b). The semi-quantitative EDS analyzes conducted during the SEM observations allow the estimation of the compositions of the four phases observed: • a "residual" vitreous matrix mainly composed of SiO_2, Na_2O, Al_2O_3, and Cao — note that B cannot be analyzed by EDS, • crystals presenting a "dark" chemical contrast (➢ on Figure 19), mainly composed of Ca and P, crystallizing with a typical apatite morphology, • crystals with a "clear" chemical contrast (★ on Figure 19), grouped into clusters (*e.g.*, Figure 20.a), and containing predominantly Cr and Zn, • white beads (● on Figure 19) crystallizing in the vicinity of the clear crystals (*e.g.*, Figure 20.a), containing almost exclusively Bi.

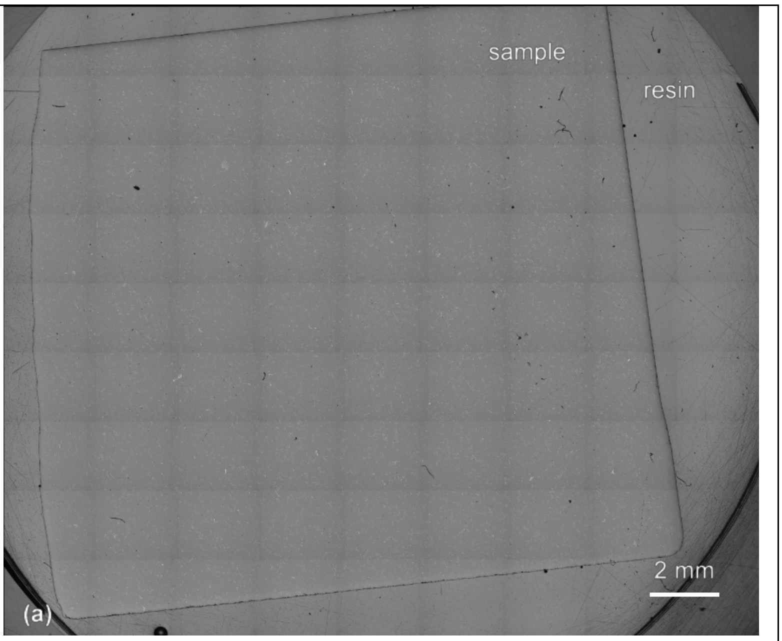

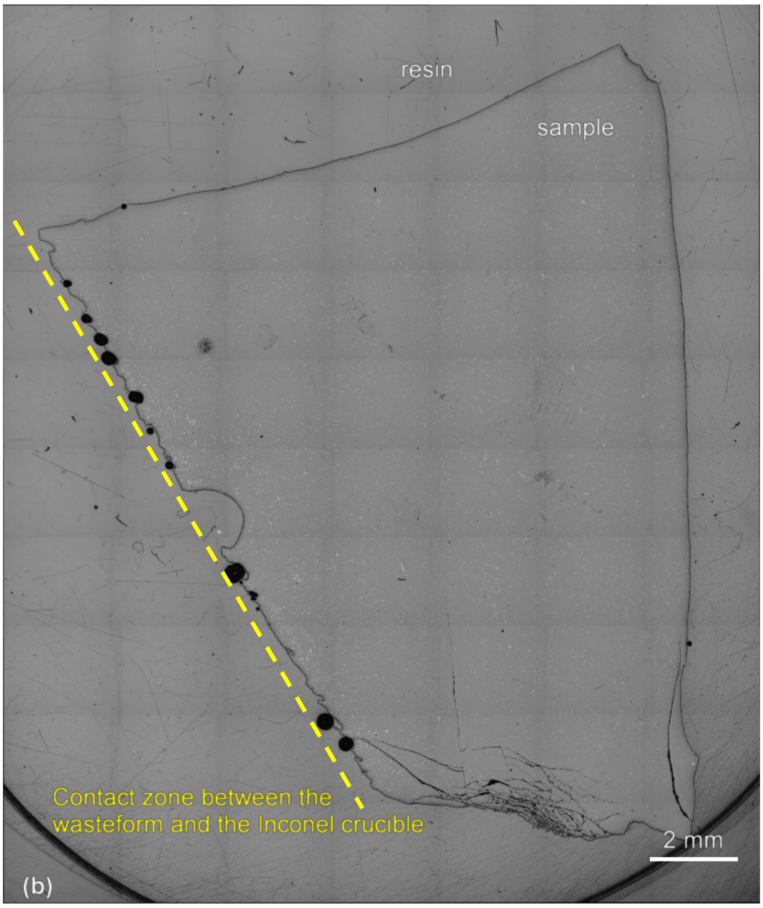

Figure 18: Preliminary observation by optical microscopy of the samples taken from (a) the center of the INCAN-BST wasteform and (b) from a contact zone between the wasteform and the Inconel crucible. Light gray crystals

embedded in a vitreous matrix are discernible.

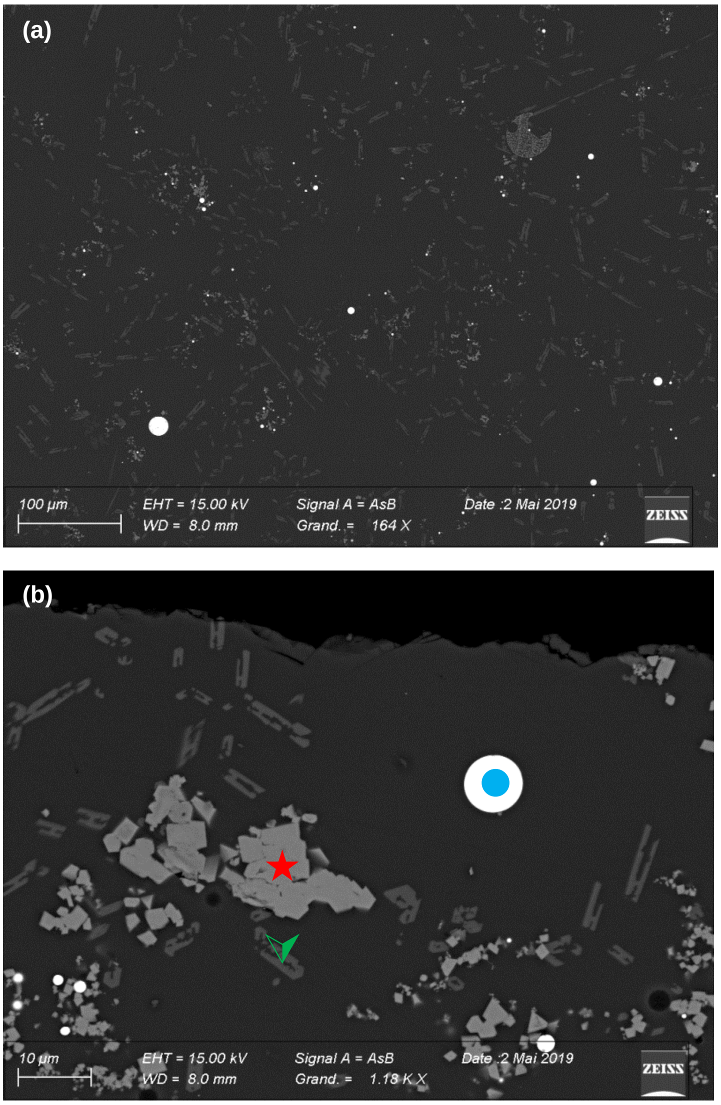

Figure 19: SEM observation of the sample taken from the center of the INCAN-BST wasteform.

	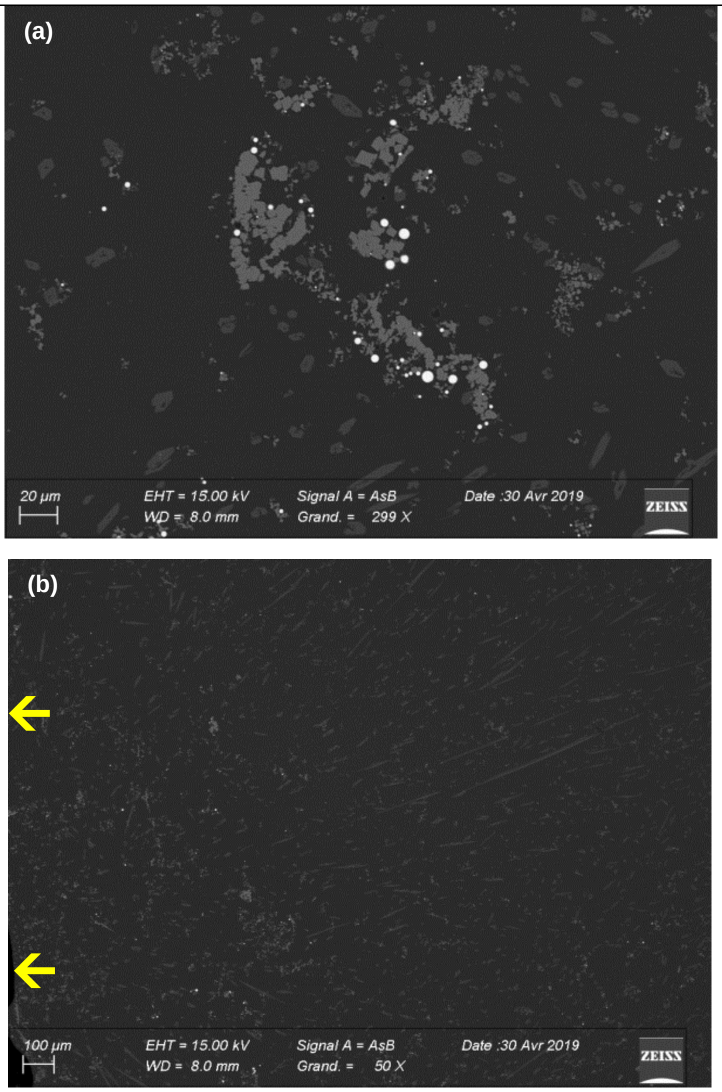 *Figure 20: SEM observation of samples taken from a contact zone between the INCAN-BST wasteform and the Inconel crucible. The yellow arrows in figure b indicate the location of the wasteform/crucible interface*
Free liquid or gas:	Absence
Crystalline composition:	The XRD pattern (Figure 21) acquired between 10 and 90° (2θ) shows the crystallizations of hydroxyapatites $Ca_5(PO_4)_3(OH)$ (ICDD card 00-034-0010), zincochromites $ZnCr_2O_4$ potentially incorporating Al (01-084-7094, $ZnCr_{1.6}Al_{0.4}O_4$), and bismuth (04-006-7762) or bismuth-antimony alloys (04-007-5316, $Bi_{0.97}Sb_{0.03}$). These identifications are consistent with the analyzes performed by SEM/EDS.

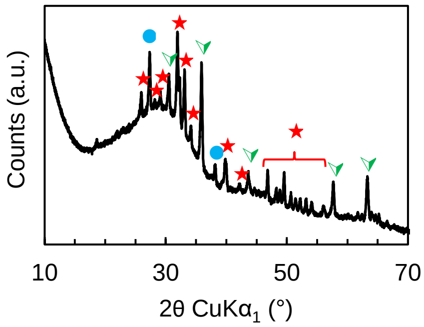

Figure 21: XRD pattern of the bench scale wasteform showing characteriztic peaks of hydroxyapatites (★), zincochromites (▽), and bismuth-antimony alloys (●).

Comments and discussion:

The wasteform is a crystallized glass. The vitreous matrix includes three types of crystallization: hydroxyapatites, zincochromites, and bismuth or bismuth-antimony alloys. The crystals are homogeneously distributed in the matrix, although they may be more numerous in a layer of about one millimeter thick in contact with the wall of the Inconel crucible.

Chemical composition

Method(s): ☐ EMP ☐ ICP-OES/MS ☒ XRF ☒ Other: SEM/EDS

Operating conditions: **SEM/EDS:** The SEM described in the section “Microstructure” is coupled with a lithium-doped silicon detector for elemental analysis in energy-dispersive X-ray spectrometry.

Chemical composition:

The chemical composition of the ash was analyzed by XRF (Table 7): it is mainly composed of Al, Zn, Ca, Si, Bi, K, Mg, and P; and contains also: Ba, Cl, Cr, Fe, Na, Ni, S, Sb, and Ti. The theoretical chemical composition of the wasteform (Table 7) is calculated with the hypothesis of a complete reaction to produce a homogeneous glass. The calculation is based on the compositions of the glass frit and ash, and the proportions of each in the mixture.

Element	Ash (XRF)	Glass fritt	Wasteform (calc)	Oxide	Wasteform (calc.)
Al	**11.9**	0.0	**6.0**	Al_2O_3	**11.2**
B	0.0	10.0	**5.0**	B_2O_3	**16.2**
Ba	0.7	0.0	0.4	BaO	0.4
Bi	**4.0**	0.0	2.0	Bi_2O_3	2.2
Ca	**9.9**	0.0	**5.0**	CaO	**6.9**
Cl	1.4	0.0	0.7	Cl	0.7
Cr	0.1	0.0	0.1	Cr_2O_3	0.1

Fe	0.5	0.0	0.3	Fe_2O_3	0.4
K	**2.3**	0.0	1.1	K_2O	2.7
Mg	**1.6**	0.0	0.8	MgO	1.3
Na	0.6	23.7	**12.1**	Na_2O	**16.4**
Ni	0.7	0.0	0.3	NiO	0.4
P	**1.6**	0.0	0.8	P_2O_5	1.9
S	0.3	0.0	0.2	SO_3	0.4
Sb	0.2	0.0	0.1	Sb_2O_4	0.1
Si	**7.5**	16.6	**12.0**	SiO_2	**25.7**
Ti	0.5	0.0	0.2	TiO_2	0.4
Zn	**8.1**	0.0	**4.1**	ZnO	**5.1**

Table 7: Compositions of the ash (analyzed by XRF) and INCAN-BST wasteform (calculated), expressed in wt.%.

For each of the two samples presented in Figure 18, the vitreous matrix and the three types of crystallization were analyzed in 12 distinct zones (*i.e.*, 48 EDS analyzes). The measurement uncertainty generally considered for this number of analyzes is 2σ with σ the standard deviation.

For all the phases composing the wasteform, the analyzed compositions of both samples are similar (Table 8 to Table 11). It shows homogeneous compositions of the matrix and crystals in the wasteform.

The vitreous matrix consists mainly of SiO_2, Na_2O, Al_2O_3 and CaO (≈ 70 wt.%) — note that B_2O_3 content cannot be analyzed by EDS. The differences observed between the calculated composition of the wasteform and the analyzed composition of its vitreous part are due to the precipitation of crystals (Table 8).

Oxide	**Wasteform (calc)**	**Figure 18.a**		**Figure 18.b**	
		Mean	**σ**	**Mean**	**σ**
Al_2O_3	**11.2**	**18.2**	0.43	**17.3**	0.44
B_2O_3	**16.2**	n.a.	n.a.	n.a.	n.a.
BaO	0.4	< LD	-	< LD	-
Bi_2O_3	2.2	0.2	0.29	< LD	-
CaO	**6.9**	**5.0**	0.39	**4.9**	0.72
Cl	0.7	0.7	0.04	0.5	0.12
Cr_2O_3	0.1	< LD	-	< LD	-
Fe_2O_3	0.4	0.8	0.15	1.0	0.06
K_2O	2.7	1.9	0.15	1.9	0.09
MgO	1.3	2.6	0.22	2.4	0.10

Na_2O	**16.4**	**18.0**	2.62	**19.0**	0.40
NiO	0.4	< LD	-	< LD	-
P_2O_5	1.9	1.5	0.11	1.4	0.51
SO_3	0.4	0.4	0.21	< LD	-
Sb_2O_4	0.1	< LD	-	< LD	-
SiO_2	**25.7**	**30.5**	0.99	**28.8**	0.53
TiO_2	0.4	1.0	0.11	0.7	0.14
ZnO	**5.1**	3.9	0.21	3.2	0.27

Table 8: Composition of the vitreous part of the INCAN-BST wasteform, analyzed by SEM/EDS and expressed in oxide wt.% (< LD: below the limit of detection).

Hydroxyapatites mobilize a part of the P and Ca (Table 9). The stoichiometry calculated from the EDS analyzes is $Ca_{4.8}P_{2.9}Si_{0.3}\ Na_{0.2}Al_{0.1}Cl_{0.1}$ consistent with the theoretical stoichiometry of hydroxyapatites $Ca_5(PO_4)_3(OH)$.

Element	**Figure 18.a**		**Figure 18.b**	
	Mean	**σ**	**Mean**	**σ**
Al	0.4	0.4	0.2	0.5
Ca	**36.8**	1.5	**33.1**	1.7
Cl	0.5	0.1	0.5	0.1
Na	0.7	0.4	0.6	0.3
P	**16.3**	1.7	**15.8**	1.1
Si	1.5	0.7	1.1	0.8

Table 9: Composition of hydroxyapatites (★), analyzed by SEM/EDS and expressed in wt.%.

Zincochromites mobilize Zn and Cr (Table 10). The stoichiometry calculated from the EDS analyzes is $ZnCr_{2.6}Na_{0.5}Mg_{0.2}Al_{0.1}Fe_{0.1}\ Ni_{0.1}$ consistent with the theoretical stoichiometry of zincochromites $ZnCr_2O_4$.

Element	**Figure 18.a**		**Figure 18.b**	
	Mean	**σ**	**Mean**	**σ**
Al	1.5	1.27	0.9	0.35
Ca	0.1	0.07	0.2	0.05
Cr	**43.3**	3.68	**38.3**	1.28
Fe	1.0	0.27	0.8	0.13

Mg	1.9	0.21	1.8	0.03
Na	< LD	-	3.4	0.05
Ni	0.9	0.23	1.0	0.33
Si	0.2	0.08	0.2	0.05
Ti	0.4	0.18	0.6	0.29
Zn	**22.2**	1.04	**17.6**	0.14

Table 10: Composition of zincochromites (⋎),analyzed by SEM/EDS and expressed in wt.% (< LD: below the limit of detection).

The metal alloy incorporates the majority of the Bi (Table 11). As Sb is not assayed in any of the phases by EDS analysis, the hypothesis that it may be Bi-Sn alloys containing a large majority of Bi is not ruled out.

Element	**Figure 18.a**		**Figure 18.b**	
	Mean	**σ**	**Mean**	**σ**
Bi	95.2	3.35	87.3	2.16
Ni	0.4	0.49	< LD	-
Sn	< LD	-	< LD	-
Zn	0.9	0.25	0.5	0.30

Table 11: Composition of Bi alloys (●), analyzed by SEM/EDS and expressed in wt.% (< LD: below the limit of detection).

Comments and discussion:

The wasteform is mainly composed of a vitreous matrix made of 80 wt.% of SiO_2, Na_2O, B_2O_3, Al_2O_3, and CaO (note that the B_2O_3 content was obtain by calculation). Crystals of hydroxyapatite, zincochromite and Bi are embedded in the matrix. The crystallization of these phases leads to a relative decrease in the content of the glassy matrix in Bi, Ca, Cr, P and Zn.

Chemical durability

Method(s):

☒ As described in MS12 Report (p. 12-13), adapted from ASTM C1285

☐ As described in MS12 Report (p. 14), adapted from ASTM C1220

☐ Other:

Clarifications:	Solution samples, taken at regular intervals, are filtered with a cutoff of 0.45 µm, acidified with ultrapure grade HNO_3 and analyzed by ICP-OES (Thermo Scientific iCAP^{TM} 6000 Series). The concentrations are used to calculate normalized mass losses NL_i: $\mathrm{NL}_i = C_i/(x_i \times S/V)$ with C_i the concentration of the element i, x_i the mass percentage of i in the wasteform, S/V the specific-surface-area-to-solution-volume ratio. The alteration rate, $r = \mathrm{d}NL_i/\mathrm{d}t$, is calculated by linear regression. Note that B is known to be an alteration tracer, that means that it is not retained in alteration products while released from the glass.
Results and discussion:	Figure 22.a shows the normalized mass losses in Al, B, Na, and Si over time. Only elements that are mainly integrated into the vitreous matrix are considered. Thus, the mass fractions (x_i) considered to normalize the mass losses are those resulting from SEM/EDS analyzes for Al, Na, and Si in the vitreous matrix (Table 8) and from calculation for B. The dissolution rates of the crystalline phases are therefore not considered. This choice is justified because when a vitreous matrix includes durable crystals — such as apatites or spinels — the wasteform dissolution is controlled by that of the vitreous phase [Nicoleau *et al*., 2015, Nicoleau *et al*., 2016]. The congruence of the boron and sodium releases - tracers of the dissolution - gives confidence in the corresponding x_i values used for the normalization of the alteration rates. During the first day of leaching, the alteration rate of the BST vitreous part of the wasteform is ≥ 2.4 g·m^{-2}·d^{-1}. At three days, it is ≈ 1.5 g·m^{-2}·d^{-1}. The alteration rate is therefore decreasing from the first points. The dissolution of the vitreous matrix quickly becomes non-congruent: Si and Al are retained at about 30-40 % after one month. Such a retention rate for Si remains quite low: the alteration layer is still depleted in silicon and the hydrolysis regime remains important. The high dissolution rate at the first instants rapidly leads to a pH value of about 8.2 at 90°C, which seems a stabilizing value. The leaching test is duplicated (Figure 22.b). The tests are quite repeatable and the trends similar. The Na concentrations are slightly higher in one of the two tests, which leads to the difference observed in the Si release. Indeed, a slightly higher pH leads to a slightly higher hydrolysis rate in test #2. The reaction progress is therefore a little more important in test #2, the alteration rate drops faster and the retention of Si is higher.

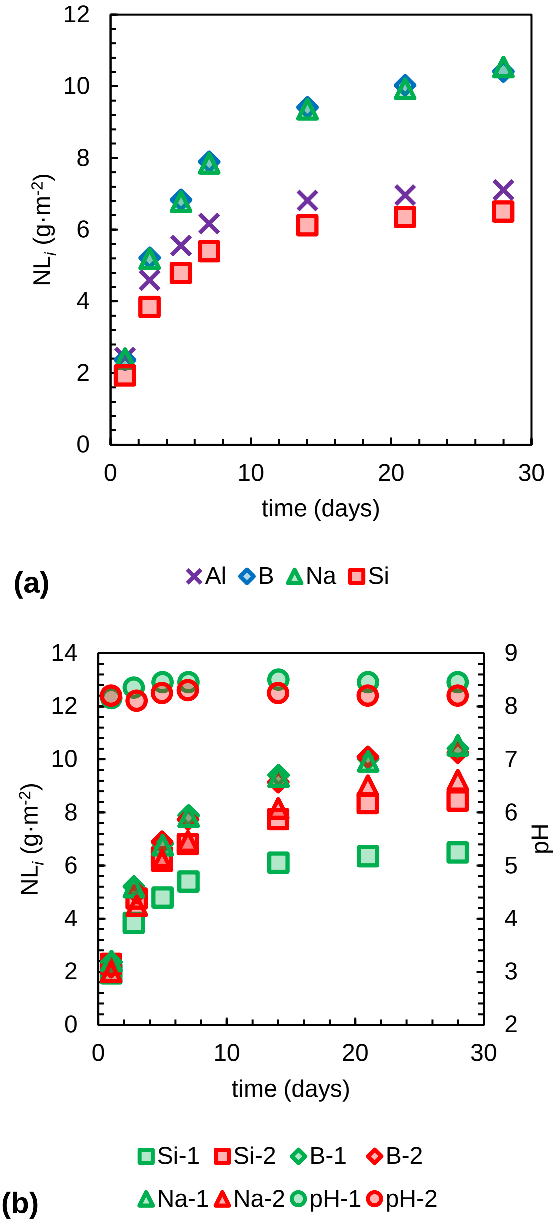

Figure 22: Evolution (a) of NL as a function of time at 90°C, S/V = 10 m^{-1} without stirring and (b) of pH and NL$_{B, Na, Si}$ during duplicate leaching tests of INCAN-BST sample.

The comparison of the results obtained with the INCAN-BST and ISG samples (Figure 23) shows similar and “classical” trends in these experimental conditions (90°C and low *S/V* ratio).

- Because of its composition, INCAN-BST vitreous matrix has a higher rate of hydrolysis. Indeed, it contains large fractions of Na_2O and B_2O_3, which are unfavorable to the glass durability. Therefore, in the early stages of dissolution, the evolutions of the concentrations in solution are faster for INCAN-BST wasteform. This conclusion is also valid for the pH.

- The growth of the alteration layer is faster for the INCAN-BST sample. Thus, its alteration rate drops faster. Between 14 and 28 days, the alteration rate of the INCAN-BST vitreous matrix (0.07 $g \cdot m^{-2} \cdot d^{-1}$) is almost 1.5 time lower than the one of the ISG (0.10 $g \cdot m^{-2} \cdot d^{-1}$), while the hydrolysis rate of the BST vitreous phase after 1 day is greater. This result is well known for simple glasses [Jégou, 1998; Gin et al., 2012]: the glasses that are hydrolyzed the fastest are also those who have the earliest rate drops.
- The ISG stays longer in a regime close to the initial rate at this low *S/V* ratio.

If the hydrolysis rate of INCAN-BST wasteform is greater than that of ISG, the data trends tend to show that, in the longer term, an alteration layer will form causing a decrease of the alteration rate similar to the one observed for the ISG.

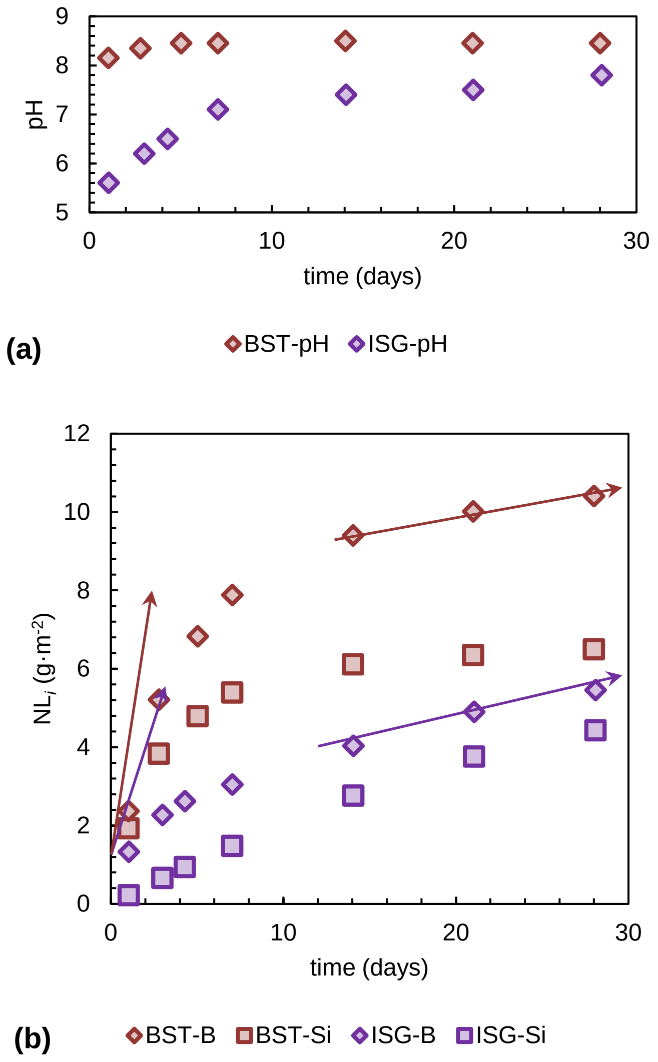

Figure 23: Compared evolutions of (a) pH and (b) NL of Si and B during the leaching of ISG and INCAN-BST samples. The

arrows are a guide for the eyes to estimate the alteration rates of the matrices.

Other tests and characterizations

Specific surface area measurement

The specific surface area of the glass powder is measured by krypton adsorption on the surface of the sample (Micromeritics ASAP 2020). The samples were degassed at 200°C under vacuum of 0.13 Pa minimum for 24 hours. The quantity of gas required to form a monoatomic layer on the surface of the sample is estimated by the Brunauer–Emmett–Teller theory.

The specific surface of the INCAN-BST powder (125-250 µm) is **259 $cm^2 \cdot g^{-1}$**. This value gives a classical shape factor of ≈ 2.1 with respect to the geometric surface area of the grains assimilated to spheres.

Comparison between materials from BST and FST

In the time allocated before the delivery of this report, the material resulting from the FST test was characterized by SEM associated with non-quantitative EDS analyzes and XRD. The results of these analyzes are compared with those from the material resulting from the BST previously described.

The can resulting from the FST test was cored (Figure 24) and a sample from the coring underwent the above mentioned analyzes under the same conditions as those described in the “Microstructure” section.

Figure 24: Coring of the wasteform from the FST.

The SEM/EDS (Figure 25) and XRD (Figure 27) analyzes show the same phases — morphology, size, and composition — as those identified during the analysis of the material resulting from the BST: hydroxyapatites, zincochromites, and Bi-alloys embedded in a vitreous phase mainly composed of SiO_2, Na_2O, B_2O_3, Al_2O_3, and CaO.

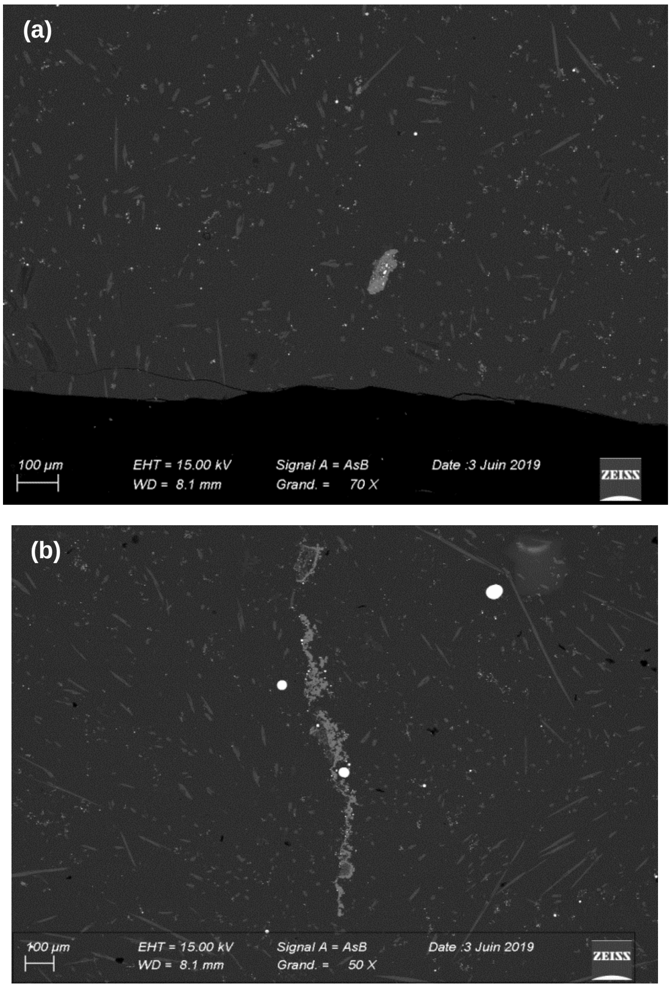

Figure 25: SEM observation of samples taken from the FST.

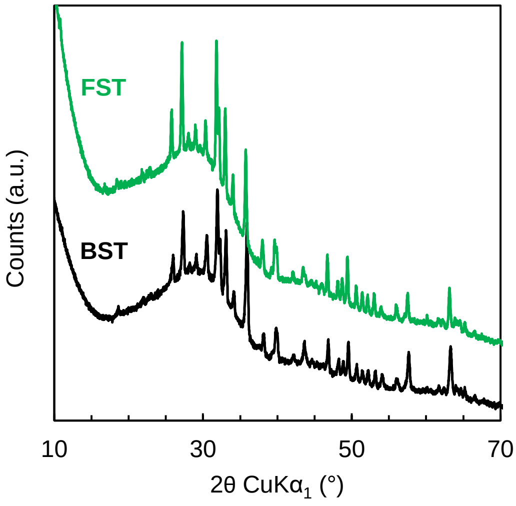

Figure 26: Compared XRD patterns of the INCAN-BST (black) and FST (green) wasteforms.

Conclusions and Outlooks

The INCAN-BST wasteform is produced by the vitrification of ash from the incineration of technological waste (cotton, plastics...) The wasteform consists in a crystallized glass mainly composed of SiO_2, Na_2O, B_2O_3, Al_2O_3, and CaO. The term “crystallized glass” refers to a vitreous matrix including crystals of hydroxyapatite, zincochromite and bismuth alloy. The crystals are distributed homogeneously in the characterized sample.

The crystalline phases being durable, the durability of the wasteform is controlled by that of the vitreous matrix. The hydrolysis rate of this vitreous part is relatively high because of its high contents of B_2O_3 and Na_2O. However, the “classical” trends observed suggest that, in the long-term, an alteration layer will form, leading to a decrease in the alteration rate.

It should be noted that the characterizations presented were conducted with the material resulting from the bench scale test (BST). The first comparisons made with the material from the full-scale trial (FST) tend to show that the microstructures of these two materials are very close.

4.3 Sample from JÜV 50/2 (FZJ)

General information

Partner:	FZJ
Sample id:	JÜV 50/2
Contact person:	Natalia Daniels

Origin and macroscopic description

The JÜV 50/2 is a multi-chamber incinerator for mixed radioactive waste. The final product after thermal treatment at the JÜV50/2 multi-chamber incinerator is ash (Figure 27). Five ash samples were randomly taken from the incineration batch, whereas only sample 1 was characterized; remaining four samples could not be characterized using proposed methodology due to the time constraints.

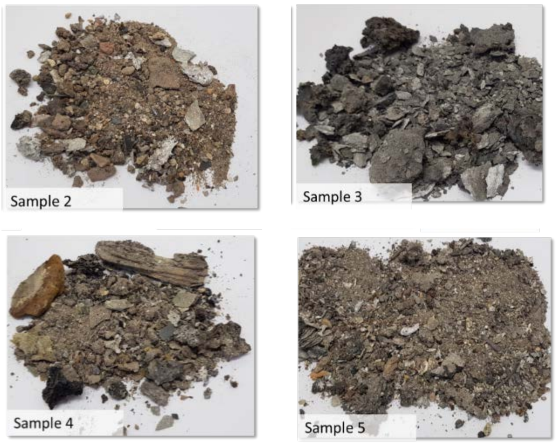

Figure 27: Ash samples – products of incineration of mixed radioactive wastes in the multi-chamber incinerator JÜV50/2 (Copyright JEN).

Due to the strong dependence of the ash product on the raw waste, one of the main goals concerning the ash characterization was to identify phases, select those structures responsible for binding radionuclides and link this information to their behaviour under neutral and cementitious conditions, defined by the partners of the project as relevant conditions for final disposal. For this purpose, the original ash sample (sample 1) was fractionated by sieving. As a result 8 fractions were collected (Figure 28. top). Fraction F1 with R > 1000 μm was not characterized.

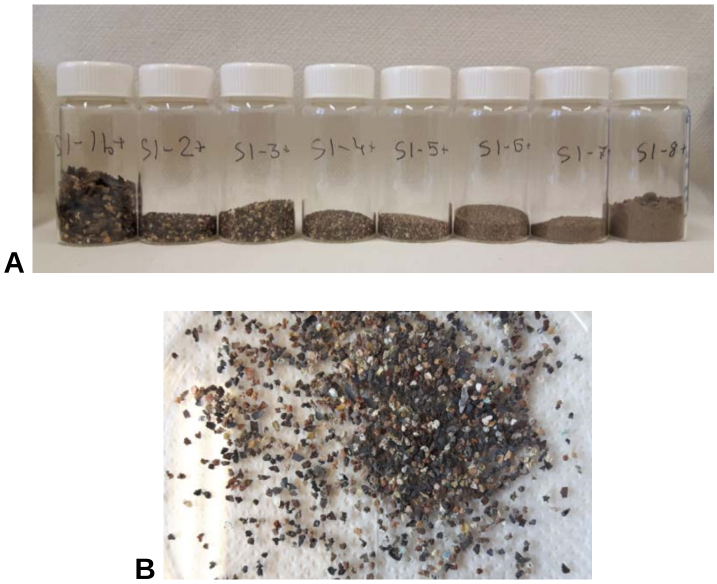

*Figure 28: Fractionated ash sample: **A** – 8 fractions collected for further characterization, **B** – fraction 2 800<R<1000 μm.*

Microstructure

Method(s):	☒ SEM ☒ XRD ☐ Other:
Operating conditions:	Powder X-ray diffraction (XRD, Brucker D4 Endeavor diffractometer) was used to characterize the phase composition of sub-samples (fractioned ash sample). The XRD-patterns were recorded using CuKα radiation (λ = 1.5418 Å) at ambient temperature in the 2Θ-range from 10 to 90° with 0.02° step size and 2 second recording time for every step. Prior to the measurements the ash samples were thoroughly ground and homogenized in an agate mortar. The microstructure and morphology of the ash fractions was investigated by SEM combined with energy dispersive X-Ray spectroscopy (EDX) using a Quanta 200 FEG (FEI Comp.) coupled to an EDX-Modul (EDAX, Inc.).
Homogeneity:	Inhomogeneous
Free liquid or gas:	None
Crystalline composition:	*N.B: Microscopic investigation was carried out on particles, selected with help of autoradiography. The autoradiography results are presented in "Chemical composition" Section.* The phase composition of each fraction F2-F8 was investigated by means of powder XRD. Figure 29.A shows patterns from each fraction. As expected, a complex phase composition was found for the treated waste-product samples. Furthermore, all identified reflexes are found in every fraction, however with different intensity. This indicates a qualitatively rather similar phase assemblage in samples F2-F8. As can be seen from Figure 29.A, reflex intensity at 2Θ ~ 26.6º and ~ 20.85º is especially well pronounced for F4 and F5 respectively, indicating a slight enrichment of corresponding phases in these fractions. Figure 29.A also demonstrates a presence of two broad humps in the XRD patterns at low 2Θ, i.e. ~ 15º and ~ 22º, which indicates that a fraction of solid phases is amorphous. Identification of single reflexes resulted in a few phases, summarized below (the numbers in brackets correspond to the phase number in the database of Match3 software with respective shortenings): 1) Fe_2O_3 Hematite (N:96-101-1241, H) 2) SiO_2 Quartz (N:96-900-0776, Q) 3) Al_2O_3 Corundum (N:96-900-8082, C) 4) CaO Lime (N:96-900-6735, L) 5) $Al_{2.826}Si_{0.174}O_{4.588}$ Mullite (N:96-900-1622, M) 6) $Al_{5.35}Ca_{2.676}Si_{2.65}O_{16}$ Yoshiokaite (N:96-900-1301, Y) 7) KCl Sylvite (N:96-900-3141, S) 8) NaCl Halite (N:96-900-0042, Ha) In Figure 29.B, the identified reflexes are respectively assigned. Mainly these are phases containing Fe, Si, Al, and Ca, which is in a good agreement with an average elemental

composition of ashes (presented in Table 14). The complex phase assemblage did not allow for a quantitative evaluation of the amounts of the different phases.

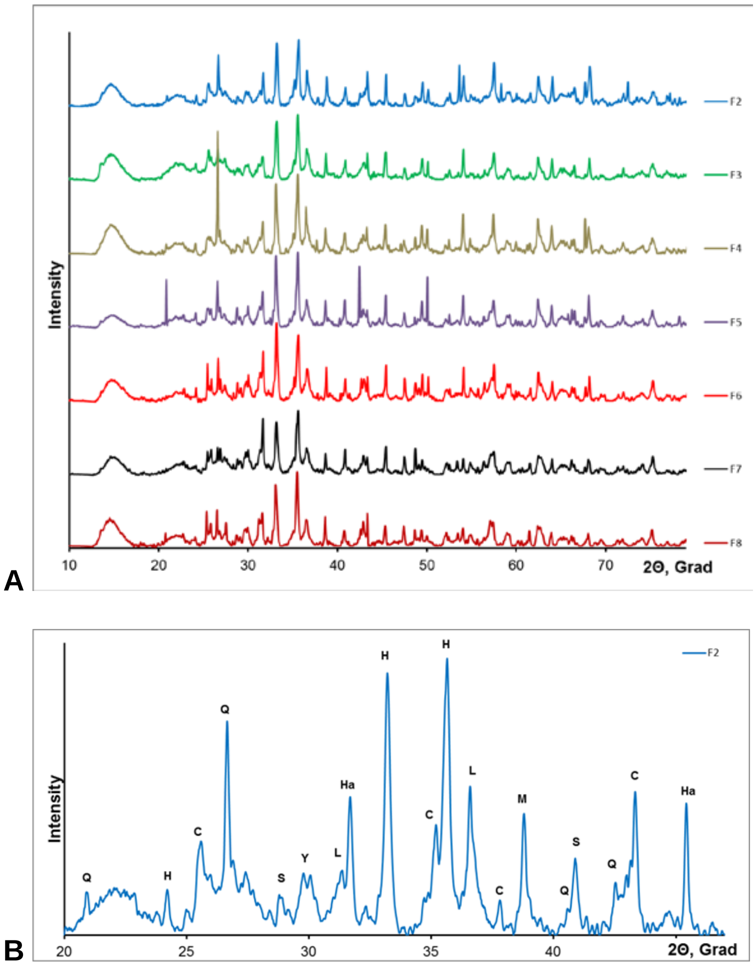

Figure 29: Powder XRD patterns: ***A*** *- for ash fractions F2 – F8,* ***B*** *– detailed evaluation of phase composition of ash fraction F2. Indexes represent shortenings for respective mineral phase names.*

Detailed phase evaluation was also performed for other fractions F3-F8, and is given in the Appendix B. Similar to F2, other fractions also contain Fe oxide (hematite), SiO_2 (Quartz), Al_2O_3 (Corundum) and CaO (Lime), however the relative concentration of phase changes.

The correlative microscopic characterization of selected particles consisted of three steps. In the first step, optical microscopy was carried out in reflected light in order to identify a shape of the particles, whereas the colour can help to identify metallic inclusions, like the white inclusion in the Figure 30.A in a shape of a heart. Secondly, SEM was used to obtain zoomed-in images of areas of interests and to obtain information on the morphology of the particles. Then, EDX analysis was carried out to determine the elemental composition of areas of interest.

An example is shown in Figure 30 – a microscopic analysis of a highly radioactive particle from specimen F2-D (particle from F2 marked in red in Figure 38: F2-D). The particle has big internal pores. According to the EDX analyzes, the particle consists mostly of Si, Ca, Al, and Fe. White inclusions on SEM image (area C) are rich in Cl, Ti, and Ba. The heart-shaped area on SEM image (area D) of the particle represents the inclusion with high content of Al, most probably in metallic form. Presence of Al_2O_3, which was determined by the XRD analysis, cannot be excluded.

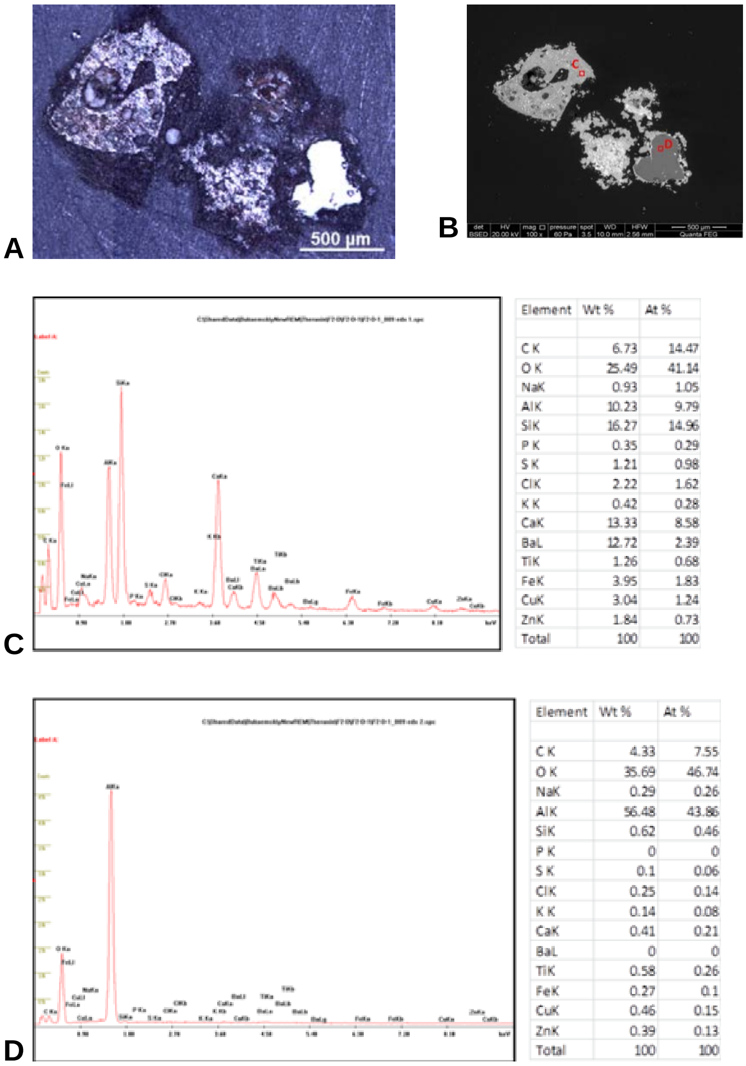

Element	Wt %	At %
C K	6.73	14.47
O K	25.49	41.14
NaK	0.93	1.05
AlK	10.23	9.79
SiK	16.27	14.96
P K	0.35	0.29
S K	1.21	0.98
ClK	2.22	1.62
K K	0.42	0.28
CaK	13.33	8.58
BaL	12.72	2.39
TiK	1.26	0.68
FeK	3.95	1.83
CuK	3.04	1.24
ZnK	1.84	0.73
Total	100	100

Element	Wt %	At %
C K	4.33	7.55
O K	35.69	46.74
NaK	0.29	0.26
AlK	56.48	43.86
SiK	0.62	0.46
P K	0	0
S K	0.1	0.06
ClK	0.25	0.14
K K	0.14	0.08
CaK	0.41	0.21
BaL	0	0
TiK	0.58	0.26
FeK	0.27	0.1
CuK	0.46	0.15
ZnK	0.39	0.13
Total	100	100

Figure 30: Microscopic analysis of a highly radioactive particle from specimen F2-D: ***A*** *– optical microscopy,* ***B*** *– SEM image in BSE mode,* ***C*** *and* ***D*** *– EDX of respective selected areas of the particle.*

Another example is given in Figure 31, which shows a highly radioactive particle from specimen F2-E (particle from F2 marked in red in Figure 38: F2-E). Similar to the particle F2-D, particle F2-E has large pores in the bulk. As indicated in Figure 31.C, the particle is mainly composed of Si, Al, Ca and Fe. This composition agrees well with the results of XRD investigations, where phases like SiO_2, Al_2O_3, Fe_2O_3, CaO and mixed (Si, Al, Ca)-oxide were found.

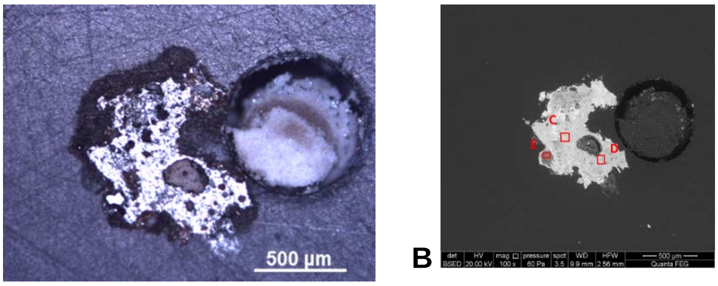

C

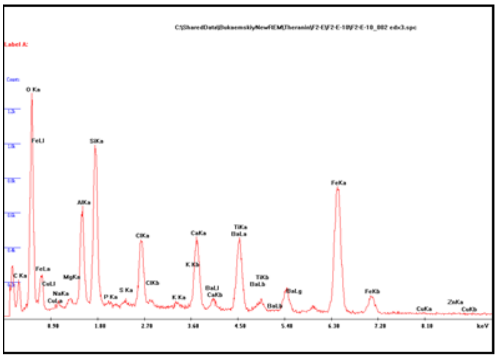

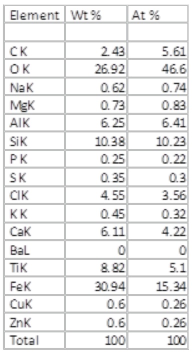

Element	Wt %	At %
C K	2.43	5.61
O K	26.92	46.6
NaK	0.62	0.74
MgK	0.73	0.83
AlK	6.25	6.41
SiK	10.38	10.23
P K	0.25	0.22
S K	0.35	0.3
ClK	4.55	3.56
K K	0.45	0.32
CaK	6.11	4.22
BaL	0	0
TiK	8.82	5.1
FeK	30.94	15.34
CuK	0.6	0.26
ZnK	0.6	0.26
Total	100	100

D

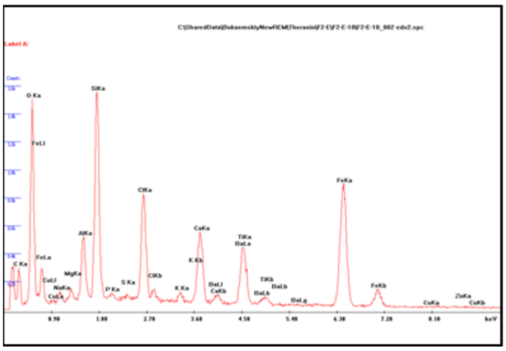

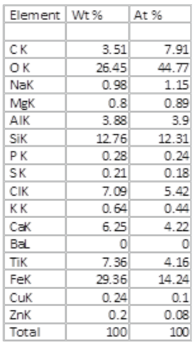

Element	Wt %	At %
C K	3.51	7.91
O K	26.45	44.77
NaK	0.98	1.15
MgK	0.8	0.89
AlK	3.88	3.9
SiK	12.76	12.31
P K	0.28	0.24
S K	0.21	0.18
ClK	7.09	5.42
K K	0.64	0.44
CaK	6.25	4.22
BaL	0	0
TiK	7.36	4.16
FeK	29.36	14.24
CuK	0.24	0.1
ZnK	0.2	0.08
Total	100	100

E

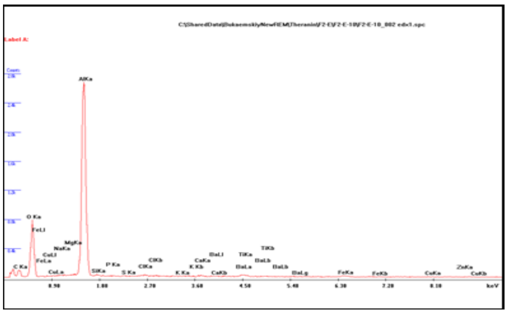

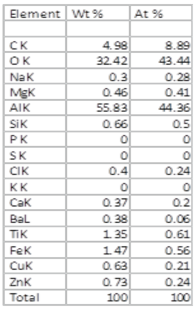

Element	Wt %	At %
C K	4.98	8.89
O K	32.42	43.44
NaK	0.3	0.28
MgK	0.46	0.41
AlK	55.83	44.36
SiK	0.66	0.5
P K	0	0
S K	0	0
ClK	0.4	0.24
K K	0	0
CaK	0.37	0.2
BaL	0.38	0.06
TiK	1.35	0.61
FeK	1.47	0.56
CuK	0.63	0.21
ZnK	0.73	0.24
Total	100	100

Figure 31: Microscopic analysis of a highly radioactive particle from specimen F2-E: ***A*** *– optical microscopy,* ***B*** *– SEM image,* ***C, D, E*** *– EDX of respective selected areas of the particle.*

During systematic examination of a few radionuclide-bearing particles, matrixes composed of oxides Fe, Si and Al were found. It can assume that Fe- and Al-oxides might be responsible for binding of radionuclides. For instance, it was earlier observed that ^{60}Co can be stabilized in solid solutions with Fe(III) oxide and oxyhydroxide [Krupka *et al*., 2002; Li *et al*., 2012; Abdel-Karim *et al*., 2019]. ^{137}Cs may be also associated with oxides phases, however presence of relatively high amount of chlorides (e.g. NaCl, KCl) can also mean that Cs, having rather similar chemical behaviour to Na, can be present as CsCl.

In Figure 32.A and B, SEM images of zoomed in areas of particle F2-E show crystalline white inclusions composed of Ba, Ti and Cl.

It has to be mentioned that Ba- and Ti-enriched inclusions with similar composition were systematically identified in a number of other particles as well, indicating that (Ba,Ti)Cl_x might be a typical phase present in the ashes. The measured Ba/Ti ratio is 3.1 ± 0.1 for the respective white inclusions in Figure 32.A and B, whereas the ratio Cl / (Ba+Ti) is 1.9 ± 0.1 respectively (uncertainties are calculated from EDX measurements made on 7 different particles containing typical Ba- and Ti-enriched inclusions).

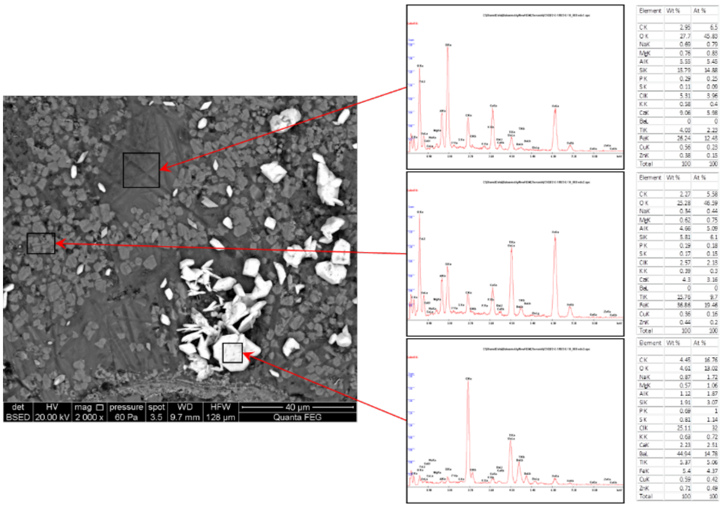

Element	Wt %	At %
C K	2.95	6.5
O K	27.7	45.83
NaK	0.69	0.79
MgK	0.76	0.83
AlK	5.55	5.45
SiK	15.79	14.88
P K	0.29	0.25
S K	0.11	0.09
ClK	5.31	3.96
K K	0.58	0.4
CaK	9.06	5.98
BaL	0	0
TiK	4.08	2.23
FeK	26.24	12.48
CuK	0.56	0.23
ZnK	0.38	0.15
Total	100	100

Element	Wt %	At %
C K	2.27	5.58
O K	25.28	46.59
NaK	0.34	0.44
MgK	0.62	0.75
AlK	4.66	5.09
SiK	5.81	6.1
P K	0.19	0.18
S K	0.17	0.15
ClK	2.57	2.13
K K	0.39	0.3
CaK	4.3	3.16
BaL	0	0
TiK	15.76	9.7
FeK	36.86	19.46
CuK	0.36	0.16
ZnK	0.44	0.2
Total	100	100

Element	Wt %	At %
C K	4.45	16.76
O K	4.61	13.02
NaK	0.87	1.72
MgK	0.57	1.06
AlK	1.12	1.87
SiK	1.91	3.07
P K	0.69	1
S K	0.81	1.14
ClK	25.11	32
K K	0.63	0.72
CaK	2.23	2.51
BaL	44.94	14.78
TiK	5.37	5.06
FeK	5.4	4.37
CuK	0.59	0.42
ZnK	0.71	0.49
Total	100	100

A

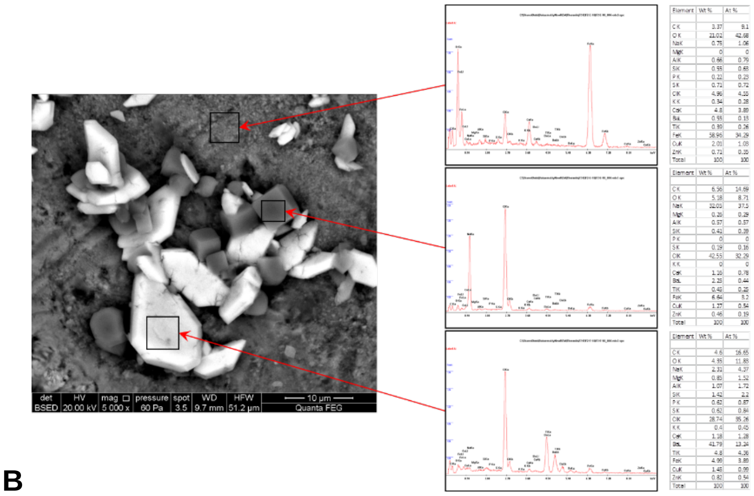

Element	Wt %	At %
C K	3.37	9.1
O K	21.02	42.68
NaK	0.75	1.06
MgK	0	0
AlK	0.66	0.79
SiK	0.59	0.68
P K	0.22	0.23
S K	0.71	0.72
ClK	4.96	4.55
K K	0.34	0.28
CaK	4.8	3.89
BaL	0.59	0.13
TiK	0.39	0.26
FeK	58.96	34.29
CuK	2.01	1.03
ZnK	0.71	0.35
Total	100	100

Element	Wt %	At %
C K	6.56	14.69
O K	5.18	8.71
NaK	32.03	37.5
MgK	0.26	0.29
AlK	0.57	0.57
SiK	0.41	0.39
P K	0	0
S K	0.19	0.16
ClK	42.55	32.29
K K	0	0
CaK	1.16	0.78
BaL	2.25	0.44
TiK	0.43	0.25
FeK	6.64	3.2
CuK	1.27	0.54
ZnK	0.46	0.19
Total	100	100

Element	Wt %	At %
C K	4.6	16.65
O K	4.35	11.88
NaK	2.31	4.37
MgK	0.85	1.52
AlK	1.07	1.72
SiK	1.42	2.2
P K	0.62	0.87
S K	0.62	0.84
ClK	28.74	35.26
K K	0.4	0.45
CaK	1.18	1.28
BaL	41.79	13.24
TiK	4.8	4.36
FeK	4.99	3.89
CuK	1.43	0.99
ZnK	0.82	0.54
Total	100	100

Figure 32: SEM/EDX analysis of a highly radioactive particle of F2-E specimen: ***A*** *and* ***B*** *–two zoomed in representative areas.*

Well-shaped crystals is an indication that the local temperature during the waste treatment exceeded the respective melting point, regardless of whether this compound was initially present in the raw wastes of formed during the incineration. At the same time, the treatment temperature should not exceed the boiling point, so the substance is not removed during treatment by evaporation.

Another scenario of crystallization is possible in the pores when the substance sublimates in the closed pores, if treatment temperature exceeds the boiling point.

Table 12 summarizes properties of some selected chlorides that meet this requirement, $BaCl_2$ and $TiCl_2$ included. The other two chlorides of Ti, i.e. $TiCl_3$ (T_{melt} = 440°C with decomposition) and $TiCl_4$ (T_{boil} = 136.4°C), are either unstable or evaporate at much lower temperature. Stabilization of reduced form of titanium Ti(II) in the mixed $(Ba,Ti)Cl_x$ form can be, however, questionable, as oxides like Fe_2O_3 are determined in the ash fractions in the macro-concentrations by powder XRD. This means that redox conditions during treatment were rather oxidizing, therefore stabilization of titan in form of TiO_2 is more probable. In this case TiO_2 must be present before incineration, or can be formed from less stable titanium compounds. In favor of this suggestion is relatively high oxygen content measured in Ba- and Ti-enriched phase. Nonetheless, neither titanium chlorides, nor TiO_2 were detected during XRD examination, pointing out that Ti phase, is only a minor phase in the ash sample. It has to be mentioned that measurements of oxygen local concentration using EDX is usually concerned with a high uncertainty, therefore direct stoichiometric correlation of Ti and O content is not possible. However, EDX measurements demonstrate that Ba- and Ti-enriched phase correlates with low Fe amount, i.e. stabilization of reduced Ti(II) in form of (Ba,Ti)Cl_x can be also possible.

Compound	$T_{melting}$, °C	$T_{boiling}$, °C
NaCl	801	1465
KCl	776	1407
$CaCl_2$	772	1935
$TiCl_2$	1035	1500
$TiCl_3$	440	-
$TiCl_4$	-	136.4
TiO_2	1855	2900
$BaCl_2$	926	1560
CsCl	646	1382
$CoCl_2$	735	1049

Table 12: Melting and boiling points of selected chlorides [Wagman et al., 1982].

Supplementary information on microscopic and microanalytical investigation of ash particles by means of SEM/EDX are presented in Appendix C.

Comments and discussion:

Chemical composition

Method(s): ☐ EMP ☒ ICP-OES/MS ☐ XRF ☒ Other: TOC-analysis and radiological analysis

Operating conditions:

For characterization of their chemical composition ten waste-product samples were taken from incinerated charges between 2006 and 2010. The samples were dissolved by acid digestion and analyzed using established analytical methods (e.g. ICP-OES and IC).

The average radionuclide content of the ashes is the result of characterization of ash obtained in the period from 2004 to 2017.

For characterization of radionuclide concentration in each ash fraction, several techniques have been performed: Table 13 also indicates typical detection limit (DL) for these radionuclides regarding the methodology to be used for quantification.

Radionuclide	Method	Detection limit, Bq/g*
^{60}Co	γ-spectrometry	0.5
^{137}Cs		0.6
^{154}Eu		0.5
^{14}C	Digestion/LSC	0.9
^{241}Am	γ-spectrometry	0.4 $6.8 \cdot 10^{-2}$

	Digestion/α-spectrometry	
^{238}U	Digestion/α-spectrometry	$4.6 \cdot 10^{-2}$
^{238}Pu		$4.6 \cdot 10^{-2}$
$^{239/240}Pu$		$4.6 \cdot 10^{-2}$
$^{243/240}Cm$		$6.5 \cdot 10^{-2}$

Table 13: Radionuclides which can be potentially present in the ash fractions with DL (for 1 g of ash sample) of respective measurement technique.

For γ-spectrometry, a semi-conductor coaxial HPGe detector (Type PGC 2018) with beryllium window (Model Gr3018 by Canberra) was used (voltage +2500 V). Samples of the respective ash fractions were placed directly on the detector, and spectra were acquired for 24 h. The evaluation of the spectra was performed using the GammaVision software (ORTEC). For data evaluation an efficiency calibration was carried out using an ^{152}Eu standard.

For autoradiography, parts of the subsamples F2 - F8 were embedded in an epoxy resin made of 30 parts of Araldite 2020/A and 10 parts of 2020/B (purchased from Huntsman International LLC), as demonstrated in Figure 33. Three steps of polishing were applied after embedding ash fractions. For that abrasive sand-paper with 35.0 μm (P400), 21.8 μm (P800) and 15.3 μm (P1200) grain-sized (purchased from Buehler, Austria) was used. Given that smaller particles are easier to remove during polishing, some amount of material in the finer fractions (e.g. F7 and F8) was lost.

Autoradiographic investigations were carried out by placing the ash fractions embedded in the resin on Fuji RX photo-plates sensitive to radiation. After an exposure time of 4 days (experimentally verified to be an optimum exposure time) the photo-plates were scanned by a laser scanner HD-CR 35 from Fa. Raytest (Germany) using a red laser (wavelength 635 nm) and 12.5 μm scanning steps (Raytest, Germany). The image data analysis program AIDA (Raytest, Germany) was used for data evaluation.

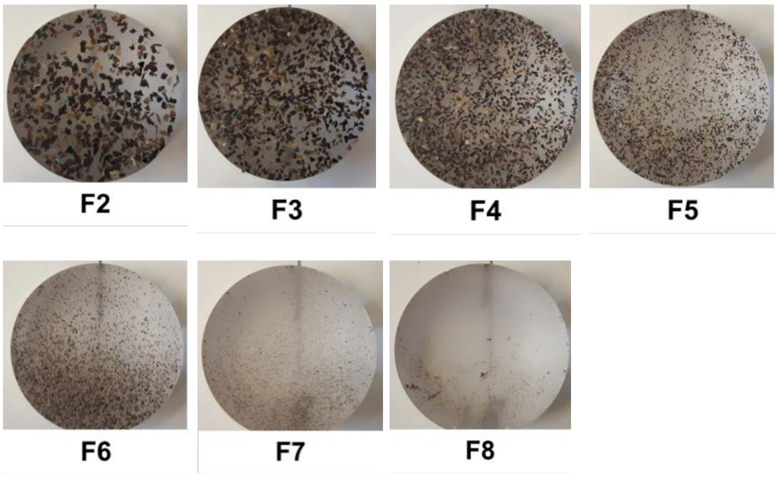
F2 F3 F4 F5

F6 F7 F8

Figure 33: Ash fractionated embedded in the araldite resin.

Chemical composition:

The average elemental composition is summarized in the Table 14.

Element	Conc., mg/g, <average>	Element	Conc., mg/g, <average>
Si	106 ± 11	Pb	6.18 ± 1.06
Al	119 ± 7	Mn	0.94 ± 0.08
Ca	80.7 ± 7.0	Cr	2.50 ± 0.52
Mg	8.01 ± 0.58	B	3.47 ± 0.73
K	13.8 ± 1.5	Ni	1.98 ± 0.49
Na	16.6 ± 3.5	Sr	0.37 ± 0.04
Fe	81.8 ± 8.8	Co	0.17 ± 0.03
Cu	9.64 ± 2.15	Bi	0.05 ± 0.3
Zn	8.85 ± 1.08	Hg	$(1.29 \pm 0.56)\cdot 10^{-4}$

Table 14: Average elemental composition of thermally treated waste product (ashes) of the incinerator JÜV50/2.

The results show that Si and Al are the most abundant components in the ashes, indicating Al_2O_3 and SiO_2 as plausible dominating phases. Along with that, high content of Ca was measured in the phases, and can be either present as single CaO phase or stabilized in form of mixed (Al, Si, Ca)-phases. A relatively high concentration of Fe was measured as well. This might be due to the presence of some metallic parts originating from the raw wastes arising from decommissioning of nuclear facilities. Further elements, like Cu, Pb, Cr und Ni were measured in minor concentrations.

These results on elemental composition in combination with PXRD data were used in the analysis of the phase composition.

It was additionally demonstrated (using TOC-Analysis) that the remaining content of organic substances is relatively low.

The average radionuclide content of the ashes is listed in Table 15. Besides typical radionuclides present in LILW (e.g. ^{137}Cs, ^{60}Co, etc.), a number of actinide isotopes, like ^{238}Pu and ^{241}Am, were identified.

RN	Conc., Bq/g, <average>	RN	Conc., Bq/g, <average>
^{238}U	0.035	^{54}Mn	0.16
^{238}Pu	0.0465	^{60}Co	6.22
$^{239/240}$Pu	0.03	^{137}Cs	2.16
^{241}Am	39.1	^{154}Eu	0.14
$^{243/244}$Cm	0.02	^{14}C	0.61

Table 15: Typical average radionuclide content in thermally treated waste products (ashes) of the incinerator JÜV50/2.

For characterization of radionuclide concentration in each ash fraction, γ-spectrometry was used. It indicated that reliably measured can be only activity of ^{60}Co and ^{137}Cs, whereas ^{154}Eu and ^{241}Am, indicated to be present in the ashes by JEN's analyzes, are below the DL of used analytical technique.

As shown in Figure 34 specific activity of ^{60}Co increases with decreasing of ash particle size. The highest activity of 5.74 ± 0.23 Bq/g was determined in fraction F8, while the lowest activity of 2.70 ± 0.39 Bq/g was measured for fraction F2, respectively (uncertainty is defined from the γ-spectrometric measurements). No distinct correlation of the specific activity of ^{137}Cs with particle size was found (Figure 34). For that reason, only these radionuclides ^{60}Co and ^{137}Cs remained in the focus of the leaching tests, whereas their specific activity, determined in the solid phases, was used to evaluate the release fraction.

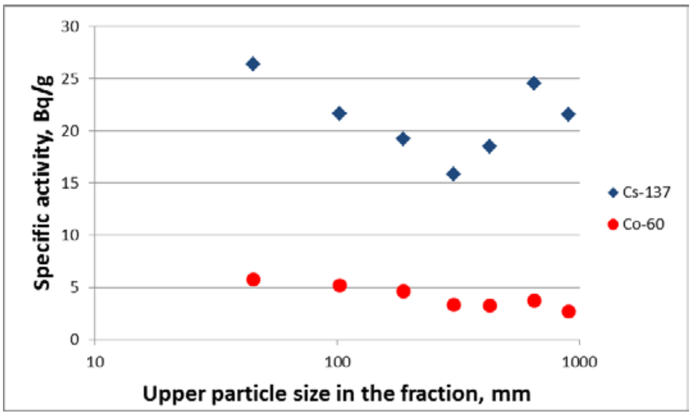

Figure 34: Results of characterization of ash sub-samples F2 – F8: evolution of ^{137}Cs and ^{60}Co specific activity, in Bq/g.

Characterization of local distribution of radionuclides in the ash fractions and linking of radionuclides to the specific phases was carried out by autoradiography in a few steps.

In the first step, the proper measurement conditions were evaluated by varying the exposure time. Figure 35 shows the results of the autoradiography of the different grain size fractions. Almost in all fractions the radioactivity was detected to be unevenly distributed. Well measurable signals were obtained for F2 – F5; F6 showed only a weak response, and F7 and F8 did not reveal any signals distinguishable from the background. The reason might be a lack of material in the polymeric matrices, which remains after the polishing of the surface: small particles are easier to lose during polishing than bigger ones. The response on the autoradiography depends on a few factors: specific activity, energy of emitted particles, and geometrical position of the radioactive particle towards the photo-plate. As no energy calibration for the autoradiography was carried out in our study and equal distance towards the photo plate cannot be assured, these images cannot be used for quantitative determination of the activity in the respective fractions.

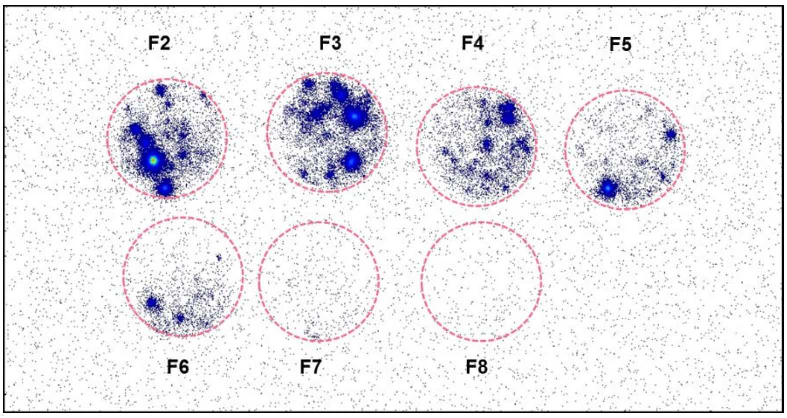

Figure 35: Autoradiographic images of ash fractions embedded in araldite resin: exposure time 4 days.

On the second step of the autoradiographic investigation, the aim was to locate the RN-bearing particles and to perform electron microscopy on selected locations, in order to investigate elemental composition of these particles. This information is complementary to the powder XRD results and will help to identify mineral phases carrying radionuclides.

As shown in Figure 36, the further processing of the autoradiographic images revealed a certain difficulty in the identification of radioactive particles, due to limited spatial resolution of the detector. Radiographic responses from the particles embedded in resin appear like clouds. The higher the activity of a particle, the bigger is the cloud and the higher is the contrast. Furthermore, if the distance between the radioactive particles is not large enough, the clouds may overlap. Therefore, it was difficult to link the autoradiographic images to isolated single RN-bearing particles using this approach.

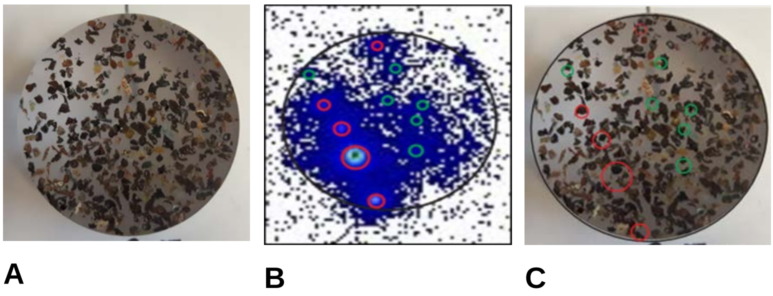

Figure 36: Processing of autoradiographic images of ash fraction F2: ***A*** *– original fraction embedded in araldite resin,* ***B*** *– autoradiographic image with the positions of radioactive*

particles (red – highly radioactive, green – lowly radioactive), ***C*** *–positions of radioactive particles in embedded specimen.*

In order to improve the methodology for the identification of radioactive particles, a second series of embedded specimens was prepared, as shown in Figure 37. Here, a lower density of embedded particles was used, with the particles located at a fixed distance from each other, in order to ease linking the autoradiographic response to a respective particle.

Identification was carried out only for particles from F2, as it was technically easier to isolate and handle bigger particles. However, taking into account results of XRD investigation, where phase composition was shown to vary only slightly among fractions, results of coupled autoradiographic-SEM/EDX investigation might be used as a first estimates (indicative) for other ash fractions. In total, nine specimens (F2-A-…-J) were prepared containing 155 particles. Due to the lower number of particle, the radiographic response appears much more distinct (Figure 37.B), which allows identification of single radioactive particles for further microscopic investigations.

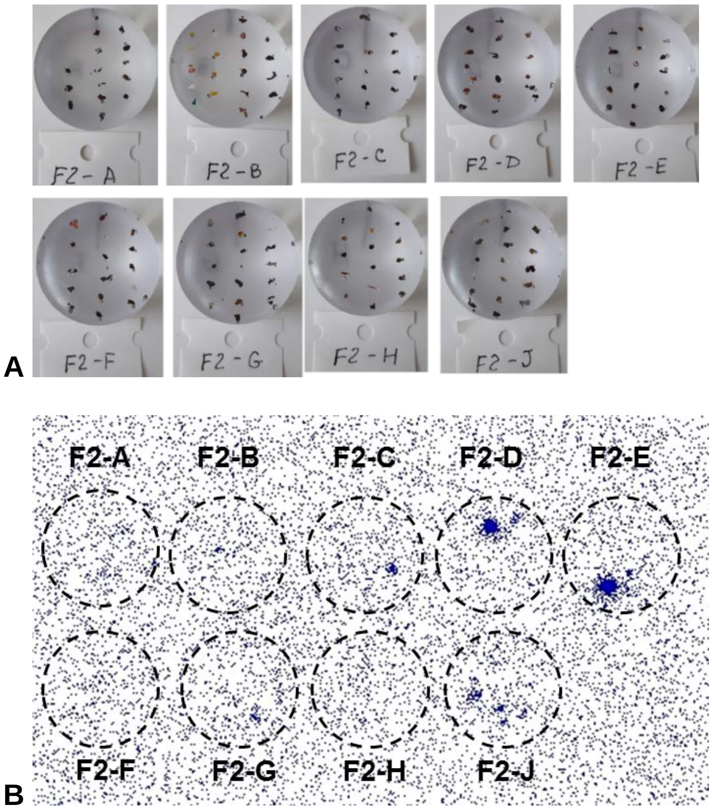

Figure 37: Processing of autoradiographic images of ash fraction F2 using a lower density of embedded particles: ***A*** *– 155 embedded particles of F2,* ***B*** *– autoradiographic image with the identified positions of radionuclide-bearing particles.*

Among 155 particles analyzed in total, 2 highly and 11 weekly radioactive particles were identified. On the third step, the radioactive particles identified in specimens F2-G, F2-D, F2-E and F2-J, as shown in Figure 38, were characterized by SEM/EDX. Along with that 33 inactive particles were analyzed as well.

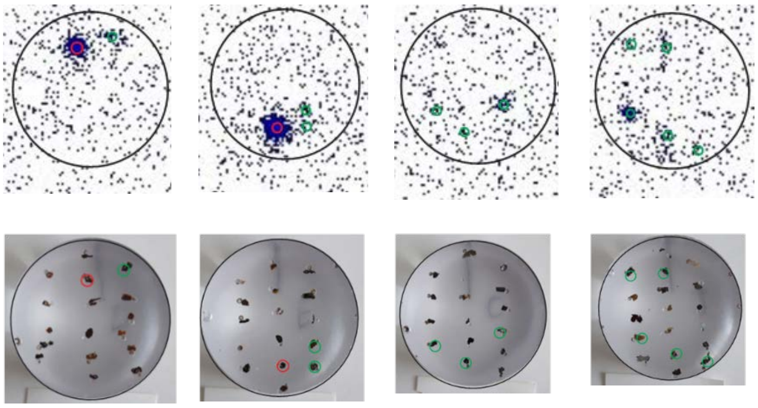

F2-D F2-E F2-G F2-J

Figure 38: Detailed processing of autoradiographic images of ash fraction F2 with lower particles density and localization of radionuclide-bearing particles.

Comments and discussion: .

Chemical durability

Method(s):

☐ As described in MS12 Report (p. 12-13), adapted from ASTM C1285
☐ As described in MS12 Report (p. 14), adapted from ASTM C1220
☒ Other:

Clarifications:

The chemical durability of the ash fractions (F2-F8) in aqueous environments was investigated in batch leaching tests. The methodology of the leaching tests is based on the ASTM C1285-14 product consistency test "Standard test method for determining chemical durability of nuclear, hazardous and mixed waste glasses and multiphase glass ceramics: the product consistency test (PCT)" [ASTM, 2014]. Leaching was carried out in teflon flasks at ambient atmospheric conditions (i.e. air as a gas phase at atmospheric pressure). Ash sub-samples (F-2 – F-8) of known mass (1 g), were leached either in 10 mL of deionized water (DIW) or 0.1 M NaOH solution, simulating cementitious pH conditions. The flasks were sealed and left at constant temperature, i.e. room temperature (RT) or 90°C (thermostated in an oven). In accordance with the ASTM procedure, the solutions were sampled after 1, 3, 7, 14, 28 days and right after the termination of the experiments and the separation of residual solids for post-leaching examinations (after 70-80 days). After sampling, the solution removed was replaced with an identical volume of the respective fresh solution (DIW or 0.1 M NaOH) in order to keep the solid to solution ratio within the whole leaching test constant. Prior to sample analysis, an aliquot of the sampled solution was filtered through a 0.45 μm membrane filter. The radionuclide concentrations in aliquots of the leachates were determined using γ-spectrometry (acquisition time 86400 s).

In parallel to the experiments carried out with ash fraction, leaching behaviour of standard glass ISG powder (MO-SCI Corp., GL 1634, L12012601) with 125-250 μm particle size was investigated [Gin *et al.*,

	2013]. Specific surface area of applied ISG is 345 cm^2/g. Leaching was carried out using (0.0725 ± 0.0069) g of ISG powder and (200 ± 0.74) mL of leaching solution, resulting in the S/V ratio of 12.55 m^{-1}. As in case of radioactive ash fractions, deionized water (DIW) and 0.1 M NaOH solution were used an aqueous media. Besides, two temperature regimes, i.e. RT and 90°C were applied. Regular sampling of the liquid phase was performed in order to measure evolution of the concentration of selected elements in the solution: Ca, Al, Si, and Zr. Concentration of these elements in the leachate were measured using ICP-OES. The concentration of these elements was used to calculate the normalized mass loss NLi as following: $NL_i=C_i/(x_i*S/V)$ Where C_i – the concentration of respective element in the solution, xi the mass percentage of I element in the glass (x_{Al} = 0.03, x_{Ca} = 0.03, x_{Si} = 0.273), S/V is a specific surface area to volume ratio (in our case equal to 0.1255 cm^{-1} or 12.55 m^{-1}). The alteration rate R was calculated as following: $R=\Delta NLi/\Delta t$ At the end of the leaching tests, the solid phase was separated from the aqueous solution, dried at 90°C and used for analyzes of remaining radionuclide concentration using γ-spectrometry. Grains with bound radionuclides were identified using autoradiography. Identical to pre-leaching characterization, autoradiographic measurements ran for 4 days, in order to enable comparison of the results before and after leaching tests. Evolution of phase composition and morphology was investigated using XRD and SEM.
Results and discussion:	Leaching behaviour of all ash fractions was investigated on above described conditions. As example, the results on ^{137}Cs release from fraction F2 are shown in Figure 39. A comparison of the release fractions at RT and 90°C in DIW demonstrates that equilibrium is reached within 3 - 7 days of monitoring. All release curves indicate instant release of a major content of ^{137}Cs (60 - 80 %) on the first stage of the leaching test. Figure 39.A and B show that elevated temperature has only a slight effect on the release of ^{137}Cs from ash fraction F2, which is more distinct in DIW than in NaOH solution. Differences of ^{137}Cs release kinetics in DIW and 0.1 M NaOH at RT (Figure 39.C) are not significant, which is in agreement with a suggestion that the majority of ^{137}Cs can be present in the chloride form. The only difference between equilibrium released fractions was observed at 90°C (Figure 39.D), where ^{137}Cs soluble fraction was measured to be higher in DIW, than in NaOH. This effect may be concerned with adsorption of ^{137}Cs$^+$ on oxide matrices of ash particles at high pH range. The equilibrium released fraction of ^{137}Cs from ash fraction F2 are summarized in the Table 16.

	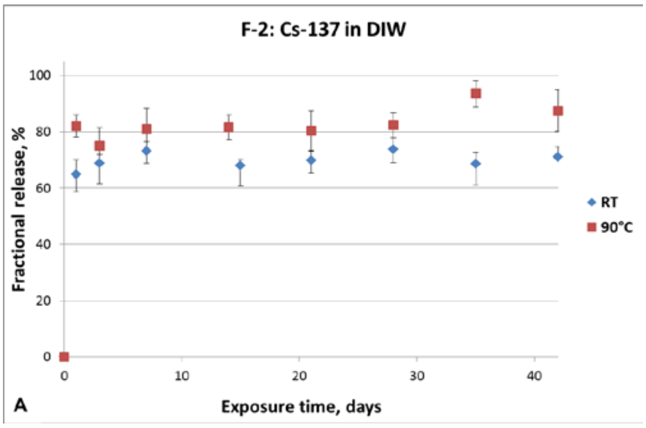 F-2: Cs-137 in DIW Fractional release, % 0 20 40 60 80 100 0 10 20 30 40 Exposure time, days A RT 90°C 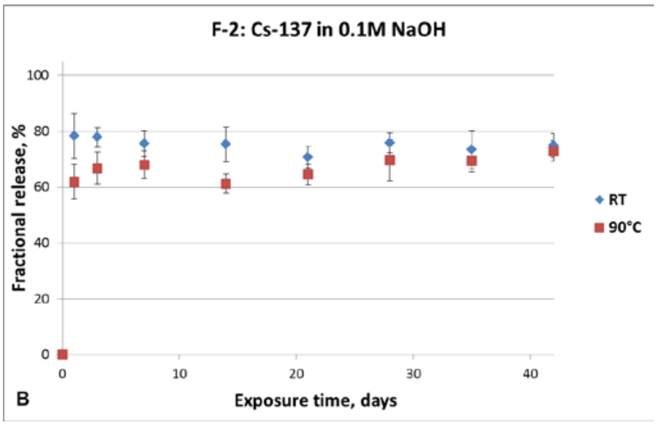 F-2: Cs-137 in 0.1M NaOH Fractional release, % 0 20 40 60 80 100 0 10 20 30 40 Exposure time, days B RT 90°C 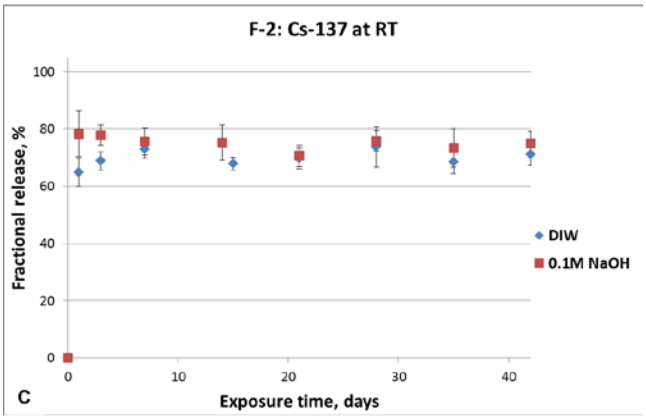 F-2: Cs-137 at RT Fractional release, % 0 20 40 60 80 100 0 10 20 30 40 Exposure time, days C DIW 0.1M NaOH 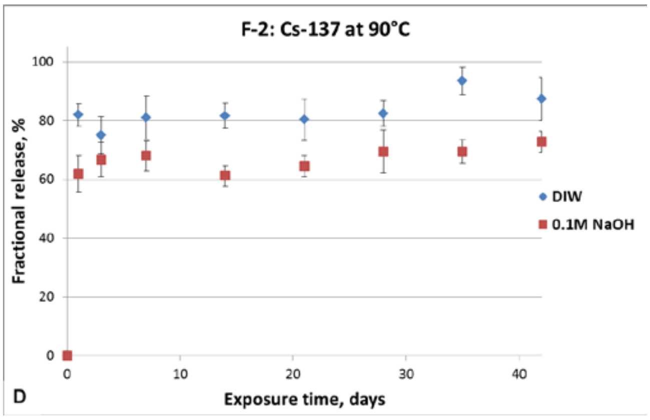 F-2: Cs-137 at 90°C Fractional release, % 0 20 40 60 80 100 0 10 20 30 40 Exposure time, days D DIW 0.1M NaOH

Figure 39: Cumulative fraction of ^{137}Cs released into leaching solution from ash fraction F2 (800<R<1000 μm): ***A*** *– in DIW,* ***B*** *– in 0.1M NaOH,* ***C*** *– at RT,* ***D*** *– at 90°C.*

Temperature	Released fraction, %	Released fraction, Bq/g
DIW		
RT	70.7 ± 2.4	15.3 ± 0.5
90°C	84.4 ± 5.1	18.2 ± 0.1
0.1M NaOH		
RT	74.3 ± 2.0	16.0 ± 0.4
90°C	67.6 ± 4.1	14.6 ± 0.9

Table 16: Equilibrium released fractions of ^{137}Cs from ash fraction F2 measured in the leaching solution using γ-spectrometry.

Results on ^{137}Cs release from a finer fraction F8 are shown in Figure 40. Similar to the ash fraction F2, instant release of a major content of ^{137}Cs was observed from F8, however it comprised 80-100 % of total ^{137}Cs content. This may be defined by higher specific surface area of F8 compared to F2, providing larger area for interaction between solids and leaching solution.

A slight decrease of ^{137}Cs released fraction in the leaching solution was observed with the time, which is more pronounced for 0.1 M NaOH. This effect may be concerned with kinetic effects of ^{137}Cs^{+} uptake by oxide matrices.

Equilibrium in the release of ^{137}Cs from fraction F8 is reached slower, during 30 days of contact with aqueous solution. When comparing the release behaviour in DIW and 0.1 M NaOH (Figure 40.B), no significant effect of the simulated cementitious environment was observed.

Figure 40.A and B also show no effect of the elevated temperature on the release kinetics. Compared to F2, F8 demonstrated a slightly higher equilibrium released fraction of ^{137}Cs, independent on the leaching conditions, namely (81.3.0 ± 4.5) %, or 21.5 ± 1.2 Bq/g.

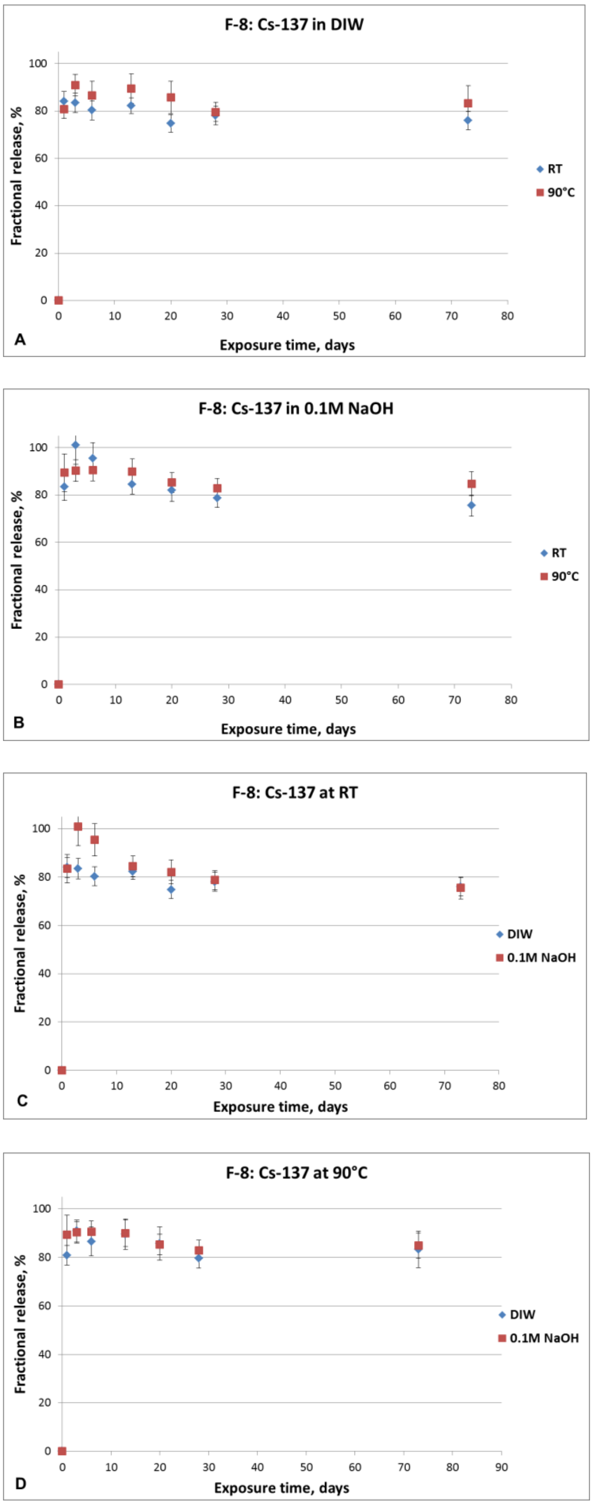

*Figure 40: Release kinetics of ^{137}Cs from ash fraction F8 (R<80 μm): **A** – in DIW, **B** – in 0.1M NaOH, **C** – at RT, **D** – at 90°C.*

Results on release behaviour for remaining fractions, F3-F6 are summarized in the Appendix D.

Although the solid to solution ratio in the experiments was relatively high, i.e. 1/10, no release of ^{60}Co was measured above detection limit (0.5 Bq/g). This confirms that Co may be present in a stable oxide-form or incorporated in mixed-oxide Fe phase.

Results of leaching tests with ISG glass (received from CEA) using the methodology based on ASTM C1282-14 are presented in Figure 41, comparing the leaching behaviour of Ca, Si and Al (evolution of elemental concentration measured by ICP-OES is given in Appendix E). It has to be mentioned that concentration of Zr was below the detection limit of the applied analytical method (DL: 0.2 mg/L). Na and B were not measured in the solution.

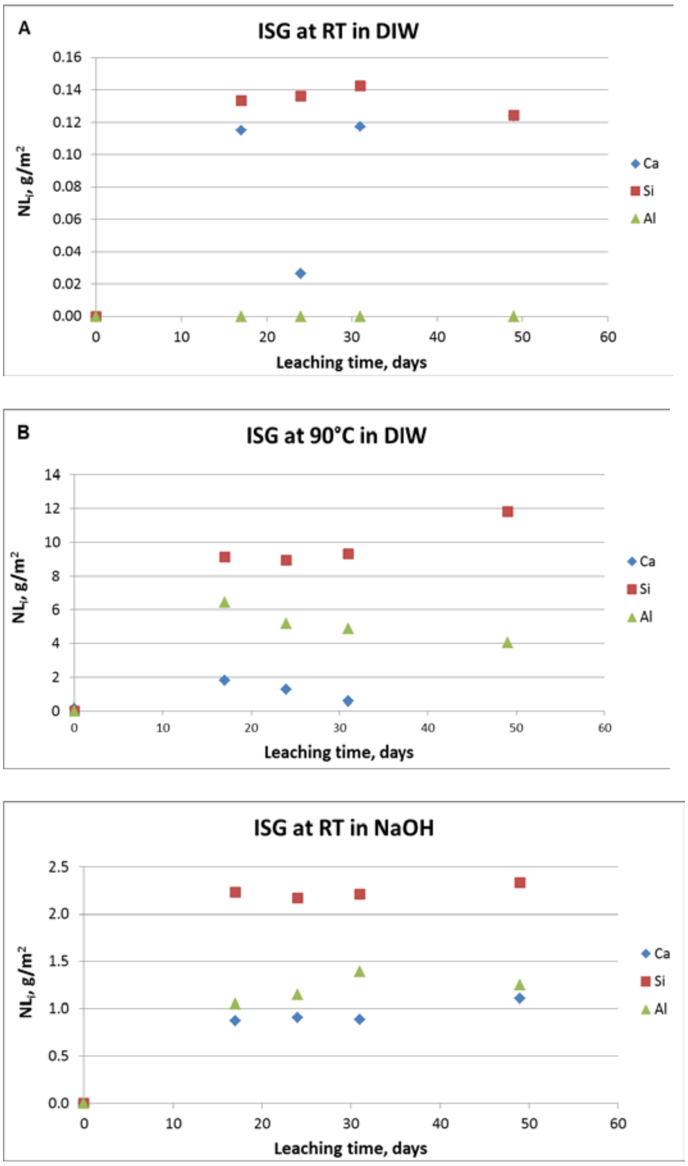

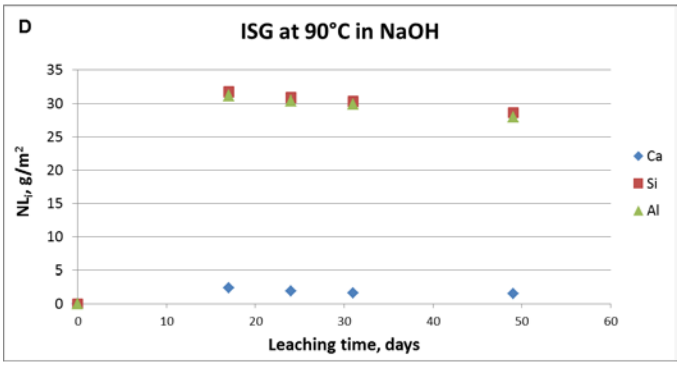

Figure 41: Leaching behaviour of Ca, Al and Si from ISG glass: ***A*** *– in DIW at RT,* ***B*** *– in DIW at 90°C,* ***C*** *– in 0.1M NaOH at RT,* ***D*** *– in 0.1M NaOH at 90°C.*

Figure 42 compares the effects of different leaching conditions on the leaching behaviour of Si. The results show that all investigated systems reach equilibrium relatively fast. As expected, the released fraction of Si is higher 0.1M NaOH solution, compared to pure water at the same temperature conditions. Increase of temperature consistently enhances the soluble fraction of Si both in pure water and 0.1M NaOH.

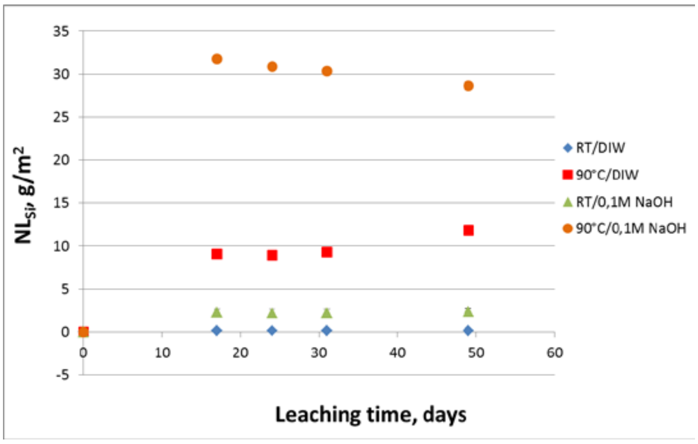

Figure 42: Comparison of leaching behaviour of Si from ISG glass for different leaching conditions.

The evolution of the Si concentration in the solution on the initial leaching step (Δt=17 days) was used for the calculation of the glass alteration rate. Table 17 summarizes evaluated alteration rates.

Conditions	R, $g \cdot m^{-2} \cdot d^{-1}$
DIW at RT	$7.84 \cdot 10^{-3}$
DIW at 90°C	$5.35 \cdot 10^{-1}$
0.1M NaOH at RT	$1.31 \cdot 10^{-1}$
0.1M NaOH at 90°C	1.87

Table 17: Alteration rate of ISG evaluated for different leaching conditions.

Obviously, the alteration rate increases with temperature in both, pure water and 0.1M NaOH solution, mimicking cementitious media. Besides that, as expected, the alteration rate is higher in the 0.1M NaOH solution compared to water at the same temperature.

Other tests and characterizations

Particle size distribution and specific surface area measurement

After the ash fractionation as indicated in the Table 18, particle size distribution was analyzed by weighing each fraction. Relatively equal mass fractions were determined for F2 to F8. Results on the investigation of each ash fraction's specific surface area (SSA), shown in Figure 43, revealed a slightly higher SSAs in the finer fractions, i.e. F8 – F6.

Fraction code	Sieve set, μm	Particle size range R, μm
F1	1000	R>1000
F2	800	800<R<1000
F3	500	500<R<800
F4	355	355<R<500
F5	250	250<R<355
F6	125	125<R<250
F7	80	80<R<125
F8		R<80

Table 18: The particle size of each collected ash fraction.

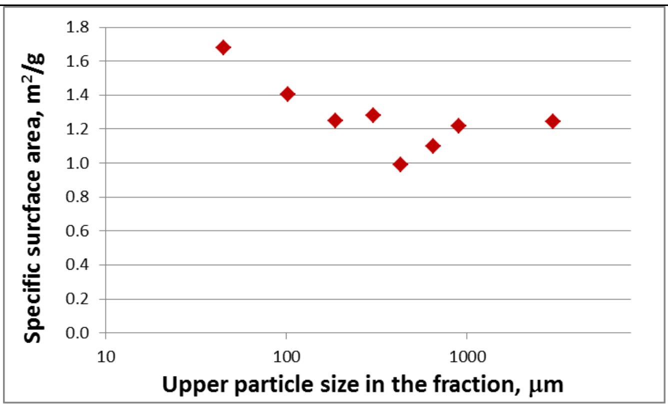

Figure 43: Results of pre-leaching characterization: evolution of specific surface area (SSA, in m²/g) of ash fractions F2 – F8.

Post-leaching examination of the solids

After approximately 80 days of leaching, the solids were separated from the aqueous solution, dried and analyzed by γ-spectrometry, autoradiography and powder XRD in order to investigate the evolution in radionuclide and phase composition. The results of the γ-spectrometric investigations of the F8 after leaching given in Figure 44 demonstrated evolution of specific activity of ^{137}Cs and ^{60}Co in the ash fractions F2.

The remaining activity of ^{137}Cs in the solids varies between 36.2 ± 1.6 % and 29.4 ± 1.3 % of initial activity depending on the leaching conditions. This result is also in a good agreement with the ^{137}Cs fraction measured in the solution. At the same time, the remaining activity of ^{60}Co decreased only slightly compared to the respective initial activity. An unexpected imbalance was measured for ^{60}Co, namely the measured activity after leaching was higher than the one initial detected in the original ash sample. This result points out that despite fractionation of the ash sample, large ash fractions still have a certain degree of inhomogeneity regarding the radionuclide distribution. General conclusion can be made about most of ^{60}Co activity remaining in the solids after leaching. This finding for F2 is also consistent with low ^{60}Co activity released into the aqueous solution, where no reliably measurable ^{60}Co activity was detected.

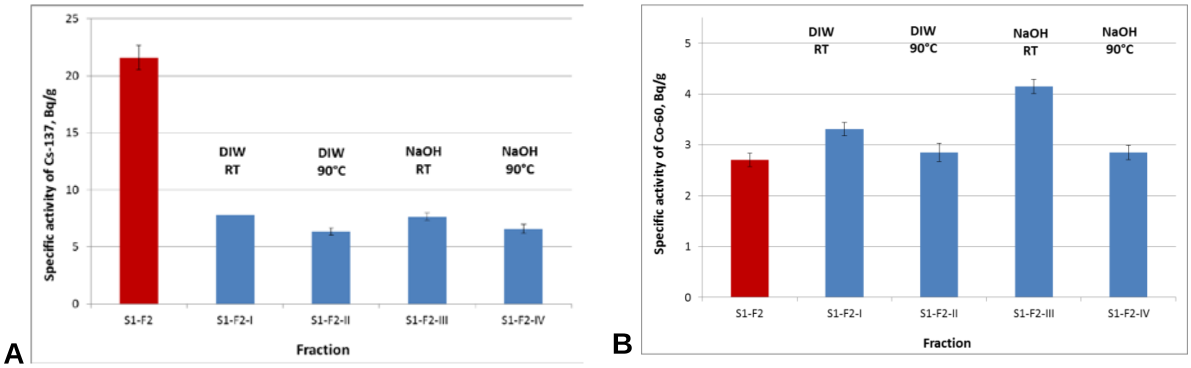

*Figure 44: Results of γ-spectrometric examination of solids of ash fraction F2 (800<R<1000 μm) after leaching: **A** – specific activity of ^{137}Cs, **B** – specific activity of ^{60}Co; in red – initial activity, in blue – activity after leaching on respective conditions.*

Rather similar results were obtained for the ash fraction F8 presented in Figure 45. Obviously, a larger fraction of ^{137}Cs was removed from the solids during leaching test. Remaining ^{137}Cs activity does not change much depending on the leaching conditions applied. In average, 31.5 ± 1.7 % of initial activity of ^{137}Cs remained in the solids. This value is in a good agreement with activity measured in the leaching solutions. In contrast, for ^{60}Co smaller changes in the specific activity in the solids were observed after leaching: in average 81.6 ± 8.4 % of the initial ^{60}Co activity was found in the solids. The fact, such a high ^{60}Co fraction remained in the solids is consistent with low ^{60}Co activity regularly monitored in the leaching solution (i.e. below the respective detection limit of 0.5 Bq/g). However it can be also concerned with a slow kinetics of ^{60}Co release, i.e. the equilibrium is not reached within the exposure time of 42 days. In order to answer this question, different methodology has to be applied, for instance, monitoring of ^{60}Co activity in the solids with time, rather than in a leaching solution.

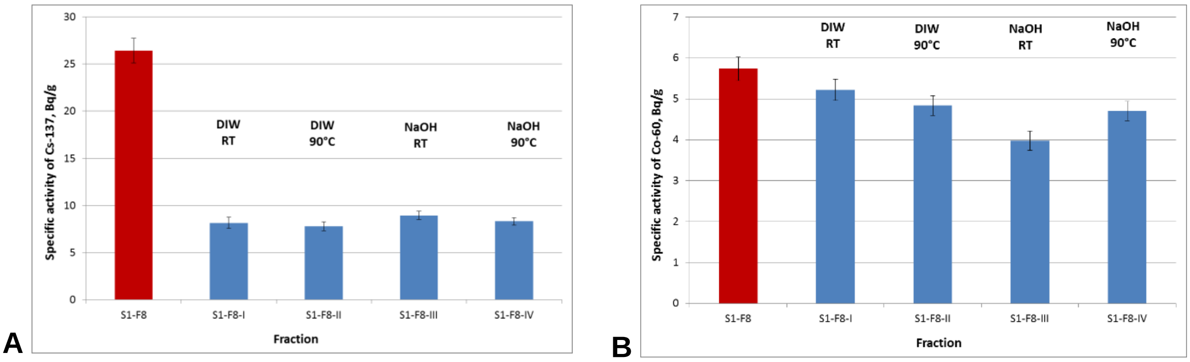

Figure 45: Results of γ-spectrometric examination of solids of ash fraction F8 (R<80 μm) after leaching: ***A*** *– specific activity of ^{137}Cs,* ***B*** *– specific activity of ^{60}Co; in red – initial activity, in blue – activity after leaching on respective conditions.*

Autoradiography on the solids subjected to the leaching was performed in order to identify the evolution heterogeneity of radionuclides distribution in the ash fractions. For that, similar to the methodology described in "Chemical composition" part, solids collected after leaching were embedded in araldite resin, polished and examined by autoradiography.

Figure 46 shows the autoradiographic images obtained for leached solids of fraction F2 (grain size 800<R<1000 μm), i.e. F2-I, F2-II, F2-III, F2-IV, in comparison to the original F2. Based on the obtained images conclusion about the evolution of radionuclide distribution cannot be done. Moreover, the selected approach also does not allow qualitative or quantitative evaluation of radionuclide content.

Taking into account that most of ^{137}Cs, which might have contributed significantly to the autoradiographic response, was removed by leaching, significant contribution of ^{60}Co can still be observed.

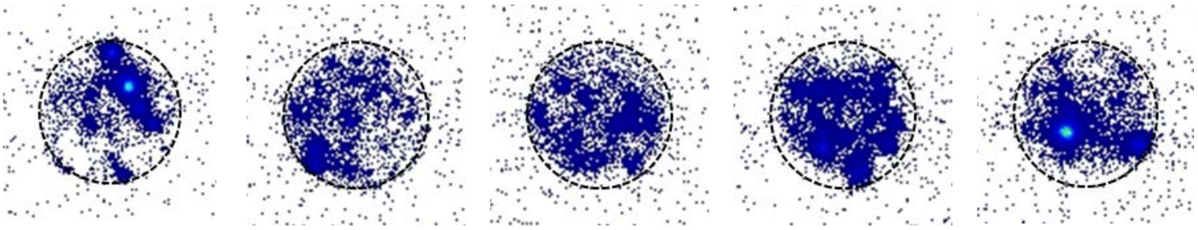

F2 F2-I F2-II F2-III F2-IV

Figure 46: Autoradiographic images of original ash fraction F2 and solids collected after leaching: F2-I – F2 leached in DIW at RT, F2-II - F2 leached in DIW at 90°C, F2-III - F2 leached in 0.1M NaOH at RT, F2-IV - F2 leached in 0.1M NaOH at 90°C.

Results of post-leaching XRD-examination are shown in Figure 47. Comparison of XRD-patterns indicates similar phase composition of solids before and after leaching. As for the unleached material, the spectra look rather similar with most reflexes present in all difractograms, however with different intensity.

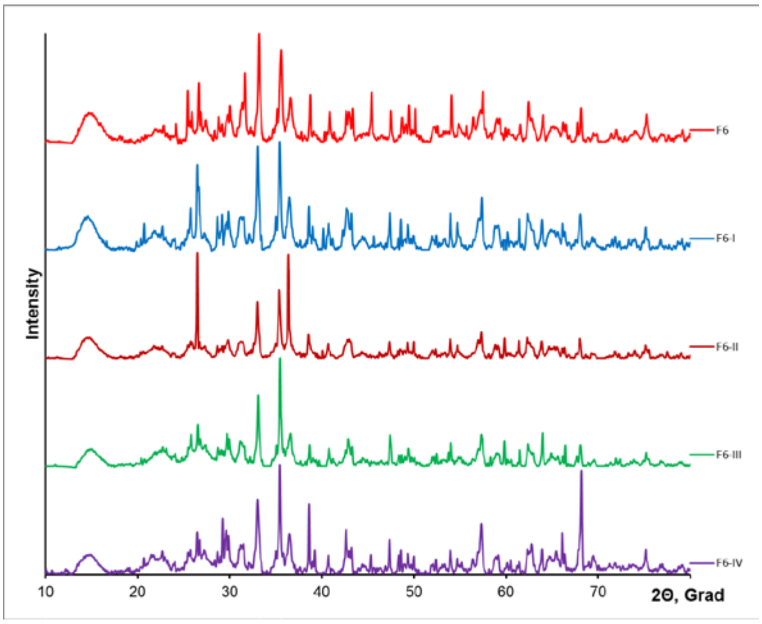

Figure 47: XRD-patterns of initial solid of ash fraction F6 and respective solids after leaching F6-I – IV.

A detailed evaluation of the phases present, given in Figure 48, shows presence of all initially identified phases, besides NaCl (at 2 Θ of 32 and 45.5 degrees).

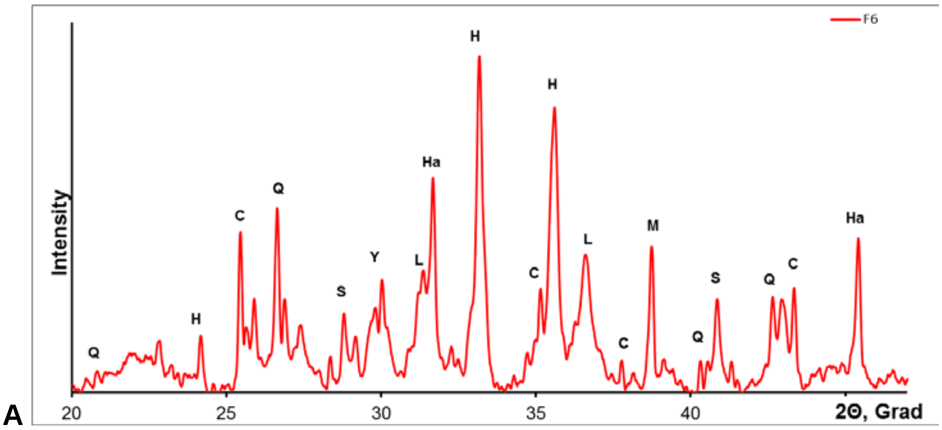

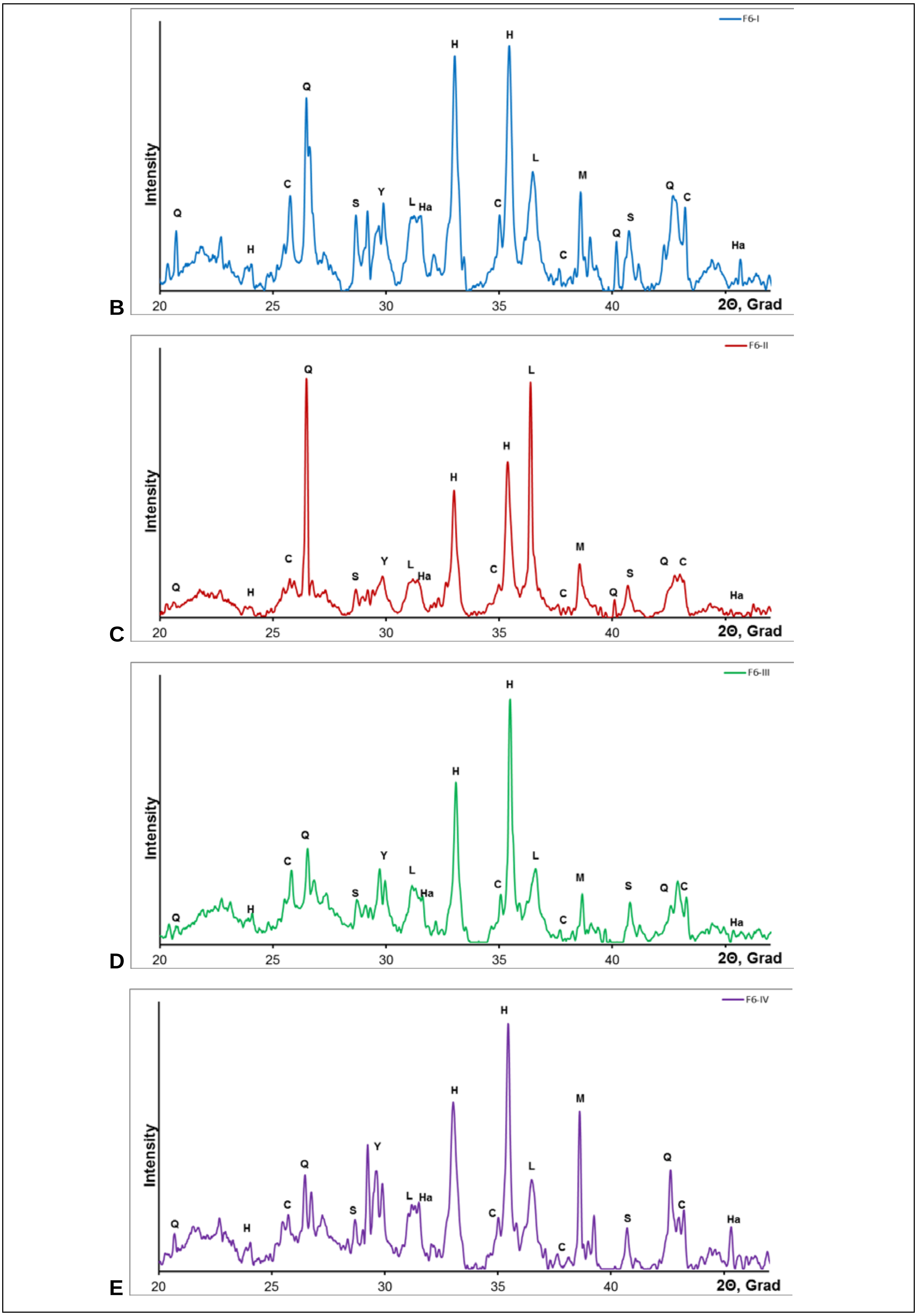
F6-I
Intensity
Q
H
C
Q
S
Y
L
Ha
H
C
H
L
C
M
Q
S
Q
C
Ha
20
25
30
35
40
2Θ, Grad
B
F6-II
Intensity
Q
H
C
Q
S
Y
L
Ha
H
C
H
L
C
M
Q
S
Q
C
Ha
20
25
30
35
40
2Θ, Grad
C
F6-III
Intensity
Q
H
C
Q
S
Y
L
Ha
H
C
H
L
C
M
S
Q
C
Ha
20
25
30
35
40
2Θ, Grad
D
F6-IV
Intensity
Q
H
C
Q
S
Y
L
Ha
H
C
H
L
C
M
S
Q
C
Ha
20
25
30
35
40
2Θ, Grad
E

*Figure 48: Detailed evaluation of XRD-patterns of initial solid of ash fraction F6 (**A**) and respective solids after leaching in DIW at RT (**B**), in DIW at 90°C (**C**), in 0.1M NaOH at RT (**D**) and in 0.1M NaOH at 90°C (**E**). Indexes on difractograms represent shortenings of respective mineral phase names.*

Reflexes of NaCl are much lower after leaching. This finding is consistent with the suggestion made after microanalytical examination of parent solid F6: NaCl and KCl were observed at SEM images, and these phases are expected to be dissolved during leaching tests. Similar behaviour was expected for KCl (sylvite) however reflexes, corresponding to the KCl phase are to see for every solid after leaching. Additionally, in samples leached in NaOH (F6-III and F6-IV) the intensities of the reflexes of quartz (SiO_2) and corundum (Al_2O_3) seem to be lower compared to the respective reflexes for parent sample F6 (not leached) and samples F6-I and F6-II leached in DIW. This is a result of a higher solubility of both SiO_2 and Al_2O_3 in alkaline media, compared to DIW.

Similar results were obtained for F2 (see Appendix F).

Conclusions and Outlooks

The obtained ash samples were fractionated in 8 fractions by sieving. Characterization of fractions F2 – F8 demonstrated a higher specific surface area for finer fractions.

The radioanalytical characterization revealed no significant measurable activity of radionuclides besides ^{137}Cs and ^{60}Co. The distribution of these radionuclides seems to be rather heterogeneous, hot-spots in radionuclide distribution were observed by autoradiography.

A detailed investigations of the phase composition revealed a similar matrix for all ash fractions composed mainly of oxide SiO_2 (Quartz), Al_2O_3 (Corundum), CaO (Lime) and Fe_2O_3 (Hematite), or mixed (Si, Al, Ca)-oxides (Mullite and Yoshiokaite), and chloride phases, i.e. KCl and NaCl. Particles bearing radionuclides were systematically composed of Fe-, Si- and Al-oxides. Ba- and Ti-reach phases were systematically observed by SEM/EDX examination, they were not, however identified by powder XRD analysis, indicating only minor amount of (Ba, Ti)-phase.

The stability of the ash fractions was evaluated in leaching tests, which revealed a measurable release only for ^{137}Cs, whereas release of ^{60}Co was determined by measurement of solid phases after leaching. Radionuclides ^{241}Am or ^{154}Eu, initially present in the ash (according to the radioanalytical data provided by JEN) were not detected in the leaching solution. The leaching tests showed that for large fractions (e.g. sample F2, grain size $800<R<1000$ µm) about 60 % to 80 % of the ^{137}Cs inventory is released within a first few days. Equilibrium ^{137}Cs content was slightly higher for DIW at 90°C. Lower release of ^{137}Cs in alkaline media can be presumably due to partial uptake of Cs^+ uptake by the ash.

Release of ^{60}Co from F2 was possible to determine only from post-leaching examination of ash fraction; ^{60}Co activity in the leaching solution was below the DL. The residual ^{60}Co activity in the F2 solid comprised 81.6 ± 8.4% of the initial ^{60}Co activity. The results of the leaching tests are in a good agreement with post-leaching γ-spectrometric examinations, showing significant decrease in ^{137}Cs specific activity, and slight drop in specific activity of ^{60}Co. For finer fractions (e.g. F8, grain size $R<80$ µm) leaching tests similarly demonstrated high ^{137}Cs instant release fraction within first 3 days of leaching, i.e. 80 % to 100 % of the ^{137}Cs inventory.

Irrespective of the leaching conditions release fraction of ^{137}Cs was determined to be (81.3.0 ± 4.5) %, or 21.5 ± 1.2 Bq/g. The findings on high release of ^{137}Cs are consistent for all ash fractions and imply that ^{137}Cs is present in easily soluble form, e.g. in a chloride form. Systematically low activity of ^{60}Co that could not be reliably measured in the leaching solution may be due to the slow kinetics of Co dissolution. Furthermore, ^{60}Co may be associated with Fe-oxide phases, providing for a low Co solubility in aqueous solution in neutral and high pH-range. Examination of the phase composition before and after leaching revealed significant decrease of NaCl (easily soluble). Besides that, after leaching in alkaline conditions, relative amounts of quartz and corundum were found to decrease compared to the initial ash fraction, which was not observed after leaching experiments performed in DIW.

Alteration rates for ISG glass were determined in pure water and 0.1M NaOH at RT and 90°C. Direct comparison of leaching behaviour of ashes and ISG is not possible though, as results of matrix dissolution for ashes are not available due to the technical reasons.

4.4 TH 01 Geomelt ICV sample – vitrification of sea dump drums (NNL)

General information	
Partner:	NNL
Sample id:	TH 01 Geomelt ICV vitrification of sea dump drums
Contact person:	C R Scales
Origin and macroscopic description	
 *Figure 49: TH 01Geomelt ICV sample.*	Waste feeds comprised of surrogate sea dump drums with added soils and glass frit as fluxing agents. **Details are noted in the WP3 report**. Product appears to be macroscopically homogeneous as indicated visually (Figure 49).
Microstructure	
Method(s):	☐ SEM ☐ XRD ☐ Other:
Operating conditions:	
Homogeneity:	
Free liquid or gas:	
Crystalline composition:	
Comments and discussion:	
Chemical composition	
Method(s):	☐ EMP ☐ ICP-OES/MS ☒ XRF ☐ Other: SEM/EDS
Operating conditions:	
Chemical composition:	Chemical composition is shown below (Table 19). Sampling points taken SP1 (one sample at 0-100mm) and SP2 (3 samples at 0-100, 100-200, and 200-300) at horizontal axes at approx. 200 mm from base of product. SP3 taken from top (0-100).

Sample	Na_2O	MgO	Al_2O_3	SiO_2	K_2O	CaO	Ti	Cr	Fe_2O_3	Ce	Cs^{137} Bq/g
SP1.1	13.60	0.73	7.48	65.81	1.20	2.59	0.14	0.19	2.76	0.03	n/a
SP2.1	14.18	0.54	6.71	64.89	1.13	2.54	0.14	0.13	2.45	0.01	82.8
SP2.2	14.26	0.54	6.46	67.39	1.21	2.63	0.15	0.10	2.33	0.00	80.5
SP2.3	13.38	0.48	6.34	64.31	1.14	2.56	0.14	0.11	2.38	0.00	82.4
SP3.1	13.48	0.51	7.48	66.50	1.17	2.53	0.14	0.14	2.68	0.00	76.5

Table 19: TH 01 Geomelt ICV chemical composition (n.a.: not analyzed)

Comments and discussion:	**The vitrified block was examined through use of XRF on the major glass forming elements. (Note lighter elements not included in this analysis). Analyzes at various points in the block demonstrate homogeneity of product at the macroscopic level. Consistent measurements of iron throughout the block suggest that the contents of the surrogate sea dump drums have been well mixed in the melt. (Note sea dump drum surrogate is the only source of iron in the melt). 25MBq Cs-137 was loaded into a single can in the central row of the staged melt. Gamma scans show that the caesium is evenly distributed throughout the vitrified block and at a level which suggests that good mixing is taking place in the melt.**

Chemical durability

Method(s):	☒ As described in MS12 Report (p. 12-13), adapted from ASTM C1285 ☐ As described in MS12 Report (p. 14), adapted from ASTM C1220 ☐ Other:
Clarifications:	28 day PCT leach test, boron concentration in ug/L shown in table below for ISG and TH01 glass samples. Test in triplicate from each of three sample points.
Results and discussion:	Boron concentration in the leachate was measured following 28 day PCT test. The ISG has 16 % B_2O_3 content compared to 11.8 % B_2O_3 estimated for TH01. Based on feeds added and a correction made for losses of volatile components particularly water during processing, the data below shows that the resulting boron concentration is lower than that observed for ISG by an order of magnitude (Table 20).

ISG			TH01		
Jar	***Sample***	**B ug/L**	***Jar***	***Sample***	**B ug/L**
575	ISG	13.8	627	SP1.1	2.63
576	ISG	22.7	628	SP1.1	2.49
577	ISG	38.1	629	SP1.1	2.92
			630	SP2.2	1.83
			631	SP2.2	1.83
			632	SP2.2	2.26
			633	SP3.1	1.22
			634	SP3.1	1.44
			635	SP3.1	8.13

Table 20: Boron concentration (ug/L) measured in the leachate: comparison with the ISG glass

Other tests and characterizations

N/A

Conclusions and Outlooks

Vitrification has been successfully carried out surrogate sea dump drums. XRF analysis across the block shows a homogeneous wasteform at a macroscopic level. The iron content throughout the block suggests thorough mixing within the melt. Note that the only iron source is from the surrogate sea dump drums.

PCT leach tests show a superior durability to ISG glass under the conditions applied. It should also be noted that as a one off demonstration melt, optimization of the product has not been attempted. Under current GDF requirements in the UK for disposal of ILW, no credit is taken for durability of the product and as such may not be a discriminator for disposal.

4.5 TH 02 Geomelt ICV sample – vitrification of sludge and clinoptilolite (NNL)

General information

Partner:	NNL
Sample id:	TH 02 Geomelt ICV vitrification sludge and clinoptilolite
Contact person:	C R Scales

Origin and macroscopic description

Figure 50: TH 02- Geomelt ICV sample.

Waste feeds comprised of a simulated Magnox sludge plus clinoptilolite simulating ion exchange materials. The co-vitrification illustrates the capability of thermal to reduce overall wasteform volumes. Feed data is included in the WP3 report.

Illustrated (Figure 50) is the surface of the vitrified product (lower) and a bagged sample of a core drilled for analysis.

In both cases the product appears homogeneous at the macroscopic level.

Microstructure

Method(s):	☐ SEM ☐ XRD ☐ Other:
Operating conditions:	
Homogeneity:	
Free liquid or gas:	
Crystalline composition:	
Comments and discussion:	

Chemical composition

Method(s):	☐ EMP ☐ ICP-OES/MS ☒ XRF ☐ Other:

Operating conditions:	
Chemical composition:	Chemical composition using XRF is shown below. SP1 samples were drilled from the surface of the block vertically down into the block at 3 points, 0-100, 100-200, 200-300. SP2 samples were taken from a sampling point approx. 200mm from the base of the block drilled through the block at 3 points, 0-110, 100-200, 200-300.

Sample	Na_2O	MgO	Al_2O_3	SiO_2	K_2O	CaO	Ti	Cr	Fe_2O_3	Ce	Cs^{137} Bq/g	Sr^{85} Bq/g
SP1.1	12.93	9.45	9.75	63.16	2.13	1.10	0.03	0.21	1.69	0.00	93.7	60.2
SP1.2	13.42	9.62	6.13	59.37	2.09	1.02	0.03	0.13	1.19	0.00	100.7	65.3
SP1.3 R3	12.90	9.58	6.81	60.69	2.18	1.04	0.03	0.18	1.44	0.00	85.9	56.1
SP1.3 R2	13.41	9.74	6.93	61.69	2.18	1.05	0.03	0.18	1.46	0.00		
SP1.3 R1	13.05	9.71	6.87	60.88	2.18	1.05	0.03	0.17	1.44	0.00		
SP2.1	13.11	9.80	7.46	59.58	2.14	1.06	0.04	0.13	1.22	0.01	91.0	57.5
SP2.2	13.13	9.90	6.23	60.26	2.17	1.06	0.03	0.14	1.25	0.00	107.8	69.3
SP2.3	13.45	10.15	6.36	60.91	2.21	1.04	0.03	0.15	1.42	0.00	106.4	68.6

Table 21: TH 02 Geomelt ICV chemical composition (n.a.: not analyzed)

Comments and discussion:	**Homogeneity across the vitrified block has been examined through use of XRF on the major glass forming elements. (Note lighter elements not included in this analysis). Data provides evidence for good mixing in the melt.** **Both caesium and strontium were added to the feeds in the centre of the batch prior to the melting operation. Activity levels measured suggest good mixing of the radioactive dopants in the melt, with consistent ratios between the activity of Cs and Sr throughout.**

Chemical durability

Method(s):	☒ As described in MS12 Report (p. 12-13), adapted from ASTM C1285 ☐ As described in MS12 Report (p. 14), adapted from ASTM C1220 ☐ Other:
Clarifications:	28 day PCT leach test carried out
Results and discussion:	Boron concentration in the leachate was measured following 28 day PCT test. The ISG has 16 % B_2O_3 content compared to 10.3 % B_2O_3 estimated for TH02 based on feeds added and a correction made for losses of volatile components particularly water during processing.

Data below shows that the resulting boron concentration is largely equivalent that observed for ISG (Table 22).

ISG			TH02		
Jar	***Sample***	**B ug/L**	***Jar***	***Sample***	**B ug/L**
575	ISG	13.8	636	SP21.1	13.8
576	ISG	22.7	637	SP21.1	12.5
577	ISG	38.1	638	SP21.1	6.97
			639	SP21.2	7.91
			640	SP21.2	10.3
			641	SP21.2	12.5
			642	SP21.3	10.3
			643	SP21.3	21.1
			644	SP21.3	11.1

Table 22: Boron concentration (ug/L) measured in the leachate: comparison with the ISG glass

Other tests and characterizations

N/A

Conclusions and Outlooks

Vitrification has been successfully carried out on surrogate for Magnox sludge using another wastestream, clinoptilolite, to provide glass forming components. XRF analysis and gamma scanning of active components across the block shows good homogeneity and thus infers good mixing of feed components during processing.

PCT leach tests show equivalent durability to ISG glass under the conditions applied. It should also be noted that as a one off demonstration melt, optimization of the product has not been attempted. Under current GDF requirements in the UK for disposal of ILW, no credit is taken for durability of the product and as such may not be a discriminator for disposal.

4.6 HIP-1 sample (NNL)

General information

Partner:	University of Sheffield (USFD) National Nuclear Laboratory (NNL)
Sample id:	NNL-HIP-1
Contact person:	Sam Walling, Charlie Scales and Neil Hyatt

Origin and macroscopic description

Figure 51: Photograph of sectioned NNL-HIP-1

Hot isostatic pressing (HIPing) as a thermal treatment method was used during THERAMIN WP3 to develop wasteforms for further characterization.

The wasteform in this study was co-mixed containing both simulant calcined Magnox sludge and Cs-exchanged clinoptilolite. A borosilicate glass frit (MW ½ Li frit) was added to help the formation of a glassy wasteform.

The batch composition is detailed in

Borosilicate glass frit MW ½ Li frit		**NNL-HIP-1**	
SiO2	63.4	Magnox sludge	33.3 %
B2O3	22.5	Clinoptilolite	56.5 %
Na2O	11.4	MW ½ Li frit	10.2 %
Li2O	2.7	CeO2	10 g
		Cs2O	90 g

Table 23.

The sample used during this study was only a small portion of the overall HIP wasteform prepared by NNL.

Visually the sample appears a solid, heterogeneous crystalline product (Figure 51).

For sample preparation and trial details, refer to report THERAMIN D3.6.

Borosilicate glass frit MW ½ Li frit		**NNL-HIP-1**	
SiO_2	63.4	Magnox sludge	33.3 %
B_2O_3	22.5	Clinoptilolite	56.5 %
Na_2O	11.4	MW ½ Li frit	10.2 %
Li_2O	2.7	CeO_2	10 g
		Cs_2O	90 g

<table>
<tr><td></td><td>Table 23: Composition of borosilicate glass frit and NNL-HIP-1 (Data extracted from THERAMIN D3.6, pages 13-14)</td></tr>
<tr><td colspan="2">Microstructure</td></tr>
<tr><td>Method(s):</td><td>☒ SEM ☒ XRD ☐ Other:</td></tr>
<tr><td>Operating conditions:</td><td>XRD: A powdered sample was analyzed using a Bruker D2 PHASER diffractometer with a LYNXEYE detector utilising Cu Kα (λ = 1.5418 Å) radiation, a Ni foil was used to filter the K radiation. The diffraction pattern was collected between 10° < 2θ < 70° with a step size of 0.01° 2θ and dwell time of 1s per step.
SEM: A Hitachi TM3030 scanning electron microscope coupled with a Bruker Quantax 70 energy dispersive X-ray spectroscopy system (EDX) with a silicon drift detector was used. A sectioned slice of the HIP can/sample was mounted in epoxy resin, ground using SiC grit paper, polished to a 1 µm finish using diamond suspensions and carbon coated.</td></tr>
<tr><td>Homogeneity:</td><td>Heterogeneous</td></tr>
<tr><td>Free liquid or gas:</td><td>Absence</td></tr>
<tr><td>Crystalline composition:</td><td>Multi-phase glass ceramic</td></tr>
<tr><td>Comments and discussion:</td><td>In Figure 52, multiple crystalline phases were identified by powder XRD. These consisted of: forsterite ($MgSiO_3$), ceria (CeO_2), periclase (MgO), quartz (SiO_2), with minor reflections from kotoite ($Mg_3(BO_3)_2$ and potentially from albite ($NaAlSi_3O_8$). There were no reflections associated with clinoptilolite, which indicated that the zeolite structure was destroyed during the thermal treatment process. The presence of periclase suggests the $Mg(OH)_2$ waste stream was not fully incorporated into a glassy matrix, instead a portion of the waste underwent decomposition to MgO.
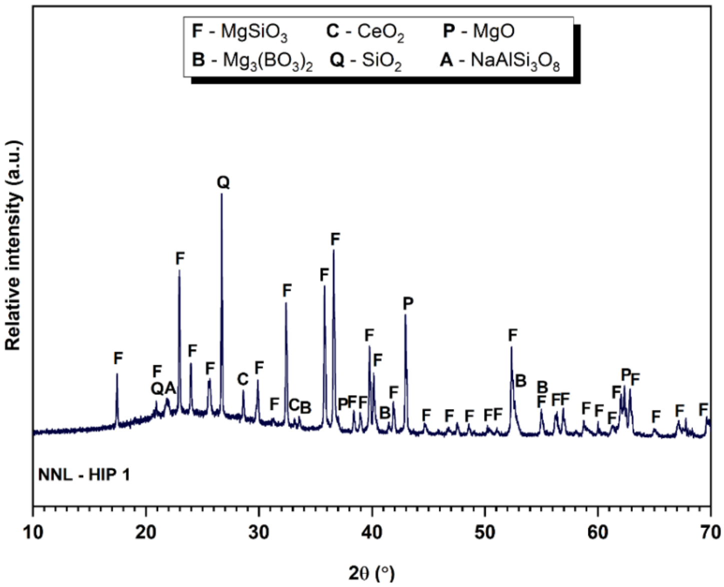
</td></tr>
</table>

Figure 52: XRD of NNL-HIP-1

The micrographs of NNL-HIP-1 are shown in Figure 53 and Figure 54, displaying a highly heterogeneous microstructure. The pale grey region represents the collapsed clinoptilolite, postulated due to a strong association of Si, Al, Na and Ca (Figure 54), which corresponds to the nominal composition of clinoptilolite; $(Na_{0.5}K_{2.5})(Ca_{1.0}Mg_{0.5})(Al_6Si_{30})O_{72}\cdot 24H_2O$.

The borosilicate glass frit and $Mg(OH)_2$ have likely reacted to form the Mg and Si rich darker region, likely this is the source of the crystallized forsterite, identified by XRD.

The CeO_2 is present as white spots in Figure 53 and Figure 54 and tend to be scattered throughout the sample.

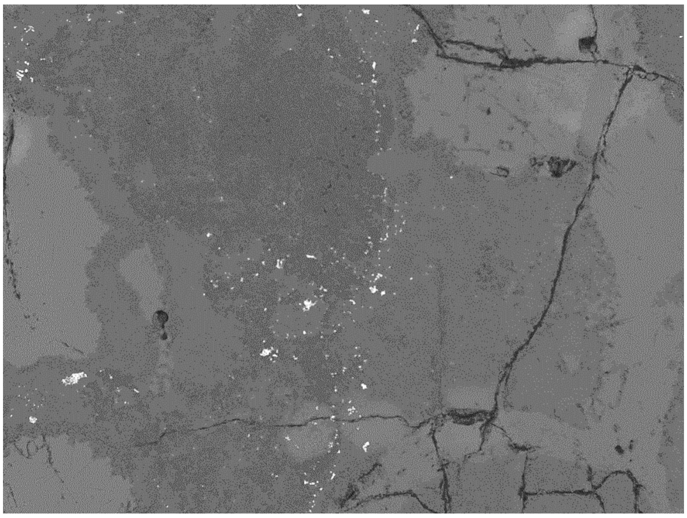

Figure 53: BSE micrograph of NNL-HIP-1 (x 100 magnification)

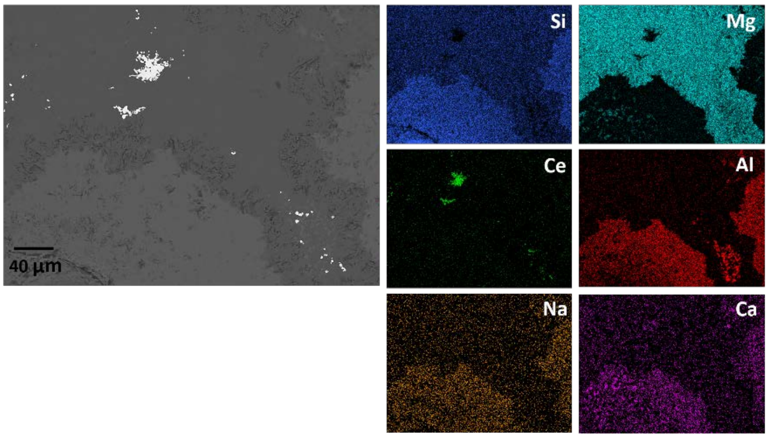

Figure 54: SEM/EDX micrograph of NNL-HIP-1 (x 500 magnification)

Chemical composition

Method(s):	☐ EMP ☒ ICP-OES/MS ☒ XRF ☐ Other:
Operating conditions:	A NNL-HIP-1 bead was prepared using bulk powdered sample and a lithium tetraborate flux at a 1:10 sample-to-flux ratio, heated to 1270 °C. This was analyzed using a PANalytical PW2404 spectrometer under vacuum using a Rh X-rays tube. Additionally samples were digested for ICP-OES analysis to determine boron and lithium contents, this was undertaken on a Thermo Iris Advantage ICP.

Chemical composition:

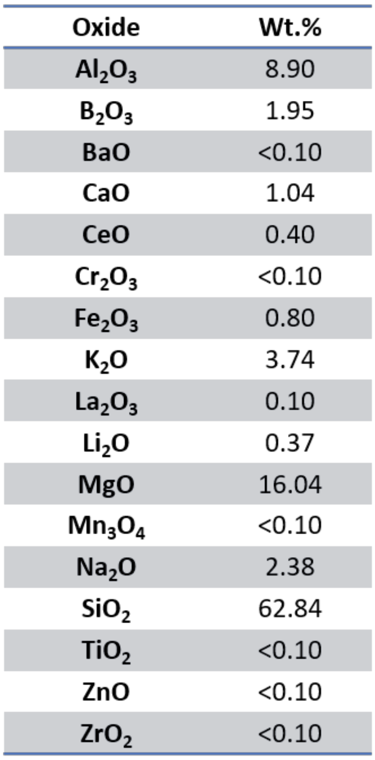

Oxide	Wt.%
Al_2O_3	8.90
B_2O_3	1.95
BaO	<0.10
CaO	1.04
CeO	0.40
Cr_2O_3	<0.10
Fe_2O_3	0.80
K_2O	3.74
La_2O_3	0.10
Li_2O	0.37
MgO	16.04
Mn_3O_4	<0.10
Na_2O	2.38
SiO_2	62.84
TiO_2	<0.10
ZnO	<0.10
ZrO_2	<0.10

Table 24: Composition of bulk NNL-HIP-1 by XRF and ICP spectroscopy

Comments and discussion:

The sample is representative of the materials used in producing this HIP can, with Al2O3 + SiO2 >70%, and 16% MgO from the calcined Magnox sludge simulant used. Only a small contribution from B2O3 is present due to being a minor component of the glass frit added.

It should be noted that the XRF composition is different to HIP-USFD-Ce, both of which were produced from the same material supplied by NNL. This suggests a degree of inhomogeneity within the larger HIP sample (of which only one section of unknown located was supplied for testing).

Chemical durability

Method(s):	☒ As described in MS12 Report (p. 12-13), adapted from ASTM C1285 ☐ As described in MS12 Report (p. 14), adapted from ASTM C1220 ☐ Other:
Clarifications:	Sample material was crushed and sieved to 125-250 µm, then washed and prepared as per ASTM C1285. PFA screw-lid pots were used, with 10 ml ASTM Type 1 water and a quantity of sample material to ensure a SA/V of 10 m^{-1}. The surface area / volume was calculated assuming a geometric surface area, as required in ASTM C1285 specifications (with density from helium pycnometry analysis). Static leaching at 90 °C was undertaken for up to 28 days, with duplicate sampling at 1, 3, 7, 14, 21 and 28 days. Sample aliquots were filtered using a 0.2 µm cellulose acetate filter. The aliquot pH was measured using a 3-point calibrated pH probe and then acidified with ultrapure NORMATOM HNO_3 and analyzed by ICP-OES (Thermo Fisher iCAP 6300 ICP-OES) and/or ICP-MS (Thermo Scientific iCAP RQ ICP-MS). Normalized mass loss was calculated using compositional data from XRF analysis.
Results and discussion:	*NB: The USFD ISG dissolution results are reported in GeoMelt-Glass 6 characterization test sheet* For the NNL-HIP-1 sample, the solution pH moves by ± 0.3 units either side of ~pH 9, at day 28 the pH was 8.9. 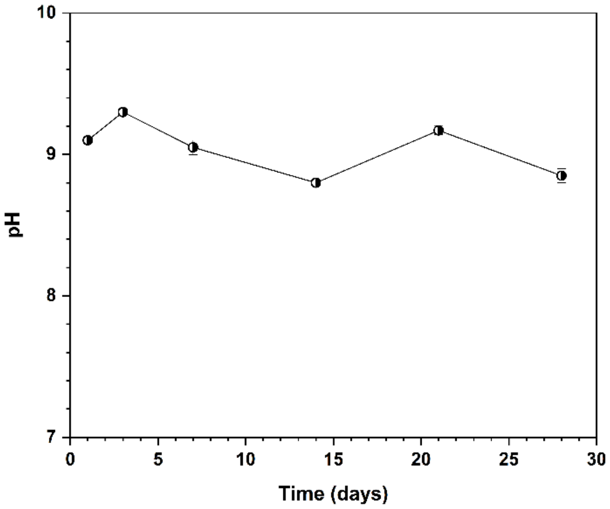 *Figure 55: pH of NNL-HIP-1 up to day 28* From day 1, there is an immediate release of Ca, Na and B (Figures 6 and 7), which steadily continue up to day 28. These are, however, minor components of this material. Though the boron release rate ends at a comparable level to ISG (24 g/m^2 for HIP-1, 28 g/m^2 for ISG – data for ISG available in GeoMelt-Glass 6 characterization test sheet), this HIP material is not a homogeneous glass and unlikely to dissolve congruently, as such the use of boron as comparative indicator of dissolution between these materials should be discouraged.

The final Si normalized mass loss (4.4 g/m^2 compared to 17 g/m^2 in ISG) might indicate an improved durability, however as this HIP material is inhomogeneous direct comparisons are still difficult. Overall the cerium within this sample was below the limits of detection for the ICP-OES, therefore widespread dissolution is unlikely to have occurred.

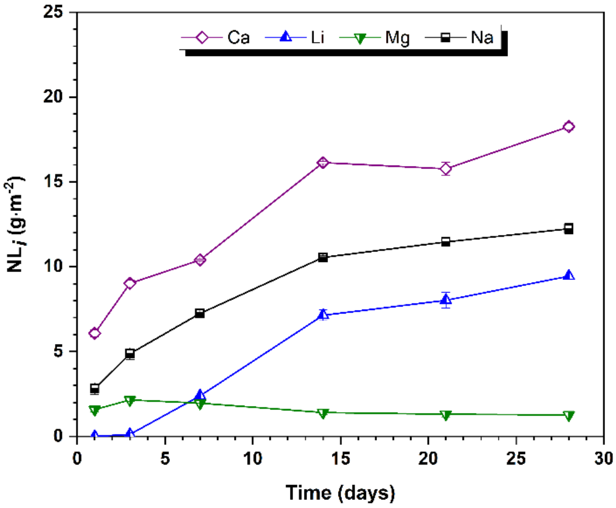

Figure 56: Normalized mass loss of Ca, Li, Mg and Na from NNL-HIP-1, up to day 28

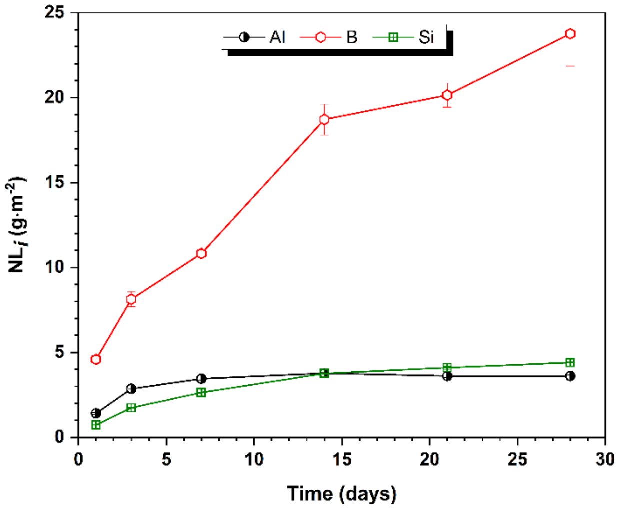

Figure 57: Normalized mass loss of Al, B and Si from NNL-HIP-1, up to day 28

Other tests and characterizations

N/A

Conclusions and Outlooks

The thermally treated product presented here has a heterogeneous glass-ceramic microstructure, with CeO_2 present as discrete particles throughout the sample. Simulant waste streams (calcined Magnox sludge and clinoptilolite) have partially, or fully reacted to form constituent phases (either glassy or crystalline), with the borosilicate glass frit assisting as a glass former. As such a high waste loading is possible with this thermal treatment.

Chemical durability assessments of this product is difficult to compare to ISG, due to the difference in dissolution mechanisms between a homogeneous glass and this multi-phase material. Overall boron normalized mass losses appear to show equal or slightly better durability to ISG, while silicon mass loss suggests improved durability, this depends on the existence or formation of any secondary precipitation products during dissolution.

The similarities between this product, produced at a larger scale, and the smaller scale product (HIP-USFD-Ce) verify the use and value of smaller wasteform development projects.

4.7 HIP-2 sample (NNL)

General information	
Partner:	University of Sheffield (USFD) National Nuclear Laboratory (NNL)
Sample id:	NNL-HIP-2
Contact person:	Sam Walling, Charlie Scales and Neil Hyatt

Origin and macroscopic description

Figure 58: Photograph of sectioned NNL-HIP-2

Hot isostatic pressing (HIPing) as a thermal treatment method was used during THERAMIN WP3 to develop wasteforms for further characterization.

The wasteform in this study was co-mixed containing both simulant calcined Magnox sludge and Cs-exchanged clinoptilolite. Borax ($Na_2B_4O_7 \cdot 10H_2O$) was added to help the formation of a glassy wasteform. The batch composition is detailed in Table 25.

The sample used during this study was only a small portion of the overall HIP wasteform prepared by NNL. Visually the sample appears a solid, heterogeneous product with no obvious porosity (Figure 58).

For sample preparation and trial details, refer to report THERAMIN D3.6.

Magnox sludge	44.8 %
Clinoptilolite	44.8 %
Borax	10.4 %
CeO_2	10 g
Cs_2O	90 g

Table 25: Composition of NNL-HIP-2 (Data extracted from THERAMIN D3.6, pages 13-14)

Microstructure

Method(s):	☒ SEM ☒ XRD ☐ Other:
Operating conditions:	**XRD:** A powdered sample was analyzed using a Bruker D2 PHASER diffractometer with a LYNXEYE detector utilising Cu Kα (λ = 1.5418 Å) radiation, a Ni foil was used to filter the K radiation. The diffraction pattern was collected between 10° < 2θ < 70° with a step size of 0.01° 2θ and dwell time of 1s per step. **SEM:** A Hitachi TM3030 scanning electron microscope coupled with a Bruker Quantax 70 energy dispersive X-ray spectroscopy system (EDX) with a silicon drift detector was used. A sectioned slice of the HIP

	can/sample was mounted in epoxy resin, ground using SiC grit paper, polished to a 1 µm finish using diamond suspensions and carbon coated.
Homogeneity:	Heterogeneous
Free liquid or gas:	Absence
Crystalline composition:	Multi-phase glass ceramic
Comments and discussion:	In Figure 59, multiple crystalline phases were identified by powder XRD. These consisted predominantly of: forsterite ($MgSiO_3$), with minor reflections from periclase (MgO) and kotoite ($Mg_3(BO_3)_2$. There were no reflections associated with clinoptilolite, which indicated that the zeolite structure was destroyed during the thermal treatment process. The relative intensity of the periclase reflections compared to those in NNL-HIP-1 were significantly lower. This suggests that the inclusion of borax as a glass former resulted in more consumption of the simulant Magnox sludge. 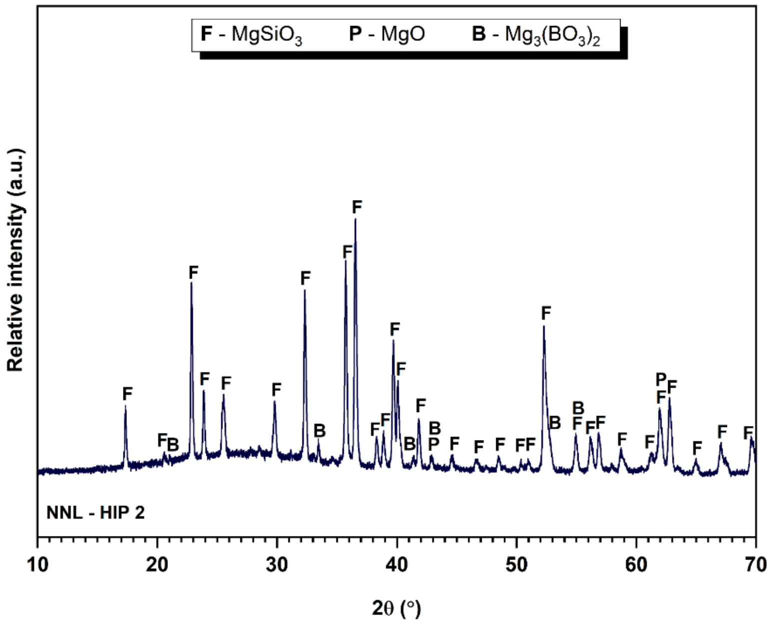 *Figure 59: XRD of NNL-HIP-2* The microstructure of NNL-HIP-2 is shown in Figure 60 and Figure 61, displaying a heterogeneous structure. The pale grey region represents the collapsed clinoptilolite particles. This is postulated due to a strong association of Si, Na and Ca, corresponding to the nominal composition of clinoptilolite; $(Na_{0.5}K_{2.5})(Ca_{1.0}Mg_{0.5})(Al_6Si_{30})O_{72}\cdot 24H_2O$. The darker regions are rich in Si and Mg, likely associated with crystalline forsterite identified via XRD analysis, from reactions between $Mg(OH)_2$ and Si from clinoptilolite. Regions richer in Mg, and deficient in other elements may be magnesium-borate phases, however the resultant x-ray

energies from boron are difficult to detect with conventional SEM-EDX analysis.

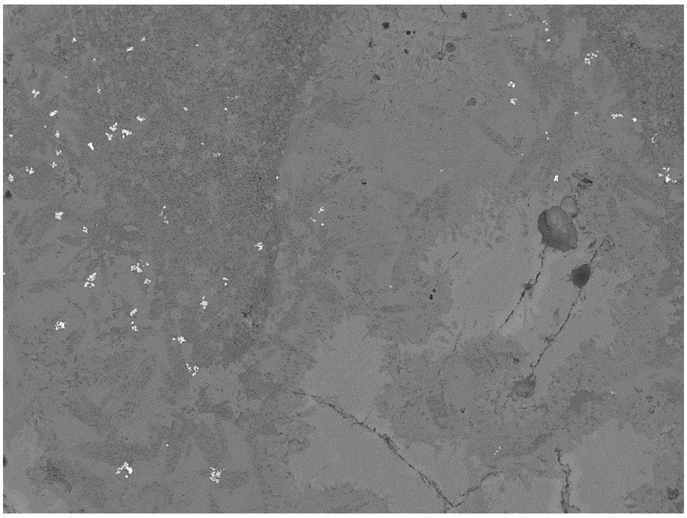

Figure 60 BSE micrograph of NNL-HIP-2 (x100 magnification)

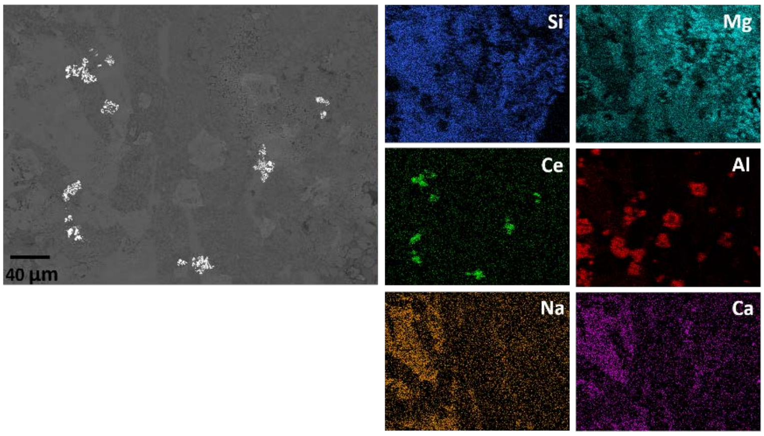

Figure 61: SEM/EDX micrograph of NNL-HIP-2 (x500 magnification)

Chemical composition

Method(s):	☐ EMP ☒ ICP-OES/MS ☒ XRF ☐ Other:
Operating conditions:	A NNL-HIP-2 XRF bead was prepared using bulk powdered sample and a lithium tetraborate flux at a 1:10 sample-to-flux ratio, heated to 1270 °C. This was analyzed using a PANalytical PW2404 spectrometer under vacuum using a Rh X-rays tube. Additionally samples were digested for ICP-OES analysis to determine boron and lithium contents, this was undertaken on a Thermo Iris Advantage ICP.

Chemical composition:

Oxide	Wt.%
Al_2O_3	6.28
B_2O_3	7.73
BaO	<0.10
CaO	0.86
CeO	0.56
Cr_2O_3	<0.10
Fe_2O_3	0.72
K_2O	2.60
La_2O_3	<0.10
Li_2O	<0.01
MgO	33.44
Mn_3O_4	<0.10
Na_2O	5.32
SiO_2	42.12
TiO_2	<0.10
ZnO	<0.10
ZrO_2	<0.10

Table 26: Composition of bulk NNL-HIP-2 by XRF and ICP spectroscopy

Comments and discussion: The XRF/ICP composition is in line with the batch composition, reflecting a fairly high proportion of MgO due to addition of Magnox sludge simulant.

Chemical durability

Method(s):	☒ As described in MS12 Report (p. 12-13), adapted from ASTM C1285 ☐ As described in MS12 Report (p. 14), adapted from ASTM C1220 ☐ Other:
Clarifications:	Sample material was crushed and sieved to 125-250 µm, then washed and prepared as per ASTM C1285. PFA screw-lid pots were used, with 10 ml ASTM Type 1 water and a quantity of sample material to ensure a SA/V of 10 m-1. The surface area / volume was calculated assuming a geometric surface area, as required in ASTM C1285 specifications (with density from helium pycnometry analysis). Static leaching at 90 °C was undertaken for up to 28 days, with duplicate sampling at 1, 3, 7, 14, 21 and 28 days. Sample aliquots were filtered using a 0.2 µm cellulose acetate filter. The aliquot pH was measured using a 3-point calibrated pH probe and then acidified with ultrapure NORMATOM HNO3 and analyzed by ICP-OES (Thermo Fisher iCAP 6300 ICP-OES) and/or ICP-MS (Thermo Scientific iCAP RQ ICP-MS). Normalized mass loss was calculated using compositional data from XRF analysis.
Results and discussion:	

NB: The USFD ISG dissolution results are reported in GeoMelt-Glass 6 characterization test sheet

For the NNL-HIP-2 sample the pH remained fairly consistent throughout the testing at between pH 9.2-9.4 (Figure 62).

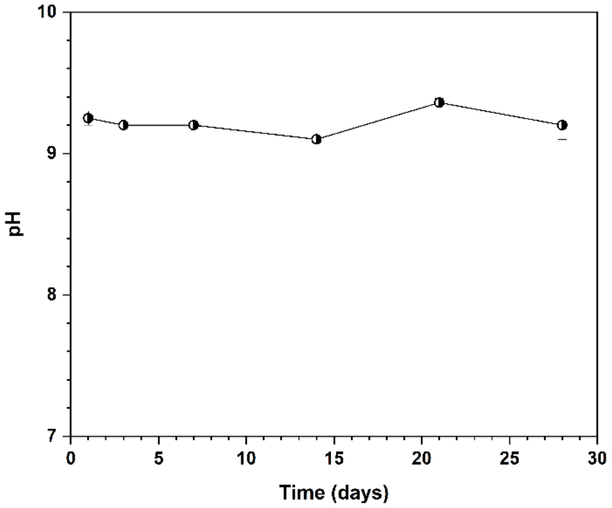

Figure 62: pH of NNL-HIP-2 up to day 28

The chemical durability of NNL-HIP-2 is different to many of the vitrified products, in that there is a high initial release rate detected within the first day. Boron, calcium and sodium elemental mass loss within 1 day (Figure 63 and Figure 64) are all >20 g/m^2. Calcium mass loss reaches a maximum at day 14 before decreasing, while sodium and boron continue to be released into solution, reaching 46 and 50 g/m^2 respectively after 28 days.

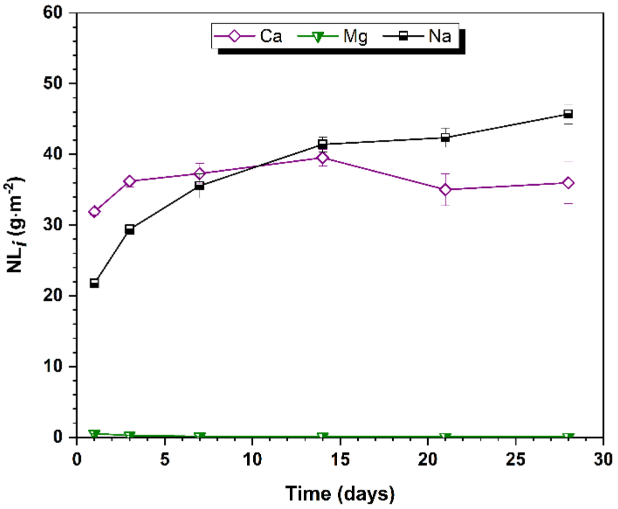

Figure 63: Normalized mass loss of Ca, Mg and Na from NNL-HIP-2, up to day 28

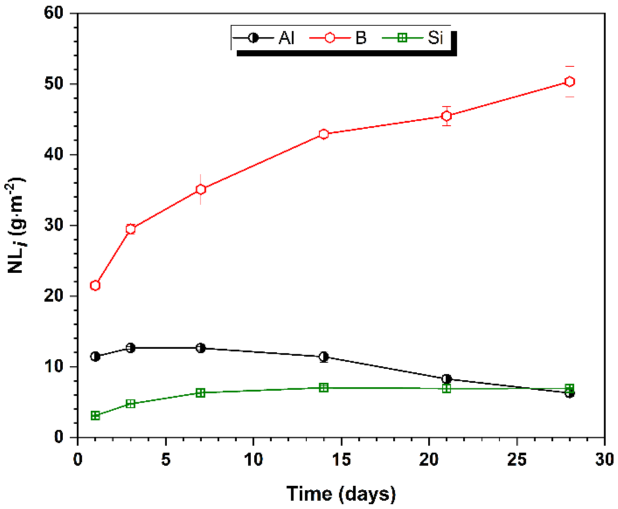

Figure 64: Normalized mass loss of Al, B and Si from NNL-HIP-2, up to day 28

Mg release is very low, varying from 0.5 g/m^2 at day 1 to 0.07 g/m^2 at day 28. Al release also follows a downward trend, while Si release increases a maximum of 6.9 g/m^2 is reached.

Comparison of these values to ISG should be taken with caution given the different compositions and the different nature of these materials (glass compared to multi-phase glass ceramic). Overall normalized boron mass losses are higher in this HIP sample, though silicon mass losses are slightly lower.

Other tests and characterizations

N/A

Conclusions and Outlooks

The thermally treated product presented here has a heterogeneous glass-ceramic microstructure, with CeO_2 present as discrete particles throughout the sample. Simulant waste streams (calcined Magnox sludge and clinoptilolite) have partially, or fully reacted to form constituent phases (either glassy or crystalline), with the borax assisting as a glass former. As such a high waste loading is possible with this thermal treatment.

The chemical durability of this product is equal to, or slightly less durable than ISG, especially if comparing boron release between the samples. Longer term chemical durability tests would be required, combined with surface analysis to determine if dissolution is congruent or phase specific.

4.8 Glass 6 – Geomelt sample (USFD)

General information

Partner:	University of Sheffield (USFD)
Sample id:	GeoMelt-Glass 6
Contact person:	Samuel Walling and Neil Hyatt

Origin and macroscopic description

Figure 65: Photograph of GeoMelt-Glass 6, denoting two phases of interest.

This glassy material is a historic Geomelt sample arising from proof of concept testing in 2009 in which simulated UK intermediate- and low-level wastes were thermally treated with various glass forming materials using the Geomelt In-Container Vitrification (ICV) technology. This trial consisted of a 200 litre melt, using a bottom-up melting process, with simulant materials and glass formers.

The formulation for GeoMelt-Glass 6 was comprised of two components: a plutonium contaminated material (PCM) simulant, and a SIXEP sand/clinoptilolite simulant. These are detailed in Table 27, extracted the from Witwer *et al.* (2010). In addition to the materials listed in the table, stable isotope tracers were added into the feed (Ce, Cs, Sr, Co, Re & Eu)

Staged – PCM Simulant

	Simulant Component	**Mass of Feed (kg)**	**% of Total**
Waste Stream Simulants	Carbon Steel Drum Fragments (representing 200 liter drums)	78.9	23.62
	Stainless Steel (reprensenting 500 liter drums)	7.1	2.13
	Misch Metal (Ce, La, Nd, Pr Mix)	0.49	0.15
	PVC as gloves	24.1	7.22
	Rubber	9.7	2.90
	Polyethylene as polyethylene grocery bags	5.4	1.62
	Portland Cement	18.7	5.60
	Cellulose, Bottle glass, Concrete	27	8.08
Other additives	Local soil and fluxant	163	48.80

	Total	334	100

FWM – SIXEP Magnox Sludge Simulant			
	Simulant Component	**Mass of Feed (kg)**	**% of Total**
Waste Stream Simulants	De-Mineralized Water	63.96	15.05
	Misch Metal (Ce, La, Nd, Pr Mix)	2.93	0.69
	Brucite $Mg(OH)_2$	82.26	19.36
Other additives	Local soil	276.25	65.00
	Total	425	100

Table 27: GeoMelt-Glass 6 composition [Witwer et al., 2010]

The sample used during this study was only a small portion of the overall melt. The sample is glassy with noticeable heterogeneity. Due to the visible heterogeneity of GeoMelt-Glass 6, XRD and SEM analysis was undertaken on both ‘phase 1’, the lighter region of the sample, and also on ‘phase 2’, the darker region. These regions of interest are noted in Figure 65.

For further details on the melt preparation, raw materials and GeoMelt technology, please refer Witwer., et al (2010)..

Microstructure

Method(s):	☒ SEM ☒ XRD ☐ Other:
Operating conditions:	**XRD:** Powdered samples was analyzed using a Bruker D2 PHASER diffractometer with a LYNXEYE detector utilising Cu Kα (λ = 1.5418 Å) radiation, a Ni foil was used to filter the K radiation. The diffraction pattern was collected between 10° < 2θ < 60° with a step size of 0.01° 2θ and dwell time of 1s per step. **SEM:** A Hitachi TM3030 scanning electron microscope coupled with a Bruker Quantax 70 energy dispersive X-ray spectroscopy system (EDX) with a silicon drift detector was used. A sectioned slice containing both phases identified in Glass 6 was mounted in epoxy resin, ground using SiC grit paper, polished to a 1 µm finish using diamond suspensions and carbon coated.
Homogeneity:	Heterogeneous
Free liquid or gas:	Absence

Crystalline composition:	Crystalline and glassy
Comments and discussion:	Crystalline features were identified in both phase 1 and 2 samples for the GeoMelt-Glass 6, as shown in Figure 66. Both diffractions patterns display a diffuse scattering characteriztic of a glassy component, with crystalline reflections from clinoenstatite ($MgSiO_3$) and α-iron. 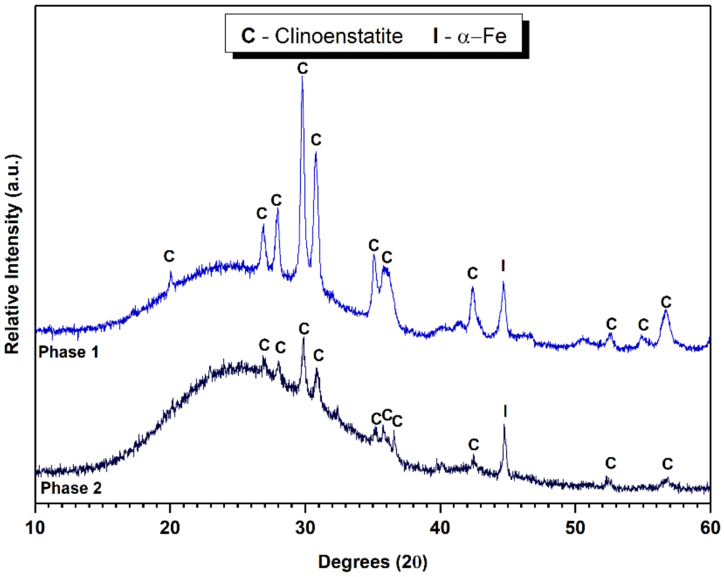 *Figure 66: XRD patterns of GeoMelt-Glass 6, phase 1 and phase 2.* The heterogeneous nature of Glass 6 is confirmed by SEM analysis of phase 1 and phase 2, in Figure 67 - Figure 70 respectively. In Figure 68, regions of crystalline magnesium silicate were clearly visible by the distinct dendritic crystals. In Figure 70, the darker regions appeared slightly enriched in magnesium, which could represent clinoenstatite as there were no discernable crystalline features at this level of magnification (albeit the same magnification as phase 1, Figure 68). Both phases consist largely of glassy regions rich in Ca, Al and Si. Equally both were observed to contain droplets of iron within the glassy matrix (Figure 67 - Figure 70).

	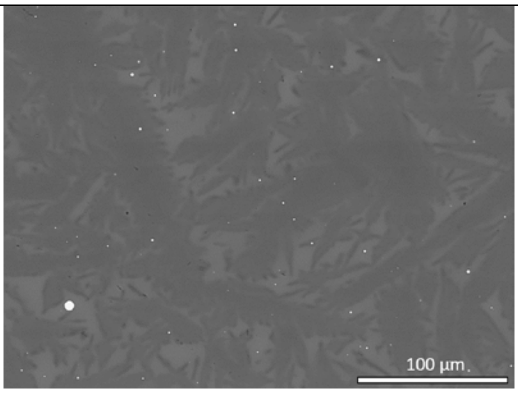 *Figure 67: BSE micrograph of GeoMelt-Glass 6, phase 1.* 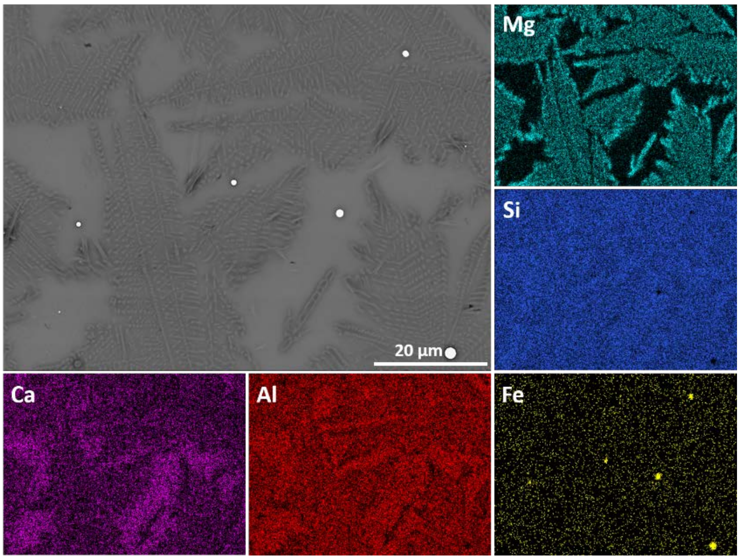 *Figure 68: SEM/EDX of GeoMelt-Glass 6, phase 1.* 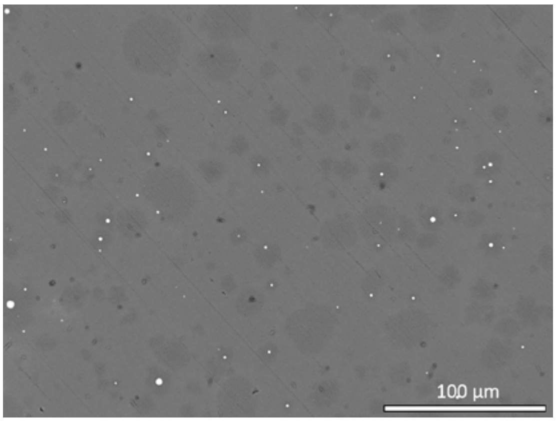 *Figure 69: BSE micrograph of GeoMelt-Glass 6, phase 2.*

	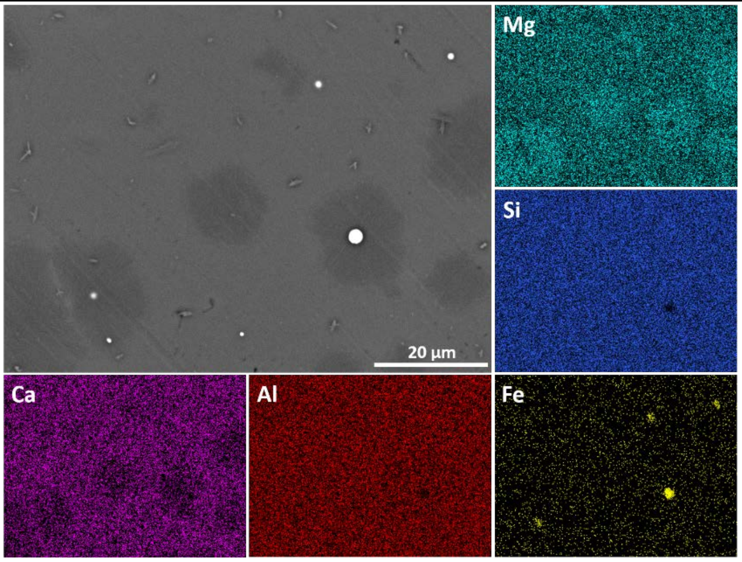 *Figure 70: SEM/EDX of GeoMelt-Glass 6, Phase 2.*
Chemical composition	
Method(s):	☐ EMP ☒ ICP-OES/MS ☒ XRF ☐ Other:
Operating conditions:	A GeoMelt-Glass 6 XRF bead was prepared using bulk powdered sample and a lithium tetraborate flux at a 1:10 sample-to-flux ratio, heated to 1270 °C. This was analyzed using a PANalytical PW2404 spectrometer under vacuum using a Rh X-rays tube. Additionally samples were digested for ICP-OES analysis to determine boron and lithium contents, this was undertaken on a Thermo Iris Advantage ICP.

Chemical composition:

Oxide	Wt.%
Al_2O_3	12.90
B_2O_3	0.03
BaO	0.10
CaO	5.56
CeO	0.50
Cr_2O_3	<0.10
Fe_2O_3	0.66
K_2O	1.40
La_2O_3	0.26
Li_2O	0.01
MgO	12.24
Mn_3O_4	0.24
Na_2O	6.08
SiO_2	61.08
TiO_2	0.92
ZnO	<0.10
ZrO_2	<0.10

Table 28: Composition of bulk GeoMelt-Glass 6 by XRF spectroscopy.

Comments and discussion:

XRF analysis has determined that SiO2 + Al2O3 >70 wt.%, combined with a lower alkali content, could help impart durability to these samples. Compared to ISG glass, this has a higher Al2O3 content, and a very high MgO component. Unlike ISG and many nuclear glasses however, the boron content is very low, which will make comparison of durability more complicated as boron is typically used as an indicator of dissolution.

Chemical durability

Method(s):

☒ As described in MS12 Report (p. 12-13), adapted from ASTM C1285
☐ As described in MS12 Report (p. 14), adapted from ASTM C1220
☐ Other:

Clarifications:

Sample material was crushed and sieved to 125-250 µm, then washed and prepared as per ASTM C1285. PFA screw-lid pots were used, with 10 ml ASTM Type 1 water and a quantity of sample material to ensure a SA/V of 10 m^{-1}. The surface area / volume was calculated assuming a geometric surface area, as required in ASTM C1285 specifications (with density from helium pycnometry analysis). Static leaching at 90 °C was undertaken for up to 28 days, with duplicate sampling at 1, 3, 7, 14, 21 and 28 days.

Sample aliquots were filtered using a 0.2 µm cellulose acetate filter. The aliquot pH was measured using a 3-point calibrated pH probe and then acidified with ultrapure NORMATOM HNO_3 and analyzed by ICP-OES

	(Thermo Fisher iCAP 6300 ICP-OES) and/or ICP-MS (Thermo Scientific iCAP RQ ICP-MS). Normalized mass loss was calculated using compositional data from XRF analysis.
Results and discussion:	Alongside these data, the chemical durability of ISG glass is also presented in Figure 71 and Figure 72. These data were collected and analysed using the same conditions, in order to compare between the sample in this study and the representative International simplified nuclear waste glass surrogate. Data for GeoMelt-Glass 6 are detailed in Figure 72, Figure 73 and Figure 74. The pH of the ISG leaching solution at day 1 begins at ~9.2 and increased to ~9.4 after 28 days leaching. This is likely due to the initial ion exchange of alkalis into the water increasing the pH, though the low SA/V tested does not permit pH levels to raise significantly. 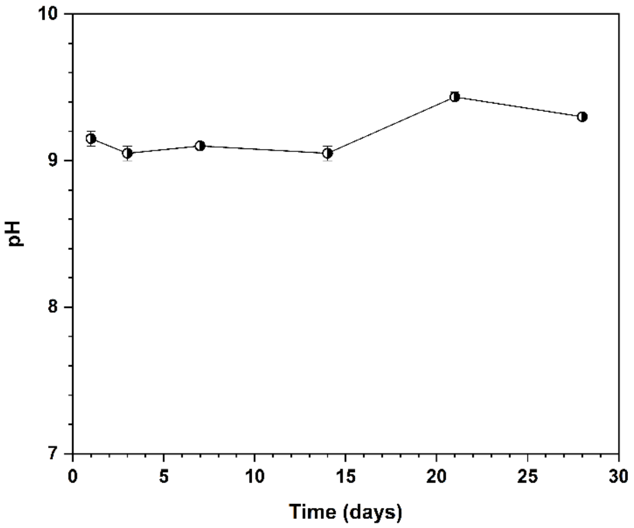 *Figure 71: pH of ISG up to day 28*

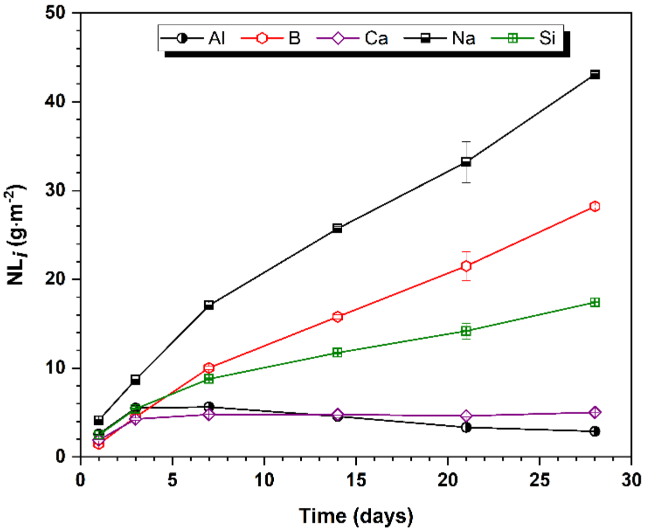

Figure 72: Normalized mass loss of Al, B, Ca, Ca, Na and Si from ISG, up to day 28

Sodium and boron release continues steadily from day 1 to day 28 with little change in release rate, reaching 43 and 28 g/m^2 respectively. Silicon release reaches 17 g/m^2, while both calcium and aluminium reach 5 and 2.9 g/m^2 respectively at the end of testing. The low release of Ca and Al likely indicate the precipitation of secondary products, which is supported by the absence of Zr (known to participate in alteration layers), which was below the limits of detection for the ICP.

The ISG elemental release and pH in Figure 71 and Figure 72 are higher than those determined by other institutions, due to varied experimental conditions. The experiments undertaken at USFD determined the quantity of glass in each leach vessel by geometric surface area and sample density (as specified in ASTM C1285), rather than using BET, which is known to over-estimate the surface area of crushed glasses. As such these data result in a higher pH due to more material being leached, which results in a lower durability compared to other studies due to the pH dependence of silica dissolution.

All chemical durability undertaken by USFD use the same geometric area setup methodology, therefore the data are directly comparable to the ISG data above.

For GeoMelt-Glass 6, the solution pH increased from 8.2 to 9.0 within the first 7 days, then slowly increased to pH ~9.2 up to day 28 (Figure 73). This is accompanied with continual release of Ca and Na (Figure 74), resulting in a normalized mass loss for sodium of 9.25 g/m^2 after 28 days leaching. Silicon release at 28 days is 5.6 g/m^2, therefore both Na and Si release were substantially lower than that of ISG after 28 days, indicating GeoMelt-Glass 6 has a higher durability over this timeframe.

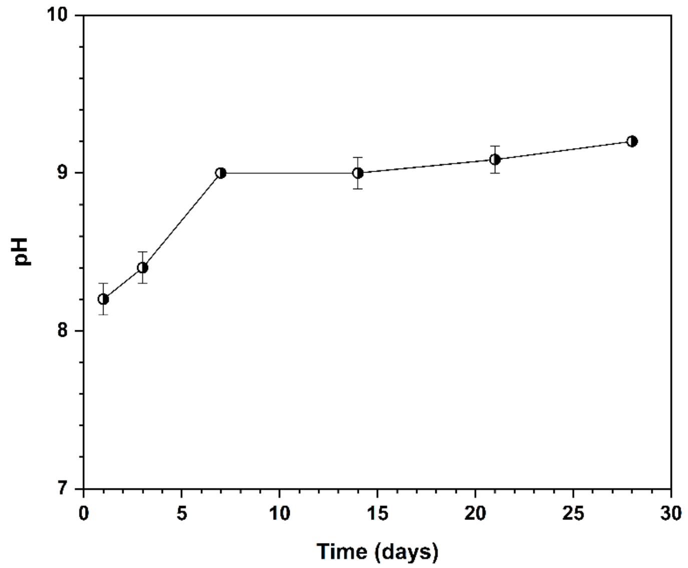

Figure 73: pH of GeoMelt-Glass 6 up to day 28

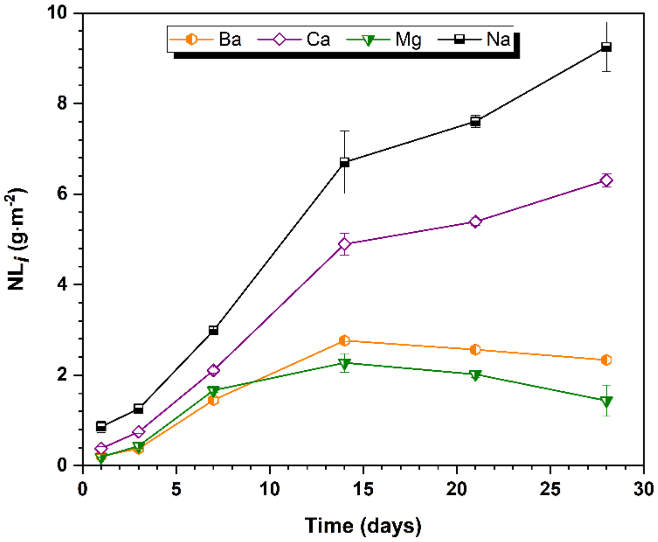

Figure 74: Normalized mass loss of Ba, Ca, Mg and Na from GeoMelt-Glass 6 up to day 28

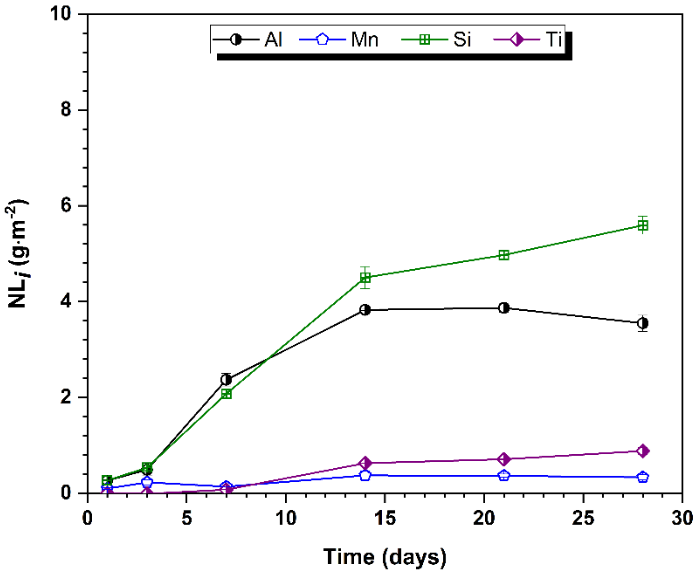

Figure 75: Normalized mass loss of Al, Mn, Si and Ti from GeoMelt-Glass 6, up to day 28

Al, Ba, and Mg release all begin to level off then decrease after 14 days leaching (Figure 74 and Figure 75). This may be indicative of secondary product formation, or perhaps reduced solubility in a slowly increasing pH environment.

Other tests and characterizations

N/A

Conclusions and Outlooks

This sample produce via the GeoMelt ICV method is a glassy heterogeneous material, largely containing substituted magnesium silicate crystals within a Ca, Al Si rich glassy matrix. Chemical durability over a 28 day timeframe is superior to that of ISG, though data suggest continued dissolution is continuing to occur suggesting longer term dissolution data could be required.

4.9 Glass 12 – Geomelt sample (USFD)

General information

Partner:	University of Sheffield (USFD)
Sample id:	GeoMelt-Glass 12
Contact person:	Samuel Walling and Neil Hyatt

Origin and macroscopic description

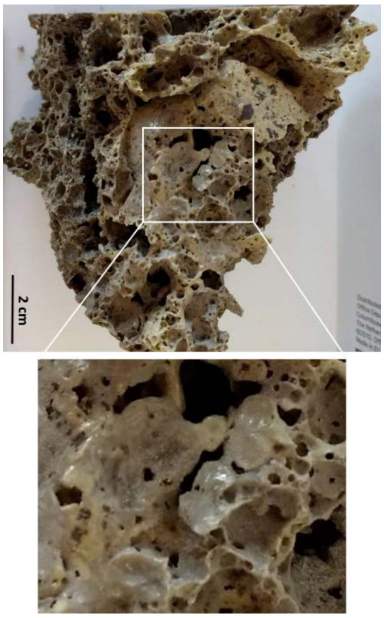

Figure 76: Top surface – denoted 'Phase 1

This glassy material is a historic GeoMelt sample arising from proof of concept testing in 2009 in which simulated UK intermediate- and low-level wastes were thermally treated with various glass forming materials using the GeoMelt In-Container Vitrification (ICV) technology. This trial consisted of a 200 litre melt, using a top-down batch approach, with simulant materials and glass formers.

The formulation for this GeoMelt-Glass 12 was comprised of two components: a pile fuel cladding silo simulant, and a SIXEP sand/clinoptilolite simulant. These are detailed in Table 29, extracted from Witwer., et al (2010). In addition to the materials listed, stable isotope tracers were added into the feed (Ce, Cs, Sr, Co, Re & Eu).

The sample used during this study was only a small portion of the overall melt. The sample is heterogeneous, with a high porosity and with noticeable crystalline features, as shown in Figure 76 and Figure 77. Due to the heterogeneity of the sample, XRD and SEM analysis was undertaken on both 'phase 1', a lighter section of the sample, and on 'phase 2', a more crystalline component which consists of the bulk sample.

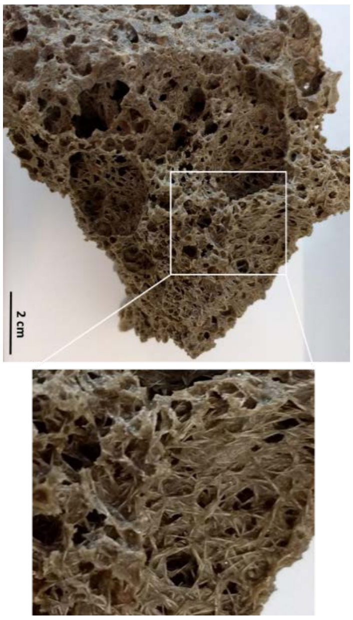

Pile Fuel Cladding Silo Simulant		
Simulant Component	**Mass of Feed (kg)**	**% of Total**
C- Graphite	13.5	3.31
$CaCO_3$ - Limestone	5.5	1.35
Fe - Steel	14.8	3.63
Mg – metal (rods)	16.0	3.93
$Mg(OH)_2$ - Brucite	4.3	1.06
Al_2O_3 - Alumina	4.3	1.06
Cellulose – Trial 1 Recycled HEPA and scurbfilter	2.2	0.54
Hydraulic Oil	0.3	0.07
SubTotal	61	15

Figure 77: Bottom surface – denoted 'Phase 2'

SIXEP Sand/Clinoptilolite Simulant		
Simulant Component	**Mass of Feed (kg)**	**% of Total**
De-Mineralized Water	34.1	8.37
Clinoptilolite	42.4	10.41
Silica Sand	10.5	2.58
Misch Metal (Ce, La, Nd, Pr Mix)	0.8	0.20
$Mg(OH)_2$ - Brucite	4.0	0.98
Al_2O_3 - Alumina	0.1	0.02
CaO - Quicklime	0.4	0.10
Fe2O3 - Hematite	0.1	0.02
Na2CO3 – Sodium Carbonate / Soda Ash	0.2	0.05
K2O - Potash	0.2	0.05
Sub-Total	92.2	23
Soil / Hematite Glass Forming Additives		
Additives	253.55	62
Final Total	407.25	100

Table 29: GeoMelt-Glass 12 composition [Witwer et al., 2010].

For further details on the melt preparation, raw materials and GeoMelt technology, please refer Witwer. *et al*. (2010)

Microstructure

Method(s):	☒ SEM ☒ XRD ☐ Other:
Operating conditions:	**XRD:** Powdered samples was analyzed using a Bruker D2 PHASER diffractometer with a LYNXEYE detector utilising Cu Kα (λ = 1.5418 Å) radiation, a Ni foil was used to filter the K radiation. The diffraction pattern was collected between 10° < 2θ < 60° with a step size of 0.01° 2θ and dwell time of 1s per step. **SEM:** A Hitachi TM3030 scanning electron microscope coupled with a Bruker Quantax 70 energy dispersive X-ray spectroscopy system (EDX) with a silicon drift detector was used. Sectioned slices of the Glass 12 (phase 1 and phase 2) were mounted in epoxy resin, ground using SiC grit paper, polished to a 1 µm finish using diamond suspensions and carbon coated.
Homogeneity:	Heterogeneous
Free liquid or gas:	Absence
Crystalline composition:	Crystalline and glassy

Comments and discussion:	Crystalline features were identified in both phase 1 and 2 samples for the GeoMelt-Glass 12. Phase 1 is comprised predominantly of forsterite (Mg_2SiO_4), which is likely iron substituted, as observed in Figure 78. In addition, reflections associated with enstatite and clinoenstatite ($MgSiO_3$) were identified. The phase assemblage of phase 2 consisted of both enstatite and clinoenstatite (both $MgSiO_3$), with α-iron and minor contributions from forsterite. 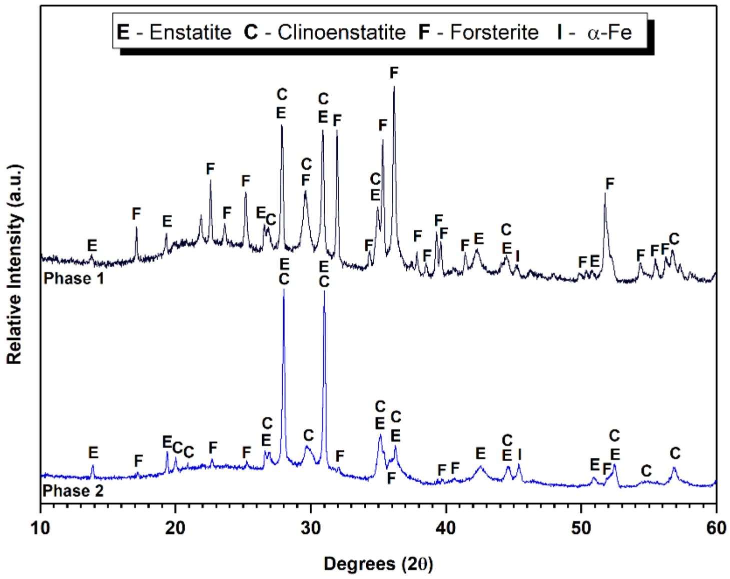 *Figure 78: XRD patterns of GeoMelt-Glass 12, phase 1 and phase 2* The heterogeneous nature of Glass 12 was confirmed by SEM analysis of phase 1 and phase 2. Figure 79 - Figure 82 highlight the presence of crystalline features embedded within a glassy matrix. Figure 80 exhibits crystalline striations running through the glass phase, rich in Mg and Fe, which support the XRD identification of an iron-substituted forsterite. Phase 2 was found to consist of two distinct crystalline features (needles and angular crystals), of which at least one is a magnesium silicate. Also observed in Phase 2 were metallic iron droplets (Figure 81 and Figure 82). Within both phases the glass appears enriched in Ca, Al and Si. This is likely to contribute positively towards wasteform chemical durability.

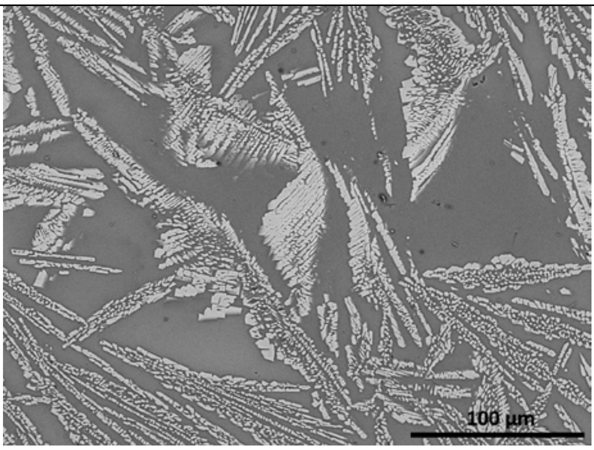

Figure 79: BSE micrograph of GeoMelt-Glass 12, phase 1

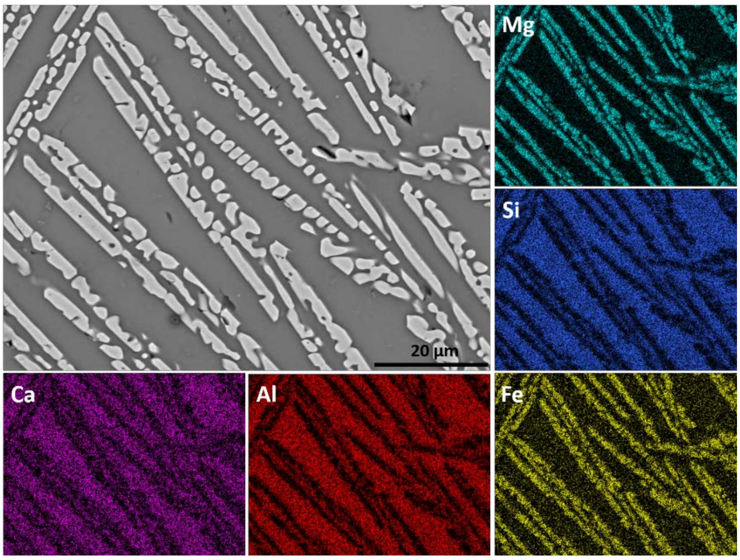

Figure 80: EM/EDX of GeoMelt-Glass 12 phase 1

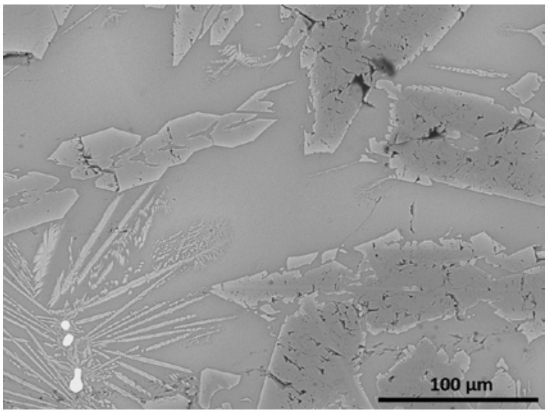

Figure 81: BSE micrograph of GeoMelt-Glass 12, phase 2

	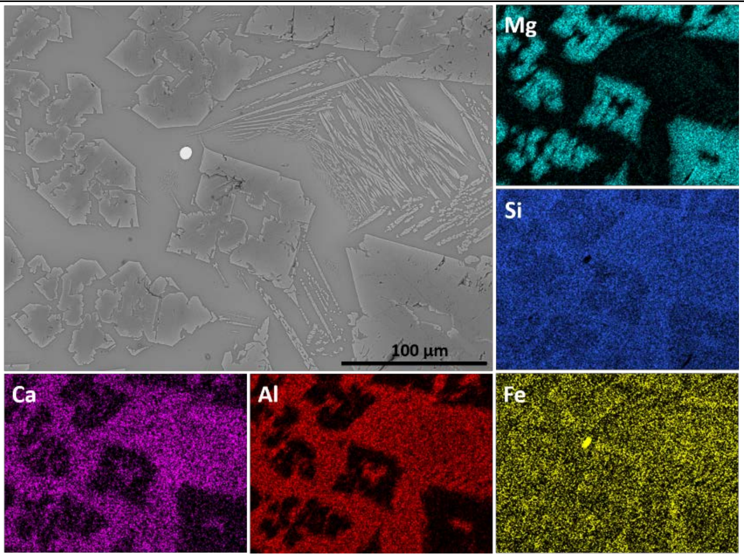 *Figure 82: SEM/EDX of GeoMelt-Glass 12 phase 2*

Chemical composition

Method(s):	☐ EMP ☒ ICP-OES/MS ☒ XRF ☐ Other:
Operating conditions:	A GeoMelt-Glass 12 XRF bead was prepared using bulk powdered sample and a lithium tetraborate flux at a 1:10 sample-to-flux ratio, heated to 1270 °C. This was analysed using a PANalytical PW2404 spectrometer under vacuum using a Rh X-rays tube. Additionally samples were digested for ICP-OES analysis to determine boron and lithium contents, this was undertaken on a Thermo Iris Advantage ICP.
Chemical composition:	

Oxide	Wt.%
Al_2O_3	11.94
B_2O_3	0.02
BaO	<0.10
CaO	2.76
CeO	0.28
Cr_2O_3	<0.10
Fe_2O_3	17.92
K_2O	1.3
La_2O_3	0.14
Li_2O	0.01
MgO	11.94
Mn_3O_4	0.16
Na_2O	1.28
SiO_2	58.58
TiO_2	0.40
ZnO	<0.10
ZrO_2	<0.10

Table 30: Composition of bulk GeoMelt-Glass 12 by XRF spectroscopy.

Comments and discussion:	XRF analysis has determined that the combined SiO_2 + Al_2O_3 content is ~64%, along with high contents of MgO and Fe_2O_3, though low overall alkali content. This composition is therefore quite different from ISG and likely to perform differently under aqueous leaching conditions

Chemical durability

Method(s):	☒ As described in MS12 Report (p. 12-13), adapted from ASTM C1285 ☐ As described in MS12 Report (p. 14), adapted from ASTM C1220 ☐ Other:
Clarifications:	Sample material was crushed and sieved to 125-250 µm, then washed and prepared as per ASTM C1285. PFA screw-lid pots were used, with 10 ml ASTM Type 1 water and a quantity of sample material to ensure a SA/V of 10 m^{-1}. The surface area / volume was calculated assuming a geometric surface area, as required in ASTM C1285 specifications (with density from helium pycnometry analysis). Static leaching at 90 °C was undertaken for up to 28 days, with duplicate sampling at 1, 3, 7, 14, 21 and 28 days. Sample aliquots were filtered using a 0.2 µm cellulose acetate filter. The aliquot pH was measured using a 3-point calibrated pH probe and then acidified with ultrapure NORMATOM HNO_3 and analyzed by ICP-OES (Thermo Fisher iCAP 6300 ICP-OES) and/or ICP-MS (Thermo Scientific iCAP RQ ICP-MS). Normalized mass loss was calculated using compositional data from XRF analysis.

Results and discussion:

NB: The USFD ISG dissolution results are reported in GeoMelt-Glass 6 characterization test sheet

For the GeoMelt-Glass 12, initially a pH 7.7 was achieved after day 1, which increased to a maximum of pH 8.8 at day 14, before dropping to pH 8.6 by day 28 (Figure 83). This is a lower pH than achieved with the ISG glass, likely due to a lower total of alkali elements within this glass.

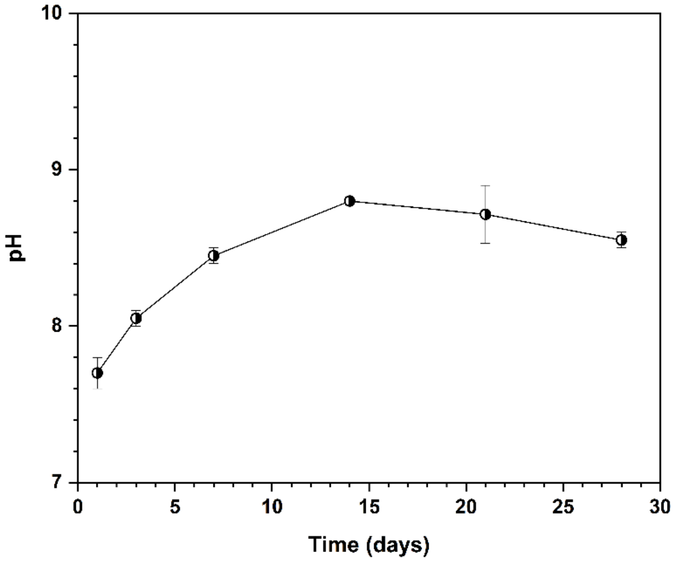

Figure 83: pH of GeoMelt-Glass 12 up to day 28

Normalized mass losses for elements in Figure 84 and Figure 85 show an upward trend for Na and Ca towards day 28 leaching, with losses of 8.6 g/m^2 and 5.8 g/m^2 for Na and Ca, respectively. Due to the lack of boron in these samples, comparing Na release rates to ISG after 28 days (43 g/m^2), this material appears to perform better over this timeframe.

Both Al and Si release reach a maximum at day 21, dropping to 4.8 g/m^2 and 3.5 g/m^2 respectively at day 28 leaching. Silicon release, indicative of structural glass dissolution is lower than ISG (17.4 g/m^2 at day 28), though the turnover of both Al and Si mass losses suggests the formation of secondary precipitates / alteration layers.

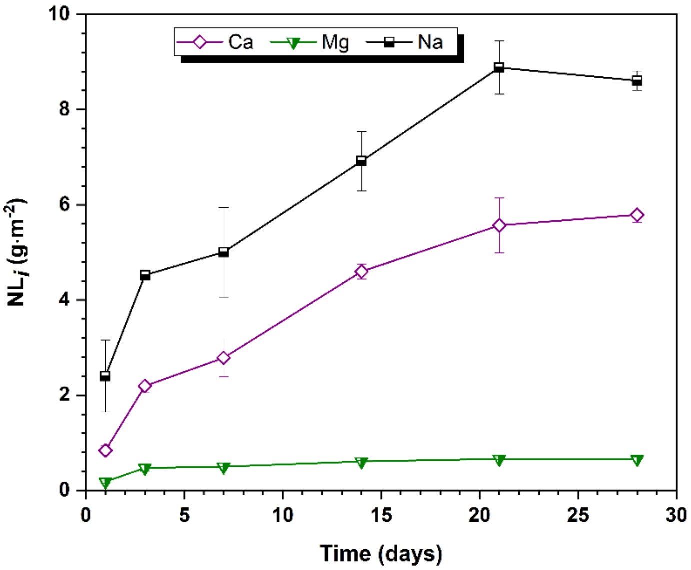

Figure 84: Normalized mass loss of Ca, Mg and Na from GeoMelt-Glass 12, up to day 28

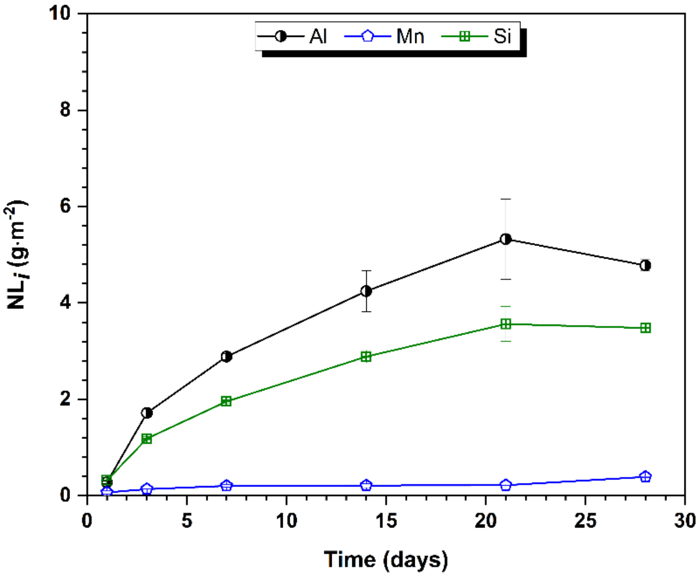

Figure 85: Normalized mass loss of Al, Mn and Si from GeoMelt-Glass 12, up to day 28

Other tests and characterizations

N/A

Conclusions and Outlooks

This sample produce via the GeoMelt ICV method is a highly heterogeneous glassy product, largely containing substituted magnesium silicate crystals within a glass matrix, itself enriched in Ca, Al and Si.

Chemical durability over a 28 day timeframe shows superior performance to ISG, although durability is more difficult to assess given the absence of boron within these samples. A reduction in the mass losses of both silicon and aluminium suggests the formation of precipitates on the glass during dissolution, and as such the effect of these on the longer term durability would need assessing.

4.10 Plasma vitrified PCM – cold crucible sample (USFD)

General information

Partner:	University of Sheffield (USFD)
Sample id:	Plasma Vitrified PCM
Contact person:	Samuel Walling and Neil Hyatt

Origin and macroscopic description

Figure 86: Photograph of PCM 54.1% sample

Figure 87: Photograph of PCM 54.1% sample

This sample is part of a historic demonstration of plasma vitrification for plutonium contaminated material [1], which contain quantities of masonry, steel, aluminium and plastic materials. The melt was undertaken using a twin torch plasma melter, and a water cooled cold crucible. The temperature of the melt was kept at ~1500 °C, enabling destruction of organic materials and the formation of a glassy slag [Hyatt *et al.*, 2007].

This specific glass was formulated to target a 54.1 wt.% PCM waste loading (using a CeO_2 spike as a PuO_2 surrogate), as detailed below in Table 31. The PCM simulant was mixed with glass forming additives consisting of (by wt. %): 29.2 % CaO, 27.7 % Al_2O_3 and 43.1 % SiO_2.

Component	Wt %
Aluminium	10
Carbon steel	28
Stainless steel	5
Soda-lime glass	2.5
HLW glass	2.5
Masonry – concrete	6
Masonry - tiles	3
Soil	5
Calcium fluoride	1
Corn cob	3
Polyethylene	12
Polyvinyl chloride	18
Polystyrene	4
Total	100
Plus 1% CeO_2 spike = 1.25 wt.%	

Table 31: Composition of PCM waste [Hyatt *et al.*, 2007].

	The sample appears glassy and black, as noted in Figure 86 and Figure 87, though heterogeneous with some open porosity.

Microstructure

Method(s):	☒ SEM ☒ XRD ☐ Other:
Operating conditions:	**XRD:** A powdered sample was analyzed using a Bruker D2 PHASER diffractometer with a LYNXEYE detector utilising Cu Kα (λ = 1.5418 Å) radiation, a Ni foil was used to filter the K radiation. The diffraction pattern was collected between 10° < 2θ < 70° with a step size of 0.01° 2θ and dwell time of 1s per step. **SEM:** A Hitachi TM3030 scanning electron microscope coupled with a Bruker Quantax 70 energy dispersive X-ray spectroscopy system (EDX) with a silicon drift detector was used. The sample was sectioned into a monolith, mounted in epoxy resin, ground using SiC grit paper, polished to a 1 µm finish using diamond suspensions and carbon coated.
Homogeneity:	Heterogeneous
Free liquid or gas:	Absence
Crystalline composition:	Semi-crystalline glass
Comments and discussion:	XRD analysis identified various crystalline phases present with the PCM 54.1 wt.% wasteform, along with diffuse scattering indicative of a glassy structure. A spinel structure ((Mg,Fe)(Fe,Cr,Al)$_2$O$_4$) is noted, in addition to corundum (Al$_2$O$_3$), mullite (Al$_6$Si$_2$O$_{13}$) and anorthite (CaAl$_2$Si$_2$O$_8$) as shown in Figure 88. 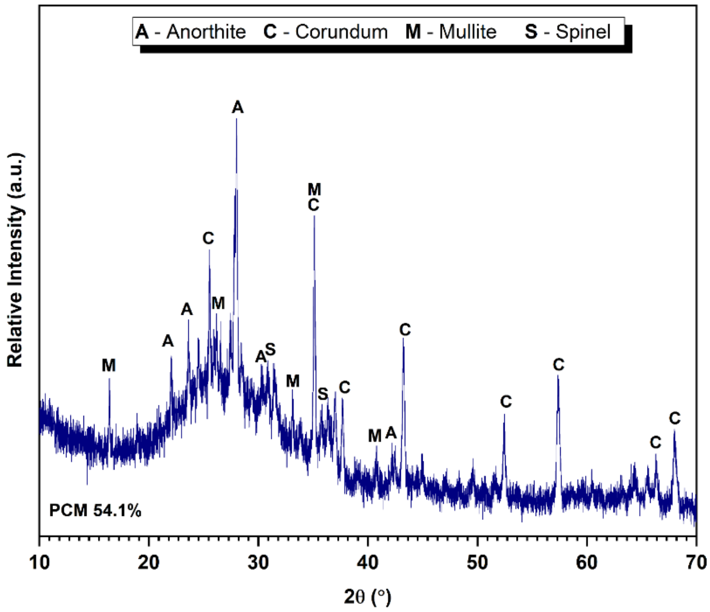 *Figure 88: XRD of PCM 54.1 wt.%* The PCM 54.1 wt.% wasteform is a slag-like glassy material with various crystalline components incorporated. Figure 89 and Figure 90 demonstrate crystalline and heterogeneous

features within an iron rich calcium aluminosilicate glass. A region rich in Al and Cr is likely a crystalline spinel, as also identified with XRD (Figure 88).

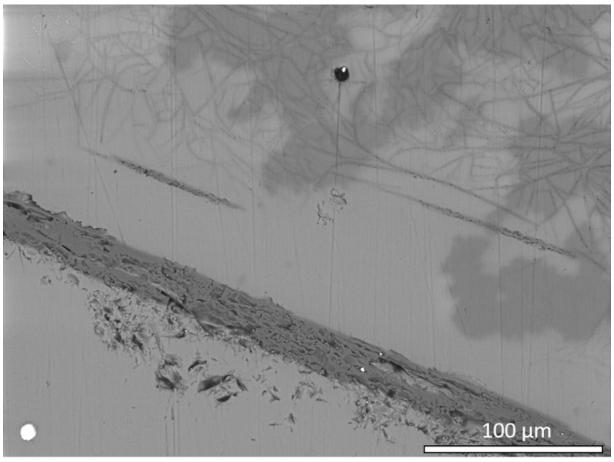

Figure 89: BSE micrograph of PCM 54.1 wt.% glass

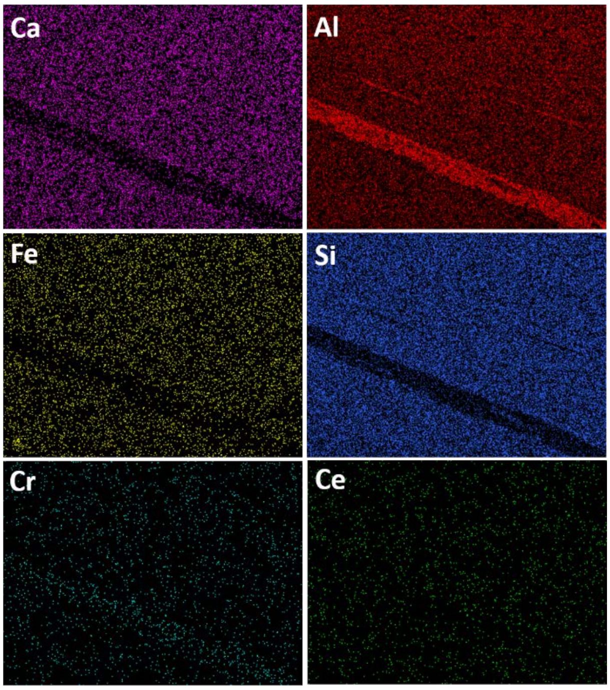

Figure 90: EDX maps of PCM 54.1 wt.% glass

Chemical composition

Method(s):	☐ EMP ☒ ICP-OES/MS ☒ XRF ☐ Other:
Operating conditions:	A Plasma Vitrified PCM XRF bead was prepared using bulk powdered sample and a lithium tetraborate flux at a 1:10 sample-to-flux ratio, heated to 1270 °C. This was analysed using a PANalytical PW2404 spectrometer under vacuum using a Rh X-rays tube. Additionally samples were digested for ICP-OES analysis to determine boron and lithium contents, this was undertaken on a Thermo Iris Advantage ICP.

Chemical composition:	see table below

Oxide	Wt.%
Al_2O_3	40.48
B_2O_3	0.21
BaO	<0.10
CaO	11.34
CeO	0.90
Cr_2O_3	0.94
Fe_2O_3	11.42
K_2O	0.12
La_2O_3	<0.10
Li_2O	0.07
MgO	0.20
Mn_3O_4	0.32
Na_2O	0.76
SiO_2	35.08
TiO_2	0.30
ZnO	<0.10
ZrO_2	<0.10

Table 32: Composition of bulk Plasma Vitrified PCM by XRF and ICP spectroscopy

Comments and discussion:	XRF analysis has determined that SiO_2 + Al_2O_3 >75 wt.%, combined with a fairly lower alkali content could help impart durability to these samples. Aluminium, silicon, calcium and iron oxides make up the majority of this sample, with minor other contributions

Chemical durability

Method(s):	☒ As described in MS12 Report (p. 12-13), adapted from ASTM C1285 ☐ As described in MS12 Report (p. 14), adapted from ASTM C1220 ☐ Other:
Clarifications:	Sample material was crushed and sieved to 125-250 µm, then washed and prepared as per ASTM C1285. PFA screw-lid pots were used, with 10 ml ASTM Type 1 water and a quantity of sample material to ensure a SA/V of 10 m^{-1}. The surface area / volume was calculated assuming a geometric surface area, as required in ASTM C1285 specifications (with density from helium pycnometry analysis). Static leaching at 90 °C was undertaken for up to 28 days, with duplicate sampling at 1, 3, 7, 14, 21 and 28 days. Sample aliquots were filtered using a 0.2 µm cellulose acetate filter. The aliquot pH was measured using a 3-point calibrated pH probe and then acidified with ultrapure NORMATOM HNO_3 and analyzed by ICP-OES (Thermo Fisher iCAP 6300 ICP-OES) and/or ICP-MS (Thermo Scientific iCAP RQ ICP-MS). Normalized mass loss was calculated using compositional data from XRF analysis.

Results and discussion:	*NB: The USFD ISG dissolution results are reported in GeoMelt-Glass 6 characterization test sheet* The pH of the Plasma Vitrified PCM sample (Figure 91) starts at pH 8.7 after day 1, increasing to to pH 9 after day 28 leaching. This is accompanied by a high initial normalized mass loss for Na (8.2 g/m^2, Figure 92), although due to the low content of Na_2O within this glass the absolute levels of Na in the leachate remain low. 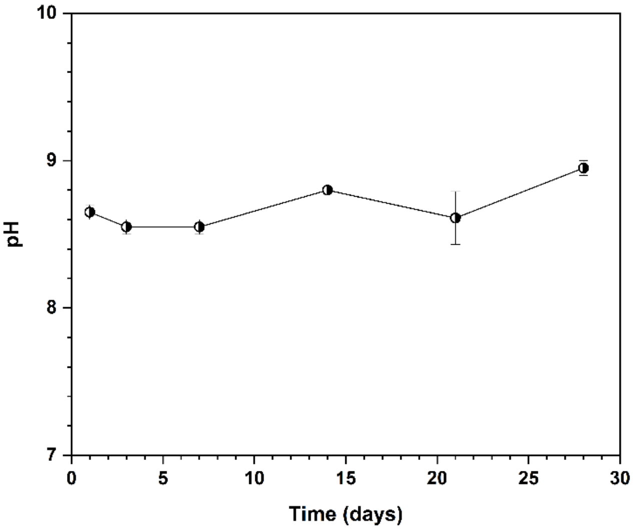 *Figure 91: pH of Plasma Vitrified PCM up to day 28* 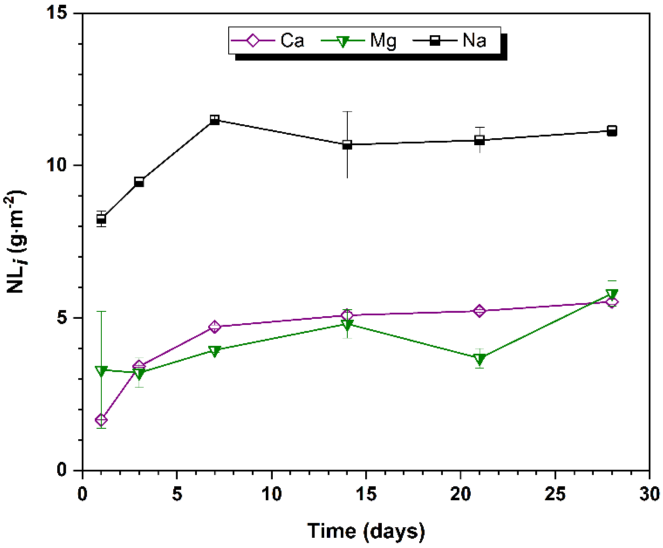 *Figure 92: Normalized mass loss of Ca, Mg and Na from Plasma Vitrified PCM, up to day 28* The structural elements, Al and Si reach a maximum at day 28 (Figure 93), with 2.6 g/m^2 and 4.8 g/m^2 respectively. The release trend is increasing, though at a very slow rate, with

both lower values than reported for ISG (2.9 g/m^2 and 17.4 g/m^2 for Al and Si, respectively). Neither Si, Al nor Ca normalized mass losses decreased by day 28, suggesting there has not yet been a step change associated with precipitation products, though further characterization would be necessary.

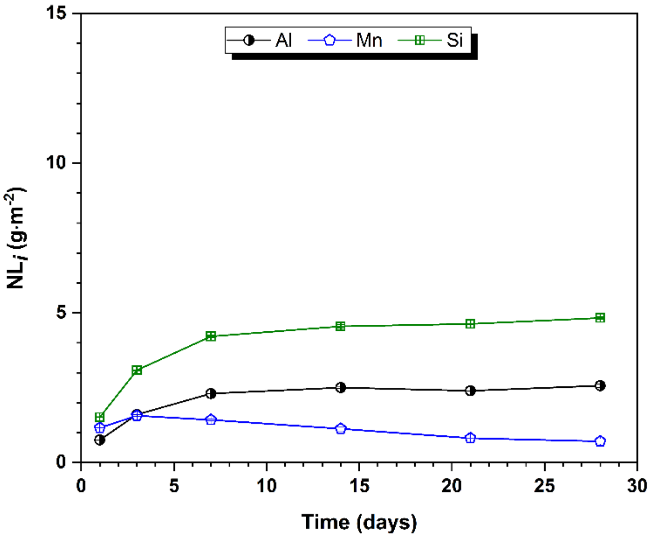

Figure 93: Normalized mass loss of Al, Mn and Si from Plasma Vitrified PCM, up to day 28

Other tests and characterizations

N/A

Conclusions and Outlooks

This plasma vitrified material presents a largely glassy structure, with some crystalline features. Simulant plutonium material, added as CeO_2 partitioned into the glass. A high waste loading (54.1 wt.%) was achieved, which would likely achieve a considerable volume consolidation for these materials.

The chemical durability of this material appears to be good, resulting in lower normalized mass losses for silicon and aluminium than for ISG. Due to the lack of boron in this material, and the low levels of sodium, there are fewer elements to compare between these samples to assess durability. Overall however, this material performs well, with longer-term leaching suggested to determine if these dissolution rates continue at a low level, or change over a longer timeframe.

4.11 HIP-Ce sample (USFD)

General information

Partner:	University of Sheffield (USFD)
Sample id:	HIP-USFD-Ce
Contact person:	Samuel Walling and Neil Hyatt

Origin and macroscopic description

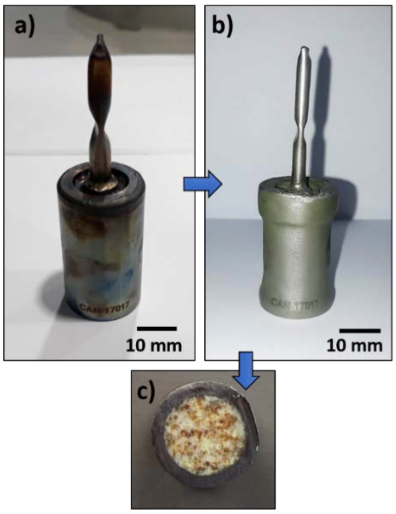

Figure 94: Photographs of a) pre-HIP can, b) post-HIP can and c) sectioned HIP can

For more information, refer to report THERAMIN D3.6.

Hot isostatic pressing (HIPing) as a thermal treatment method was used during THERAMIN WP3 to develop wasteforms for further characterization. The HIP at USFD is the only designated HIP in the UK for the processing of radioactive samples. This is achieved by using an active furnace isolation chamber (AFIC) developed by American Isostatic Press, GeoRoc Ltd and 8 AMEPT. The AFIC system facilitates the processing of single straight-walled HIP canisters using multiple filters in a lock and seal chamber, which prevents contamination of the HIP in the event of a canister breach during processing.

The wasteform in this study was co-mixed containing both simulant calcined Magnox sludge simulant (CMgS) and Cs-exchanged clinoptilolite, an aluminosilicate zeolite. MW ½ Li frit glass (a simple sodium lithium borosilicate glass) was added to help the formation of a glassy wasteform. The raw inactive materials were prepared and provided by the National Nuclear Laboratory. The batch composition is detailed in Tables 1-2.

HIP-USFD-Ce (Can No. 17017)	
CMgS (g)	16.57
MW ½ Li (g)	5.03
Clino (g)	28.12
CeO_2 (g)	0.30
Waste loading (wt. %)	89.9
MW ½ Li glass frit	
SiO_2	63.4
B_2O_3	22.5
Na_2O	11.4
Li_2O	2.7

Table 33: Composition for HIP-USFD-Ce and glass frit.

	Pre-conditioning of the wastes included calcination at 950 °C for 3 hours to remove bound water (performed by NNL for inactive components). The sample was packed into a straight-walled HIP canister using a hydraulic press to improve the packing density. The lid was welded into place, the can was evacuated (until a vacuum of <8 Pa was achieved) and then exposed to temperature (600 °C) whilst under vacuum to remove any remaining water from the sample. Once the vacuum recovered, the evacuation tube was crimped twice and welded to create a fully sealed wasteform ready for HIPing. This sample is also labelled as HIP can 17017 in report THERAMIN D3.6.

Microstructure

Method(s):	☒ SEM ☒ XRD ☐ Other:
Operating conditions:	**XRD:** A powdered sample was analyzed using a Bruker D2 PHASER diffractometer with a LYNXEYE detector utilising Cu Kα (λ = 1.5418 Å) radiation, a Ni foil was used to filter the K radiation. The diffraction pattern was collected between $10^\circ < 2\theta < 70^\circ$ with a step size of 0.02° 2θ and dwell time of 1s per step. **SEM:** A Hitachi TM3030 scanning electron microscope coupled with a Bruker Quantax 70 energy dispersive X-ray spectroscopy system (EDX) with a silicon drift detector was used. A sectioned slice of the HIP can/sample was mounted in epoxy resin, ground using SiC grit paper, polished to a 1 µm finish using diamond suspensions and carbon coated.
Homogeneity:	Heterogeneous
Free liquid or gas:	Absence
Crystalline composition:	Multi-phase glass ceramic
Comments and discussion:	In Figure 95, multiple crystalline phases were identified by powder XRD. These consisted of: forsterite ($MgSiO_3$), ceria (CeO_2), periclase (MgO), quartz (SiO_2), kotoite ($Mg_3(BO_3)_2$) and albite ($NaAlSi_3O_8$). There were no reflections associated with clinoptilolite, which indicated that the zeolite structure was destroyed during the thermal treatment process. The presence of periclase suggests the $Mg(OH)_2$ waste stream was not fully incorporated into a glassy matrix, instead a portion of the waste underwent decomposition to MgO. The microstructure of HIP-USFD-Ce is shown in Figure 96 - Figure 97, indicating a heterogeneous glass ceramic. Lighter regions richer in Ca, Al, Si and Na are likely composed of vitrified clinoptilolite regions (this natural zeolite is nominally composed $(Na_{0.5}K_{2.5})(Ca_{1.0}Mg_{0.5})(Al_6Si_{30})O_{72}\cdot 24H_2O$), with a magnesium rich region between these regions. Unreacted

ceria is encapsulated between these, scattered throughout the sample.

Reactions occurred between the MW ½ Li glass frit and $Mg(OH)_2$ likely lead to the crystallization of forsterite, identified by XRD and in the medium grey region of Figure 97, which is rich in Mg and Si. This is more clearly evident in Figure 96, where the micrograph represents a larger surface area of the HIP-USFD-Ce sample.

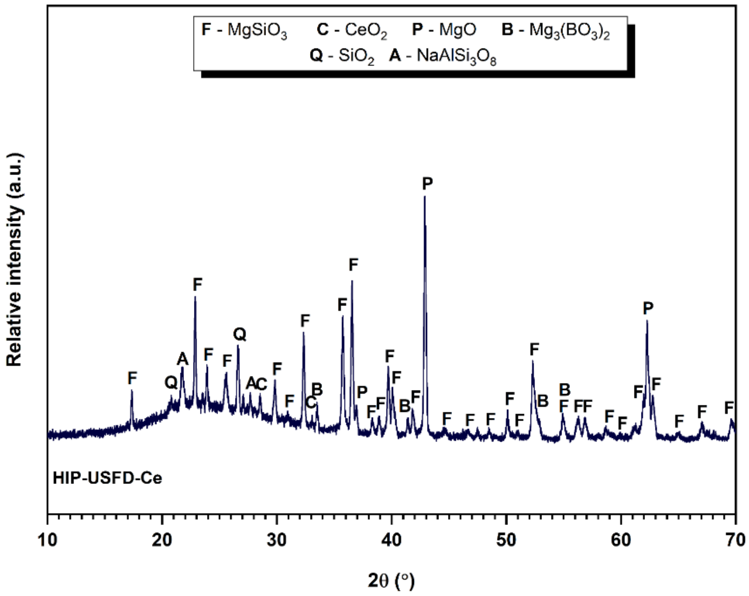

Figure 95: XRD of HIP-USFD-Ce

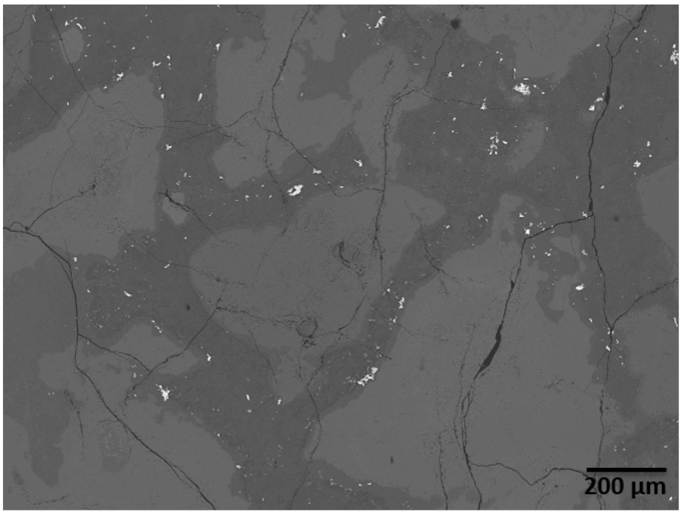

Figure 96: SE micrograph of HIP-USFD-Ce (x100 magnification)

	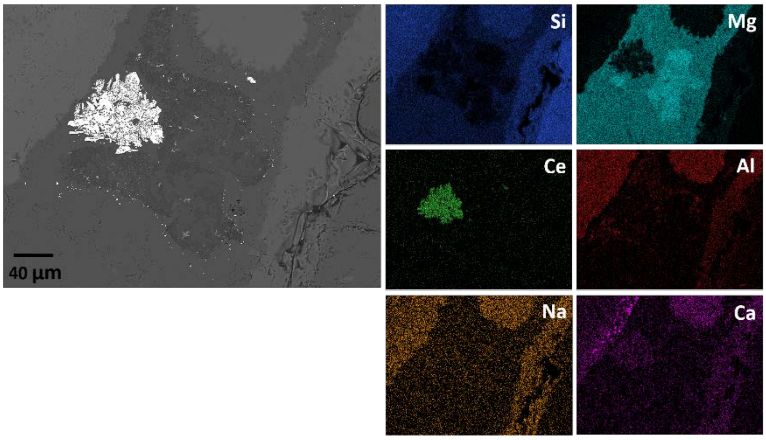 *Figure 97: SSEM/EDX micrograph of HIP-USFD-Ce (x500 magnification)* The phase assemblage and microstructure appear similar to the corresponding NNL sample (NNL-HIP-1), which was completed on a larger scale (8 kg), compared to ~20 g at USFD. This indicated that smaller wasteforms can be confidently used to mimic the wasteform likely to be produced in industrial applications, allowing more rapid and thorough testing prior to implementation

Chemical composition

Method(s):	☐ EMP ☒ ICP-OES/MS ☒ XRF ☐ Other:
Operating conditions:	A HIP-USFD-Ce XRF bead was prepared using bulk powdered sample and a lithium tetraborate flux at a 1:10 sample-to-flux ratio, heated to 1270 °C. This was analysed using a PANalytical PW2404 spectrometer under vacuum using a Rh X-rays tube. Additionally samples were digested for ICP-OES analysis to determine boron and lithium contents, this was undertaken on a Thermo Iris Advantage ICP.
Chemical composition:	*Table 34: Composition of bulk HIP-USFD-Ce by XRF and ICP spectroscopy*

Oxide	Wt.%
Al_2O_3	7.52
B_2O_3	2.23
BaO	<0.10
CaO	1.06
CeO	0.44
Cr_2O_3	<0.10
Fe_2O_3	0.76
K_2O	2.88
La_2O_3	<0.10
Li_2O	0.28
MgO	25.64
Mn_3O_4	<0.10
Na_2O	1.98
SiO_2	55.68
TiO_2	<0.10
ZnO	<0.10
ZrO_2	<0.10

Table 35: Composition of bulk HIP-USFD-Ce by XRF and ICP spectroscopy

Comments and discussion:

The sample is representative of the materials used in producing this HIP can, with Al_2O_3 + SiO_2 >70%, and 16% MgO from the calcined Magnox sludge simulant used. Only a small contribution from B_2O_3 is present due to being a minor component of the glass frit added.

It should be noted that the XRF composition is different to NNL HIP-1, though the materials are supposed to be the same. This HIP-USFD-Ce can was produced from material batched and supplied (as one powder) by NNL leftover from their larger can. This suggests either an issue with batching, or inhomogeneity within the larger NNL HIP-1 sample which has resulted in a varying chemical composition.

A uranium containing sample (HIP-USFD-U) was also produced to the same formula. This was produced and batched at USFD from individual raw materials supplied by NNL, to the recipe noted in Table 1. The XRF composition of the uranium sample is the same as this HIP-USFD-Ce sample (although with U substitution for Ce). This indicated the larger NNL HIP-1 sample was either incorrectly batched, or contains widespread large inhomogeneities such that the sample received for analysis is not representative of these smaller scale samples.

Chemical durability

Method(s):	☒ As described in MS12 Report (p. 12-13), adapted from ASTM C1285 ☐ As described in MS12 Report (p. 14), adapted from ASTM C1220 ☐ Other:
Clarifications:	Sample material was crushed and sieved to 125-250 µm, then washed and prepared as per ASTM C1285. PFA screw-lid pots were used, with 10 ml ASTM Type 1 water and a quantity of sample material to ensure a SA/V of 10 m^{-1}. The surface area / volume was calculated assuming a geometric surface area, as required in ASTM C1285 specifications (with density from helium pycnometry analysis). Static leaching at 90 °C was undertaken for up to 28 days, with duplicate sampling at 1, 3, 7, 14, 21 and 28 days. Sample aliquots were filtered using a 0.2 µm cellulose acetate filter. The aliquot pH was measured using a 3-point calibrated pH probe and then acidified with ultrapure NORMATOM HNO_3 and analyzed by ICP-OES (Thermo Fisher iCAP 6300 ICP-OES) and/or ICP-MS (Thermo Scientific iCAP RQ ICP-MS). Normalized mass loss was calculated using compositional data from XRF analysis.

Results and discussion:

NB: The USFD ISG dissolution results are reported in GeoMelt-Glass 6 characterization test sheet

For the HIP-USFD-Ce, the solution pH begins at 9.8 after day 1, falling to a minimum of 9.1 at day 14, before finally levelling off to 9.2 after 28 days leaching (Figure 98).

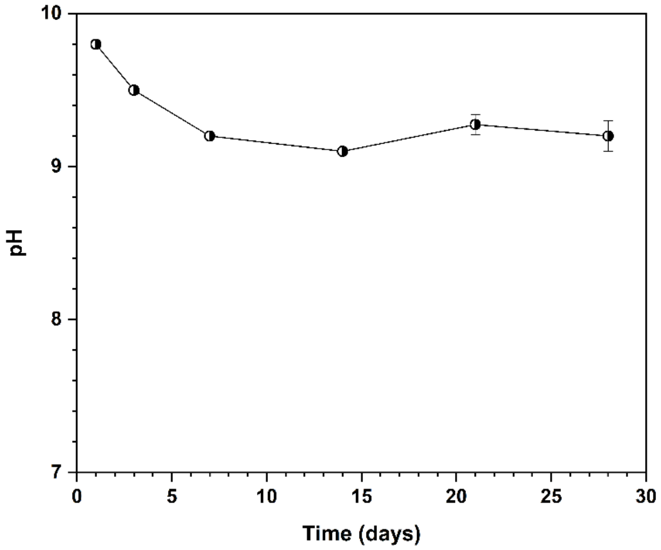

Figure 98: pH of HIP-USFD-Ce up to day 28

Similar to the larger scale NNL HIP-1 material, this sample presents an immediate release of elements within the first day, especially Ca, Na and B (Figure 99 and Figure 100). These, along with Li continue release up to day 28, where a final normalized mass loss of 21.5 g/m^2 for B, and 13.9 g/m^2 for Na are reached.

Final Si normalized mass loss (3.9 g/m^2 compared to 17 g/m^2 in ISG) again might indicate improved durability, along with a slightly reduced B normalized mass loss (28.2 g/m^2 in ISG).

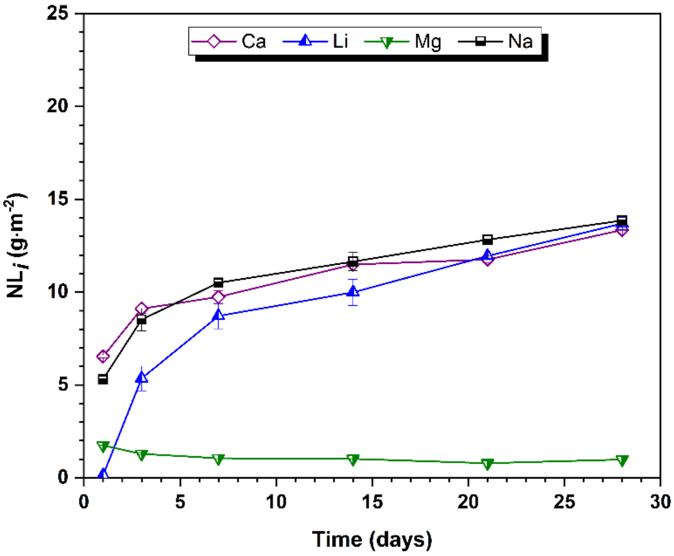

Figure 99: Normalized mass loss of Ca, Li, Mg and Na from HIP-USFD-Ce, up to day 28

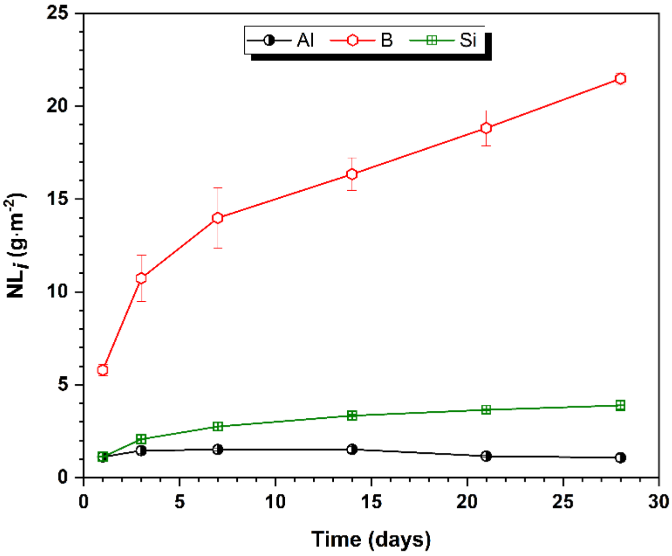

Figure 100: Normalized mass loss of Al, B and Si from HIP-USFD-Ce, up to day 28

Other tests and characterizations

N/A

Conclusions and Outlooks

This thermally treated product has formed a heterogeneous glass ceramic in which added CeO_2 has been encapsulated within the wasteform. Two of the simulant waste streams added; Magnox sludge simulant, and clinoptilolite haven been fully or partially incorporated into a glassy product. This demonstrates a high level of waste loading is possible for these products, while forming a solid product.

Chemical durability assessments of this product is difficult to compare to ISG, due to the difference in dissolution mechanisms between a homogeneous glass and this multi-phase material. Overall both boron and silicon normalized mass losses appear to show better durability to ISG, though this depends on the existence or formation of any secondary precipitation products during dissolution. The durability of this material compared to the larger scale NNL-HIP-1 product compare well. The chemical composition of the products varied due to batching or inhomogeneity issues, however the bulk dissolution trends between the products were similar. Both showed relatively slightly lower boron mass losses compared to ISG, and notably lower silicon losses. The final normalized mass losses varied slightly between the two scaled samples, but the trends remained broadly similar.

Overall, the similarities between this product, produced at a small scale, and the larger scale product (NNL-HIP-1) verify the use and value of smaller wasteform development projects.

4.12 HIP-U sample (USFD)

General information

Partner:	University of Sheffield (USFD)
Sample id:	HIP-USFD-U
Contact person:	Samuel Walling and Neil Hyatt

Origin and macroscopic description

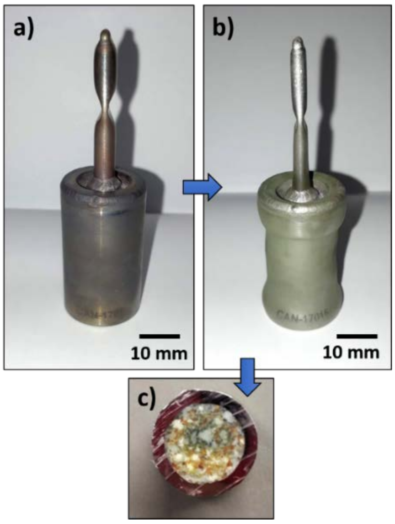

Figure 101: Photographs of a) pre-HIP can, b) post-HIP can and c) sectioned HIP can

For more information, refer

to report THERAMIN D3.6.

Hot isostatic pressing (HIPing) as a thermal treatment method was used during THERAMIN WP3 to develop wasteforms for further characterization. The HIP at USFD is the only designated HIP in the UK for the processing of radioactive samples. This is achieved by using an active furnace isolation chamber (AFIC) developed by American Isostatic Press, GeoRoc Ltd and 8 AMEPT. The AFIC system facilitates the processing of single straight-walled HIP canisters using multiple filters in a lock and seal chamber, which prevents contamination of the HIP in the event of a canister breach during processing.

The wasteform in this study was co-mixed containing both simulant calcined Magnox sludge simulant (CMgS) and Cs-exchanged clinoptilolite, an aluminosilicate zeolite. MW ½ Li frit glass (a simple sodium lithium borosilicate glass) was added to help the formation of a glassy wasteform. The raw inactive materials were prepared and provided by the National Nuclear Laboratory. At USFD, equimolar U_3O_8 replaced the Ce surrogate used in the NNL-HIP-1 and HIP-USFD-Ce samples. The batch composition is detailed in Table 36.

HIP-USFD-Ce (Can No. 17016)	
CMgS (g)	16.51
MW ½ Li (g)	5.02
Clino (g)	28.01
U_3O_8 (g)	0.48
Waste loading (wt. %)	90.0
MW ½ Li glass frit	
SiO_2	63.4
B_2O_3	22.5
Na_2O	11.4
Li_2O	2.7

Table 36: Composition for HIP-USFD-U and glass frit.

	Pre-conditioning of the wastes included calcination at 950 °C for 3 hours to remove bound water (performed by NNL for inactive components). At USFD, the U_3O_8 was also exposed to the same condition prior to batch blending. The sample was packed into a straight-walled HIP canister using a hydraulic press to improve the packing density. The lid was welded into place, the can was evacuated (until a vacuum of <8 Pa was achieved) and then exposed to temperature (600 °C) whilst under vacuum to remove any remaining water from the sample. Once the vacuum recovered, the evacuation tube was crimped twice and welded to create a fully sealed wasteform ready for HIPing. This sample is also labelled as HIP can 17016 in report THERAMIN D3.6.
Microstructure	
Method(s):	☒ SEM ☒ XRD ☐ Other:
Operating conditions:	**XRD:** A powdered sample was analyzed using a Bruker D2 PHASER diffractometer with a LYNXEYE detector utilising Cu Kα ($\lambda = 1.5418$ Å) radiation, a Ni foil was used to filter the K radiation. The diffraction pattern was collected between $10° < 2\theta < 70°$ with a step size of 0.02° 2θ and dwell time of 1s per step. **SEM:** A Hitachi TM3030 scanning electron microscope coupled with a Bruker Quantax 70 energy dispersive X-ray spectroscopy system (EDX) with a silicon drift detector was used. A sectioned slice of the HIP can/sample was mounted in epoxy resin, ground using SiC grit paper, polished to a 1 µm finish using diamond suspensions and carbon coated.
Homogeneity:	Heterogeneous
Free liquid or gas:	Absence
Crystalline composition:	Multi-phase glass ceramic
Comments and discussion:	In Figure 102, multiple crystalline phases were identified by XRD. These consisted of forsterite ($MgSiO_3$), periclase (MgO), quartz (SiO_2), kotoite ($Mg_3(BO_3)_2$, albite ($NaAlSi_3O_8$) and potentially anhydrous sodium diuranante ($Na_2U_2O_7$). There were no reflections associated with clinoptilolite, which indicated that the zeolite structure was destroyed during the thermal treatment process. The presence of periclase suggests the $Mg(OH)_2$ waste stream was not fully incorporated into a glassy matrix, instead a portion of the waste underwent decomposition to MgO. The microstructure of HIP-USFD-Ce is shown in Figure 103 and Figure 104. This reflects the heterogeneous glass ceramic nature of the material, with clusters of uranium

embedded between collapsed clinoptilolite and a magnesium rich glassy phase.

The pale grey region represents the collapsed clinoptilolite particles. This is postulated due to a strong association of Si, Al, Na and Ca (Figure 104), which corresponds to the nominal composition of clinoptilolite, $(Na_{0.5}K_{2.5})(Ca_{1.0}Mg_{0.5})(Al_6Si_{30})O_{72}\cdot24H_2O$.

Reactions between the MW ½ Li glass frit and $Mg(OH)_2$ occurred likely leading to the crystallization of forsterite, identified by XRD and in the medium grey region of Figure 104, which is rich in Mg and Si. This is more clearly evident in Figure 103, where the micrograph represents a larger surface area of the HIP-USFD-U sample.

The uranium is present as white spots in Figure 103 and Figure 104, and tend to be associated with discrete regions. The behaviour is similar to that for Ce in sample HIP-USFD-Ce, being embedded in the matrix rather than dissolved in a vitreous phase.

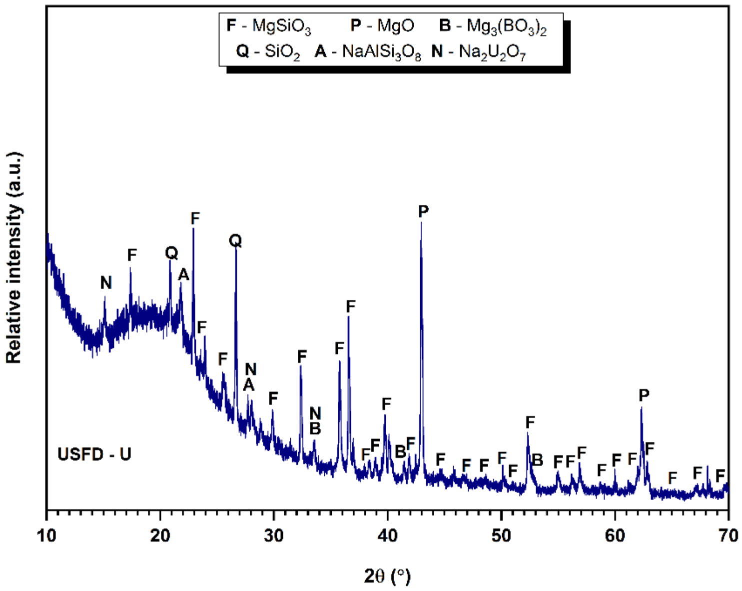

Figure 102: XRD of HIP-USFD-U

	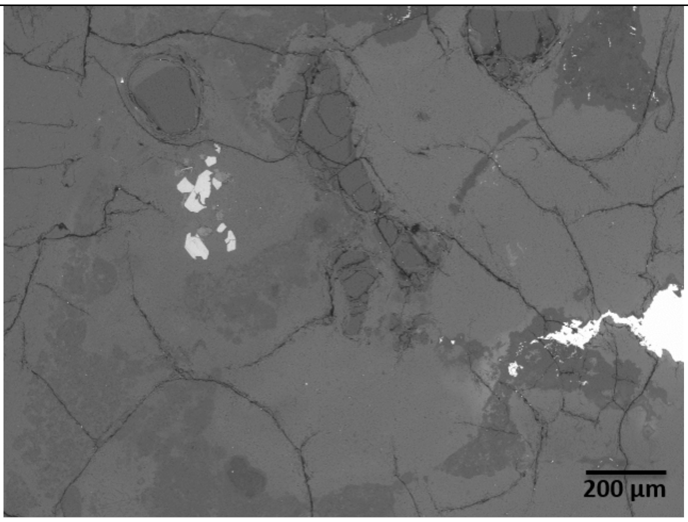 *Figure 103: BSE micrograph of HIP-USFD-U (x 100 magnification)* 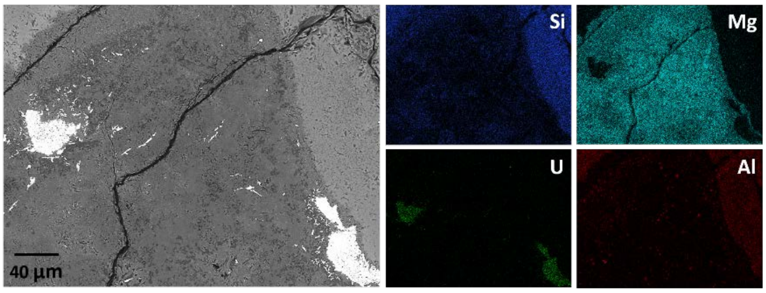 *Figure 104: SEM/EDX micrograph of HIP-USFD-U (x 500 magnification)*

Chemical composition

Method(s):	☐ EMP ☒ ICP-OES/MS ☒ XRF ☐ Other:
Operating conditions:	A HIP-USFD-U XRF bead was prepared using bulk powdered sample and a lithium tetraborate flux at a 1:10 sample-to-flux ratio, heated to 1270 °C. This was analysed using a PANalytical PW2404 spectrometer under vacuum using a Rh X-rays tube. Additionally samples were digested for ICP-OES analysis to determine boron and lithium contents, this was undertaken on a Thermo Iris Advantage ICP.
Chemical composition:	

Oxide	Wt.%
Al_2O_3	7.96
B_2O_3	2.11
BaO	<0.10
CaO	1.04
Cr_2O_3	<0.10
Fe_2O_3	1.02
K_2O	3.10
La_2O_3	<0.10
Li_2O	0.30
MgO	23.30
Mn_3O_4	<0.10
Na_2O	2.16
SiO_2	56.30
TiO_2	0.16
U_3O_8	1.12
ZnO	<0.10
ZrO_2	0.10

Table 37: Composition of bulk HIP-USFD-U by XRF and ICP spectroscopy

Comments and discussion:

The sample is representative of the materials used in producing this HIP can, with Al_2O_3 + SiO_2 >70%, and 16% MgO from the calcined Magnox sludge simulant used. Only a small contribution from B_2O_3 is present due to being a minor component of the glass frit added.

The composition of this material is within experimental error, the same as HIP-USFD-Ce, with Ce substituted on an equimolar bases for U_3O_8. The sample was batched at USFD from constituent materials supplied by NNL, which confirms that both the Ce and U samples were batched to the same recipe.

Chemical durability

Method(s):	☒ As described in MS12 Report (p. 12-13), adapted from ASTM C1285 ☐ As described in MS12 Report (p. 14), adapted from ASTM C1220 ☐ Other:
Clarifications:	Sample material was crushed and sieved to 125-250 µm, then washed and prepared as per ASTM C1285. PFA screw-lid pots were used, with 10 ml ASTM Type 1 water and a quantity of sample material to ensure a SA/V of 10 m^{-1}. The surface area / volume was calculated assuming a geometric surface area, as required in ASTM C1285 specifications (with

	density from helium pycnometry analysis). Static leaching at 90 °C was undertaken for up to 28 days, with duplicate sampling at 1, 3, 7, 14, 21 and 28 days. Sample aliquots were filtered using a 0.2 µm cellulose acetate filter. The aliquot pH was measured using a 3-point calibrated pH probe and then acidified with ultrapure NORMATOM HNO_3 and analyzed by ICP-OES (Thermo Fisher iCAP 6300 ICP-OES) and/or ICP-MS (Thermo Scientific iCAP RQ ICP-MS). Normalized mass loss was calculated using compositional data from XRF analysis.
Results and discussion:	*NB: The USFD ISG dissolution results are reported in GeoMelt-Glass 6 characterization test sheet* For the HIP-USFD-U sample, the solution pH begins at 9.8 after day 1, dropping to 9.0 by day 14, briefly rising at 21 days, before falling to a minimum of 8.9 at day 28 (Figure 105). This is very close to the behaviour of HIP-USFD-Ce 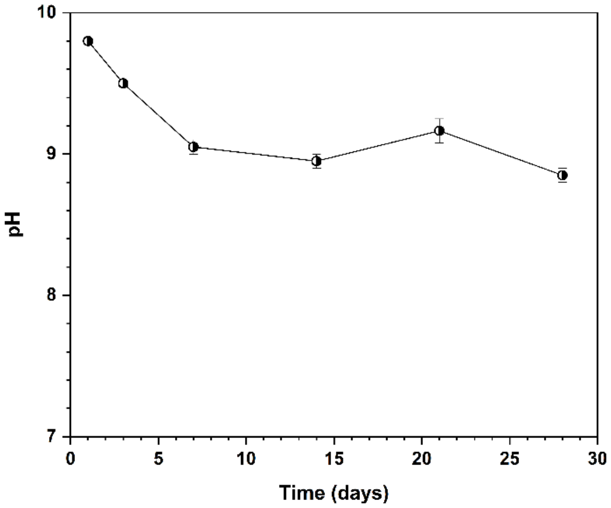 *Figure 105: pH of HIP-USFD-U up to day 28* Normalized mass loss data for this uranium containing sample are very much similar to those for HIP-USFD-Ce. The higher early pH is accompanied by immediate release of elements in the first day, especially Ca, Na and B (Figure 106 and Figure 107). These, along with Li continue release up to day 28, where a final normalized mass loss of 21.6 g/m^2 for B, and 14.1 g/m^2 for Na are reached. Final Si normalized mass loss (4.0 g/m^2 compared to 17g/m^2 in ISG) might indicate some improved durability, along with a slightly reduced B normalized mass loss (28.2 g/m^2 in ISG)

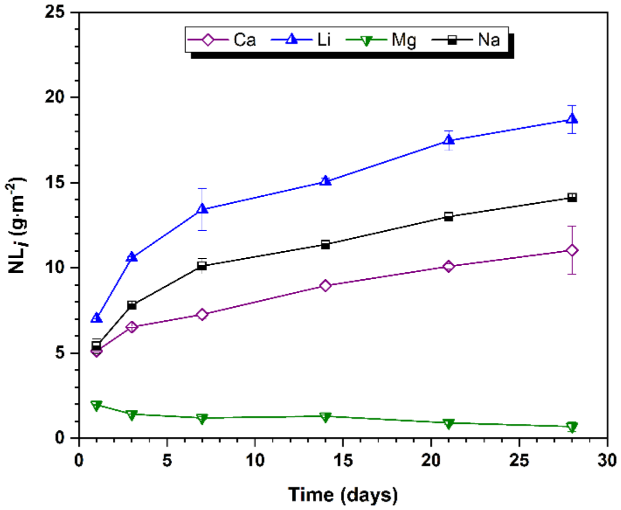

Figure 106: Normalized mass loss of Ca, Li, Mg and Na from HIP-USFD-U, up to day 28

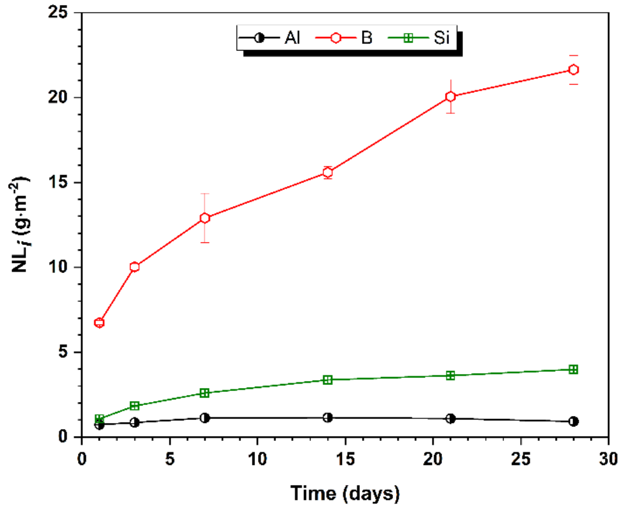

Figure 107: Normalized mass loss of Al, B and Si from HIP-USFD-U, up to day 28

Other tests and characterizations

N/A

Conclusions and Outlooks

This thermally treated product has formed a heterogeneous glass ceramic, in which the added uranium has been encapsulated within the wasteform. Similarly to the CeO_2 doped samples, the two other simulant waste streams (Magnox sludge simulant, and clinoptilolite) have partially or fully been incorporated into a glassy product. This

demonstrates a high level of waste loading is possible using a thermal treatment process.

Similar to the HIP-USFD-Ce sample, chemical durability assessments of this product is difficult to compare to ISG, due to the difference in dissolution mechanisms between a homogeneous glass and this multi-phase material. Overall both boron and silicon normalized mass losses appear to show better durability to ISG, though this depends on the existence or formation of any secondary precipitation products during dissolution.

The durability of this material compared similarly to the inactive Ce sample (HIP-USFD-Ce), this is to be expected as little in the bulk chemical composition varied. This does verify the use of producing inactive simulant samples as surrogates for active samples, particularly when assessing bulk durability.

4.13 Thermal gasification sample (VTT)

In the THERAMIN project in WP3 VTT has demonstrated processing of ion exchange resins by thermal gasification process. The product of this process is fine powder, which has to be immobilised in some way. VTT has selected geopolymerisation for immobilisation and in this section the results of characterization of the final immobilised products are presented. The characterization methods are not the same as in the case of vitrified products because the type of geopolymerised product is different.

General information

Partner:	VTT
Sample id:	Thermal gasification sample-Organic IER
Contact person:	Matti Nieminen

Origin and macroscopic description

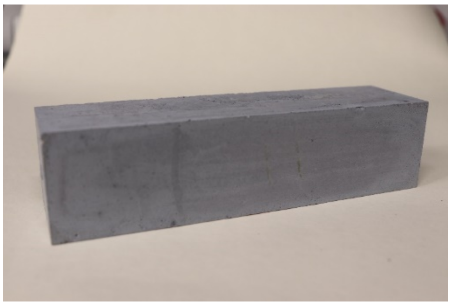

Figure 108: Gasified resin / geopolymer -sample at the age of 24 hour.

Combination of geopolymer matrix and gasification of low-and intermediate radioactive waste is a potential alternative for thermal treatment of the spent ion exchange resins. Geopolymer matrixes has presented high retention capability of radionuclides in multiple studies [Provis and Deventer, 2009]. Geopolymers have also been applied in industrial scale for encapsulation in Slovakia and Czech Republic [Provis and Deventer, 2009]. However, the practical encapsulation amount has been limited by the mechanical properties of the encapsulated matrix. Even a small amount of resin decreases the strength of the matrix and cohesion of the matrix is lost when the amount of resin exceeds 10-15%.

When thermal gasification of the resin is used as a pretreatment of the resin it reduces the resin mass to few percent of the pristine resins. Encapsulation of gasified resin with alkaline cements is a straightforward process as various ashes has been utilized in concrete technology for decades. After the gasification, practical encapsulation amount of resin is not limited by the mechanical properties of the encapsulation matrix. On-going studies have presented that the amount of encapsulated resin exceeds greatly the currently used technologies and is in some extent comparable to state-of-the art vitrification technologies.

	Geopolymer -based encapsulation is fully compatible with currently used cementing methods. If the gasification process is omitted, the encapsulation can take place in existing encapsulation plants. Geopolymers and Portland cements are both alkaline cements which manufacturing process includes mixing of solid and liquid components to form a matrix, which will self-harden. With the current studied method, solid phase consists gasified resin and thermally treated phyllosilicates, and the liquid phase consists aqueous solution of alkali silicates. The mixing procedure is not critical, as long as the selected method is able to produce homogeneous encapsulation matrix. Typical mixing time is similar to Portland cement based matrixes. Ratios of the presented raw materials are adjusted to produce self-consolidating mixture, either by changing the solid/liquid -ratio or solution pH. Mild heating increases the strength development of the formed matrix but is not necessary according to current studies. Figure 108 presents thermally treated gasified resin/ geopolymer -sample at the age of 24 hours.

Microstructure

Method(s):	☐ SEM	☐ XRD	☐ Other:
Operating conditions:			

Homogeneity:	
Free liquid or gas:	
Crystalline composition:	
Comments and discussion:	

Chemical composition

Method(s):	☐ EMP	☐ ICP-OES/MS	☐ XRF	☐ Other:
Operating conditions:				

Chemical composition:	
Comments and discussion:	

Chemical durability

Method(s):	☐ As described in MS12 Report (p. 12-13), adapted from ASTM C1285 ☐ As described in MS12 Report (p. 14), adapted from ASTM C1220 ☒ Other:
Clarifications:	Suitability of the geopolymer/gasification for low- and intermediate radioactive waste encapsulation was evaluated using method: ANSI/ANS-16.6.2003: “measurement of the leachability of the solidified low-level radioactive wastes by a short-term procedure”.

Results and discussion:

Measured apparent diffusion coefficient was 10^{-12} - 10^{-13} cm^2/s for Cesium. For comparison, apparent diffusion coefficients for Portland cement encapsulated pristine resin, gasified resin encapsulated to alkali-activated material and current developed method are presented in Figure 109.

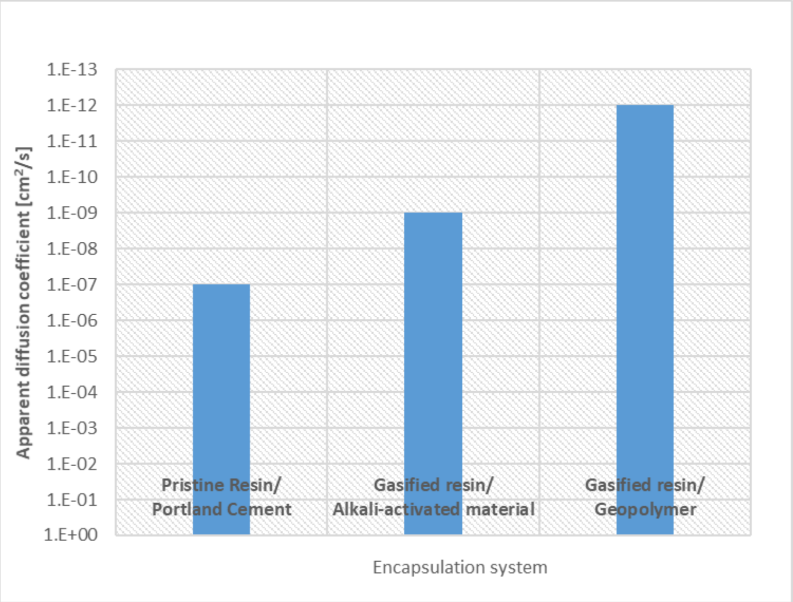

Figure 109: Apparent diffusion coefficients for Cesium in pristine resin/Portland cement -system, gasified resin /alkali-activated matrix and gasified resin /geopolymer matrix.

Other tests and characterizations

Compression strength of the studied gasified resin/ geopolymer -system is presented in Figure 110. For comparison, compression strength of pristine resin/ Portland cement is also presented. Increasing the pristine resin content in Portland cement encapsulation caused drastic decrease in compression strengths and the encapsulation became impossible with 15-20% resin content. In the studied gasified resin/ geopolymer -system, the compression strength increased as the amount of encapsulated resin increased. Compression strength of gasified resin /geopolymer -system equalized typical good quality concrete.

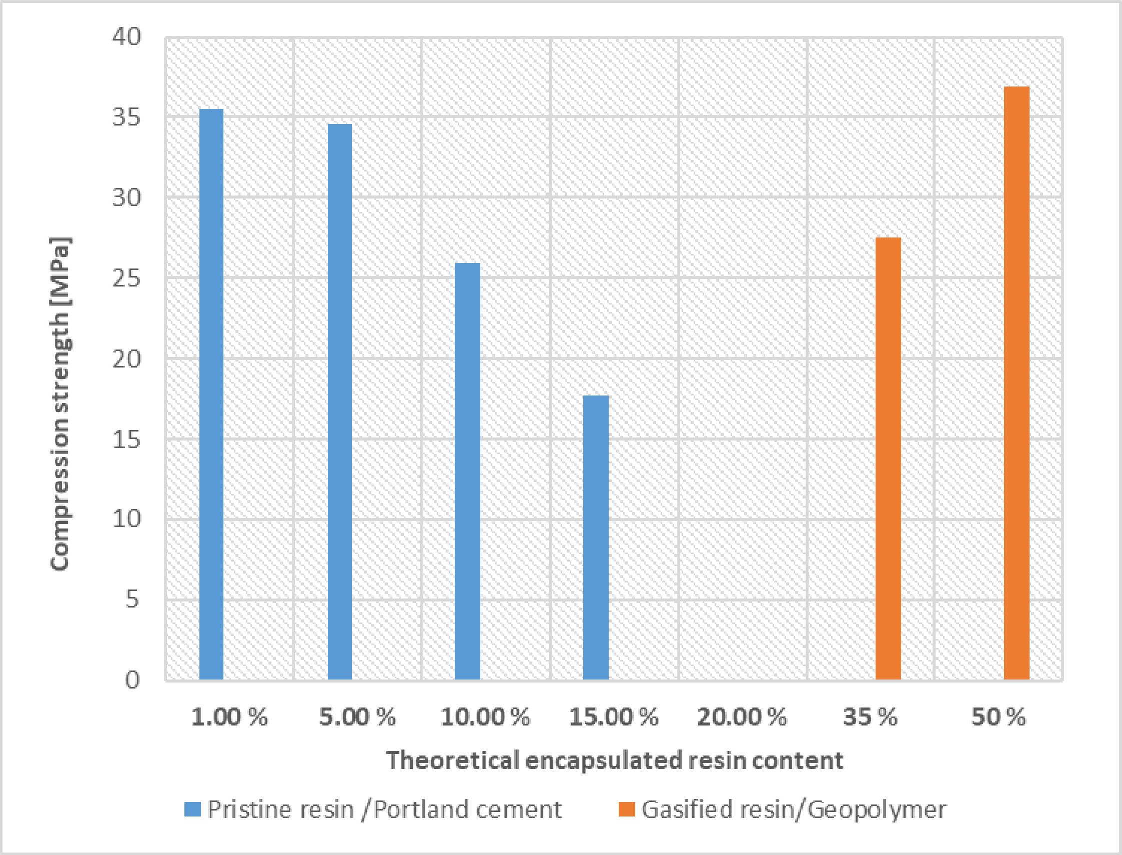

Figure 110: Compression strength of Gasified resin /geopolymer -system. For comparison, compression strengths of pristine resin /Portland cement -system is presented.

Conclusions and Outlooks

4.14 Chrompik vitrification sample (VUJE)

Both USFD and VUJE characterized VUJE Chrompik vitrification samples. These characterization results are presented distinctly.

General information

Partner:	University of Sheffield (USFD) / VUJE
Sample id:	VUJE-Chrompik-III
Contact person:	USFD: Samuel Walling and Neil Hyatt VUJE: Milan Zatkulak, Alexandra Mikusova and Zuzana Mala

Origin and macroscopic description - USFD

Figure 111:. Photograph of Chrompik-III glass block

Chrompik-III glass was produced by VUJE using the VICHR process. Glass blocks were sent to the University of Sheffield for chemical durability analysis using the modified ASTM C1285-14 methodology outlined in report MS12. Additional characterization was also performed using the standard methods C1285-14 and C1220-10 with time points extended to 504 days (18 months). Expected completion date for the extended experiments will be March 2020.

For information regarding the thermal profile and annealing stages, refer to report THERAMIN D3.7.

Origin and macroscopic description - VUJE

Figure 112: Sample of inactive Chrompik III glass block

Chrompik III- solution's pH is 9.5, it mainly contains K, HCO_3^-, CO_3^{2-} and the Cr content in the soluble form is 1 % from its original amount. Within the THERAMIN WP3, vitrification technology was used for the thermal treatment of this radwaste. WP3 demonstration trials carried out using vitrification technology at NPP A1 in Jaslovske Bohunice- trials were performed with inactive surrogate solution of chrompik III and also trials with active surrogate solution of chrompik III.

Waste feed:

- Chrompik III- (K 7.6 g/L, Cr 0.06 g/L, HCO_3^- 7.3 g/L, CO_3^{2-} 1.8 g/L, pH= 9.6- 10.0),
- 5.3 kg glass frit (SiO_2 57.0 g/L, TiO_2 5.5 g/L, Al_2O_3 5.3 g/L, B_2O_3 14.8 g/L, Na_2O 8.5 g/L, Li_2O 3.5 g/L, Fe_2O_3 4.5 g/L,
- 2.2 kg additives (based on aluminosilicates/ geopolymer)

 *Figure 113:*. Sample of active Chrompik III glass product prepared using vitrification facility	For information regarding the thermal profile and vitrification technology, refer to report THERAMIN D3.7. Preparation of monoliths in VUJE´s laboratory: Mixture of glass frit, additives and chrompik surrogate solution in ratio 40/17/43 was prepared. The mixture was dried in an oven at 100°C for 24 hours. Subsequently, the mixture was crucible melted using temperature regime of 10°C/ min to 650°C, holding time 1 hour at 650°C, 10°C/ min to 800°C, holding time 1 hour at 800°C, heating rate 10°C/ min to 1220°C, holding time 1 hour at 1220°C. Monoliths were molted on the metal pad after remelting of approx. size 1.5 x 2 x 1.5-2 cm. After cooling to about 500-600°C, the monoliths were transferred to a second furnace and tempered for 4 hours at 550°C.

Microstructure - USFD

Method(s):	☒ SEM	☒ XRD	☐ Other:
Operating conditions:	**XRD:** A Chrompik-III monolith was analyzed using a Bruker D2 PHASER diffractometer with a LYNXEYE detector utilising Cu Kα (λ = 1.5418 Å) radiation, a Ni foil was used to filter the K radiation. The diffraction pattern was collected between 5° < 2θ < 70° with a step size of 0.01° 2θ and dwell time of 1s per step. **SEM:** A Hitachi TM3030 scanning electron microscope coupled with a Bruker Quantax 70 energy dispersive X-ray spectroscopy system (EDX) with a silicon drift detector was utilised. The monolith sample was mounted in epoxy resin, ground using SiC grit paper, polished to a 1 µm finish using diamond suspensions and carbon coated.		

Homogeneity:	Homogeneous
Free liquid or gas:	Absent
Crystalline composition:	Amorphous
Comments and discussion:	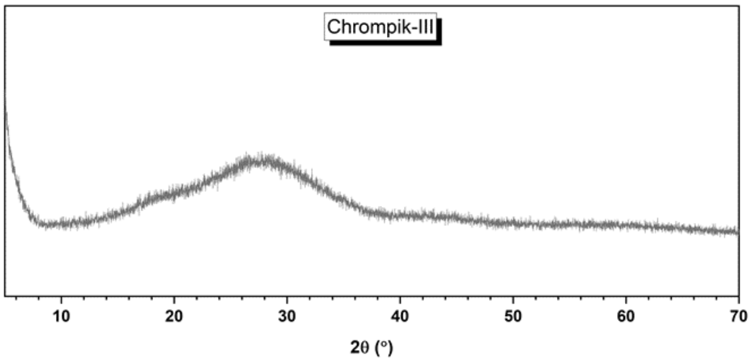 *Figure 114:* Diffraction pattern of Chrompik-III monolith

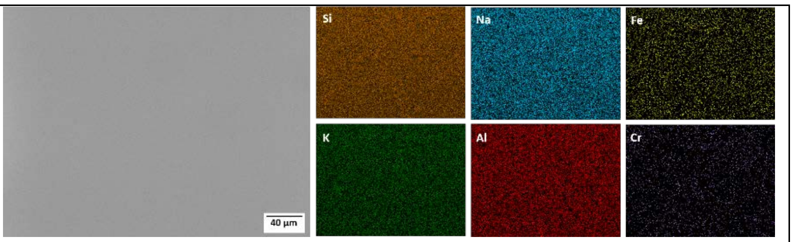

Figure 115: SEM/EDX of Chrompik-III

Chrompik-III X-ray diffraction pattern (Figure 114) is typical of a glass, evidenced by the diffuse scattering region observed between 10-40° 2θ and the noted absence of any crystalline reflections. Within SEM-EDX analysis the elemental composition was observed to be homogenously distributed throughout the microstructure (Figure 115). There was no indication of free liquid or gas contained within the sample.

Microstructure - VUJE

Method(s): ☒ SEM ☒ XRD ☐ Other:

Operating conditions:

XRD: Rigaku MiniFlex 600 Diffractometer: Cu X-ray tube + Ni Kβ filter, NaI scintillation counter: Tl detector; measurements in the range of 10° - 80° 2θ at room temperature a step of 0.02° 2θ, using an aluminum holder (compact samples with flat side). In the aluminum holder, the sample was attached using Scotch Magic Tape, resulting in a wide diffraction maximum of about 20 ° 2θ. The measured data were compared with the ICDD PDF-2 database (version 2013).

SEM: Scanning electron microscope with acceleration voltage of 15 kV in reflected electron (BEI) and secondary electron (SEI) modes using tungsten fiber. The microscope allows change the acceleration voltage in the range of 0.3 - 30kV and, depending on the sample type, the magnification up to 300,000x. Microscope is a powerful multi-purpose scanning electron microscope with low vacuum capability. The microscope is equipped with an EDS silicon based X-Max 80 Premium detector with an active area of 80 mm^2. The detector forms the basis of the analytical system AZTec Energy from Oxford Instruments.

Homogeneity:

Homogenous

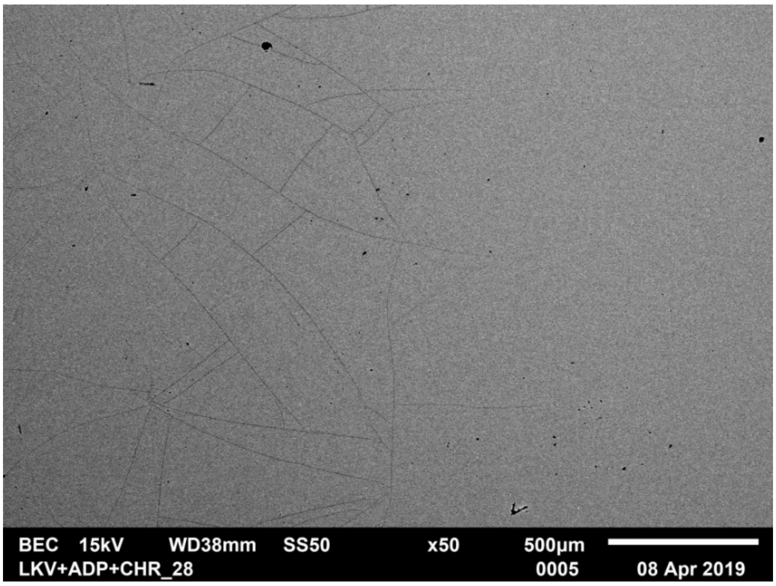

	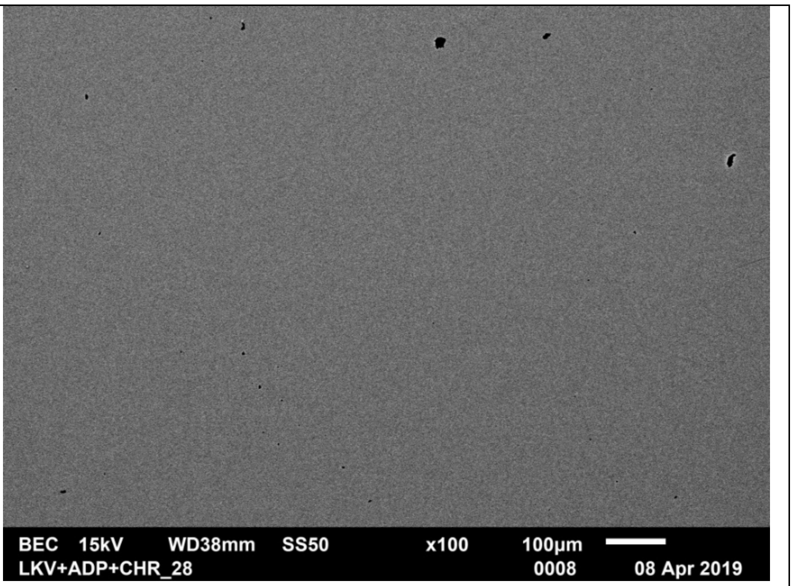 *Figure 116:* SEM observation of Chrompik III glass with two magnifications x 50 and x100. 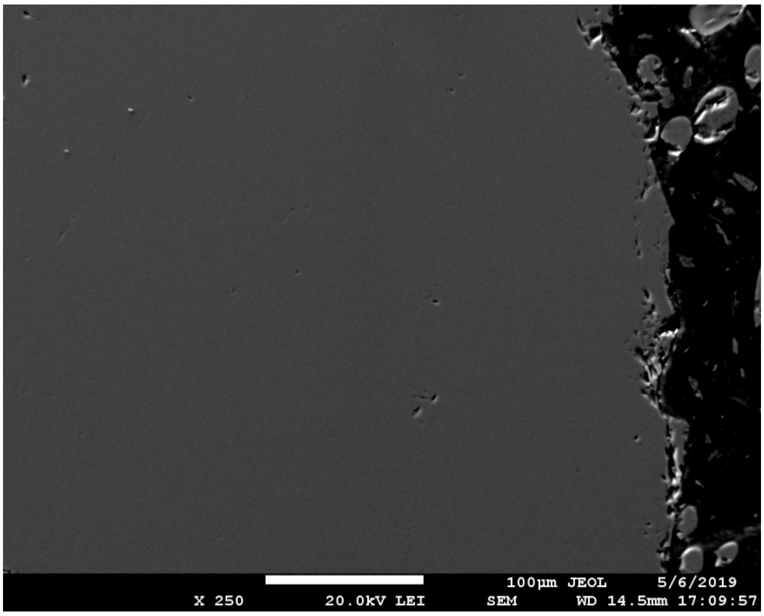 *Figure 117:* SEM/EDX observation of Chrompik III glass cross section
Free liquid or gas:	Absence. No indication of free liquid or gas contained within the sample.
Crystalline composition:	Amorphous.

	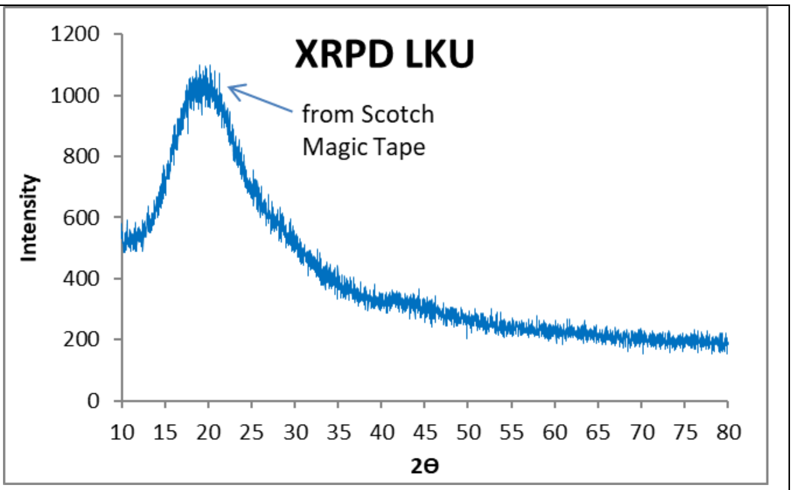 *Figure 118:* Diffraction pattern of Chrompik III glass The XRD pattern is typical of a glass, between 10- 80° 2θ shows no diffraction peak typically observed of the crystalline phases presence. Sample is predominantly amorphous (glass).
Comments and discussion:	The vitreuos sample prepared of chrompik III within the THERAMIN project is homogeneous at the micrometric scale. The matrix is amophous, wihout any evidence of crystallization visible in SEM or XRD. There was no indication of free liquid or gas.

Chemical composition - USFD

Method(s):	☐ EMP ☒ ICP-OES/MS ☒ XRF ☐ Other:
Operating conditions:	A Chrompik-III XRF bead was prepared using bulk powdered sample and a lithium tetraborate flux at a 1:10 sample-to-flux ratio, heated to 1270 °C. This was analysed using a PANalytical PW2404 spectrometer under vacuum using a Rh X-rays tube. Additionally samples were digested for ICP-OES analysis to determine boron and lithium contents, this was undertaken on a Thermo Iris Advantage ICP.

Chemical composition:

(wt.%)	VUJE Batch composition	USFD XRF
SiO_2	51.89	52.06
Al_2O_3	8.54	7.20
K_2O	5.48	7.78
Na_2O	10.24	11.16
FeO	0.03	-
Fe_2O_3	3.17	3.08
TiO_2	3.93	3.32
CaO	1.37	0.30
MnO	0.00	<0.10
MgO	0.09	0.10
B_2O_3	11.09	7.71
Li_2O	2.38	2.40
P_2O_5	0.01	<0.10
PbO	1.45	1.35
ZnO	0.13	0.20
BaO	0.12	0.26
Cr_2O_3	0.07	<0.10
Total	**99.99**	**96.92**

Table 38: Chrompik III glass composition

Comments and discussion: XRF analysis has determined that most of the elements are close to the batched composition, with this glass being largely an alkali alumino-borosilicate glass, with a quantity of lead contained.

Chemical composition - VUJE

Method(s): ☐ EMP ☐ ICP-OES/MS ☒ XRF ☒ Other: SEM-EDX

Operating conditions:

XRF: Measured on an S8 TIGER X-ray fluorescence wave dispersion spectrometer. The required amount of sample was cut to a maximum size of about 6.3 mm and was milled in a tungsten carbide ball mill for 10 minutes at 300 rpm. The ground sample was sieved on a 0.045 mm mesh screen. The following sample preparation procedure was used to determine the minor components in the sample: The required amount of sample was weighed from a portion below 0.045 mm, a wax of 0.1 times the weight of the sample was added, and the mixture was homogenized for 10 minutes at 180 rpm in a ball mill. From the homogenized mixture, the tablets were compressed in an aluminum container for 60 seconds with a force of 200 kN.

SEM/EDX: The measurement was performed on an electron microscope JEOL 7600F using an X-MAS 50 mm^2 EDX analyzer.

Chemical composition:

The theoretical chemical composition (Table 1) is calculated from the composition of glass frit, additives and surrogate solution of chrompik III. The chemical composition was verified by two methods XFR and SEM/EDX and results are presented in Table 39

wt %	Calculated composition of glass product	SEM-EDX	XRF
SiO_2	51.89	51.36	53.53
Al_2O_3	8.54	7.07	7.75
K_2O	5.48	5.76	8.07
Na_2O	10.24	6.97	11.90
Fe_2O_3	3.17	1.73	2.92
TiO_2	3.93	2.34	3.37
CaO	1.37	ND	0.23
MgO	0.09	ND	ND
B_2O_3	11.09	ND	10.44
Li_2O	2.38	ND	ND
PbO	1.45	0.2	1.20
ZnO	0.13	ND	0.14
BaO	0.12	ND	ND
Cr_2O_3	0.07	ND	ND
total	100	76.06	100.18

Table 39: Chrompik III glass composition

Comments and discussion:

The analysis of the prepared glass composition by two techniques gives consistent results between theoretical chemical composition and XRF measurements. Results of Chrompik III glass composition from University of Sheffield have not completed, will be updated for WP4 deliverable report in July.

The Chrompik III glass contains mainly SiO2, Na2O, B2O3, and K2O which present 84.6 % of the glass composition. Significant differences are in results of analyzed sample using SEM- EDX method. Boron and lithium are too light to be analyzed by this method, and due the hight theoretical content of boron in glass matrix, the total wt % is lower.

Chemical durability - USFD

Method(s):	☒ As described in MS12 Report (p. 12-13), adapted from ASTM C1285 ☐ As described in MS12 Report (p. 14), adapted from ASTM C1220 ☐ Other: ASTM C1285 (standard, SA/V ratio of 2000 m^{-1})
Clarifications:	Sample material was crushed and sieved to 125-250 µm, then washed and prepared as per ASTM C1285. PFA screw-lid pots were used, with 10 ml ASTM Type 1 water and a quantity of sample material to ensure a SA/V of 10 m^{-1}. The surface area / volume was calculated assuming a geometric surface area, as required in ASTM C1285 specifications (with density from helium pycnometry analysis). Static leaching at 90 °C was undertaken for up to 28 days, with duplicate sampling at 1, 3, 7, 14, 21 and 28 days. Sample aliquots were filtered using a 0.2 µm cellulose acetate filter. The aliquot pH was measured using a 3-point calibrated pH probe and then acidified with ultrapure NORMATOM HNO_3 and analyzed by ICP-OES (Thermo Fisher iCAP 6300 ICP-OES) and/or ICP-MS (Thermo Scientific iCAP RQ ICP-MS). Normalized mass loss was calculated using compositional data from XRF analysis.

Results and discussion:

NB: The USFD ISG dissolution results are reported in GeoMelt-Glass 6 characterization test sheet

The pH of the Chrompik-III material is initially pH 8.6 after day 1 leaching, increasing to pH 9.5 after day 28 leaching (Figure 119)

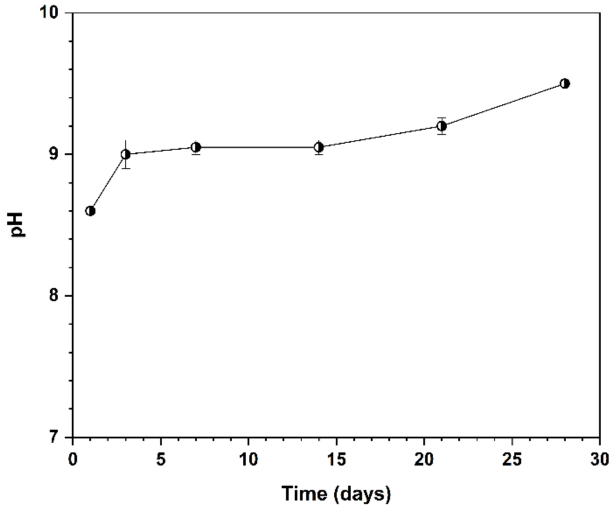

Figure 119: pH of VUJE-Chrompik-III up to day 28

Normalised mass losses for B, Li and Na follow very similar trends (Figure 5), with a steady increase up to day 28 leaching, reaching 5.4 g/m^2, 5.8 g/m^2 and 7.6 g/m^2 for B, Li and Na, respectively. These are notably lower than those for ISG, at 28.2 g/m^2 and 43 g/m^2 for B and Na, respectively.

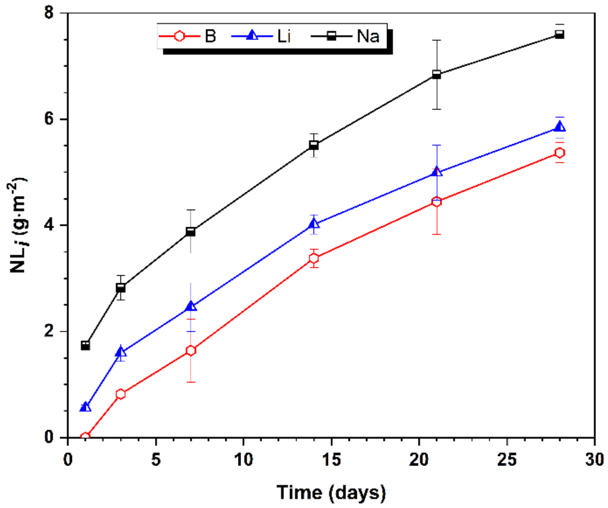

Figure 120: Normalized mass loss of B, Li and Na from VUJE-Chrompik-III, up to day 28

Silicon and aluminium release rates follow a different trend, reaching a maximum at day 21 before dropping at day 28. Interestingly, both elements report the same normalized mass loss (within error), at 3.1 g/m^2 and 3.2 g/m^2 for Si and Al respectively at 28 days. The Si normalized mass loss is lower than that for ISG (17.4 g/m^2), while Al is marginally high (2.9 g/m^2 in ISG).

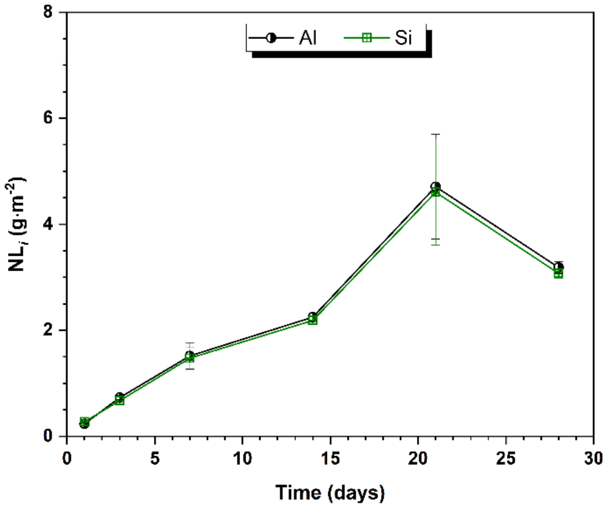

Figure 121: Normalized mass loss of Al and Si from VUJE-Chrompik-III, up to day 28

Chemical durability - VUJE

Method(s):	☐ As described in MS12 Report (p. 12-13), adapted from ASTM C1285 ☐ As described in MS12 Report (p. 14), adapted from ASTM C1220 ☒ Other: modified ASTM C1220
Clarifications:	The leachability tests on Chrompik III non- active glass samples, verification tests of water leachability according to the modified ASTM C1220. Samples were prepared by pouring into cuboid monoliths of approx. 1.5 x 2x 1.5-2 cm. The formula was used to calculate the normalized mass: $NL = \frac{(m_0 - m_t)}{S_0}$,

where m_0 is the weight of the monolith at the start of the experiment, m_t is the mass of the monolith at time t, S_0 is the surface of the sample. The amount of leaching solution was determined by the ratio $S/V = 1/10$, where V is the volume of the solution.

We tested two methods of leaching:

1. Leaching at temperature near the boiling point

Samples were leached at the boiling point. The sample was suspended on PTFE thread in a glass flask which was placed in a heating nest and the solution temperature was maintained at the boiling point. A cooler was fitted to the flask while the coolant temperature was 5°C. Every 6 hours, the sample was removed from the leaching solution, washed with water, rinsed with acetone and freely dried in the air. Subsequently, the sample was weighed and put back into the leaching solution in which the leaching was continued for a further 6 hours.

2. Leaching at 90°C in oven

a. Without stirring- without restoring the surface
The sample was suspended on PE thread and placed in a leaching solution (demi water) into a PE bottle. The volume of the leaching solution was determined by the ratio S / V = 1/10, where S is the surface of the sample and V is the volume of the solution. Leaching was carried out in an oven at 90°C. Samples were gradually removed from the oven at 1, 3, 7, 14, and 28 days. Subsequently, the samples were washed with demi water, rinsed with acetone and freely dried in the air. After drying, the samples were weighed. The pH, conductivity and determined Na + and K + content using AAS were measured in the leaching solution.

b. The sample was removed at specified time intervals, the gel layer was wiped away- the surface was being restored

The sample was suspended on PE thread and placed in a leaching solution (demi water) into a PE bottle. The volume of the leaching solution was determined by the ratio S/V = 1/10, where S is the surface of the sample and V is the volume of the solution. Leaching was carried out in an oven at 90°C. For the whole experiment, the same sample was used which was selected from the oven after the prescribed time of leaching (at 1, 3, 7, 14 and 28 days). After being removed from the oven, the sample was washed with water, rinsed with acetone and freely dried in the air. After drying, the sample was weighed. The pH and conductivity were measured in the leaching solution and approx. 20 ml to determine the Na^+ and K^+ content using AAS. The recovered amount of leaching solution was made up to the original volume with demi water. Subsequently, the sample was placed back into solution and leaching continued. The Na^+ and K^+ content was measured in the leaching solution and calculated to the amount of Na^+ and K^+ released from the sample (glass monolith) by the equation: $NL_i = \frac{c_i}{x_i \frac{S}{V}}$,

where NL_i is the normalization loss of the sample element ($i = Na^+, K^+$), c_i is the concentration of the element in the solution, x_i is the mass fraction of the element i in the glass, is the surface of the sample, V is the volume of the leaching solution.

Results and discussion:

1. Leaching at temperature near the boiling point

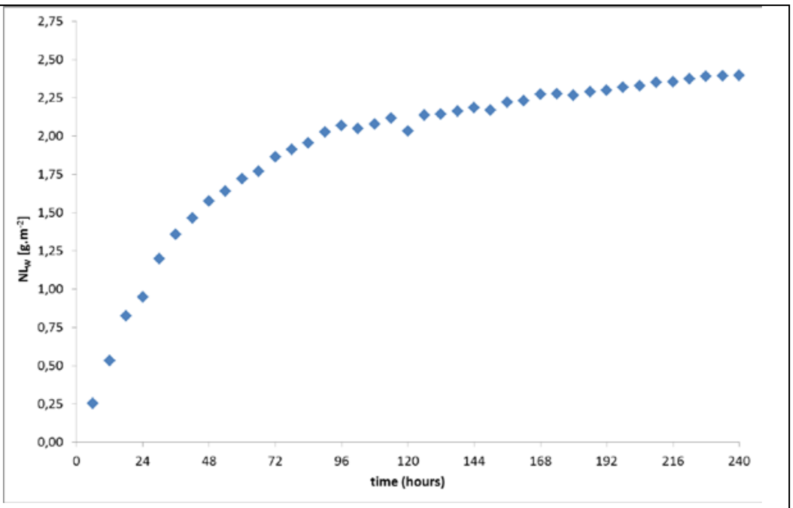

Figure 122: Evolution of NL as a function of time at temperature near the boiling point, S/V=1/10 m^{-1} during duplicate leaching tests of Chrompik III glass sample (average value)

2. Leaching at 90°C in oven

   2.a) without stirring- without restoring the surface

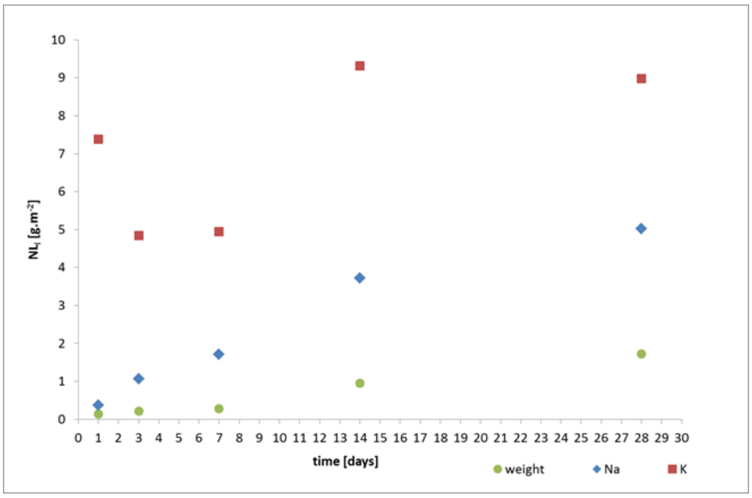

Figure 123: Evolution of NL$_{weight, Na, K}$ as a function of time at 90°C, S/V=1/10 m^{-1} without restoring the surface during repeated leaching tests of Chrompik III glass sample (average value)

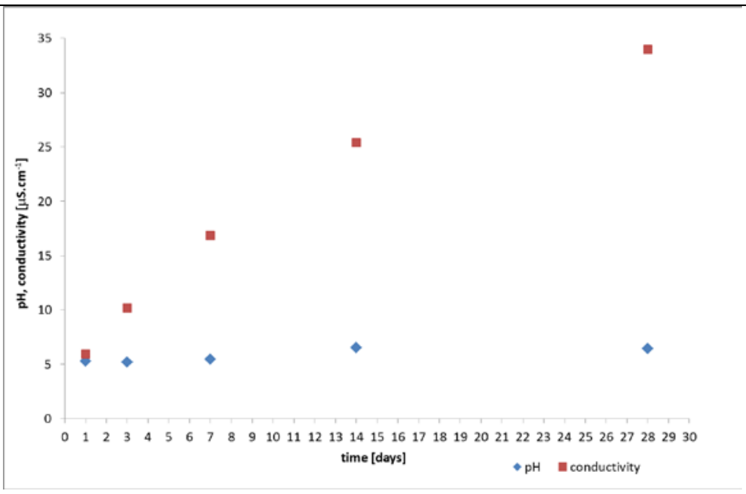

Figure 124: Evolution of pH and conductivity as a function of time at 90°C, S/V=1/10 m^{-1} without stirring during repeated leaching tests of Chrompik III glass sample (average value)

2.b) the sample was removed at specified time intervals, the gel layer was wiped away

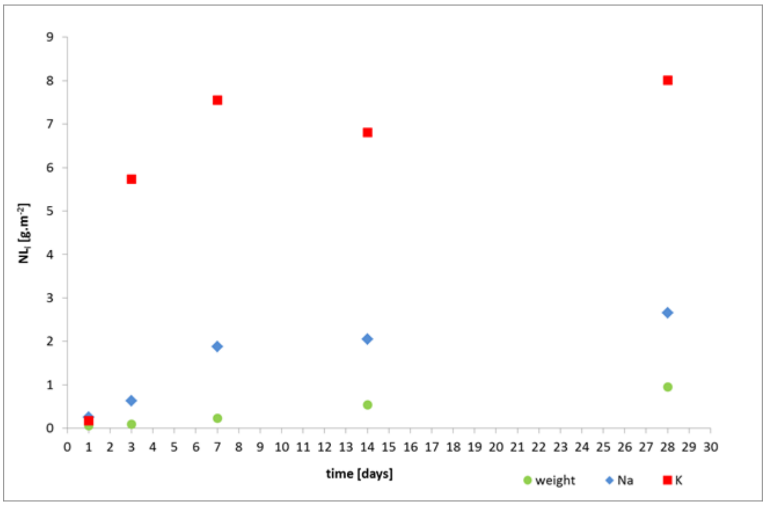

Figure 125: Evolution of $NL_{weight, Na, K}$ as a function of time at 90°C, S/V=1/10 m^{-1} with wiping away of the gel layer during repeated leaching tests of Chrompik III glass sample (average value)

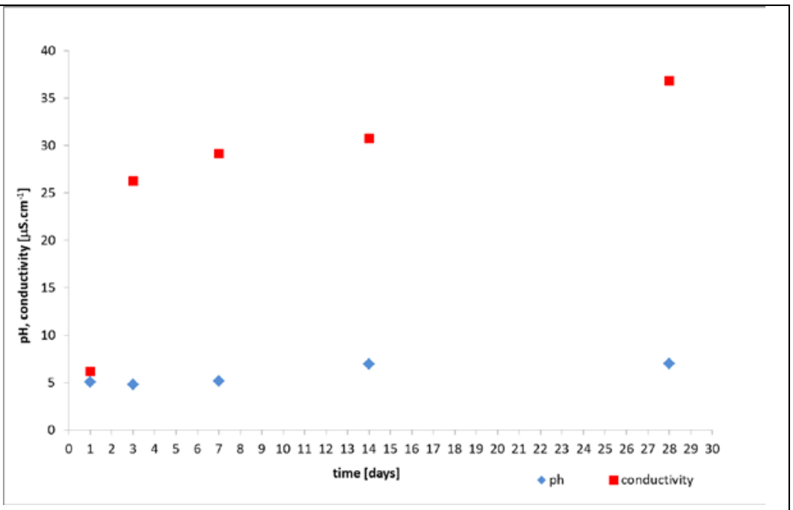

Figure 126: Evolution of pH and conductivity as a function of time at 90°C, S/V=1/10 m^{-1} with wiping away of the gel layer during repeated leaching tests of Chrompik III glass sample (average value)

<u>Chemical durability assessment:</u>

It can be seen from the measured weight loss that at a higher leaching temperature (i.e. at boiling point) and by wiping away of the gel layer at a short interval (every 6 hours) is weight loss from 7 days leaching approx. 2 times faster than leaching at 90°C without stirring. At the beginning of the experiment (1-3 days), the weight loss at boiling point and simultaneous surface renewal at a short interval is about 10 times faster.

Conversely, at a temperature of 90°C, the weight loss rate is half time lower using wiping away of the gel layer method.

The release of Na is approximately the same within 7 days for both cases, without mixing and using the wiping away of the gel layer. For a longer duration of experiment (14 and 28 days), the rate of Na loss on wiping the gel layer is only one half. The effect of removing the gel layer in K content is not unambiguous. The total amount K released is approximately the same for both cases. The pH of the leaching solution is slightly increased from 5- 6.5 for both methods and the conductivity is higher when the gel layer is wiped away. The comparison of results from pH value between methods where the gel layer was wiped away and without restoring the surface of glass monolith, shows a similar evolution of the pH value. The pH stabilizes close to 7 at 90°C under these experimental conditions.

Concluding about the long- term behaviour of the Chrompik III glass form would require further investigation but these results are encouraging for Chrompik III glass wasteform possibility to have a good behaviour for longer duration.

Other tests and characterizations – USFD

N/A

Other tests and characterizations – VUJE

Specific surface area measurement:

Samples were prepared by pouring into cuboid monoliths of approx. 1.5 x 2x 1.5-2 cm.Surface of the original surface (without cutting and polishing the sample) using a 3D scanner Zeiss Comet L3D - Optical scanner.

Surface 1213.3089 mm^2 - 1530.5875 mm^2

Volume 3282.4282 mm^3 - 4719.8349 mm^3

deviation ± 0.004 mm

Conclusions and Outlooks - USFD

Chrompik III is a glass wasteform, with no evidence of any crystalline assemblages or other inhomogeneity, with a chemical composition close to that reported as batched. The chemical durability of this material is good, with a lower normalized mass loss of boron and silicon than ISG over a 28 day leaching period. Silicon and aluminium release drops after 21 days, indicating the formation of secondary precipitates, while boron and alkalis continue to be released into solution.

Conclusions and Outlooks - VUJE

Chrompik III glass sample was produces by vitrification process using VICHR facility at NPP A1 Jaslovske Bohunice, Slovakia. Chrompik III monolithes were prepared in VUJE´s laboratory. Final product consists of an amorphous glass mainly composed of mainly SiO_2, Na_2O, B_2O_3, and K_2O which present 84.6 % of the glass composition, with no evidence of any crystalline assembleges or other inhomogeneity.

Chemical composition of glass was analyzed by two techniques, there were only small differences observed between theoretical composition and XRF results. The comparison of the results obtained from USFD and VUJE´s results for chrompik III glass are in compliance, there is no free liquid or gas, sample is homogeneous and amorphous, also the chemical composition of this wasteform is compatible with both results.

Leaching tests were performed according to the modified ASTM C1220 using two methods. Leaching test conducted at 90°C show a similar evolution of the pH value, and for chemical durability assessment seems to be better method when the gel layer was wiped away and the surface was being restored.

Concluding about the long-term behaviour of Chromium III waste glass form would require further investigation.

4.15 Concentrate slag – Simuli 2 sample (SCK•CEN)

General information

Partner:	SCK.CEN
Sample id:	Simuli 2 sample
Contact person:	Karine Ferrand, Sébastien Caes and Karel Lemmens

Origin and macroscopic description

Figure 127: Plasma incineration of conditioned wasteforms: (A) Melt blending, (B) Cooling down, (C) Demoulding.

Figure 128: Pieces of plasma slags selected for the leaching tests.

Four surrogate wastes (Simuli) were prepared by mixing concentrates (82 kg), cement (148 kg), sand (51 kg), gravel (55 kg), lime (6 kg) and water (10 L). The concentration of the chemicals used to prepare the surrogate concentrate Simuli 2 is indicated in Table 40.

Concentrations in $g.L^{-1}$			
$NaOH$	0.000	**SiO_2**	8.570
$B(OH)_3$	13.287	**Na_3PO_4**	0.000
$NaCl$	17.766	**H_3PO_4**	9.747
$AlCl_3$	2.481	**Na_2SO_4**	0.000
$Ca(OH)_2$	12.617	**$CaSO_4$**	265.137
B_2CaO_4	0.000	**H_2SO_4**	0.000
$CaCl_2$	133.453	**$NaNO_3$**	1.597
$FeCl_3$	4.232	**$CuCl_2$**	0.217
$LiOH$	0.205	**CrO_3**	0.208
$LiCl$	0.000	**NiO**	0.241
$Mg(OH)_2$	4.305	**NaF**	0.592
$ZnCl_2$	1.236	**$NH_3 . H_2O$**	0.721

Table 40: Concentration in $g.L^{-1}$ of the chemicals mixed to obtain the surrogate concentrate Simuli 2 [NIROND, 2018].

The surrogate wasteform was treated using a plasma incinerator (1200 kW torch power) at the Phoenix Solutions Hutchinson Test Facility, by intermediation of the BelgoProcess company. After this process, the different mixtures were poured in a mould to let them cool down. Then, the moulds were emptied (Figure 127).

Figure 128 shows the Simuli 2 samples used for the leaching tests that were collected from one drums (200 L) received at SCK•CEN and currently stored at the premises of the EIG EURIDICE. The samples selected for the tests were those without any surface impurities (i.e. without white large particles) and without bright surfaces. The Simuli 2 sample is matte and porous.

Microstructure

Method(s):	☒ SEM ☒ XRD ☒ Other:
Operating conditions:	
Homogeneity:	Heterogeneous. Crystalline phases are however well dispersed in the matrix
Free liquid or gas:	Absence (Based on SEM pictures)

Crystalline composition:

XRD analysis revealed that the Simuli 2 sample is partially amorphous.

SEM-EDX analysis confirmed that the samples are composed of a homogeneous glassy matrix, which mainly contains SiO_2, Fe_2O_3, CaO, Al_2O_3.

Figure 129 shows the SEM micrograph and the elemental mappings for the Simuli 2 sample. Bright and grey dendrites identified as magnetite and clinopyroxene by XRD are observed; EDX data are indicated in Table 41.

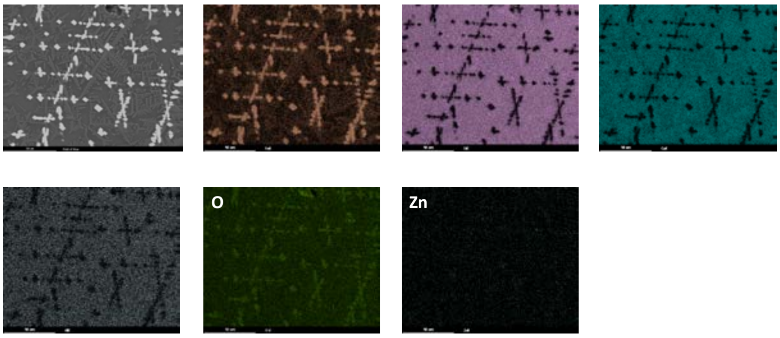

Figure 129: SEM micrograph and elemental mappings for the Simuli 2 sample.

	Bright dendrites (magnetite by XRD)	Grey dendrites (clinopyroxene by XRD)	Matrix (amorphous by XRD)
Fe_2O_3	77.8	23.3	9.1
SiO_2	11.5	45.3	51.4
CaO	4.7	22.5	30.9
Al_2O_3	3.0	5.3	6.8
ZnO	2.2		

Table 41: EDX analysis on the Simuli 2 sample (wt. %).

Comments and discussion:

Chemical composition

Method(s): ☐ EMP ☐ ICP-OES/MS ☒ XRF ☐ Other:

Operating conditions:

Chemical composition:

The composition in weight % of the plasma slags was determined by XRF and is given in Table 42.

SiO_2	Fe_2O_3	CaO	Al_2O_3	ZnO
40.1	30.5	20.7	5	1.5

Table 42: Composition of the Simuli 2 sample (in wt. %) given by XRF.

Comments and discussion:

Chemical durability

Method(s):

☒ As described in MS12 Report (p. 12-13), adapted from ASTM C1285
☐ As described in MS12 Report (p. 14), adapted from ASTM C1220
☐ Other:

Clarifications:

Static leaching tests were performed at 90 °C in ultrapure water with powders of the Simuli-2 plasma slag and ISG. The low sample surface area to solution volume (S/V) ratio of 10 m^{-1} guarantees that the concentration of rate controlling elements remains below the saturation concentration and thus the dissolution rate remains relatively high.

	Container	Weight of the container (g)	Glass (mg)	Weight of ultrapure water (g)	Weight of the system (water + glass + container) (g)
Simuli-2	TH-S2-01	198.50	28.40	220.04	418.54
	TH-S2-02	197.36	28.65	220.00	417.36
	TH-S2-03	198.12	28.37	220.02	418.14
ISG	TH-ISG-01	197.44	63.77	220.03	417.46
	TH-ISG-02	197.44	63.80	220.03	417.48
	TH-ISG-03	196.86	63.72	220.05	416.91
	TH-Bl*-01	197.95	/	220.05	418.00

Table 43: For each leaching test: mass of glass and solution volume.

After 28 days of alteration, containers were removed from the oven, manually homogenised and then cooled down to room temperature. The weight of the containers was measured to confirm that the evaporated volume was negligible. The leached solution was taken with a 5 mL syringe, then it was filtered on a 0.45 µm membrane and ultrafiltered (10k MWCO) at 6000 rpm during 20 minutes. Afterwards, the collected solutions were diluted with 5% HCl / 1% HNO_3 or 2 % HNO_3 and their chemical composition was determined by ICP-AES (Thermoscientific Iris Intrepid II dualview) or ICP-MS (Thermoscientific Xseries2).

As plasma treated surrogate wasteforms can be considered as glassy materials, their dissolution rates r in $g \cdot m^{-2} \cdot d^{-1}$ can be calculated as it is done for nuclear glass, i.e. according to Equation $r = \frac{NL(i)}{t}$.

Where t is the duration of the leaching test in days and NL(i) is the normalised mass loss for element i, expressed in $g \cdot m^{-2}$ according to Equation $NL(i) = \frac{(C_i .V .F_i)}{(f_i .SA)} = \frac{(m_i .F_i)}{(f_i .SA)}$

Where: C_i is the concentration of the element i in the aliquot of solution in $g \cdot m^{-3}$ (or $mg \cdot L^{-1}$),

V is the total volume of solution in m^3,

F_i is the factor to convert the atomic weight of element i to the molecular weight of the oxide containing the element i = molecular mass of the oxide / molecular mass of the element i in the oxide,

f_i is the weight percentage of the oxide containing the element i in the unaltered sample,

SA is the total surface area of the exposed sample in m^2,

m_i is the mass of the element i in volume V in g.

Usually for glass alteration, the rate is calculated from elements such as Na, B and Li, which are considered as good glass dissolution tracers because they are neither retained in the glass alteration layer nor in the crystalline phases that can precipitate. For the plasma slags, B_2O_3 and Li_2O are not present in their composition (B, Li). NaO was quantified only for the Simuli 3-A sample. Hence, the concentrations of the main elements (Si and Al) were used to calculate the dissolution rates.

From the normalised mass loss, the alteration layer thickness e (expressed in m) can be estimated according to Equation **e** = $\frac{NL(i)}{\rho} = \frac{NL(i) .V_{sample}}{m_{sample}}$

where NL(i) is the normalised mass loss of the element i in $g \cdot m^{-2}$, and ρ is the density of the sample in $g \cdot m^{-3}$, which is equal to the mass of the sample (m_{sample}) in g divided by the volume of the sample (V_{sample}) in m^3.

The density of the Simuli 2 sample was determined from the coupon weights and sizes prepared for the additional tests, which are not reported in Appendix H. Table 44 gives the average of the densities calculated for the Simuli-2 samples; the value found in literature for ISG is also indicated.

Samples	Density in $g \cdot m^{-3}$
Simuli 2	$3.15 \pm 0.08 \times 10^6$
ISG*	2.50*

* value reported in [Gin et al., 2015] as no ISG coupons were used in the additional tests

Table 44: Density in $g \cdot m^{-3}$ of the Simuli 2 sample used in the leaching tests (average of the values calculated for each coupon prepared for the additional tests) with the 95% confidence interval.

.Results and discussion:

Table 45 gives the pH measured at room temperature after 28 days of leaching at 90 °C in ultrapure water. The uncertainty at 2σ (95% confidence interval) on the pH measurement is equal to 0.02. For ISG, pH increases up to 8 – 8.4 whereas lower pH values of 6 – 6.5 are measured for the Simuli 2 sample.

Container	pH $_{(RT)}$
Simuli 2-01	6.55
Simuli 2-02	6.51
Simuli 2-03	5.88
ISG-01	8.38
ISG-02	8.06
ISG-03	8.02

Table 45: pH$_{(RT)}$ measured after 28 days of leaching at 90 °C in ultrapure water.

The element concentrations measured in the leachates after 28 days of alteration at 90 °C in ultrapure water are presented in Appendix G.

Table 46 gives the normalised mass losses (NL) in $g\cdot m^{-2}$ calculated from the element concentrations and Figure 130Figure *130* shows the NL as a function of time with the 95 % confidence intervals, calculated by error propagation.

Leaching days – Simuli-2 sample				
	28 (1)	**28 (2)**	**28 (3)**	Average
NL(Si)	1.28 ± 0.08	2.09 ± 0.13	1.38 ± 0.09	1.58 ± 0.10
NL(Al)	0.55 ± 0.05	0.65 ± 0.05	0.63 ± 0.05	0.61 ± 0.05
NL(Ca)	1.22 ± 0.08	1.76 ± 0.11	1.30 ± 0.09	1.43 ± 0.09
NL(Fe)	0.01 ± 0.005	0.01 ± 0.005	0.01 ± 0.005	0.01 ± 0.005
NL(Zn)	0.58 ± 0.04	0.15 ± 0.01	0.64 ± 0.04	0.46 ± 0.01
Leaching days – ISG sample				
	28 (1)	**28 (2)**	**28 (3)**	Average
NL(Si)	4.05 ± 0.25	4.17 ± 0.25	4.09 ± 0.25	4.10 ± 0.25
NL(Al)	3.33 ± 0.21	3.39 ± 0.21	3.51 ± 0.22	3.41 ± 0.21
NL(Ca)	2.84 ± 0.22	3.12 ± 0.24	3.03 ± 0.24	2.99 ± 0.23
NL(B)	5.55 ± 0.58	5.51 ± 0.59	5.56 ± 0.58	5.54 ± 0.59
NL(Na)	5.27 ± 0.80	4.68 ± 0.80	4.07 ± 0.80	4.67 ± 0.78

Table 46: Normalised mass losses (NL) in g·m^{-2} calculated from the element concentrations after 28 days of leaching.

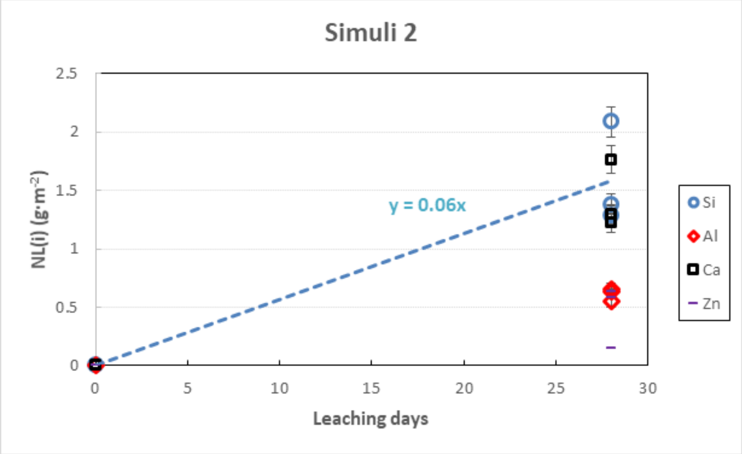

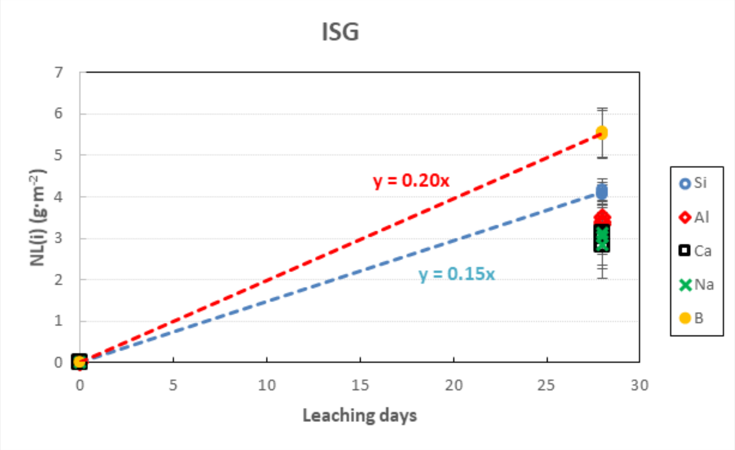

Figure 130: NL(i) as a function of the leaching time with indication of the dissolution rate between 0 and 28 days for the average NL(Si) (in blue) and average NL(B) (in red) after 28 days.

For the Simuli 2 sample, more than 50 % of Al and 5 – 10 % of Ca are retained in the alteration layer compared to Si, which is the most soluble element for all plasma slags. Fe is not released in solution and Zn is also mainly retained in the alteration layer.

The dissolution rates can be determined from the NL(Si); they are given by the slope of the linear regression between the origin (0,0) and the NL(Si) values of the triplicate after 28 days.

A rate of 0.060 ± 0.002 g·m^{-2}·d^{-1} is determined for the Simuli 2 sample.

The NL(i) values for ISG suggest that the glass does not dissolve congruently and that B can be considered as the best glass dissolution tracer at near neutral pH and 90 °C. Compared to the B release, 38% of Al, 25 % of Si, 15% of Na and 5 – 25% of Ca are retained in the alteration layer.

The dissolution rates based on NL(B) and NL(Si) are equal to 0.20 ± 0.01 $g \cdot m^{-2} \cdot d^{-1}$ and 0.15 ± 0.005 $g \cdot m^{-2} \cdot d^{-1}$, respectively.

After 28 days of alteration in ultrapure water at 90 °C, the dissolution rates found for the plasma slags and ISG are similar supporting the hypothesis that plasma slags have a similar dissolution behaviour in the investigated conditions on the short term than nuclear glass. However, the dissolution rate calculated for the Simuli 2 sample is more than three times lower than the other ones (see § 4.16 and 4.17) suggesting the formation of a more protective alteration layer for this plasma slag and/or a lower initial (or forward) dissolution rate. Note that the dissolution rate determined for ISG is in good agreement with the value reported by CEA (see § 4.1).

Table 47 gives the alteration layer thicknesses calculated from the average NL(Si) values. A very thin alteration layer of 0.5 µm is calculated for the Simuli 2 sample compared to around 2 µm for ISG sample.

Samples	**Alteration layer thickness (µm)**
Simuli 2	0.50 ± 0.07
ISG	1.64 ± 0.22

Table 47: Alteration layer thicknesses calculated from the average NL(Si) values after 28 days of leaching.

Additionnal standardised leaching tests on coupons (KOH solution at pH 13.5 and 40°C) are presented in Appendix H.

Other tests and characterizations

Specific surface area measurement

To carry out the standardised leaching tests, i.e. in ultrapure water at 90 °C, small pieces of the Simuli 2 sample were crushed and sieved to collect powder with a 125 – 250 µm size fraction (Figure 131). Then, the powder was washed with ultrapure water and dried at around 65 °C. The specific surface area was measured by BET using Kr as adsorbent gas (MICROMERITICS ASAP 2020) at the Catholic University of Louvain-la-Neuve (Institute of Condensed Matter and Nanosciences) after pre-treatment of the samples, i.e. heating up to 200 °C at 10 °C/min followed by a 4 hours plateau at 120 °C under vacuum. It was equal to 0.0780 $m^2 \cdot g^{-1}$. The experimental uncertainty on the BET measurement was not specified.

Simuli 2

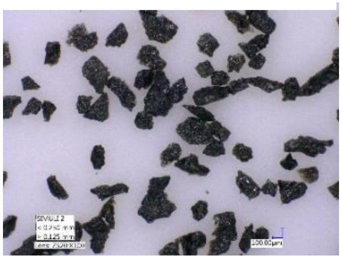

Figure 131: Picture of the Simuli-2 powder with a 125 – 250 µm size fraction.

Conclusions and Outlooks

For the WP4 of the THERAMIN project, static leaching tests following the standard procedure ASTM C1285 were carried out with a plasma slag, i.e. Simuli 2. In order to make an intercomparison, similar tests were done with ISG coming from the same batch and provided to all partner laboratories. For these tests, the following experimental conditions were selected by the THERAMIN partner laboratories: ultrapure water, 90 °C, S/V ratio of 10 m^{-1}.

For the Simuli 2 sample, more than 50 % of Al and 5 – 10 % of Ca were retained in the alteration layer compared to Si, which was the most soluble element for all plasma slags. Fe was not released in solution and Zn was also mainly retained in the alteration layer. However, the retention of these elements in the alteration layer could not be confirmed as it was not possible to perform solid analyzes.

After 28 days of alteration in ultrapure water at 90 °C, a dissolution rate of 0.060 g·m^{-2}·d^{-1} was determined for the Simuli 2 sample.

The NL(i) values for ISG suggested that the glass did not dissolve congruently and that B could be considered as the best glass dissolution tracer at near neutral pH and 90 °C. Compared to the B release, 38% of Al, 25 % of Si, 15% of Na and 5 – 25% of Ca were retained in the alteration layer. The dissolution rates based on NL(B) and NL(Si) were equal to 0.20 g·m^{-2}·d^{-1} and 0.15 g·m^{-2}·d^{-1}, respectively.

The dissolution rates found for the Simuli 2 sample- is thus three times lower than the one found for ISG suggesting the formation of a more protective alteration layer and/or a lower initial (or forward) dissolution rate for this plasma slag.

4.16 Concentrate slag – Simuli-3A sample (SCK.CEN)

General information

Partner:	SCK.CEN
Sample id:	Simuli3-A sample
Contact person:	Karine Ferrand, Sébastien Caes and Karel Lemmens

Origin and macroscopic description

Figure 132: Plasma incineration of conditioned wasteforms: (A) Melt blending, (B) Cooling down, (C) Demoulding.

Figure 133: Pieces of plasma slags selected for the leaching tests.

Four surrogate wastes (Simuli) were prepared by mixing concentrates (82 kg), cement (148 kg), sand (51 kg), gravel (55 kg), lime (6 kg) and water (10 L). The concentration of the chemicals used to prepare the surrogate concentrate Simuli3-A is indicated in Table 48.

Concentrations in $g.L^{-1}$			
$NaOH$	109.200	**SiO_2**	8.570
$B(OH)_3$	285.160	**Na_3PO_4**	16.306
$NaCl$	0.808	**H_3PO_4**	0.000
$AlCl_3$	2.481	**Na_2SO_4**	276.628
$Ca(OH)_2$	89.671	**$CaSO_4$**	0.000
B_2CaO_4	0.000	**H_2SO_4**	0.000
$CaCl_2$	0.000	**$NaNO_3$**	1.597
$FeCl_3$	4.232	**$CuCl_2$**	0.217
$LiOH$	0.205	**CrO_3**	0.208
$LiCl$	0.000	**NiO**	0.241
$Mg(OH)_2$	4.305	**NaF**	0.592
$ZnCl_2$	1.236	**$NH_3 . H_2O$**	0.721

Table 48: Concentration in $g.L^{-1}$ of the chemicals mixed to obtain the surrogate concentrates [NIROND, 2018].

The surrogate wasteform was treated using a plasma incinerator (1200 kW torch power) at the Phoenix Solutions Hutchinson Test Facility, by intermediation of the BelgoProcess company. After this process, the different mixtures were poured in a mould to let them cool down. Then, the moulds were emptied (Figure 132).

Figure 133 shows the samples used for the leaching tests that were collected from the drum (100 L) received at SCK•CEN and currently stored at the premises of the EIG EURIDICE. The samples selected for the tests were those without any surface impurities (i.e. without

	white large particles) and without bright surfaces. The Simuli 3-A sample is very glossy and looks like SON68 glass.
Microstructure	
Method(s):	☒ SEM ☒ XRD ☒ Other:
Operating conditions:	
Homogeneity:	Homogeneous
Free liquid or gas:	Absence
Crystalline composition:	XRD analysis revealed that the Simuli3-A sample is amorphous. SEM-EDX analysis confirmed that the sample is composed of a homogeneous glassy matrix, which mainly contains SiO_2, Fe_2O_3, CaO, Al_2O_3. Figure 134 shows a SEM micrograph and the elemental mappings of to the Simuli3-A sample. 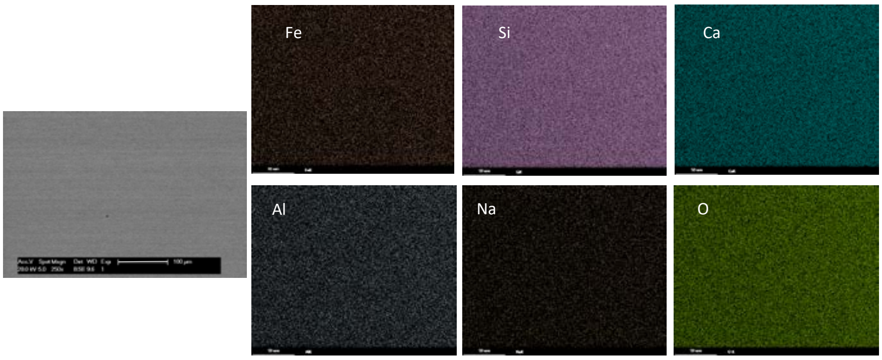 *Figure 134: SEM micrograph and elemental mappings for the Simuli3-A sample.*
Comments and discussion:	

Chemical composition

Method(s):	☐ EMP ☐ ICP-OES/MS ☒ XRF ☐ Other:
Operating conditions:	

Chemical composition:

The composition in weight % of the Simuli 3-A sample was determined by XRF and is given in Table 49.

SiO_2	Fe_2O_3	CaO	Al_2O_3	Na_2O	ZnO
49.5	14	25.6	6	2.1	1.1

Table 49: Composition of the Simuli-3A sample (in wt. %) given by XRF.

Comments and discussion:

Chemical durability

Method(s):

☒ As described in MS12 Report (p. 12-13), adapted from ASTM C1285
☐ As described in MS12 Report (p. 14), adapted from ASTM C1220
☐ Other:

Clarifications:

Static leaching tests were performed at 90 °C in ultrapure water with powders of the Simuli-3A plasma slag and ISG. The low sample surface area to solution volume (S/V) ratio of 10 m^{-1} guarantees that the concentration of rate controlling elements remains below the saturation concentration and thus the dissolution rate remains relatively high.

	Container	Weight of the container (g)	Glass (mg)	Weight of ultrapure water (g)	Weight of the system (water + glass + container) (g)
Simuli-3A	TH-S3-01	197.38	64.89	220.08	417.45
	TH-S3-02	197.61	64.84	220.10	417.72
	TH-S3-03	196.69	64.72	220.09	416.78
ISG	TH-ISG-01	197.44	63.77	220.03	417.46
	TH-ISG-02	197.44	63.80	220.03	417.48
	TH-ISG-03	196.86	63.72	220.05	416.91
	TH-Bl-01	197.95	/	220.05	418.00

Table 50: For each leaching test: mass of glass and solution volume.

After 28 days of alteration, containers were removed from the oven, manually homogenised and then cooled down to room temperature. The weight of the containers was measured to confirm that the evaporated volume was negligible. The leached solution was taken with a 5 mL syringe, then it was filtered on a 0.45 µm membrane and ultrafiltered (10k MWCO) at 6000 rpm during 20 minutes. Afterwards, the collected solutions were diluted with 5% HCl / 1% HNO_3 or 2 % HNO_3 and their chemical composition was determined by ICP-AES (Thermoscientific Iris Intrepid II dualview) or ICP-MS (Thermoscientific Xseries2).

As plasma treated surrogate wasteforms can be considered as glassy materials, their dissolution rates r in $g \cdot m^{-2} \cdot d^{-1}$ can be calculated as it is done for nuclear glass, i.e. according to Equation $r = \frac{NL(i)}{t}$.

Where t is the duration of the leaching test in days and NL(i) is the normalised mass loss for element i, expressed in $g \cdot m^{-2}$ according to Equation $NL(i) = \frac{(C_i . V . F_i)}{(f_i . SA)} = \frac{(m_i . F_i)}{(f_i . SA)}$

Where: C_i is the concentration of the element i in the aliquot of solution in $g \cdot m^{-3}$ (or $mg \cdot L^{-1}$),

V is the total volume of solution in m^3,

F_i is the factor to convert the atomic weight of element i to the molecular weight of the oxide containing the element i = molecular mass of the oxide / molecular mass of the element i in the oxide,

f_i is the weight percentage of the oxide containing the element i in the unaltered sample,

SA is the total surface area of the exposed sample in m^2,

m_i is the mass of the element i in volume V, in g.

Usually for glass alteration, the rate is calculated from elements such as Na, B and Li, which are considered as good glass dissolution tracers because they are neither retained in the glass alteration layer nor in the crystalline phases that can precipitate. For the plasma slags, B_2O_3 and Li_2O are not present in their composition (B, Li). NaO was quantified only for the Simuli 3-A sample. Hence, the concentrations of the main elements (Si and Al) were used to calculate the dissolution rates.

From the normalised mass loss, the alteration layer thickness e (expressed in m) can be estimated according to Equation $e = \frac{NL(i)}{\rho} = \frac{NL(i) . V_{sample}}{m_{sample}}$

where NL(i) is the normalised mass loss of the element i in $g \cdot m^{-2}$, and ρ is the density of the sample in $g \cdot m^{-3}$, which is equal to the mass of the sample (m_{sample}) in g divided by the volume of the sample (V_{sample}) in m^3.

The densities for the plasma slags were determined from the coupon weights and sizes prepared for the additional tests, which are reported in Appendix H. Table 51 gives the average of the densities calculated for each Simuli3-A coupons prepared for the additional tests; the value found in literature for ISG is also indicated.

Samples	Density in $g \cdot m^{-3}$
Simuli 3-A	$2.83 \pm 0.08 \times 10^6$
ISG*	2.50*

* value reported in [Gin et al., 2015] as no ISG coupons were used in the additional tests

Table 51: Density in $g \cdot m^{-3}$ of the plasma slags used in the leaching tests (average of the values calculated for each sample) with the 95% confidence interval.

Results and discussion:

Table 52 gives the pH measured at room temperature after 28 days of leaching at 90 °C in ultrapure water. The uncertainty at

2σ (95% confidence interval) on the pH measurement is equal to 0.02. For the Simuli 3-A pH reaches 9.1 – 9.5 whereas lower pH values of 8 – 8.4 are measured for the ISG sample.

Container	pH $_{(RT)}$
Simuli 3-A-01	8.7
Simuli 3-A-02	9.27
Simuli 3-A-03	9.35
ISG-01	8.38
ISG-02	8.06
ISG-03	8.02

Table 52: pH$_{(RT)}$ measured after 28 days of leaching at 90 °C in ultrapure water.

The element concentrations measured in the leachates after 28 days of alteration at 90 °C in ultrapure water are presented in Appendix G.

Table 53 gives the normalised mass losses (NL) in g·m^{-2} calculated from the element concentrations and Figure 135 shows the NL as a function of time with the 95% confidence intervals, calculated by error propagation.

Si, Al and Ca are released congruently. Fe is not released in solution and Zn is also mainly retained in the alteration layer.

Leaching days – Simuli-3A sample				
	28 (1)	**28 (2)**	**28 (3)**	Average
NL(Si)	5.43 ± 0.34	5.70 ± 0.34	5.69 ± 0.34	5.61 ± 0.35
NL(Al)	4.83 ± 0.29	5.70 ± 0.33	5.69 ± 0.31	5.06 ± 0.31
NL(Ca)	4.72 ± 0.30	5.17 ± 0.31	5.16 ± 0.31	5.02 ± 0.30
NL(Fe)	0.02 ± 0.01	0.02 ± 0.01	0.02 ± 0.01	0.02 ± 0.01
NL(Zn)	0.020 ± 0.003	0.030 ± 0.003	0.020 ± 0.003	0.025 ± 0.003
Leaching days – ISG sample				
	28 (1)	**28 (2)**	**28 (3)**	Average
NL(Si)	4.05 ± 0.25	4.17 ± 0.25	4.09 ± 0.25	4.10 ± 0.25
NL(Al)	3.33 ± 0.21	3.39 ± 0.21	3.51 ± 0.22	3.41 ± 0.21
NL(Ca)	2.84 ± 0.22	3.12 ± 0.24	3.03 ± 0.24	2.99 ± 0.23
NL(B)	5.55 ± 0.58	5.51 ± 0.59	5.56 ± 0.58	5.54 ± 0.59
NL(Na)	5.27 ± 0.80	4.68 ± 0.80	4.07 ± 0.80	4.67 ± 0.78

Table 53: Normalised mass losses (NL) in g·m^{-2} calculated from the element concentrations, with the 95% confidence interval.

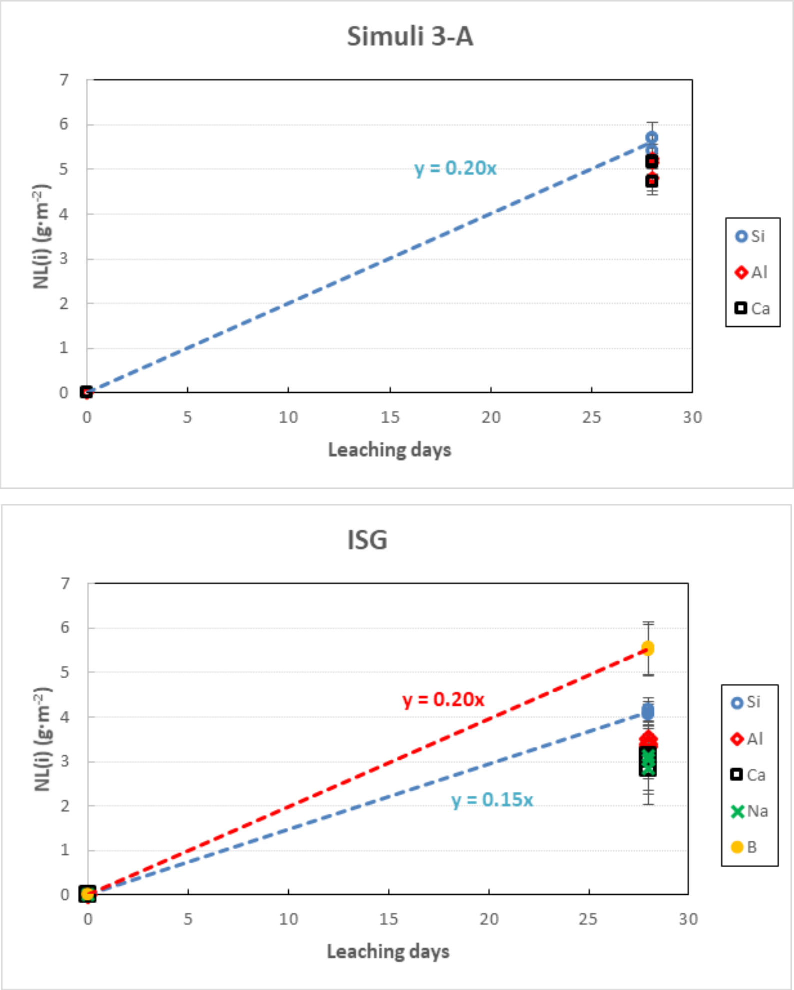

Figure 135: NL(i) as a function of the leaching time with indication of the dissolution rate between 0 and 28 days for the average NL(Si) (in blue) and average NL(B) (in red) after 28 days.

The dissolution rates can be determined from the NL(Si); they are given by the slope of the linear regression between the origin (0,0) and the NL(Si) values of the triplicate after 28 days.

A rate of 0.20 ± 0.07 g·m^{-2}·d^{-1} is determined for the Simuli 3-A sample. The NL(i) values for ISG suggest that the glass does not dissolve congruently and that B can be considered as the best glass dissolution tracer at near neutral pH and 90 °C. Compared to the B release, 38% of Al, 25 % of Si, 15% of Na and 5 – 25% of Ca are retained in the alteration layer. The dissolution rates based on NL(B) and NL(Si) are equal to 0.20 ± 0.01 $g \cdot m^{-2} \cdot d^{-1}$ and 0.15 ± 0.005 $g \cdot m^{-2} \cdot d^{-1}$, respectively.

After 28 days of alteration in ultrapure water at 90 °C, the dissolution rates found for the Simuli 3-A sample and ISG are similar supporting the hypothesis that plasma slags have a similar dissolution behaviour on the short term than nuclear glass. Note that the dissolution rate determined for ISG is in good agreement with the value reported by CEA (see § 4.1).

Table 54 gives the alteration layer thicknesses calculated from the average NL(Si) values after 28 days of leaching.

Samples	Alteration layer thickness (µm)
Simuli 3-A	1.98 ± 0.27
ISG	1.64 ± 0.22

Table 54: Alteration layer thicknesses calculated from the average NL(Si) values after 28 days of leaching.

Additionnal standardised leaching tests on coupons (KOH solution at pH 13.5 and 0°C) are presented in appendix H.

Other tests and characterizations

Specific surface area measurement

To carry out the standardised leaching tests, i.e. in ultrapure water at 90 °C, small pieces of the Simuli 3-A sample were crushed and sieved to collect powders with a 125 – 250 µm size fraction (Figure 136). Then, the powder was washed with ultrapure water and dried at around 65 °C. The specific surface area was measured by BET using Kr as adsorbent gas (MICROMERITICS ASAP 2020) at the Catholic University of Louvain-la-Neuve (Institute of Condensed Matter and Nanosciences) after pre-treatment of the samples, i.e. heating up to 200 °C at 10 °C/min followed by a 4 hours plateau at 120 °C under vacuum. It was equal to 0.0340 $m^2 \cdot g^{-1}$. The experimental uncertainty on the BET measurement was not specified.

Figure 136: Picture of the Simuli3-A powder with a 125 – 250 µm size fraction.

Conclusions and Outlooks

For the WP4 of the THERAMIN project, static leaching tests following the standard procedure ASTM C1285 were carried out with a plasma slag Simuli 3-A. In order to make an intercomparison, similar tests were done with ISG coming from the same batch and provided to all partner laboratories. For these tests, the following experimental conditions were selected by the THERAMIN partner laboratories: ultrapure water, 90 °C, S/V ratio of 10 m^{-1}.

For the Simuli 3-A sample, Si, Al and Ca were released congruently. Fe was not released in solution and Zn was also mainly retained in the alteration layer. However, the retention of these elements in the alteration layer could not be confirmed as it was not possible to perform solid analyzes.

After 28 days of alteration in ultrapure water at 90 °C, a dissolution rate of 0.20 $g{\cdot}m^{-2}{\cdot}d^{-1}$ was determined for the Simuli 3-A sample. The NL(i) values for ISG suggested that the glass did not dissolve congruently and that B could be considered as the best glass dissolution tracer at near neutral pH and 90 °C. Compared to the B release, 38% of Al, 25 % of Si, 15% of Na and 5 – 25% of Ca were retained in the alteration layer. The dissolution rates based on NL(B) and NL(Si) were equal to 0.20 $g{\cdot}m^{-2}{\cdot}d^{-1}$ and 0.15 $g{\cdot}m^{-2}{\cdot}d^{-1}$, respectively.

The dissolution rates found for the Simuli 3-A sample and ISG were similar supporting the hypothesis that the Simuli 3-A sample has a similar dissolution behaviour on the short term in the investigated conditions than nuclear glass.

4.17 Resin slag – R2 IRN 78 sample (SCK.CEN)

General information	
Partner:	SCK.CEN
Sample id:	R2IRN78 sample
Contact person:	Karine Ferrand, Sébastien Caes and Karel Lemmens

Origin and macroscopic description

Figure 137: Plasma incineration of conditioned wasteforms: (A) Melt blending, (B) Cooling down, (C) Demoulding.

Figure 138: Pieces of plasma slags selected for the leaching tests.

Two surrogate wastes originating from resins were also made: one from an anionic resin loaded with $B(OH)_3$ (15 kg) and NaOH (to obtain a pH>9.14) mixed with cement (83 kg), sand (55 kg), gravel (55 kg), lye (3 kg), BFS (83 kg), resin (75 L) and water (40 L); and another one from a cationic resin loaded with LiOH (10 kg) mixed with cement (83 kg); sand (55 kg), gravel (150 kg), lye (3 kg), BFS (83 kg), resin (75 L) and water (40 L).

All surrogate wasteforms were treated using a plasma incinerator (1200 kW torch power) at the Phoenix Solutions Hutchinson Test Facility, by intermediation of the BelgoProcess company. After this process, the different mixtures were poured in a mould to let them cool down. Then, the moulds were emptied (Figure 137).

Figure 138 shows the sample R2 IRN 78 used for the leaching tests. The sample selected for the tests was those without any surface impurities (i.e. without white large particles) and without bright surfaces. The R2 IRN 78 sample is very glossy and looks like SON68 glass.

Microstructure

Method(s):	☒ SEM ☒ XRD ☒ Other: X-Ray Fluorescence (XRF)
Operating conditions:	
Homogeneity:	Homogeneous
Free liquid or gas:	Absence

Crystalline composition:

XRD analysis revealed that the R2 IRN 78 sample is amorphous.

SEM-EDX analysis confirmed that the sample is composed of a homogeneous glassy matrix, which mainly contains SiO_2, Fe_2O_3, CaO, Al_2O_3. Figure 139 shows a SEM micrograph and the elemental mappings of a sample (Simuli-1A) very similar to R2 IRN 78 sample. Note that for the R2 IRN 78 sample, a few crystals looking like magnetite dendrites were present.

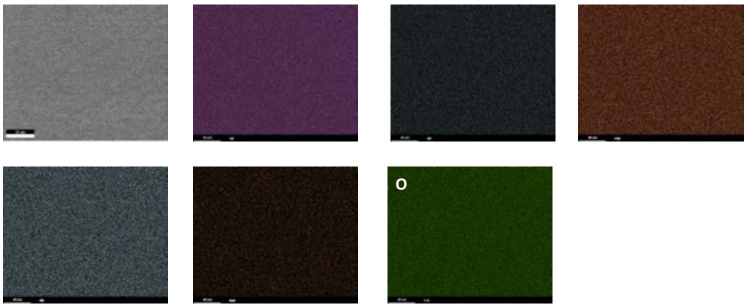

Figure 139: SEM micrograph and elemental mappings for the Simuli-1A sample, very similar to R2 IRN 78 sample.

Comments and discussion:

Chemical composition

Method(s):	☐ EMP ☐ ICP-OES/MS ☒ XRF ☐ Other:
Operating conditions:	

Chemical composition:

The composition in weight % of the plasma slags was determined by XRF and is given in Table 55.

SiO_2	Fe_2O_3	CaO	Al_2O_3	MgO
45.6	11.8	27.9	9.0	2.2

Table 55: Composition of the R-IRN-8 sample (in wt. %) given by XRF.

Comments and discussion:

Chemical durability

Method(s):

☒ As described in MS12 Report (p. 12-13), adapted from ASTM C1285
☐ As described in MS12 Report (p. 14), adapted from ASTM C1220
☐ Other:

Clarifications:

Static leaching tests were performed at 90 °C in ultrapure water with powders of the R2 IRN 78 plasma slag and ISG. The low sample surface area to solution volume (S/V) ratio of 10 m^{-1} guarantees that the concentration of rate controlling elements remains below the saturation concentration and thus the dissolution rate remains relatively high.

	Container	Weight of the container (g)	Glass (mg)	Weight of ultrapure water (g)	Weight of the system (water + glass + container) (g)
R2 IRN 78	TH-R2-01	197.46	65.07	220.05	417.51
	TH-R2-02	197.00	64.67	220.04	417.04
	TH-R2-03	197.41	64.85	220.05	417.46
ISG	TH-ISG-01	197.44	63.77	220.03	417.46
	TH-ISG-02	197.44	63.80	220.03	417.48
	TH-ISG-03	196.86	63.72	220.05	416.91
	TH-Bl-01	197.95	/	220.05	418.00

Table 56: For each leaching test: mass of glass and solution volume.

After 28 days of alteration, containers were removed from the oven, manually homogenised and then cooled down to room temperature. The weight of the containers was measured to confirm that the evaporated volume was negligible. The leached solution was taken with a 5 mL syringe, then it was filtered on a 0.45 µm membrane and ultrafiltered (10k MWCO) at 6000 rpm during 20 minutes. Afterwards, the collected solutions were diluted with 5% HCl / 1% HNO_3 or 2 % HNO_3 and their chemical composition was determined by ICP-AES (Thermoscientific Iris Intrepid II dualview) or ICP-MS (Thermoscientific Xseries2).

As plasma treated surrogate wasteforms can be considered as glassy materials, their dissolution rates r in $g \cdot m^{-2} \cdot d^{-1}$ can be calculated as it is done for nuclear glass, i.e. according to Equation $r = \frac{NL(i)}{t}$.

Where t is the duration of the leaching test in days and NL(i) is the normalised mass loss for element i, expressed in $g \cdot m^{-2}$ according to Equation $NL(i) = \frac{(C_i .V .F_i)}{(f_i .SA)} = \frac{(m_i .F_i)}{(f_i .SA)}$

Where: C_i is the concentration of the element i in the aliquot of solution in $g \cdot m^{-3}$ (or $mg \cdot L^{-1}$),

V is the total volume of solution in m^3,

F_i is the factor to convert the atomic weight of element i to the molecular weight of the oxide containing the element i = molecular mass of the oxide / molecular mass of the element i in the oxide,

f_i is the weight percentage of the oxide containing the element i in the unaltered sample,

SA is the total surface area of the exposed sample in m^2,

m_i is the mass of the element i in volume V, in g.

Usually for glass alteration, the rate is calculated from elements such as Na, B and Li, which are considered as good glass dissolution tracers because they are neither retained in the glass alteration layer nor in the crystalline phases that can precipitate. For the plasma slags, B_2O_3 and Li_2O are not present in their composition (B, Li). NaO was quantified only for the Simuli 3-A sample. Hence, the concentrations of the main elements (Si and Al) were used to calculate the dissolution rates.

From the normalised mass loss, the alteration layer thickness e (expressed in m) can be estimated according to Equation $\mathbf{e} = \frac{NL(i)}{\rho} = \frac{NL(i)\,.V_{sample}}{m_{sample}}$

where NL(i) is the normalised mass loss of the element i in $g \cdot m^{-2}$, and ρ is the density of the sample in $g \cdot m^{-3}$, which is equal to the mass of the sample (m_{sample}) in g divided by the volume of the sample (V_{sample}) in m^3.

The densities for the plasma slags were determined from the coupon weights and sizes prepared for the additional tests, which are not reported here. Table 57 gives the average of the densities calculated for R2IRN 78 and ISG samples.

Samples	Density in $g \cdot m^{-3}$
R2 IRN 78	$2.88 \pm 0.08 \times 10^6$
ISG*	2.50*

* value reported in [Gin et al., 2015] as no coupons were used in the additional tests

Table 57: Density in $g \cdot m^{-3}$ of the plasma slags used in the leaching tests (average of the values calculated for each sample) with the 95% confidence interval.

Results and discussion:

Table 58 gives the pH measured at room temperature after 28 days of leaching at 90 °C in ultrapure water. The uncertainty at 2σ (95% confidence interval) on the pH measurement is equal to 0.02. For the R2 IRN 78 sample pH reaches 9.1 – 9.5 whereas lower pH values of 8 – 8.4 are measured for the ISG sample.

Container	pH (RT)
R2 IRN 78-01	9.51
R2 IRN 78-02	9.53
R2 IRN 78-03	9.52
ISG-01	8.38
ISG-02	8.06
ISG-03	8.02

Table 58: pH$_{(RT)}$ measured after 28 days of leaching at 90 °C in ultrapure water.

Te element concentrations measured in the leachates after 28 days of alteration at 90 °C in ultrapure wate rare presented in Appendix G.

Table 59 gives the normalised mass losses (NL) in g·m^{-2} calculated from the element concentrations and Figure 140 shows the NL as a function of time with the 95% confidence intervals, calculated by error propagation.

Leaching days – R2 IRN 78 sample				
	28 (1)	**28 (2)**	**28 (3)**	Average
NL(Si)	5.31 ± 0.32	5.11 ± 0.31	5.33 ± 0.32	5.25 ± 0.32
NL(Al)	4.60 ± 0.28	4.39 ± 0.27	4.52 ± 0.27	4.50 ± 0.28
NL(Ca)	5.27 ± 0.33	5.11 ± 0.31	5.29 ± 0.34	5.23 ± 0.33
NL(Fe)	0.024 ± 0.010	0.024 ± 0.010	0.024 ± 0.010	0.020 ± 0.010
Leaching days – ISG sample				
	28 (1)	**28 (2)**	**28 (3)**	Average
NL(Si)	4.05 ± 0.25	4.17 ± 0.25	4.09 ± 0.25	4.10 ± 0.25
NL(Al)	3.33 ± 0.21	3.39 ± 0.21	3.51 ± 0.22	3.41 ± 0.21
NL(Ca)	2.84 ± 0.22	3.12 ± 0.24	3.03 ± 0.24	2.99 ± 0.23
NL(B)	5.55 ± 0.58	5.51 ± 0.59	5.56 ± 0.58	5.54 ± 0.59
NL(Na)	5.27 ± 0.80	4.68 ± 0.80	4.07 ± 0.80	4.67 ± 0.78

Table 59: Normalised mass losses (NL) in g·m^{-2} calculated from the element concentrations after 28 days of leaching.

Remark: for the R2 IRN 78 sample, Na concentrations measured after 28 days are similar as the one in the blank so NL(Na) cannot be calculated.

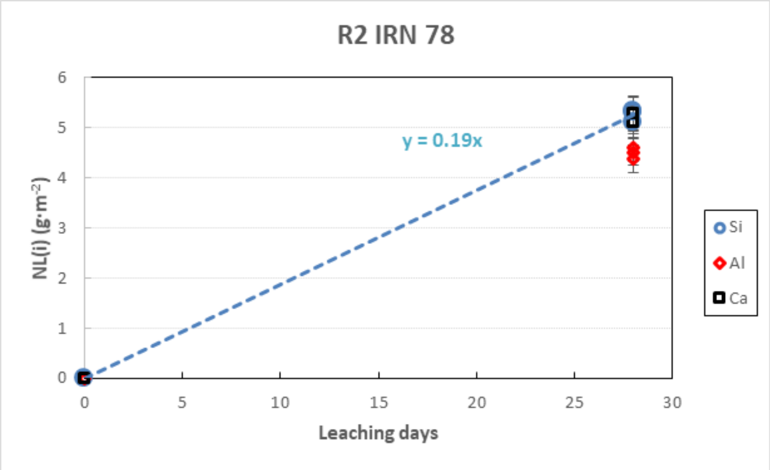

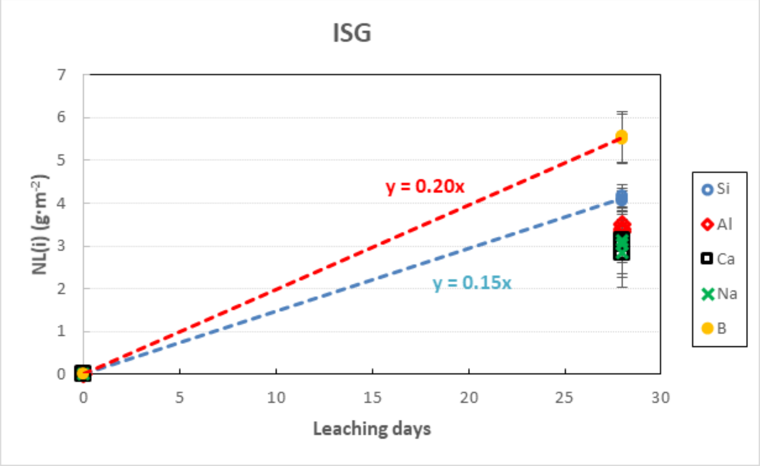

Figure 140: NL(i) as a function of the leaching time with indication of the dissolution rate between 0 and 28 days for the average NL(Si) (in blue) and average NL(B) (in red) after 28 days.

Si, Al and Ca are released congruently. Fe is not released in solution.

The dissolution rates can be determined from the NL(Si); they are given by the slope of the linear regression between the origin (0,0) and the NL(Si) values of the triplicate after 28 days.

A rate of 0.19 ± 0.07 $g \cdot m^{-2} \cdot d^{-1}$ is determined for the R2 IRN 78 sample. The NL(i) values for ISG suggest that the glass does not dissolve congruently and that B can be considered as the best glass dissolution tracer at near neutral pH and 90 °C. Compared to the B release, 38% of Al, 25 % of Si, 15% of Na and 5 – 25% of Ca are retained in the alteration layer. The dissolution rates based on NL(B) and NL(Si) are equal to 0.20 ± 0.01 $g \cdot m^{-2} \cdot d^{-1}$ and 0.15 ± 0.005 $g \cdot m^{-2} \cdot d^{-1}$, respectively.

After 28 days of alteration in ultrapure water at 90 °C, the dissolution rates found for the plasma slags and ISG are similar supporting the hypothesis that plasma slags have a similar dissolution behaviour on the short term than nuclear glass. Note that the dissolution rate determined for ISG is in good agreement with the value reported by CEA (see § 4.1).

Table 60 gives the alteration layer thicknesses calculated from the average NL(Si) values after 28 days of leaching..

Samples	**Theoretical alteration layer thickness (µm)**
R2 IRN 78	1.83 ± 0.24
ISG	1.64 ± 0.22

Table 60: Alteration layer thicknesses calculated from the average NL(Si) values after 28 days of leaching.

Additionnal standardised leaching tests on coupons (KOH solution at pH 13.5 and at 40°C) are presented in appendix H.

Other tests and characterizations

Specific surface area measurement

To carry out the standardised leaching tests, i.e. in ultrapure water at 90 °C, small pieces of the R2 IRN 78 samples were crushed and sieved to collect powder with a 125 – 250 µm size fraction (Figure 141). Then, the powder was washed with ultrapure water and dried at around 65 °C. The specific surface area was measured by BET using Kr as adsorbent gas (MICROMERITICS ASAP 2020) at the Catholic University of Louvain-la-Neuve (Institute of Condensed Matter and Nanosciences) after pre-treatment of the samples, i.e. heating up to 200 °C at 10 °C/min followed by a 4 hours plateau at 120 °C under vacuum. It was equal to 0.0340 $m^2 \cdot g^{-1}$. The experimental uncertainty on the BET measurement was not specified.

Figure 141: Picture of the R2 IRN 78 powder with a 125 – 250 µm size fraction.

Conclusions and Outlooks

For the WP4 of the THERAMIN project, static leaching tests following the standard procedure ASTM C1285 were carried out with a resin plasma slag identified as R2 IRN 78. In order to make an intercomparison, similar tests were done with ISG coming from the same batch and provided to all partner laboratories. For these tests, the following experimental conditions were selected by the THERAMIN partner laboratories: ultrapure water, 90 °C, S/V ratio of 10 m^{-1}.

For the R2 IRN 78 sample, Si, Al and Ca were released congruently. Fe was not released in solution. However, the retention of this element in the alteration layer could not be confirmed as it was not possible to perform solid analyzes.

After 28 days of alteration in ultrapure water at 90 °C, a dissolution rate based on NL(Si) of around 0.20 $g \cdot m^{-2} \cdot d^{-1}$ was determined for the R2 IRN 78 sample. The NL(i) values for ISG suggested that the glass did not dissolve congruently and that B could be considered as the best glass dissolution tracer at near neutral pH and 90 °C. Compared to the B release, 38% of Al, 25 % of Si, 15% of Na and 5 – 25% of Ca were retained in the alteration layer. The dissolution rates based on NL(B) and NL(Si) were equal to 0.20 $g \cdot m^{-2} \cdot d^{-1}$ and 0.15 $g \cdot m^{-2} \cdot d^{-1}$, respectively.

The dissolution rates found for the R2 IRN 78 sample and ISG were similar supporting the hypothesis that the R2 IRN 78 sample has a similar dissolution behaviour on the short term in the invenstigated conditions than nuclear glass.

5 Conclusion

This report covers the whole scope of the second task of WP4, task 4.2. It compiles the results of characterization tests carried out on thermally treated waste products by different THERAMIN partners.

The first part of this report briefly recalls the characterization tests which were selected for the project, and the parameters of these tests. These tests were defined to help the evaluation of the disposability of thermally treated waste.

The second part is a reminder of the studied samples and the form of the initial waste (before thermal treatment). Futhermore, a description of the International Simplified Glass (ISG) is also provided. ISG has been chosen as the basis for intercomparison of the results of leaching tests.

The last part of this document is a description of the characterization results obtained by the different partners. The results were homogenenised in a frame defined during the WP4 meeting.

The table below presents, for each characterized samples, the final wasteform after thermal treatment.

THERAMIN partner	Sample identification	Initial waste	Final wasteform
CEA	THERAMIN-SHIVA-VDM1 sample	Mixture of zeolites, diatoms and IER	Glass
CEA	THERAMIN-INCAN-BST sample	Ashes from technological waste incineration	
FZJ	Sample from JÜV 50/2	Mixed radioactive waste from German research reactor	Ashes
NNL	TH 01 Geomelt ICV sample	Simulated cemented package representing conditioned waste such as failing cemented packages and sea dump drums	Glass
NNL	TH 02 Geomelt ICV sample	Heterogenous sludge	
NNL	HIP-1 sample	Surrogates for uranium	HIP matrix
NNL	HIP-2 sample		
USFD	Glass 6 – Geomelt sample	PCM/Magnox sludge simulants	Glass
USFD	Glass 12 – Geomelt sample	Pile fuel cladding/SIXEP	
USFD	Plasma vitrified PCM – cold crucible	PCM	
USFD	HIP-Ce sample	Magnox sludge simulant	
USFD	HIP-U sample		
VTT	Thermal gasification sample	Organic IER	Ashes
VUJE	Chrompik vitrification	Chrompik liquors	Glass
SCK.CEN	Concentrate slag – Simuli-2	Cemented concentrates	
SCK.CEN	Concetrate slag – Simuli-3A	Cemented concentrates	
SCK.CEN	Resin slag – R2 IRN-78	Cemented anionic resins	

The final wasteform of the studied samples can be categorised in three classes of wasteforms: ashes, vitreous wasteform, or HIP matrix.

Only FZJ and VTT samples are ashes, namely powders. The stability of the ash sample JÜV50/2 was evaluated in leaching tests, and revealed an important release of the ^{137}Cs inventory within a first few days. Such wasteform requires to be immobilised in some way. VTT has selected geopolymerisation and characterized the final immobilised products; the apparent diffusion coefficients for cesium, 10^{-12} - 10^{-13} cm^2/s, is 5 orders of magnitude lower than apparent diffusion coefficients for Portland cement encapsulated pristine resin and 3 orders of magnitude lower than gasified resin encapsulated in alkali-activated material.

75% of the studied samples are vitreous ones and their characterization allow to get a good overview of the interest of (incineration/)vitrification process for a various panel of initial wasteforms.

The final vitreous wasteforms after treatment are not necessarily completely amorphous as SHIVA, Chrompik, Simuli-2 or R2 IRN 78 samples; they can exhibit crystallization (e. g. INCAN-BST, Glass 6 USFD, Glass 12 USFD, PCM samples). The types of crystals can then be identified by XRD and SEM/EDS observation. The latter technique can also give information on the distribution of the different crystals in the vitreous matrix.

Based on the leaching tests, the intercomparison of these different samples with the ISG glass gives some first results about the long-term behaviour.

Of course, it is important to note that the relevance of this intercomparison strongly depends on the chemical composition of the investigated samples. A vitreous matrix and the presence of boron (e.g. SHIVA sample) — known to be a tracer of the alteration — make it possible to apply the proven methodologies for the study of chemical durability and long-term behaviour and to compare “directly” this matrix to the ISG glass. It is also possible for a vitreous sample with durable crystalline phases (e.g. INCAN-BST sample): the durability of the wasteform is controlled by that of the vitreous matrix. In other case, it can be more difficult with chemical composition very different from ISG glass (e. g. Glass 6 USFD and Glass 12 USFD samples)

The leaching tests highlight different behaviour of the invenstigated samples. For borosilicate samples, a “typical” evolution of normalized mass losses (NL) are observed, suggesting a long-term behaviour similar to ISG glass: hydrolysis, formation of an alteration layer with a decrease of the alteration rate. Hydrolysis rates can be lower (e.g. SHIVA sample, TH 01 Geomelt ICV sample, Simuli-2 sample) or higher (e.g. INCAN-BST sample) than the one measured for the ISG glass: it depends on the chemical composition of the sample.

These first results are encouraging considering the objective of demonstration of durability the waste. However, concluding about the long-term behaviour of the different vitreous wasteforms would require further investigations. It is also important to keep in mind that durability of the product may not be a discriminator for disposal (current GDF requirements in the UK for disposal of ILW).

It should also be noted that to obtain initial information about chemical durability and alteration mechanisms the characterization tests were mainly performed under standardised conditions. This choice was made to avoid the findings to be limited to a specific repository concept and to allow a broader use of the results. Then, this aspect has to be taken into account for the use of the characterization results for safety case implication (task 4.3), especially if the safety case implication is site and disposal concept specific.

6 References

Abdel-Karim, A.A.M., Zaki, A.A., Elwan, W., El-Naggar, M.R., Gouda, M.M. (2019). Geochemical and contaminant transport assessment of a low-level radioactive waste disposal site. J. Geochem. Explor. 197, 174-184.

ASTM International (2017). Standard Test Method for Static Leaching of Monolithic Waste Forms for Disposal of Radioactive Waste. ASTM Standard C1220/17, West Conshohocken, PA, UnitedStates.

ASTM Internationa (2014). Standard test method for determining chemical durability of nuclear, hazardous and mixed waste glasses and multiphase glass ceramics: the product consistency test (PCT). ASTM Standard C1285/14, West Conshohocken, PA, United States.

Deliverable Report D3.3 (2019). SHIVA and In-Can Melting technologies and demonstration test trials.

Deliverable Report D4.1 (2018). THERAMIN, Waste Acceptance Criteria and requirements in terms of characterization.

Fournier M. and Vallat C. (2019). Essais conduits par le DE2D/SEVT dans le cadre du projet européen THERAMIN (Work Package 4), Bilan au 31 janvier 2019. Note technique DEN/MAR/DE2D/SEVT/NT/2019-07.

Gin S., Beaudoux X., Angéli F., Jégou C., Godon N. (2012). Effect of composition on the short-term and long-term dissolution rates of ten borosilicate glasses of increasing complexity from 3 to 30 oxides. Journal of Non-Crystalline Solids, 358(18-19): 2559-2570.

Gin S., Abdelouas A., Criscenti L.J., Ebert W.L., Ferrand K., Geisler T., Harrison M.T., Inagaki Y., Mitsui S., Mueller K.T., Marra J.C., Pantano C.G., Pierce E.M., Ryan J.V., Schofield J.M., Steefel C.I., Vienna J.D. (2013). An international initiative on long-term behaviour of high-level nuclear waste glass. Materials Today, 16(6): 243-248

Gin S., Jolliver P., Fournier M., Berthon C., Wang Z., Mitroskov A., Zhu Z., Ryan J.V. (2015). The fate of silicon during glass corrosion under alkaline conditions: A mechanistic and kinetic study with the International Simple Glass. Geochimica et Cosmochimica Acta 151; pp. 68–85.

Hyatt, et al. (2007). Characterization of plasma vitrified simulant plutonium contaminated material waste. Mater. Res. Soc. Symp. Proc. Vol. 985, 393-398

Jégou C. (1998). Mise en évidence expérimentale des mécanismes limitant l'altération du verre R7T7 en milieu aqueux. Critique et proposition d'évolution du formalisme cinétique. Thèse de l'Université des Sciences et Techniques du Languedoc.

Krupka, K.M., Serne, R.J. (2002). Geochemical factors affecting the behaviour of Antimony, Cobalt, Europium, Technetium and Uranium in vodose sediments. Technical report PNNL-14126.

Li, D, Kaplan, D.I. (2012). Sorption coefficients and molecular mechanisms of Pu, U, Np, Am and Tc to Fe (hydr)oxides: A review. J. Hay. Mat. 243. 1-18.

Milestone Report MS12 (2018). THERAMIN, Definition and adaptation of characterization tests.

Nicoleau E., Schuller S., Angeli F., Charpentier T., Jollivet P., Le Gac A., Fournier M., Mesbah A., Vasconcelos F. (2015). Phase separation and crystallization effects on the structure and durability of molybdenum borosilicate glass. Journal of Non-Crystalline Solids, 427: 120-133.

Nicoleau E., Angeli F., Schuller S., Charpentier T., Jollivet P., Moskura M. (2016). Rare-earth silicate crystallization in borosilicate glasses: Effect on structural and chemical durability properties. Journal of Non-Crystalline Solids, 438: 37-48.

NIROND NIRAS/ONDRAF (2018). Methodology for the formulation of surrogate cemented concentrates for the assessment of the plasma torch technique. Note 2017-2475,

Provis L., van Deventer J. (2009) Geopolymers Structure, processing, properties and industrial applications. Woodhead Publishing Limited, Abington Hall, Cambridge CB21 6AH, UK

Wagman, D.D. et al. (1982). The NBS tables of chemical thermodznamic properties. Selected values for inorganic and C1- and C2- organic substances in SI units. J. Phys. Chem. Ref. Data, V.11, N.2.

Witwer, et al. (2010). Thermal treatment of UK intermediate and low level radioactive waste: a demonstration of the GeoMelt process towards treatment of Sellafield waste. WM 2010 Conference, Phoenix, AZ

Appendix A: Template used for the presentation of characterization results (section 4)

General information

Partner:	
Sample id:	
Contact person:	

Origin and macroscopic description

Microstructure

Method(s):	☐ SEM ☐ XRD ☐ Other:
Operating conditions:	
Homogeneity:	
Free liquid or gas:	
Crystalline composition:	
Comments and discussion:	

Chemical composition

Method(s):	☐ EMP ☐ ICP-OES/MS ☐ XRF ☐ Other: SEM/EDS
Operating conditions:	
Chemical composition:	
Comments and discussion:	

Chemical durability

Method(s):	☐ As described in MS12 Report (p. 12-13), adapted from ASTM C1285 ☐ As described in MS12 Report (p. 14), adapted from ASTM C1220 ☐ Other:

Clarifications:	
Results and discussion:	

Other tests and characterizations

Please report here other tests or characterizations that are not described before (eg other solid or solution analyzes, leaching tests in cementitious solution, etc.)

Conclusions and Outlooks

.

Appendix B: Powder XRD patterns for initial ash fractions F3-F8 with evaluation (FZJ)

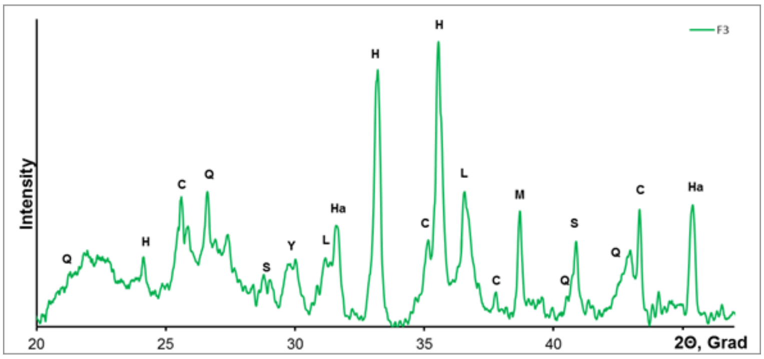

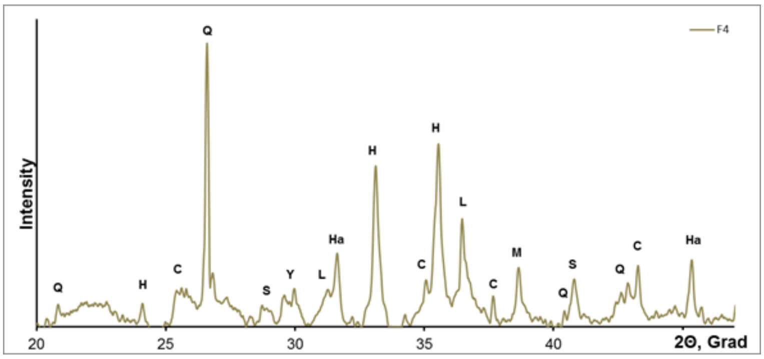

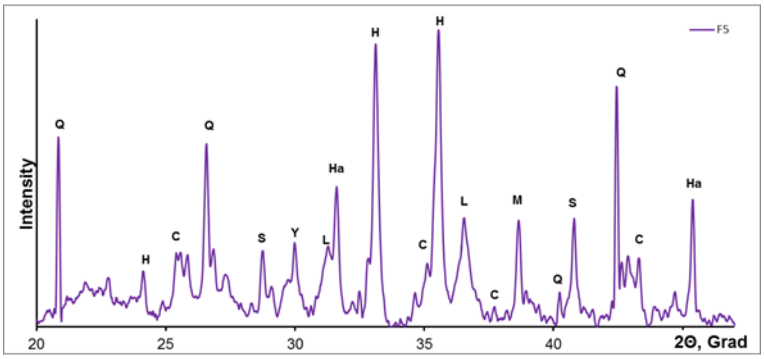

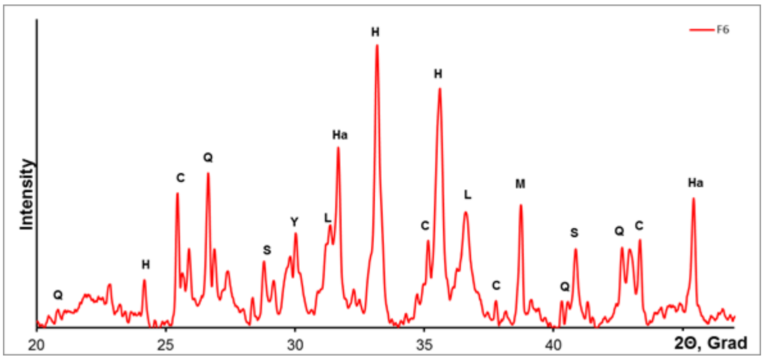

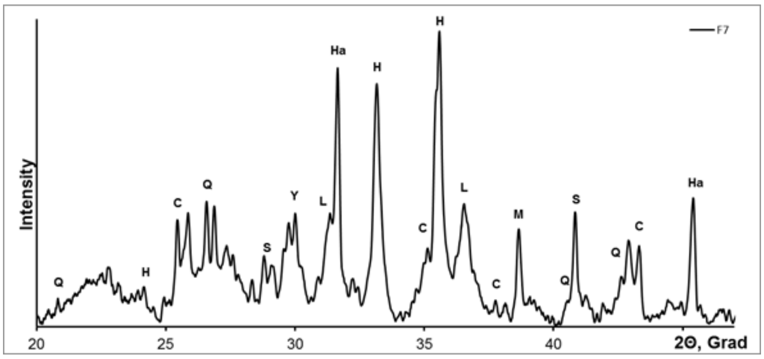

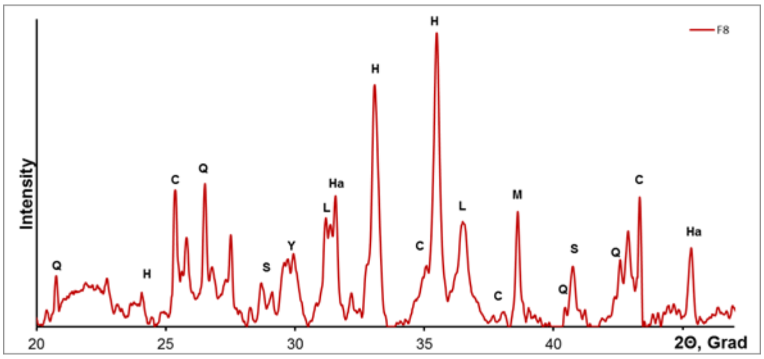

Respective shortenings used as indexes on the diffractograms:

1) Fe_2O_3 Hematite (H)
2) SiO_2 Quartz (Q)
3) Al_2O_3 Corundum (C)
4) CaO Lime (L)
5) $Al_{2.826}Si_{0.174}O_{4.588}$ Mullite (M)
6) $Al_{5.35}Ca_{2.676}Si_{2.65}O_{16}$ Yoshiokaite (Y)
7) KCl Sylvite (S)
8) NaCl Halite (Ha)

Appendix C: Supplementary information on microscopic and microanalytical investigation of ash particles by means of SEM/EDX (FZJ)

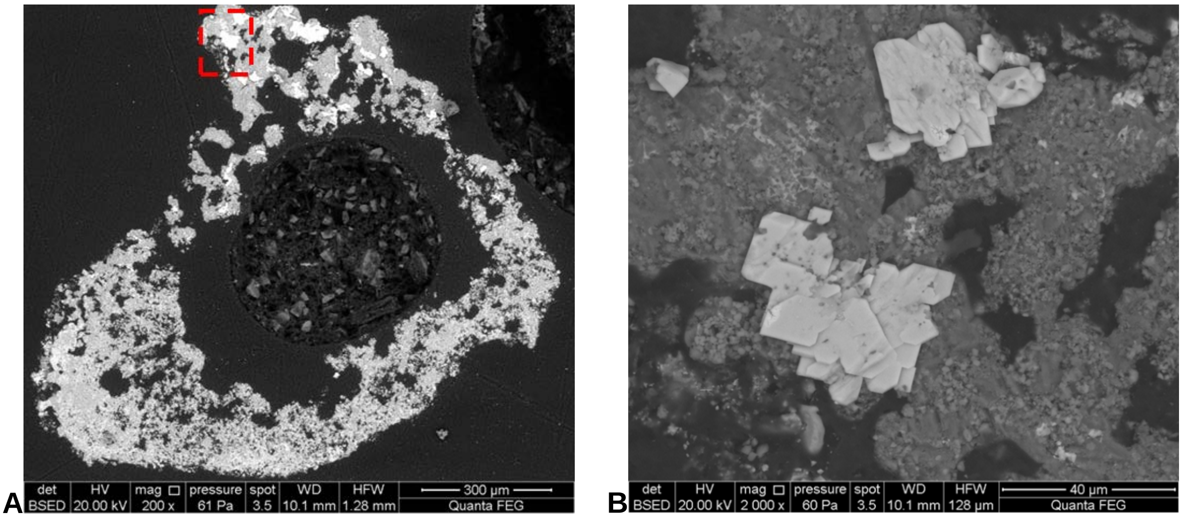

Figure C.1: SEM image of the highly radioactive particle F2-D8 from specimen F2-D: **A** – the whole particle, **B** – zoom in of selected area demonstrating white crystals of (Ba,Ti)-rich phase.

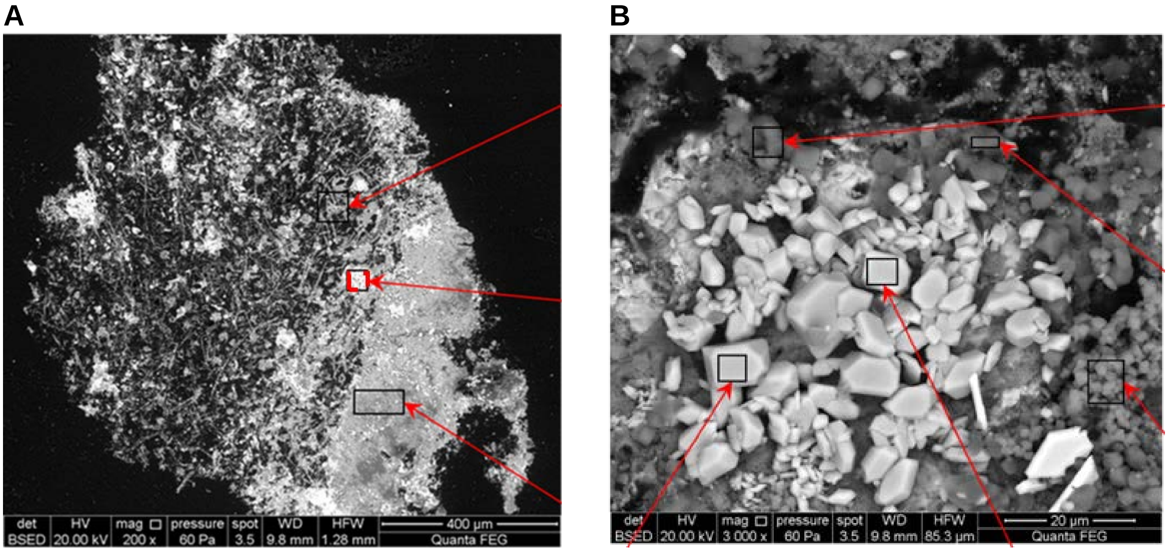

Figure C.2: SEM image of the highly radioactive particle F2-E4 from specimen F2-E: **A** – the whole particle, **B** – zoom in of selected area demonstrating white crystals of (Ba,Ti)-rich phase.

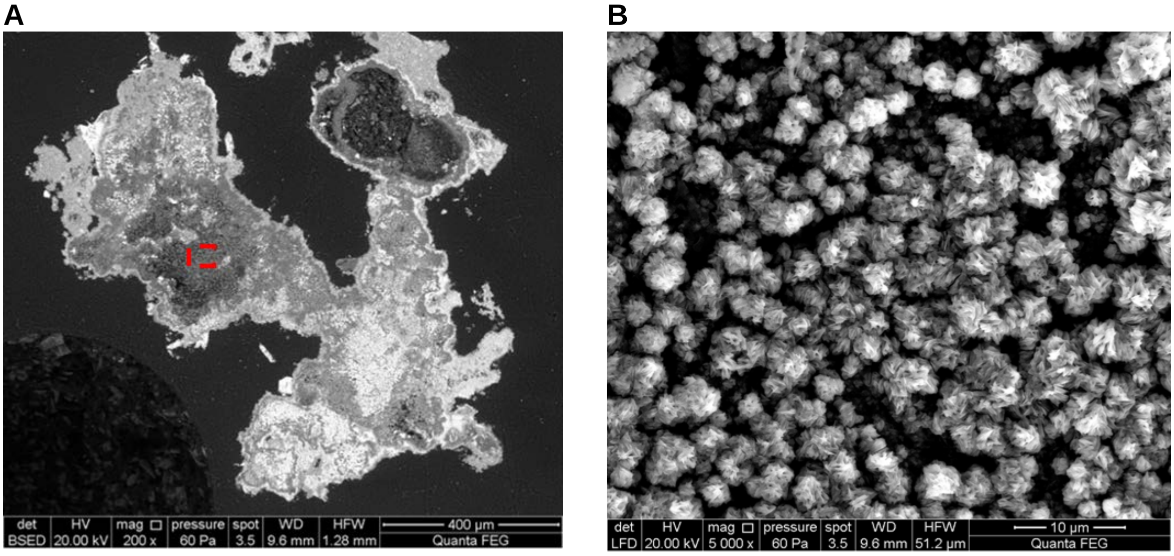

Figure C.3: SEM image of the inactive particle F2-E5 from specimen F2-E:
A – the whole particle, **B** – zoom in of selected area demonstrating agglomerates rich in chloride phases: Cl/ΣMe = 1.1.

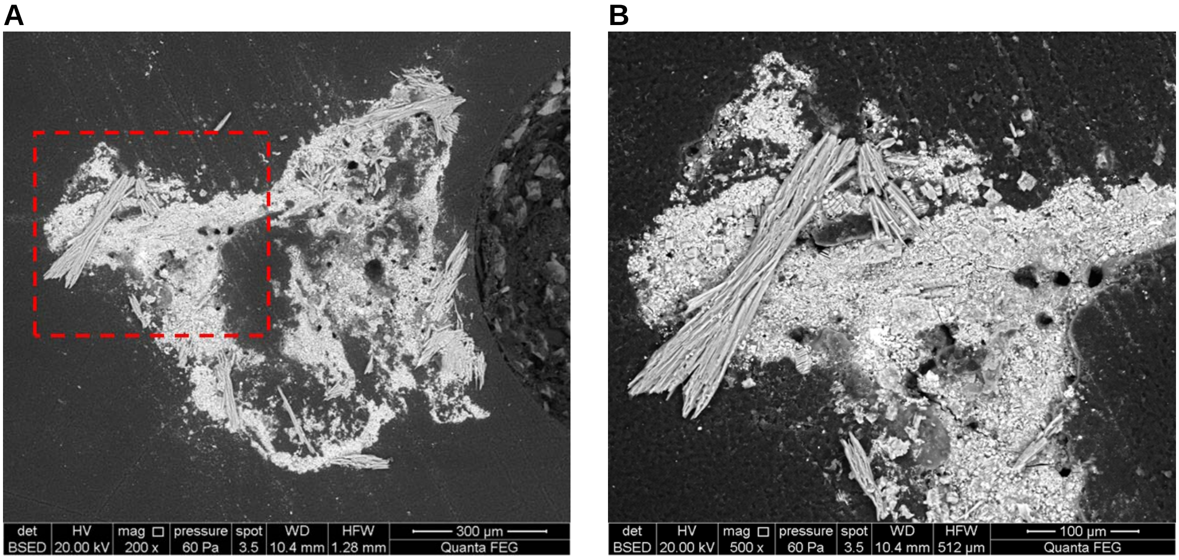

Figure C.4: SEM image of the inactive particle F2-E12 from specimen F2-E:
A – the whole particle, **B** – zoom in of selected area demonstrating white agglomerates rich in $CaCl_2$.

Appendix D: Evolution of some radionuclide in the solution during the leaching tests with ash-fractions 3, 4 and 6, evaluated by γ-spectrometry (FZJ)

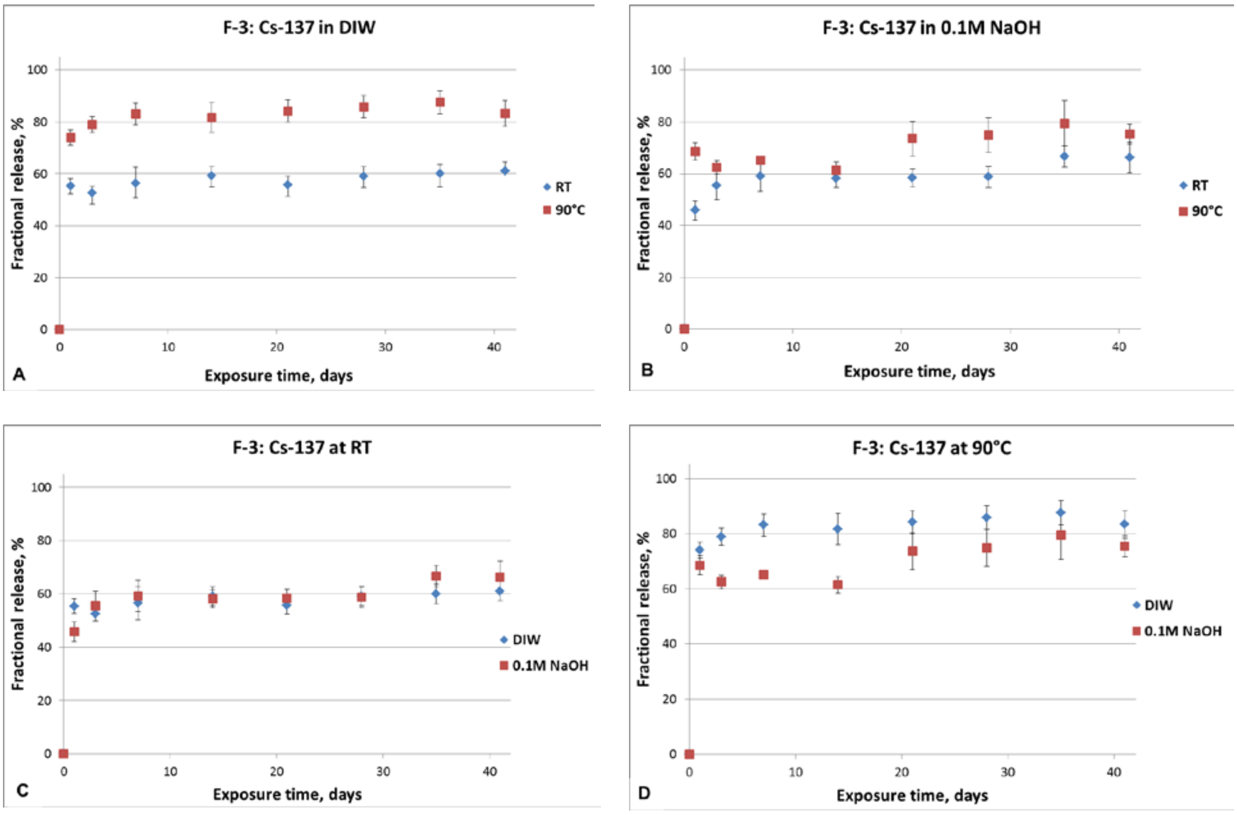

Figure D.1: Release kinetics of ^{137}Cs from ash fraction F3 (grain size of 500<R<800 μm): **A** – in DIW, **B** – in 0.1M NaOH, **C** – at RT, **D** – at 90°C.

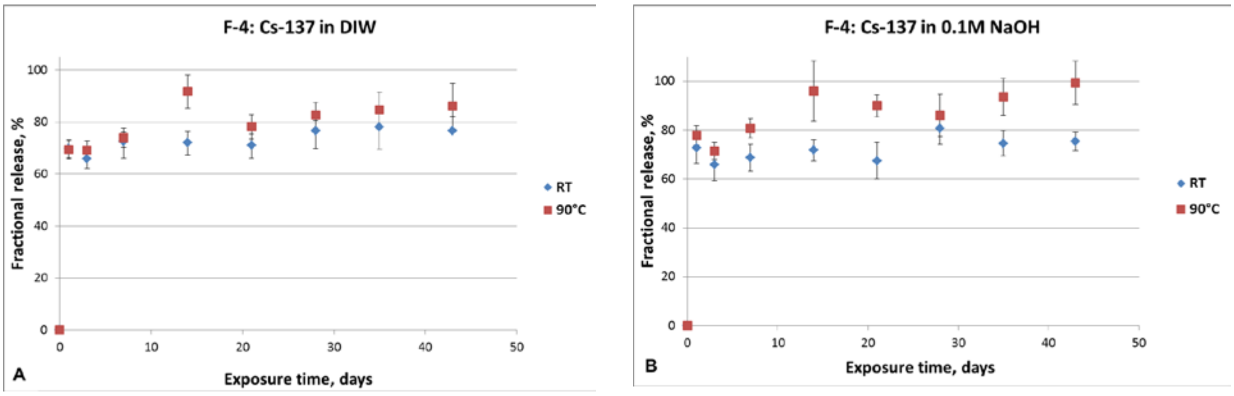

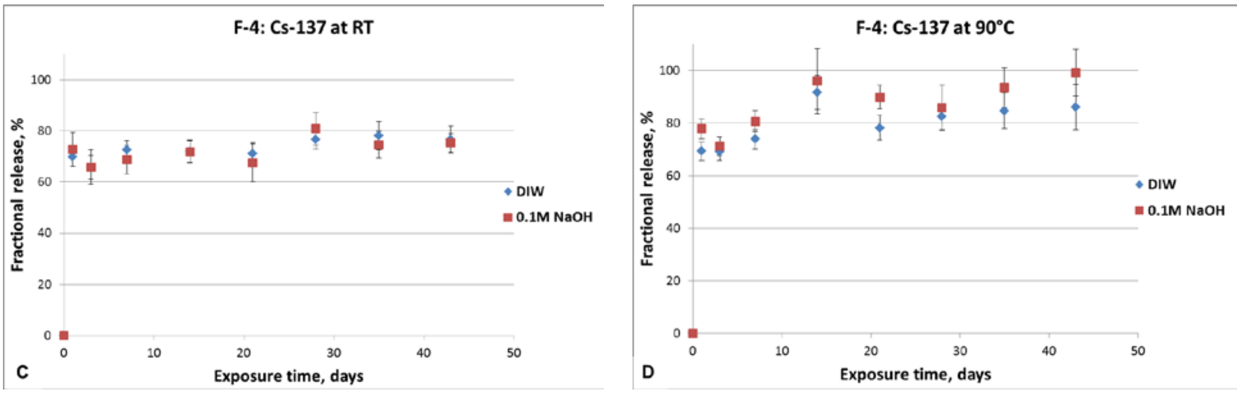

Figure D.2: Release kinetics of ^{137}Cs from ash fraction F4 (grain size of 355<R<500 μm): **A** – in DIW, **B** – in 0.1M NaOH, **C** – at RT, **D** – at 90°C.

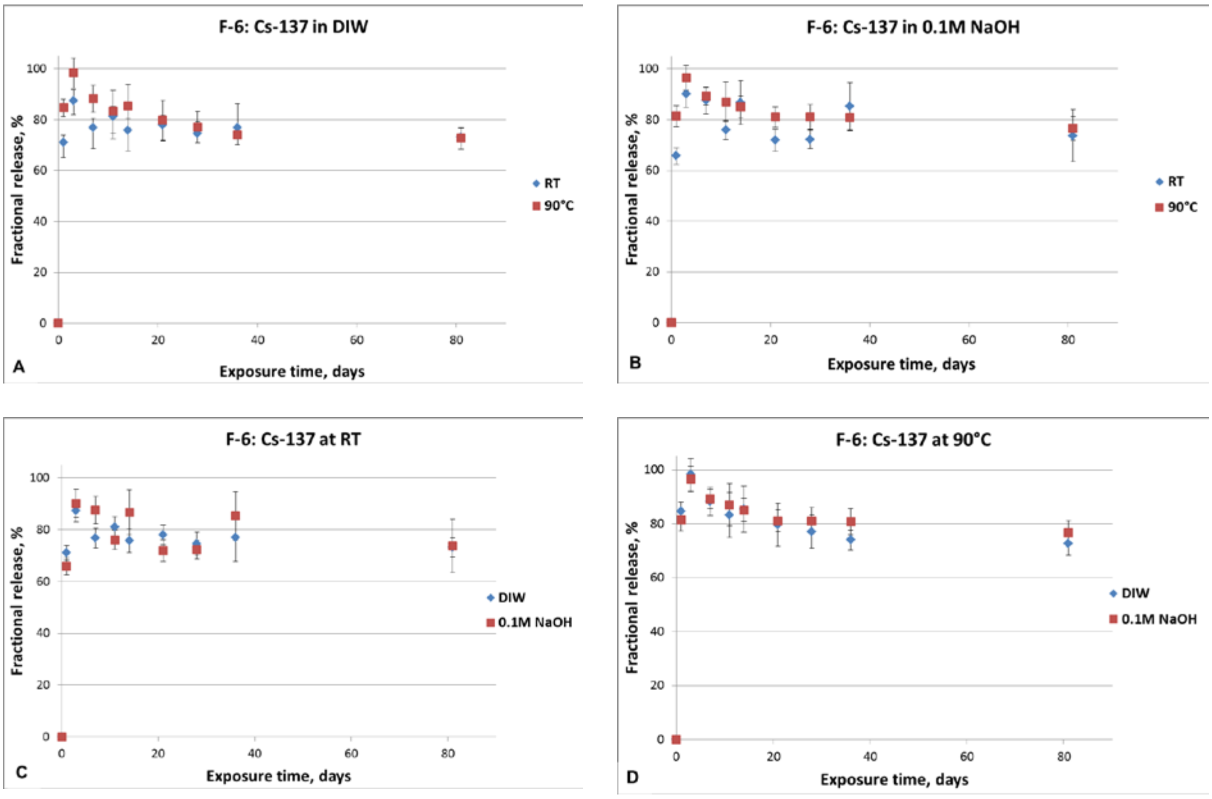

Figure D.3: Release kinetics of ^{137}Cs from ash fraction F6 (125<R<250 μm): **A** – in DIW, **B** – in 0.1M NaOH, **C** – at RT, **D** – at 90°C.

Appendix E: Evolution of concentration of some elements in the solution during the leaching experiments with ISG glass, measured by means of ICP-OES (FZJ)

Δt	**C_{Ca}**	**SD**	**C_{Si}**	**SD**	**C_{Al}**	**SD**
[days]	**[mg/L]**	**[mg/L]**	**[mg/L]**	**[mg/L]**	**[mg/L]**	**[mg/L]**
DIW/RT						
0	<0.002	-	<0.001	-	<0.1	-
17	0.052	0.004	0.44	0.06	<0.1	-
24	0.0118	0.0005	0.45	0.15	<0.1	-
31	0.053	0.002	0.47	0.13	<0.1	-
49	0.056	0.003	0.41	0.15	<0.1	-
DIW/90°C						
0	<0.002	-	<0.001	-	<0.1	-
17	0.06	0.005	30.03	0.17	2.57	0.05
24	0.81	0.009	29.39	0.13	22.08	0.05
31	0.56	0.005	30.7	0.3	1.95	0.09
49	0.25	0.004	39.0	0.2	1.61	0.05
0.1M NaOH/RT						
0	<0.002	-	<0.001	-	<0.1	-
17	0.393	0.018	7.37	0.15	0.42	0.04
24	0.41	0.02	7.15	0.07	0.46	0.06
31	0.4	0.02	7.3	0.1	0.56	0.16
49	0.5	0.02	7.69	0.08	0.5	0.06
0.1M NaOH/90°C						
0	<0.002	-	<0.001	-	<0.1	-
17	1.09	0.03	104.7	0.3	12.5	0.12
24	0.84	0.02	101.9	0.6	12.19	0.08
31	0.73	0.02	100.0	0.4	11.98	0.09
49	0.67	0.02	94.5	0.5	11.23	0.13

Appendix F: Powder XRD patterns for ash fractions F2 before and after leaching (FZJ)

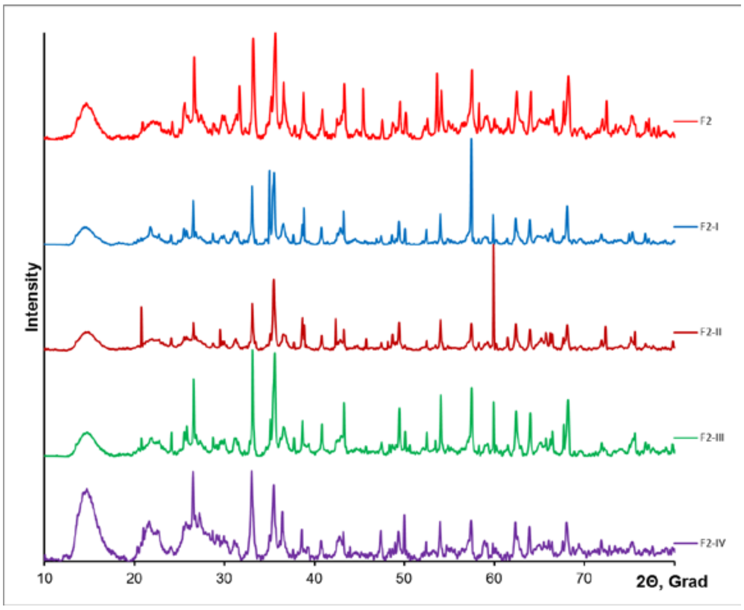

Figure F.1: XRD-patterns of initial solid of ash fraction F2 and respective solids after leaching F2-I – IV.

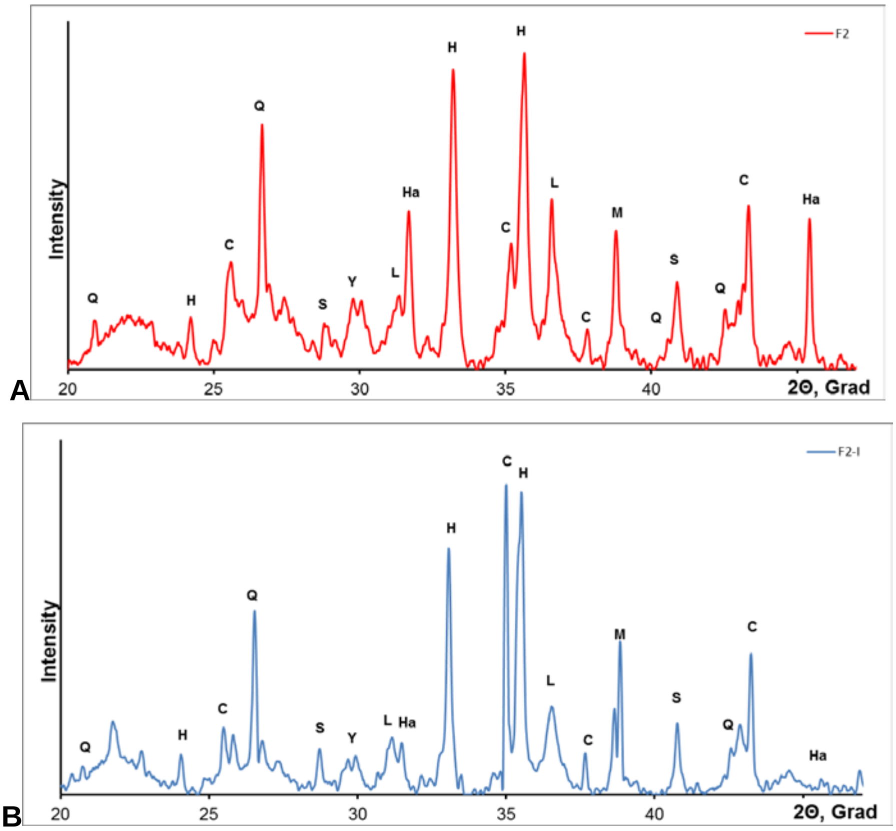

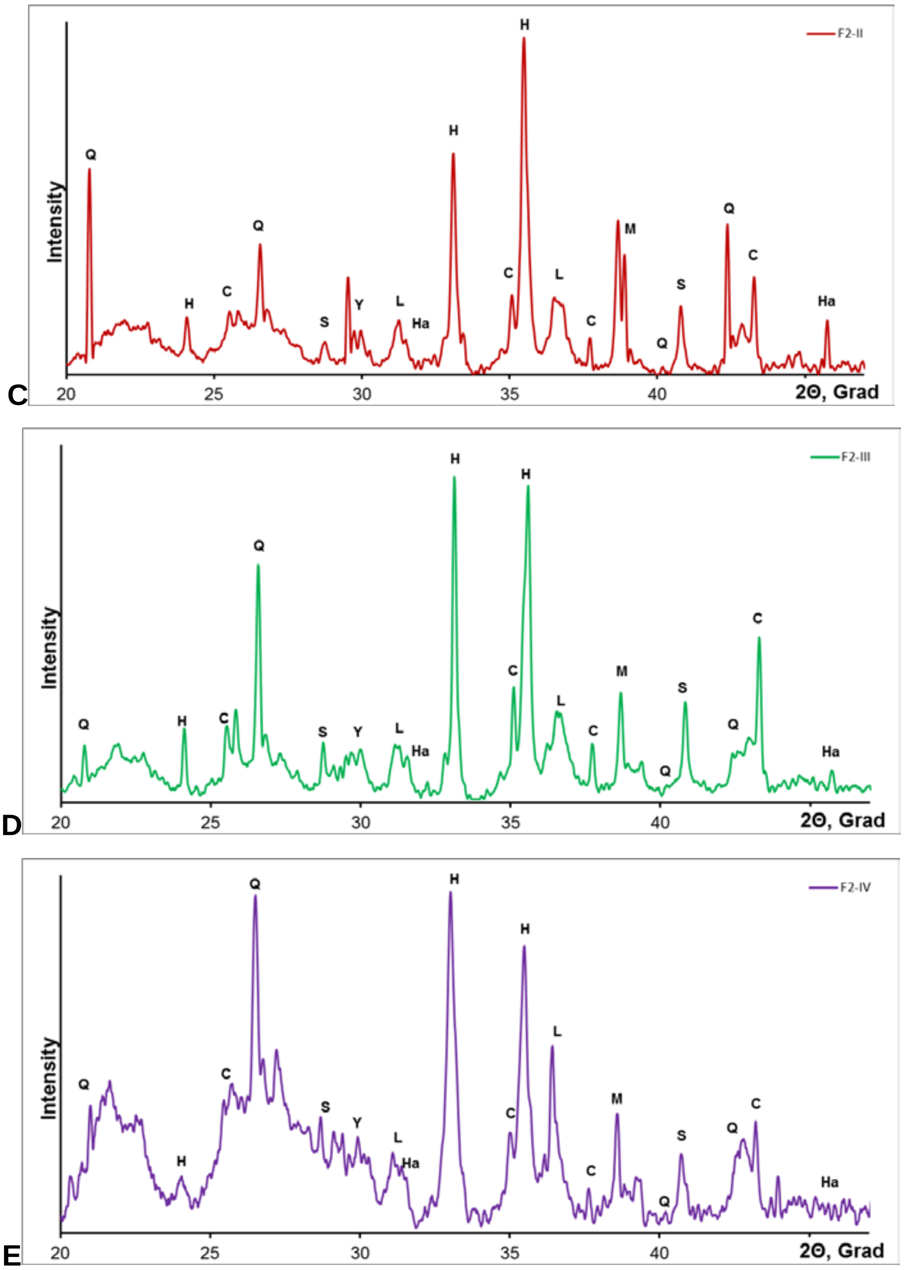

Figure F.2: Detailed evaluation of XRD-patterns of initial solid of ash fraction F2 (**A**) and respective solids after leaching in DIW at RT (**B**), in DIW at 90°C (**C**), in 0.1M NaOH at RT (**D**) and in 0.1M NaOH at 90°C (**E**). Indexes on the difractograms represent shortenings of respective mineral phases and are given below.

Respective shortenings used as indexes on the diffractograms:

1) Fe_2O_3 Hematite (H)
2) SiO_2 Quartz (Q)
3) Al_2O_3 Corundum (C)
4) CaO Lime (L)
5) $Al_{2.826}Si_{0.174}O_{4.588}$ Mullite (M)
6) $Al_{5.35}Ca_{2.676}Si_{2.65}O_{16}$ Yoshiokaite (Y)
7) KCl Sylvite (S)
8) NaCl Halite (Ha)

Appendix G: Element concentrations measured after 28 days of leaching at 90 °C in ultrapure water (SCK.CEN)

Sample	[Si] mg/L	± 2σ mg/L	[Si] mol/L	± 2σ mol/L	[Al] mg/L	± 2σ mg/L	[Al] mol/L	± 2σ mol/L	[Ca] mg/L	± 2σ mg/L	[Ca] mol/L	± 2σ mol/L	[Na] mg/L	± 2σ mg/L	[Na] mol/L	± 2σ mol/L
Simuli 2-01	2.44	0.26	8.7E-5	0.9E-5	0.148	0.025	5.5E-6	0.9E-6	1.83	0.21	4.6E-5	0.5E-5	2.80	1.00	1.2E-4	0.4E-4
Simuli 2-02	4.00	0.40	1.4E-4	0.1E-4	0.176	0.027	6.5E-6	1.0E-6	2.67	0.29	6.7E-5	0.7E-5	2.90	1.00	1.3E-4	0.4E-4
Simuli 2-03	2.62	0.28	9.3E-5	1.0E-5	0.170	0.026	6.3E-6	1.0E-6	1.94	0.22	4.8E-5	0.6E-5	2.40	1.00	1.0E-4	0.4E-4
Simuli 2 average	3.02	0.31	1.1E-4	0.1E-4	0.160	0.026	6.1E-6	1.0E-6	2.15	0.24	5.4E-5	0.6E-5	2.70	1.00	1.2E-4	0.4E-4
Simuli 3-A-01	12.5	1.3	4.4E-4	0.5E-4	1.52	0.15	5.6E-5	0.6E-5	8.60	0.90	2.1E-4	0.2E-4	4.20	1.10	1.8E-4	0.5E-4
Simuli 3-A-02	13.1	1.3	4.7E-4	0.5E-4	1.65	0.17	6.1E-5	0.6E-5	9.40	0.90	2.3E-4	0.2E-4	4.10	1.10	1.8E-4	0.5E-4
Simuli 3-A-03	13.1	1.3	4.7E-4	0.5E-4	1.63	0.16	6.0E-5	0.6E-5	9.40	0.90	2.3E-4	0.2E-4	4.10	1.10	1.8E-4	0.5E-4
Simuli 3-A average	12.9	1.3	4.6E-4	0.5E-4	1.60	0.16	5.9E-5	0.6E-5	9.10	0.90	2.3E-4	0.2E-4	4.10	1.10	1.8E-4	0.5E-4
R2 IRN 78-01	11.3	1.1	4.0E-4	0.4E-4	2.19	0.22	8.1E-5	0.8E-5	10.5	1.1	2.6E-4	0.3E-4	4.00	1.10	1.7E-4	0.5E-4
R2 IRN 78-02	10.8	1.1	3.8E-4	0.4E-4	2.07	0.21	7.7E-5	0.8E-5	10.1	1.0	2.5E-4	0.3E-4	2.70	1.00	1.2E-4	0.4E-4
R2 IRN 78-03	11.3	1.1	4.0E-4	0.4E-4	2.14	0.21	7.9E-5	0.8E-5	10.5	1.1	2.6E-4	0.3E-4	3.10	1.00	1.3E-4	0.4E-4
R2 IRN 78 average	11.1	1.1	4.0E-4	0.4E-4	2.10	0.21	7.9E-5	0.8E-5	10.4	1.1	2.6E-4	0.3E-4	3.30	1.00	1.4E-4	0.4E-4
ISG-01	10.7	1.1	3.8E-4	0.4E-4	1.08	0.11	4.0E-5	0.4E-5	1.02	0.14	2.5E-5	0.4E-5	8.80	1.30	3.8E-4	0.6E-4
ISG-02	11.1	1.1	4.0E-4	0.4E-4	1.11	0.11	4.1E-5	0.4E-5	1.13	0.15	2.8E-5	0.4E-5	8.30	1.30	3.6E-4	0.6E-4
ISG-03	10.8	1.1	3.8E-4	0.4E-4	1.14	0.12	4.2E-5	0.4E-5	1.09	0.15	2.7E-5	0.4E-5	7.70	1.30	3.3E-4	0.6E-4
ISG average	10.9	1.1	3.9E-4	0.4E-4	1.10	0.11	4.1E-5	0.4E-5	1.10	0.10	2.7E-5	0.4E-5	8.30	1.30	3.6E-4	0.6E-4
Blank	0.1		3.6E-6		0.02	/	7.4E-7	/	0.1	/	2.5E-6	/	4.00	1.10	1.7E-4	0.5E-4

	[Fe]	± 2σ	[Fe]	± 2σ	[Zn]	± 2σ	[Zn]	± 2σ
Sample	**mg/L**	**mg/L**	**mol/L**	**mol/L**	**µg/L**	**µg/L**	**mol/L**	**mol/L**
Simuli 2-01	0.02	/	3.6E-07	/	71.0	7.0	1.1E-6	0.1E-06
Simuli 2-02	0.02	/	3.6E-07	/	18.4	1.9	2.8E-7	0.3E-07
Simuli 2-03	0.02	/	3.6E-07	/	78.0	8.0	1.2E-6	0.1E-06
Simuli 2 average	0.02	/	3.6E-07	/	55.8	5.6	8.5E-7	0.9E-07
Simuli 3-A-01	0.02	/	3.6E-07	/	2.10	0.50	3.2E-8	0.8E-08
Simuli 3-A-02	0.02	/	3.6E-07	/	2.50	0.50	3.8E-8	0.8E-08
Simuli 3-A-03	0.02	/	3.6E-07	/	2.00	/	3.1E-8	
Simuli 3-A average	0.02	/	3.6E-07	/	2.20	0.50	3.3E-8	0.8E-08
R2 IRN 78-01	0.02	/	3.6E-07	/	2.00	/	3.1E-8	/
R2 IRN 78-02	0.02	/	3.6E-07	/	2.00	/	3.1E-8	/
R2 IRN 78-03	0.02	/	3.6E-07	/	2.00	/	3.1E-8	/
R2 IRN 78 average	0.02	/	3.6E-07	/	2.00	/	3.1E-8	/
Blank	0.02	/	3.6E-07	/	2.00	/	3.06E-8	/

	[B]	± 2σ	[B]	± 2σ	[Zr]	± 2σ	[Zr]	± 2σ
Sample	**mg/L**	**mg/L**	**mol/L**	**mol/L**	**µg/L**	**µg/L**	**mol/L**	**mol/L**
ISG-01	3.0	0.6	2.8E-4	0.6E-04	0.30	/	3.3E-9	/
ISG-02	3.0	0.6	2.8E-4	0.6E-4	0.64	0.33	7.0E-9	3.6E-9
ISG-03	3.0	0.6	2.8E-4	0.6E-4	0.30	/	3.3E-9	/
ISG average	3.0	0.6	2.8E-4	0.6E-4	0.40	0.30	4.5E-9	3.6E-9
Blank	0.5	/	4.6E-5	/	0.30	/	3.3E-9	/

Appendix H: Additional standardised leaching tests on coupons (KOH solution at pH 13.5

H-1 pH evolution

Figure 142 shows the pH evolution for the plasma slags leaching tests in a KOH solution at pH 13.5 and 40 °C.. For all samples, the pH values stay close to the initial value of 13.5 ± 0.2.

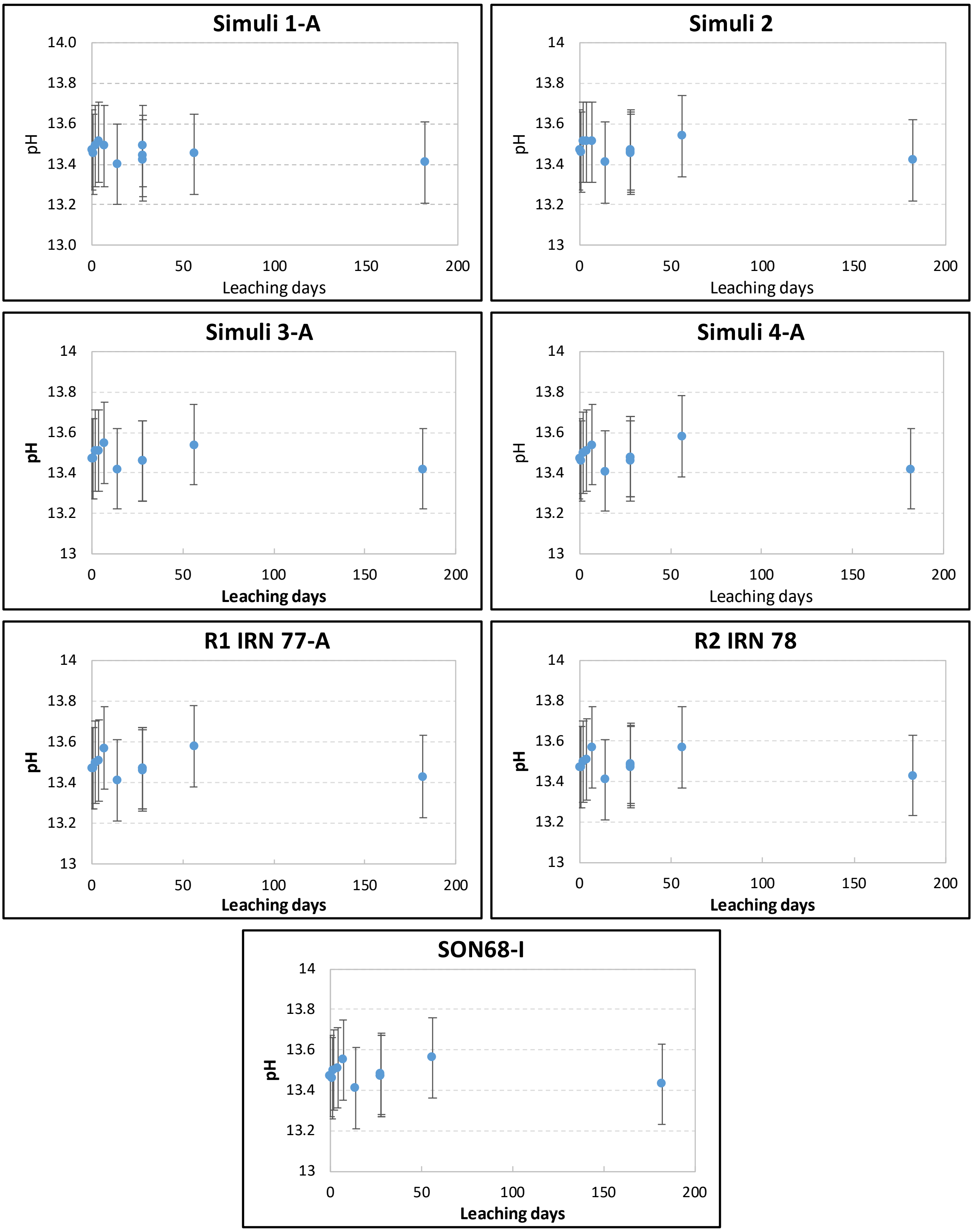

Figure 142: pH evolution in the additional tests (KOH solution at pH 13.5 and 40 °C).

H-2 Element concentration in the leachate

Figure 143 to Figure 145 give the element concentrations measured in the leachate solutions after 7, 28, 56, and 182 days of alteration in a KOH solution at pH 13.5 and 40 °C.

For the plasma slags, the silicon concentration increases from 1 – 2 mg·L^{-1} up to 19 – 31 mg·L^{-1}. The Si concentrations measured until 56 days for the R2 IRN 78 sample are lower than those measured for the R1 IRN 77-A samples but are similar to those determined for the Simuli samples. It has to be noted that after 182 days, the Si concentration is the same for Simuli 1-A and R1 IRN 77-A.

The calcium concentration slightly increases up to 7 – 13 mg·L^{-1}, and then decreases down to 5 – 8 mg·L^{-1} after 56 days.

A low aluminium increase is observed from 0.4 up to 18 mg·L^{-1} in the whole measured timeframe with the higher concentration measured for the R1 IRN 77-A sample.

Very low iron concentration is measured (< 1 mg·L^{-1}) indicating that this element is highly retained in the alteration layer.

For the Simuli samples, the zinc concentration increases from 50 – 60 µg·L^{-1} up to 440 – 830 µg·L^{-1} and seems to reach a plateau after 56 days. The higher concentration is measured for the Simuli 3-A sample. For the R1 IRN 77-A and R2 IRN 78 samples, it increases from 116 µg·L^{-1} up to 1340 µg·L^{-1} and 56 µg·L^{-1} to 581 µg·L^{-1}, respectively. For all samples, a plateau is reached between 56 and 182 days.

The potassium and sodium concentrations are the same as in the blank solution, i.e. around 12000 mg·L^{-1} and 56 mg·L^{-1}, respectively.

For SON68-I, the silicon concentration increases up to 56 mg·L^{-1}; it is thus 2 – 3 times higher than the silicon concentrations measured for the plasma slags.

Before 28 days, it was not possible to quantify the boron concentration in solution then it increases from 4 up to 13 mg·L^{-1}.

Caesium and molybdenium concentrations increase from 1000 up to 2900 µg·L^{-1} and from 0.12 to 3.3 mg·L^{-1}, respectively. An Al increase from 0.4 up to 9 mg·L^{-1} is also observed.

As for the plasma slags, iron concentrations are lower than 1 mg·L^{-1} and low Ca concentrations of 0.7 – 2 mg·L^{-1} are measured indicating a strong retention of these elements in the alteration layer. The zirconium concentration first peaks around 40 mg·L^{-1}, and then decreases suggesting Zr retention in the alteration layer.

The Na concentration increases from 56 mg·L^{-1} up to 81 mg·L^{-1} and the K concentration is the same as in the blank.

Note that for SON68-I, Si, Mo, and Cs dissolve congruently with B suggesting that these latter elements are good dissolution indicator for SON68-I glass dissolution. It should be noted that the Al concentrations calculated by considering congruent glass dissolution are slightly lower than those measured. As Ca and Fe are not dissolved congruently, they are most probably retained in the alteration layer.

The concentrations measured for SON68-I are in good agreement with those reported in [Ferrand et al., 2019] performing the same leaching tests indicating a good reproducibility.

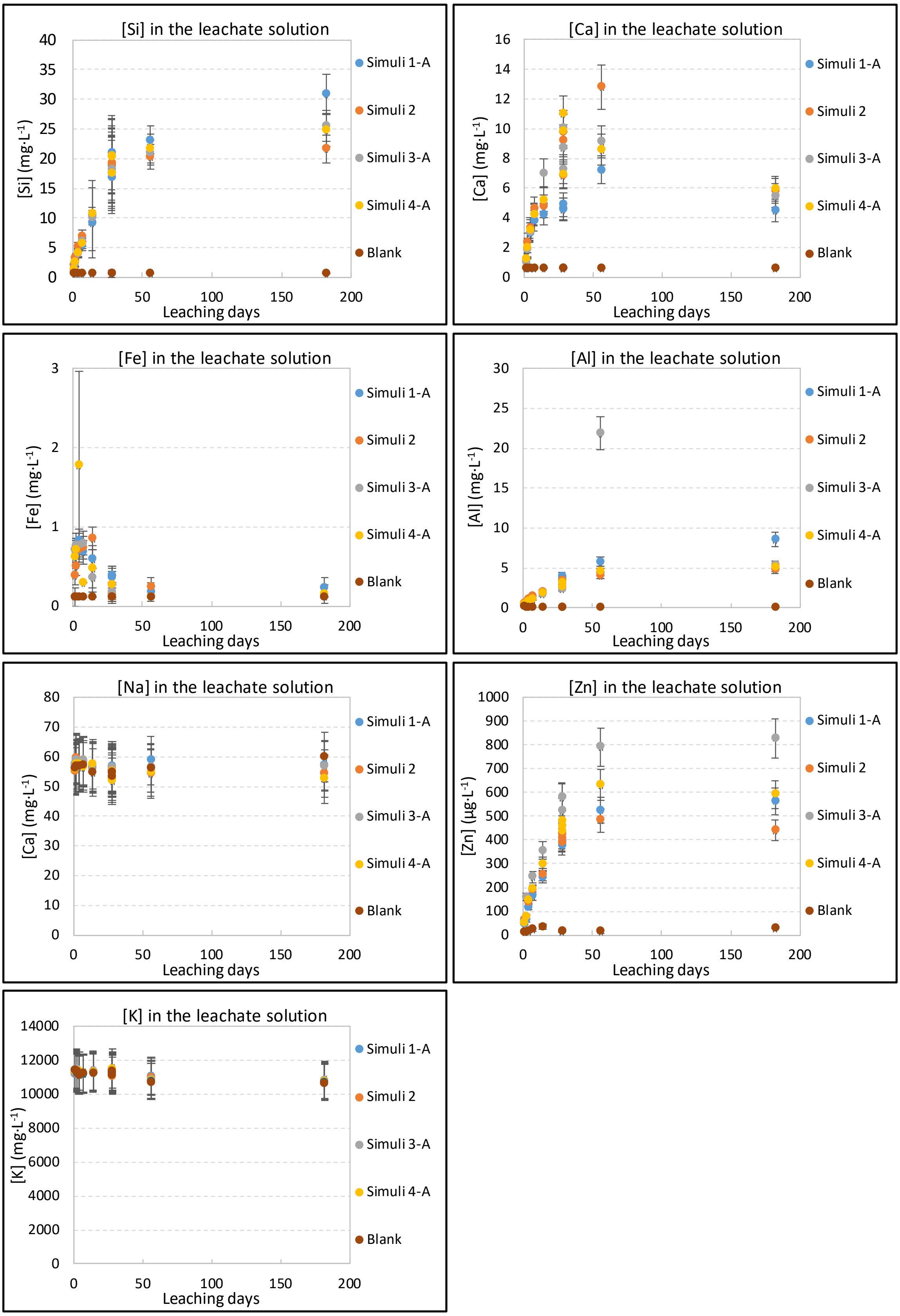

Figure 143: Element concentrations measured for the Simuli 1-A, Simuli 2, Simuli 3-A and Simuli 4-A samples in the additional tests (KOH solution at pH 13.5 and 40 °C).

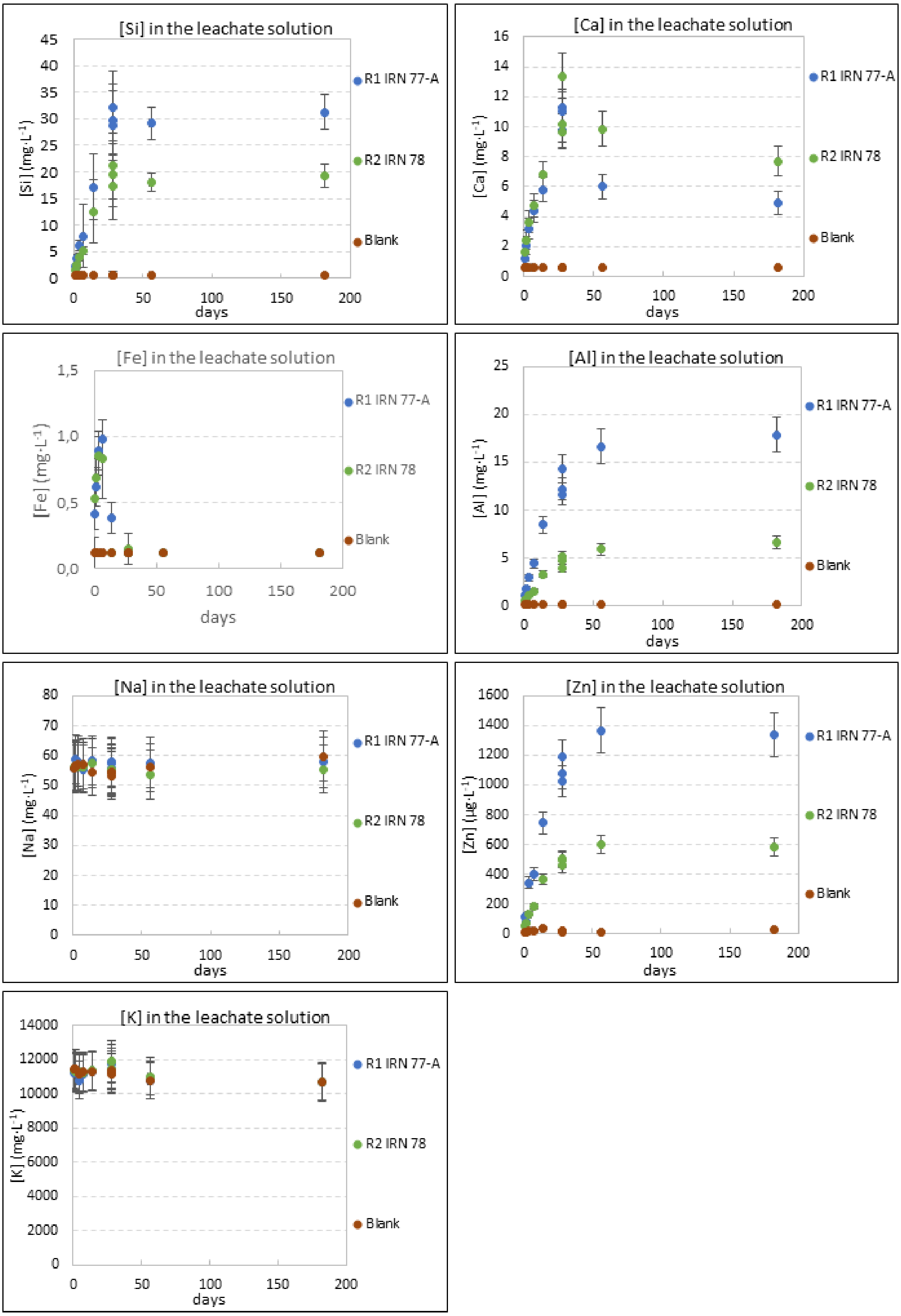

Figure 144: Element concentrations measured for the R1 IRN 77-A and R2 IRN 78 samples in the additional tests (KOH solution at pH 13.5 and 40 °C).

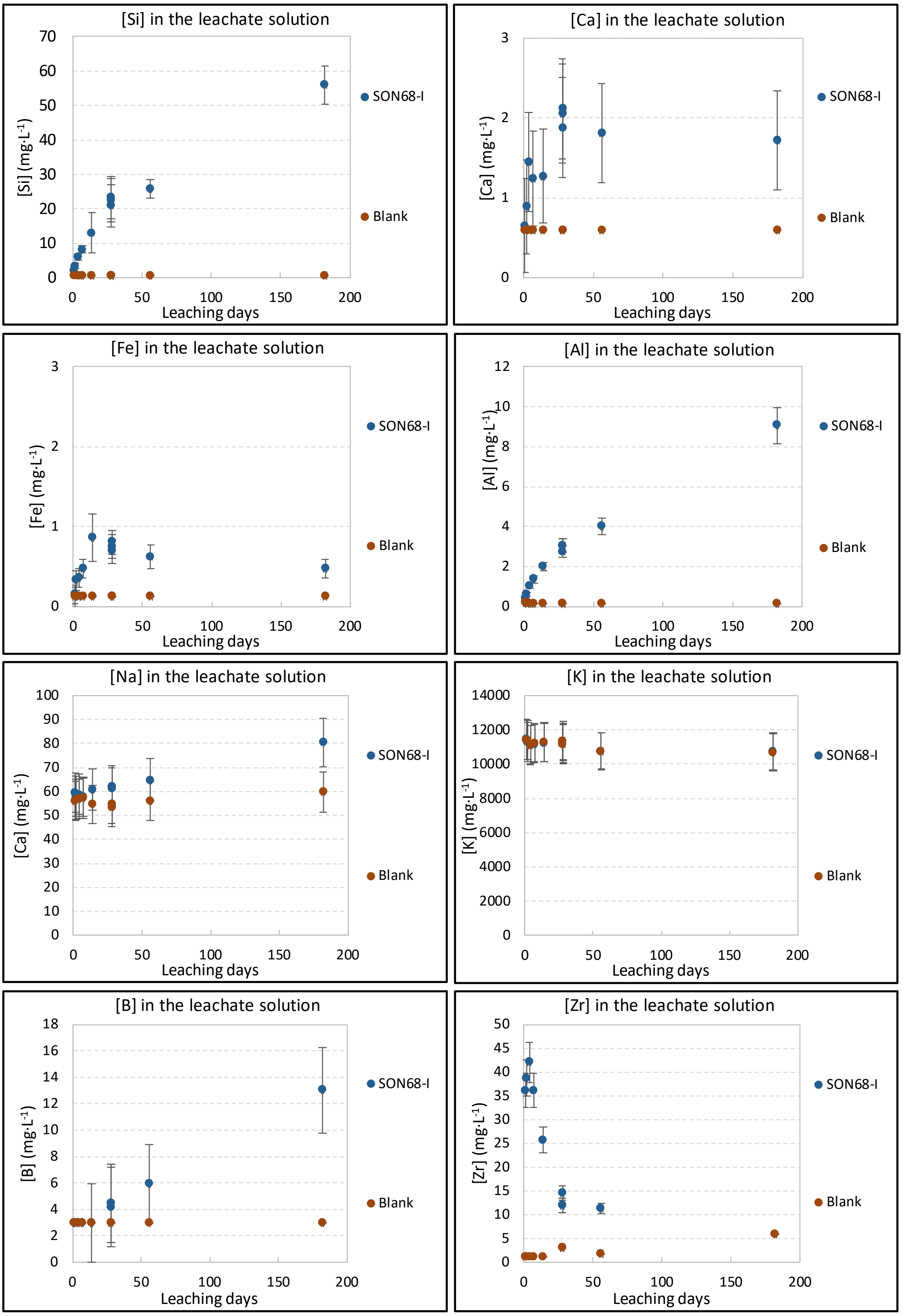

Figure 145: Element concentrations measured for the SON68-I in the additional tests (KOH solution at pH 13.5 and 40 °C).

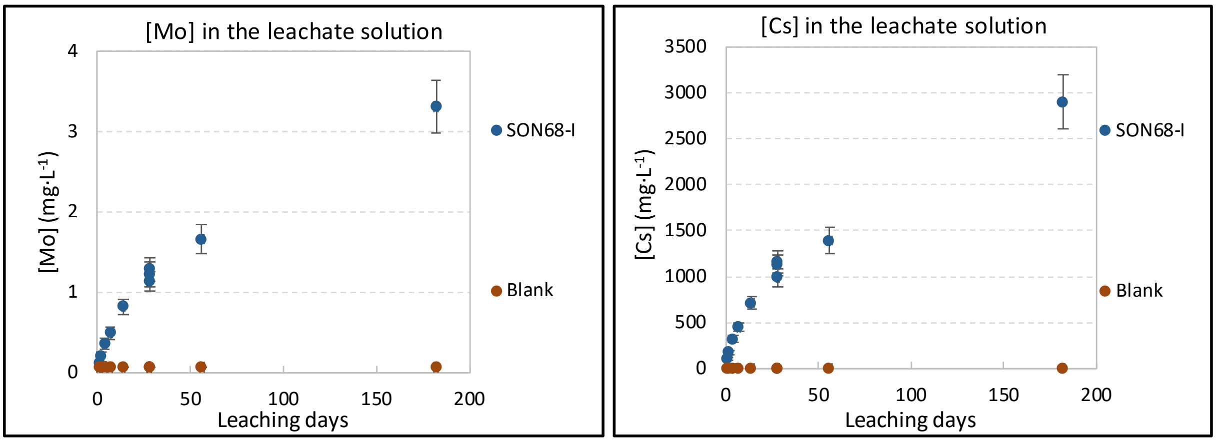

Figure 145 (continued): Element concentrations measured for the SON68-I in the additional tests (KOH solution at pH 13.5 and 40 °C).

H-3 Dissolution rates

The evolution of the Si and Al normalised mass losses as a function of time are given in Figure 146 and Figure 147 with the 95% confidence intervals, calculated by error propagation.. For the calculations of these normalised mass losses, it was not necessary to remove the background concentrations because the values in the blank tests were below the detection limit. The slopes of the linear regressions give the sample dissolution rates. In

Table 61, the dissolution rates calculated from NL(Si) and NL(Al) in the period 0 – 1 days, 1 – 2 days, 2 – 4 days , 4 – 7 days, 7 – 14 days, 14 – 28 days 14 and 56 – 182 days of leaching are given[1]. Figure 148 and Figure 149 present the evolution of these dissolution rates. It should be remarked that to determine the dissolution rates in the periods 14 – 28 days and 28 – 56 days for the R2 IRN 78 sample, and in the period 28 – 56 days for the R1 IRN 77-A sample, only one or two NL(Si) after 28 days have been considered to obtain a positive slope of the linear regression.

The maximum dissolution rates are obtained by the slopes connecting the first data point (after 1 day) with the origin (0,0). As for glass alteration under alkaline conditions, the results show that the plasma slags dissolve first at a maximum rate and then the alteration rate decreases; this latter rate can be up to two orders of magnitude lower than the maximum rate. It can also be noted that the maximum rates do not last for a long time, as the rate show already a significant decrease after 4 days.

In the period 0 – 1 day, the maximum dissolution rates based on NL(Si) are in the range of 0.6 – 1.3 $g \cdot m^{-2} \cdot d^{-1}$ with the minimum rate for the Simuli 4-A sample and the maximum rate for the R1 IRN 77-A sample. The maximum rates based on NL(Al) are in the range of 1 – 1.9 $g \cdot m^{-2} \cdot d^{-1}$ with the minimum rate for the Simuli 1-A sample and the maximum rate for the Simuli 2. Note that the uncertainties on the dissolution rates calculated from NL(Si) are very high because of the high uncertainties on the Si concentrations in solution. The dissolution rates based on NL(Al) are thus more accurate due to lower uncertainties on the Al concentrations. Until 28 days, higher rates are found for the Simuli 2 and R1 IRN 77-A samples which are both porous plasma slags containing crystalline phases identified as magnetite and clinopyroxene.

The maximum rates based on NL(Si) and NL(Al) established for SON68-I in the period 0 – 1 day are equal to 0.94 ± 0.29 $g \cdot m^{-2} \cdot d^{-1}$ and 1.46 ± 0.45 $g \cdot m^{-2} \cdot d^{-1}$, respectively.

As observed for nuclear glass alteration, for the investigated plasma slags a maximum dissolution rate is first observed, followed by a rate drop which may be due to the increase of the main element concentrations (Si, Al) in solution. For all samples, the dissolution rates between 56 and 182 days are quite similar, i.e. around 0.01 – 0.03 $g \cdot m^{-2} \cdot d^{-1}$, except for the R2 IRN 78 sample for which a rate one order of magnitude lower is found (0.004 $g \cdot m^{-2} \cdot d^{-1}$). For this latter sample, the Si and Al concentration in solution were quite similar to those measured for the other plasma slags.

---

[1] For some samples, the dissolution rate was also calculated in the period 1-4 days or 28 – 182 days to have a positive slope of the linear regression.

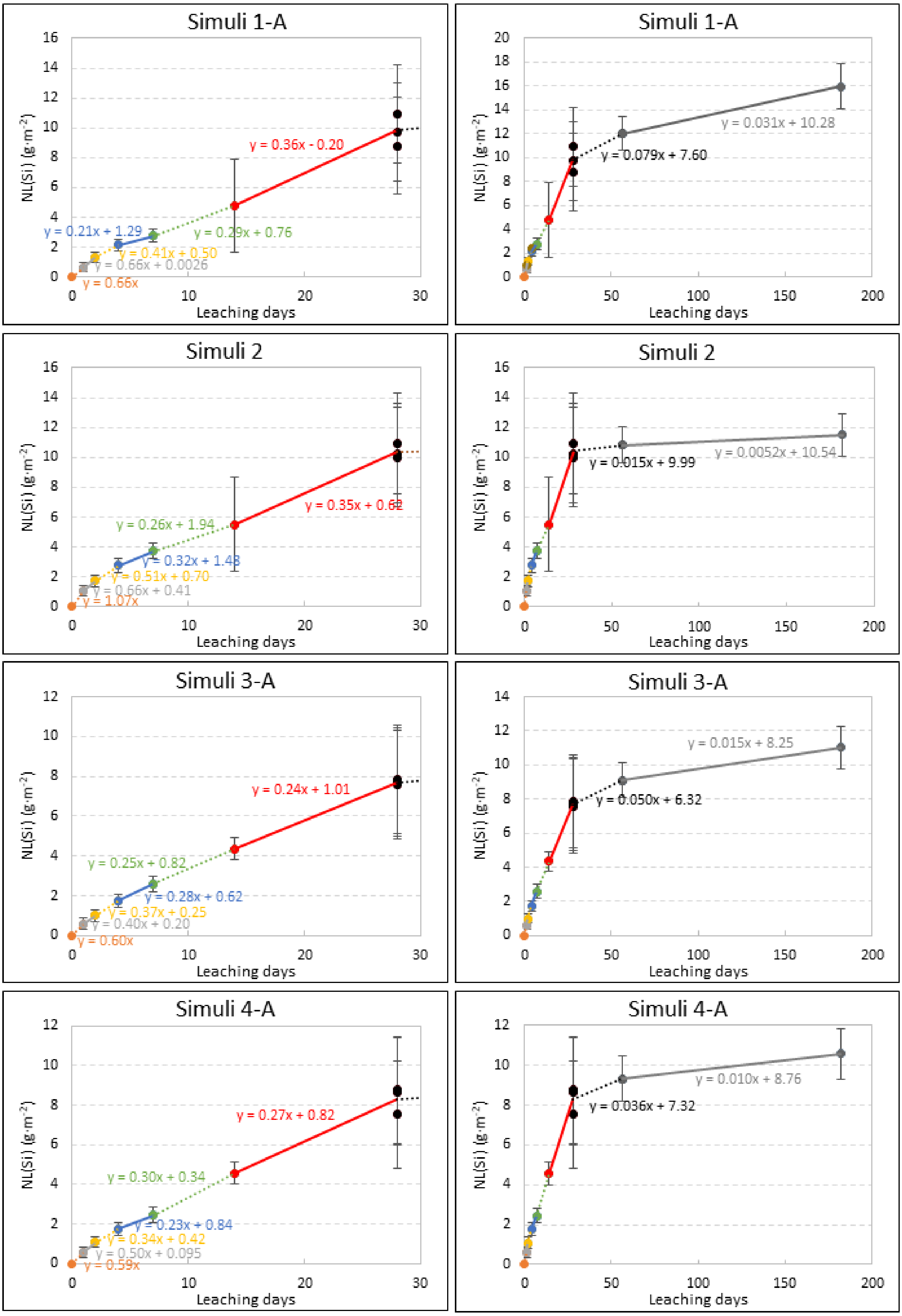

Figure 146: NL(Si) in g·m^{-2} as a function of leaching days.

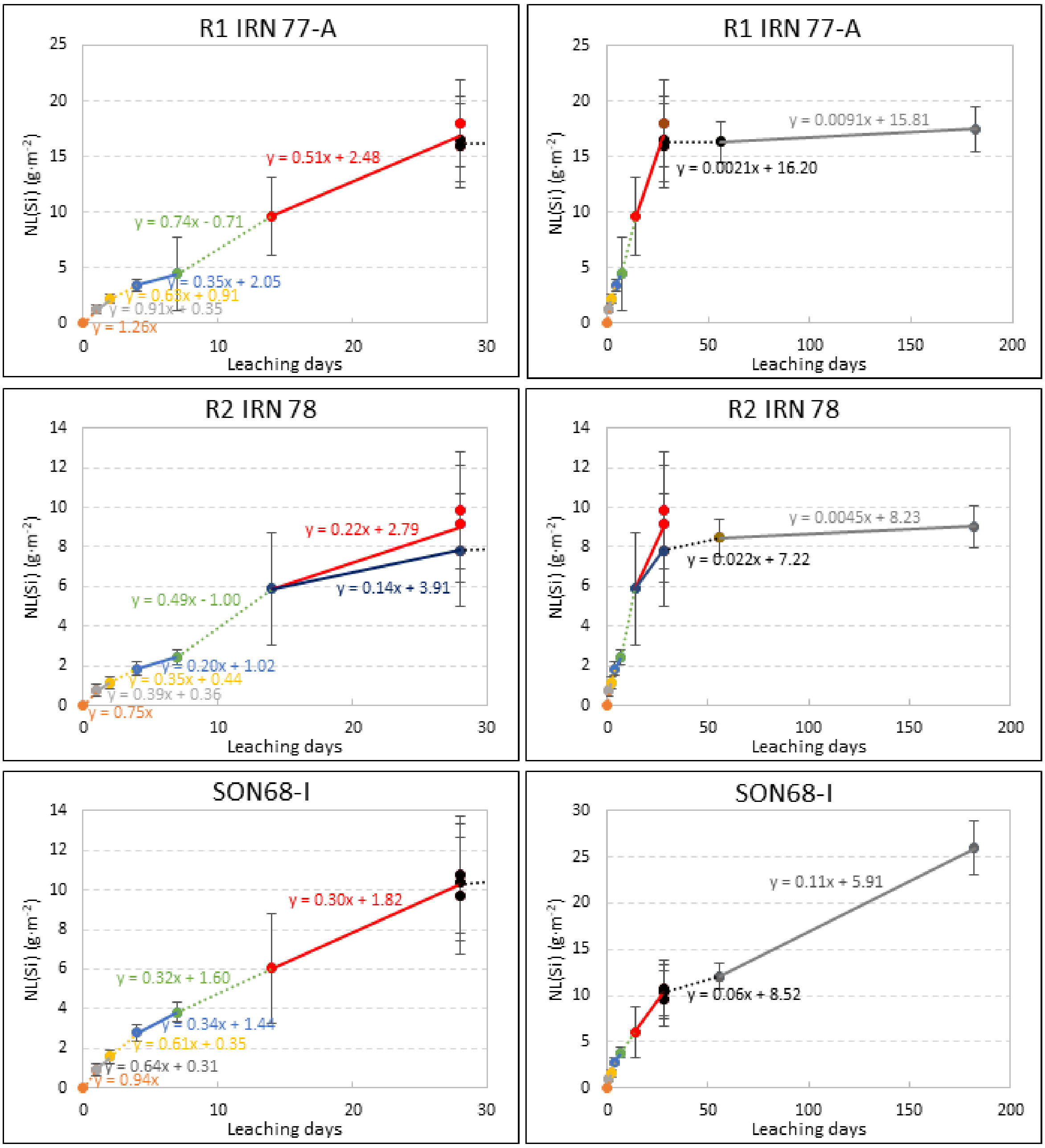

Figure 146 (continued): NL(Si) in g·m^{-2} as a function of leaching days.

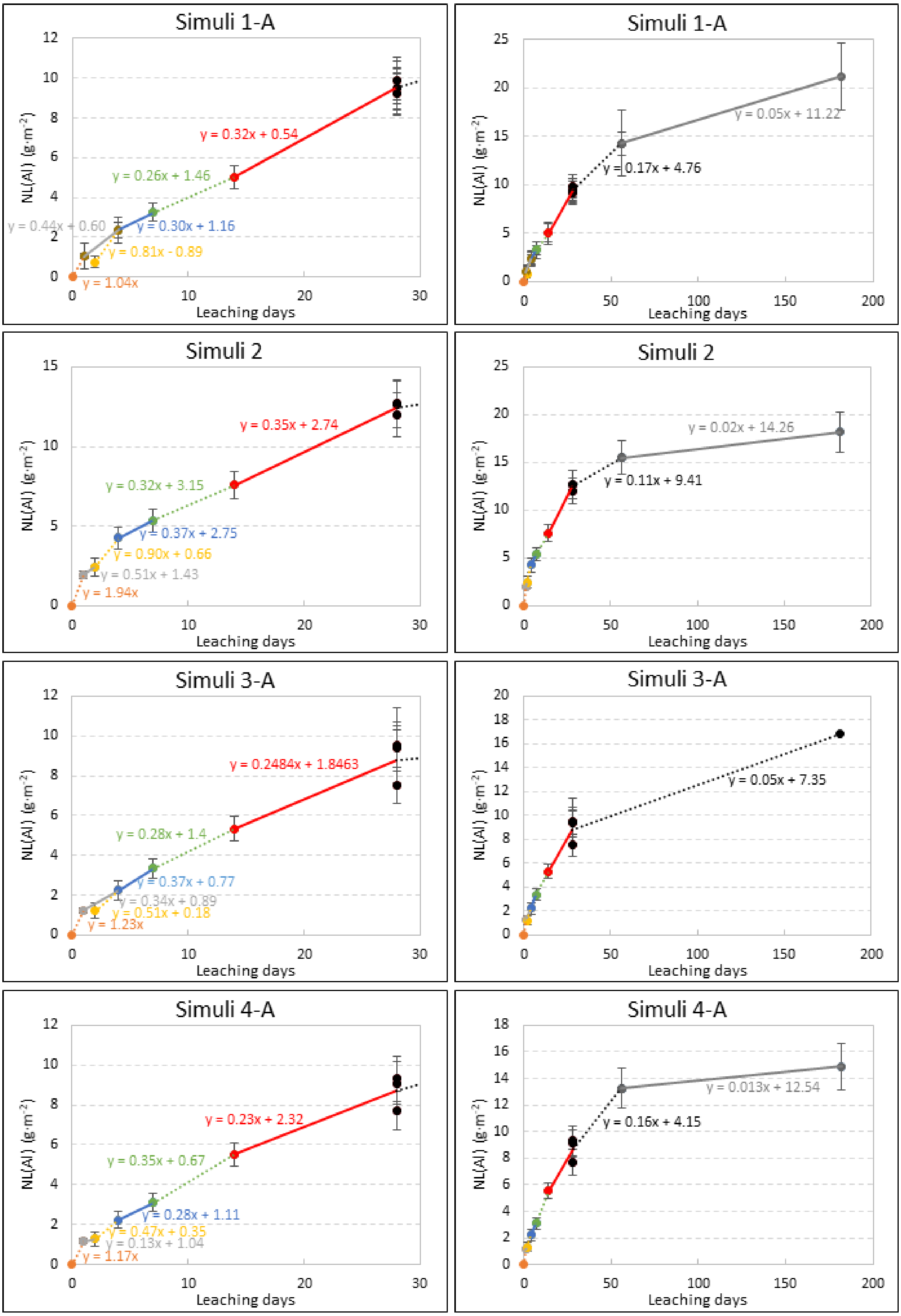

Figure 147: NL(Al) in g·m^{-2} as a function of leaching days.

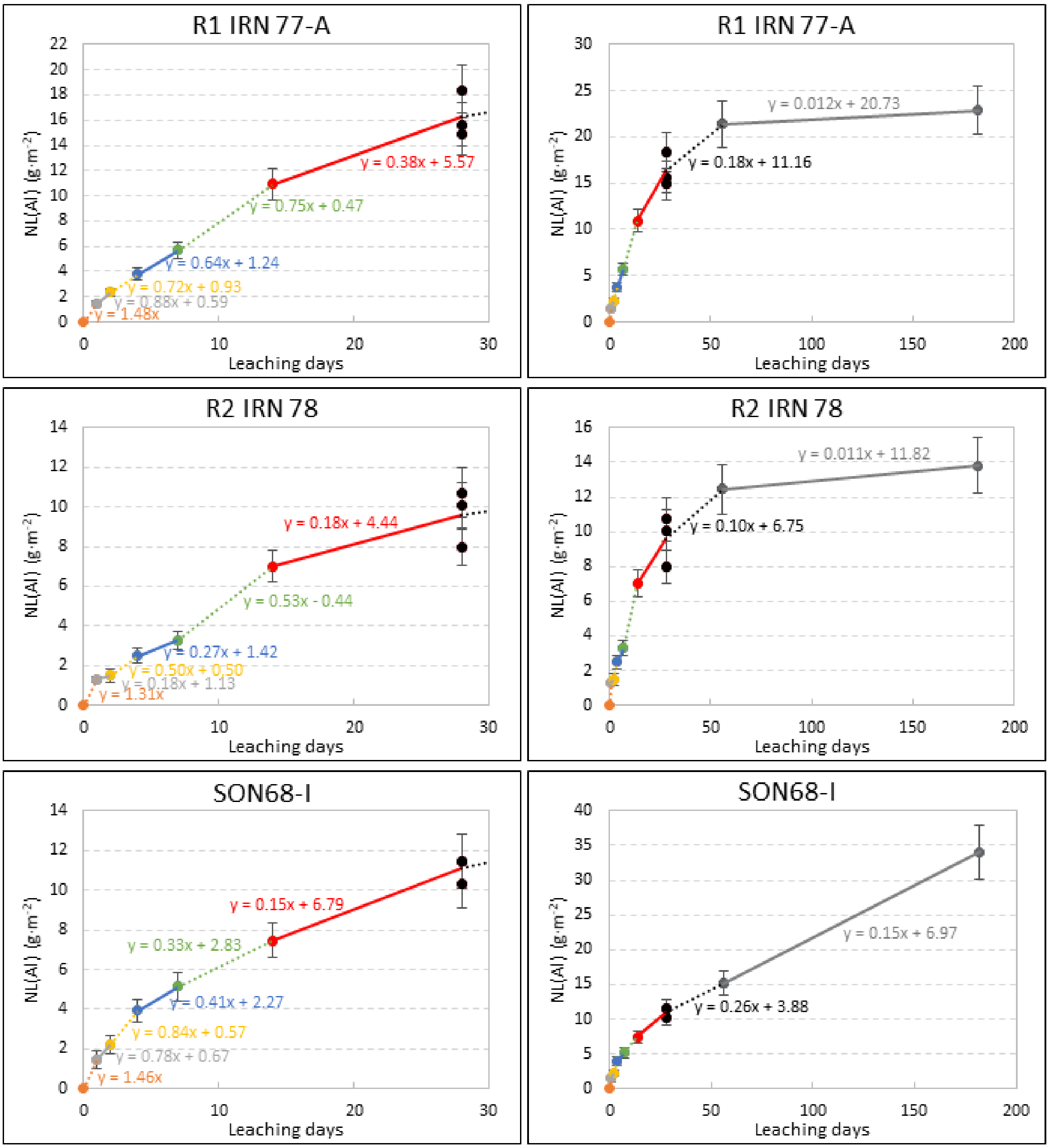

Figure 147 (continued): NL(Al) in g·m^{-2} as a function of leaching days.

Table 61: Dissolution rates calculated from NL(Si), and NL(Al) in the periods 0 – 1 day, 1 – 2 days or 1 – 4 days, 2 – 4 days, 4 – 7 days, 7 – 14 days, 14 – 28 days, 28 –56 days and 56 – 182 days.

Samples	**Dissolution rate in the period 0 – 1 day ($g \cdot m^{-2} \cdot d^{-1}$)**	
	From NL(Si)	**From NL(Al)**
Simuli 1-A	0.66 ± 0.31	1.04 ± 0.12
Simuli 2	1.07 ± 0.34	1.94 ± 0.22
Simuli 3-A	0.60 ± 0.27	1.23 ± 0.14
Simuli 4-A	0.59 ± 0.27	1.17 ± 0.13
R1 IRN 77-A	1.26 ± 0.35	1.48 ± 0.17
R2 IRN 78	0.75 ± 0.29	1.31 ± 0.15
SON68-I	0.94 ± 0.29	1.46 ± 0.45

Samples	**Dissolution rate in the period 1 – 2 days ($g \cdot m^{-2} \cdot d^{-1}$)**	
	From NL(Si)	**From NL(Al)**
Simuli 2	0.66 ± 0.50	0.51 ± 0.61
Simuli 4-A	0.50 ± 0.39	0.13 ± 0.38
R1 IRN 77-A	0.91 ± 0.54	0.88 ± 0.34
R2 IRN 78	0.39 ± 0.43	0.18 ± 0.35
SON68-I	0.64 ± 0.44	0.78 ± 0.65

Samples	**Dissolution rate in the period 1 – 4 days ($g \cdot m^{-2} \cdot d^{-1}$)**	
	From NL(Si)	**From NL(Al)**
Simuli 1-A	0.66 ± 0.46	0.44 ± 0.13
Simuli 3-A	0.40 ± 0.38	0.34 ± 0.17

Table 61 (continued): Dissolution rates calculated from NL(Si), and NL(Al) in the periods 0 – 1 day, 1 – 2 days or 1 – 4 days, 2 – 4 days, 4 – 7 days, 7 – 14 days, 14 – 28 days, 28 –56 days and 56 –182 days.

Samples	**Dissolution rate in the period 2 – 4 days ($g\cdot m^{-2}\cdot d^{-1}$)**	
	From NL(Si)	**From NL(Al)**
Simuli 1-A	0.41 ± 0.26	0.81 ± 0.24
Simuli 2	0.51 ± 0.29	0.90 ± 0.45
Simuli 3-A	0.37 ± 0.21	0.51 ± 0.31
Simuli 4-A	0.33 ±0.21	0.47 ± 0.28
R1 IRN 77-A	0.63 ± 0.33	0.72 ± 0.27
R2 IRN 78	0.35 ± 0.23	0.13 ± 0.25
SON68-I	0.61 ± 0.26	0.84 ± 0.38

Samples	**Dissolution rate in the period 4 – 7 days ($g\cdot m^{-2}\cdot d^{-1}$)**	
	From NL(Si)	**From NL(Al)**
Simuli 1-A	0.21 ± 0.20	0.30 ± 0.20
Simuli 2	0.32 ± 0.23	0.37 ± 0.34
Simuli 3-A	0.28 ± 0.17	0.37 ± 0.23
Simuli 4-A	0.23 ± 0.16	0.28 ± 0.21
R1 IRN 77-A	0.35 ± 1.12	0.64 ± 0.27
R2 IRN 78	0.20 ± 0.18	0.27 ± 0.20
SON68-I	0.34 ± 0.22	0.41 ± 0.31

Samples	**Dissolution rate in the period 7 – 14 days ($g\cdot m^{-2}\cdot d^{-1}$)**	
	From NL(Si)	**From NL(Al)**
Simuli 1-A	0.29 ± 0.45	0.26 ± 0.11
Simuli 2	0.26 ±- 0.46	0.32 ± 0.16
Simuli 3-A	0.25 ± 0.10	0.28 ± 0.11
Simuli 4-A	0.30 ± 0.10	0.35 ± 0.11
R1 IRN 77-A	0.74 ± 0.69	0.75 ± 0.20
R2 IRN 78	0.49 ± 0.41	0.53 ± 0.13
SON68-I	0.32 ± 0.40	0.33 ± 0.16

Table 61 (continued): Dissolution rates calculated from NL(Si), and NL(Al) in the periods 0 – 1 day, 1 – 2 days or 1 – 4 days, 2 – 4 days, 4 – 7 days, 7 – 14 days, 14 – 28 days, 28 –56 days and 56 –182 days.

Samples	**Dissolution rate in the period 14 – 28 days (g·m⁻²·d⁻¹)**	
	From NL(Si)	**From NL(Al)**
Simuli 1-A	0.36 ± 0.26	0.32 ± 0.06
Simuli 2	0.35 ± 0.27	0.35 ± 0.09
Simuli 3-A	0.24 ± 0.12	0.25 ± 0.06
Simuli 4-A	0.27 ± 0.12	0.23 ± 0.06
R1 IRN 77-A	0.51 ± 0.30	0.38 ± 0.22
R2 IRN 78	0.14 ± 0.29*	/
R2 IRN 78	0.22 ±- 0.23	0.18 ± 0.07
SON68-I	0.30 ± 0.23	0.26 ± 0.08

* with the lowest NL(Si) after 28 days.

Samples	**Dissolution rate in the period 28 – 56 days (g·m⁻²·d⁻¹)**	
	From NL(Si)	**From NL(Al)**
Simuli 1-A	0.08 ± 0.08	0.17 ± 0.06
Simuli 2	0.02 ± 0.08	0.11 ± 0.07
Simuli 3-A	0.05 ± 0.07	/
Simuli 4-A	0.04 ± 0.07	0.16 ± 0.06
R1 IRN 77-A	0.002 ± 0.12*	0.76 ± 0.09
R2 IRN 78	0.02 ± 0.11**	0.44 ± 0.05
SON68-I	0.06 +/- 0.08	0.15 ± 0.07

* with the two lower NL(Si) values after 28 days; ** with the lowest NL(Si) after 28 days.

Table 61 (continued): Dissolution rates calculated from NL(Si), and NL(Al) in the periods 0 – 1 day, 1 – 2 days or 1 – 4 days, 2 – 4 days, 4 – 7 days, 7 – 14 days, 14 – 28 days, 28 –56 days and 56 –182 days.

Samples	**Dissolution rate in the period 56 – 182 days ($g\cdot m^{-2}\cdot d^{-1}$)**	
	From NL(Si)	**From NL(Al)**
Simuli 1-A	0.03 ±0.02	0.05 ± 0.02
Simuli 2	0.01 ± 0.01	0.02 +/- 0.02
Simuli 3-A	0.02 ± 0.01	(0.05 ± 0.01)*
Simuli 4-A	0.01 ± 0.01	0.01 ± 0.02
R1 IRN 77-A	0.01 ± 0.02	0.01 ± 0.03
R2 IRN 78	0.004 ± 0.01	0.011 ± 0.02
SON68-I	0.11 ± 0.03	0.15 ±0.03

* rate between 28 and 182 days.

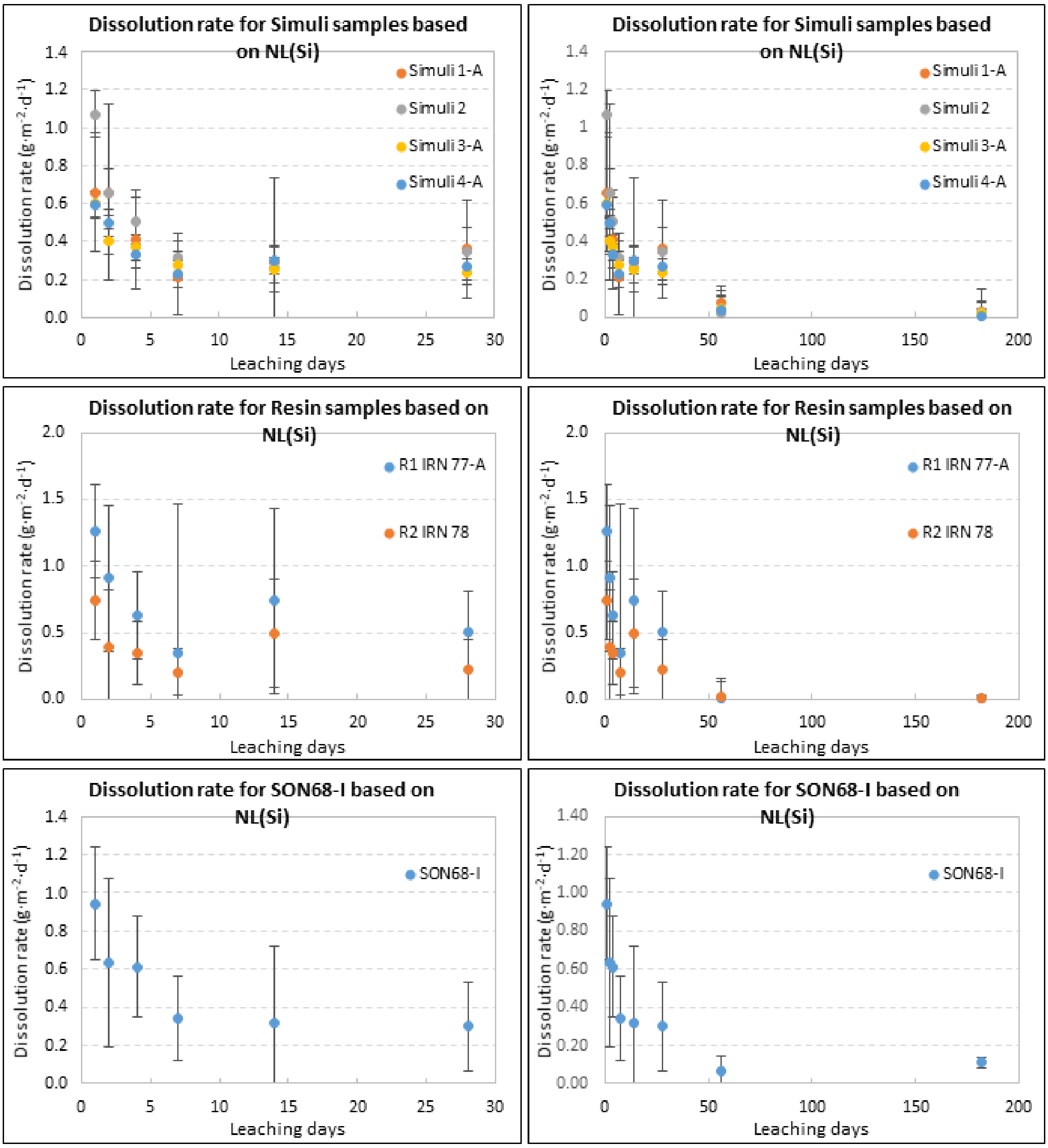

Figure 148: Evolution of the dissolution rates calculated from NL(Si) as a function of the leaching days.

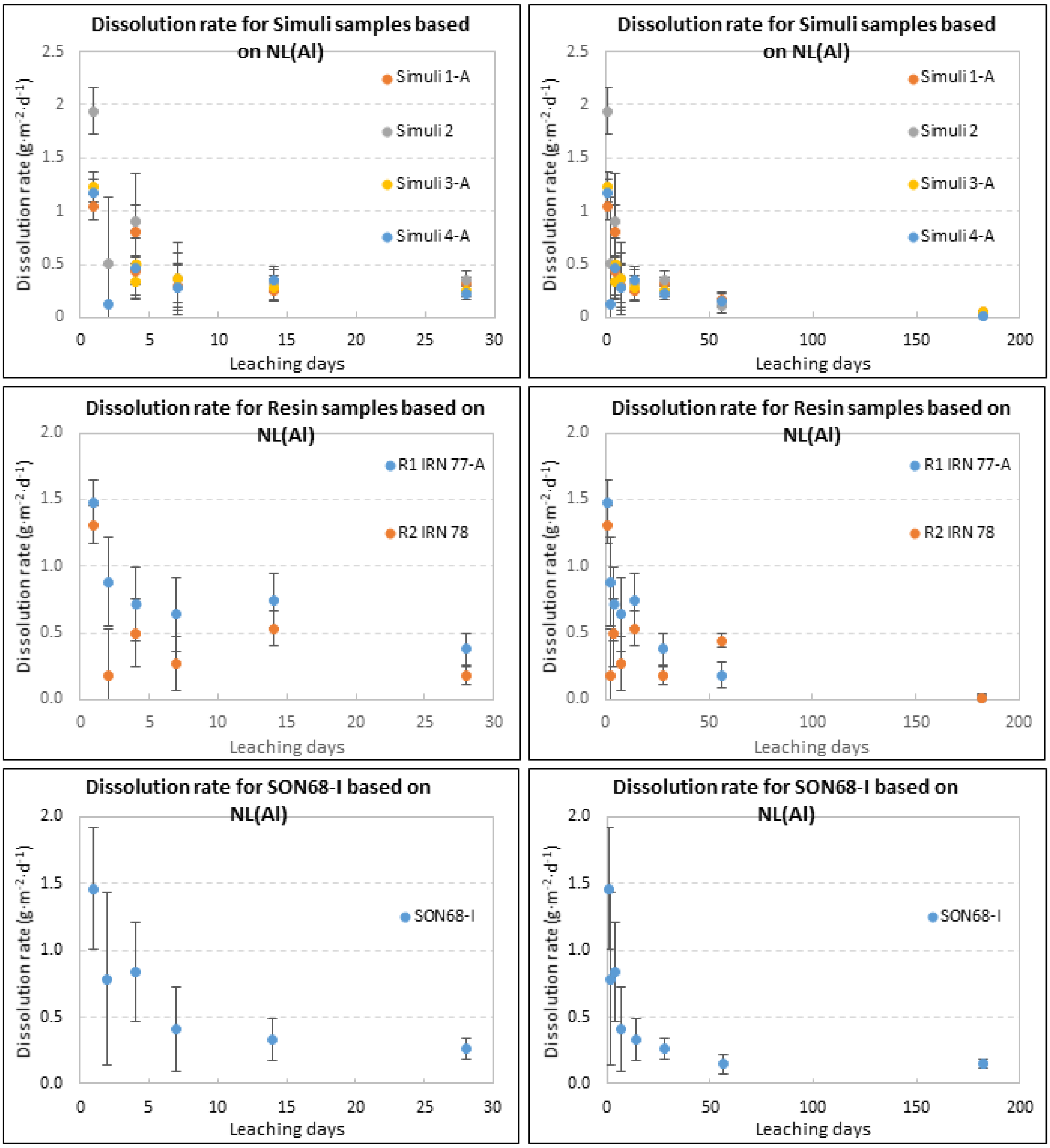

Figure 149: Evolution of the dissolution rates calculated from NL(Al) as a function of the leaching days.

H-4 Alteration layer thicknesses from NL(Si) and NL(Al)

Table 62 indicates the alteration layer thicknesses in µm calculated from NL(Si) and NL(Al) for the plasma slags altered for 182 days in a KOH solution at $pH_{(25°C)}$ 13.5 and 40 °C.

The calculations are made by dividing the normalised mass losses by the density of the samples given in Table 44, Table 51 and Table 57.

Based on the NL(Si) and NL(Al), the calculated alteration layer thicknesses are in the range of 3 - 10 µm and 5 – 13 µm, respectively, with the minimum value for the R2 IRN 78 sample and the maximum one for SON68-I.

Table 62: Alteration layer thicknesses after 182 days of alteration calculated from NL(Si) and NL(Al).

Samples	**Alteration layer (µm)**	
	From NL(Si)	**From NL(Al)**
Simuli 1-A	5.6 ± 0.7	7.4 ± 0.9
Simuli 2	3.6 ± 0.5	5.8 ± 0.7
Simuli 3-A	3.9 ± 0.5	5.9 ± 0.7
Simuli 4	3.7 ± 0.5	5.2 ± 0.6
R1 IRN 77-A	5.6 ± 0.7	7.3 ± 0.8
R2 IRN 78	3.1 ± 0.4	4.8 ± 0.6
SON68	9.5 ± 1.1	12.5 ± 1.5